Distribution Agreement

In presenting this thesis or dissertation as a partial fulfillment of the requirements for an advanced degree from Emory University, I hereby grant to Emory University and its agents the non-exclusive license to archive, make accessible, and display my thesis or dissertation in whole or in part in all forms of media, now or hereafter known, including display on the world wide web. I understand that I may select some access restrictions as part of the online submission of this thesis or dissertation. I retain all ownership rights to the copyright of the thesis or dissertation. I also retain the right to use in future works (such as articles or books) all or part of this thesis or dissertation.

Signature:

_____ _____

Aaron Bruce Reeve Date

Compartmentalization, Tissue-Specific Selection and Mutation of Envelope V1 Region, Nef and Integrase of Neuropathogenic SIVsmmFGb in the Central Nervous System and Lymph Nodes of Infected Pigtailed Macaques at One Week and Two Months Post-Infection

By

Aaron Bruce Reeve
Doctor of Philosophy

Graduate Division of Biological and Biomedical Science
Immunology and Molecular Pathogenesis

_____
Francis J. Novembre, Ph.D.
Advisor

_____
Rama R. Amara, Ph.D.
Committee Member

_____
Arash Grakoui, Ph.D.
Committee Member

_____
Paul Rota, Ph.D.
Committee Member

_____
William Tyor, M.D.
Committee Member

Accepted:

_____
Lisa A. Tedesco, Ph.D.
Dean of the James T. Laney School of Graduate Studies

_____
Date

Compartmentalization, Tissue-Specific Selection and Mutation of Envelope V1 Region, Nef and Integrase of Neuropathogenic SIVsmmFGb in the Central Nervous System and Lymph Nodes of Infected Pigtailed Macaques at One Week and Two Months Post-Infection

By

Aaron Bruce Reeve
B.Sc., University of Calgary, 2004

Advisor: Francis J. Novembre, Ph.D.

An abstract of
A dissertation submitted to the Faculty of the
James T. Laney School of Graduate Studies of Emory University
in partial fulfillment of the requirements for the degree of Doctor of Philosophy in the
Graduate Division of Biological and Biomedical Science
Immunology and Molecular Pathogenesis
2010

Abstract

Compartmentalization, Tissue-Specific Selection and Mutation of Envelope V1 Region, Nef and Integrase of Neuropathogenic SIVsmmFGb in the Central Nervous System and Lymph Nodes of Infected Pigtailed Macaques at One Week and Two Months Post-Infection

By Aaron Bruce Reeve

The simian lentivirus quasispecies SIVsmmFGb induces neuropathology in over 90% of infected pigtailed macaques and is a reliable model of HIV neuropathogenesis. However, little is understood about the genetic diversity of this virus, development of the quasispecies over the course of infection, whether the virus compartmentalizes between tissues and how these compartments develop over time. Initial seeding of the CNS and lymph node reduced Env V1 region and Int genetic diversity but had a variable effect on Nef. By two mpi, selective pressures affected the diversity of Nef sequences between tissues, but changes to Env V1 region and Int variety were similar across all tissues. At both one wpi and two mpi, *env* V1 region and *int* genes formed separate compartments between areas of the CNS, as well as between the CNS regions and the lymph nodes. The *nef* genes compartmentalized separately between all tissues at one wpi, but no longer segregated between lymph nodes at two mpi. Negative selection on *nef* and *int* genes increased in the brain regions and one lymph node over time, while positive selection of *env* V1 region increased over time in some CNS regions. Convergent evolution of both *nef* and *env* V1 region sequences, and divergent evolution of *int* genes, was noted between compartments. Intra-tissue temporal segregation occurred for all three genes and was stronger in the CNS for *env* V1 region and *nef*. Functional differences in *int* and *env* V1 region genes decreased between tissues over time, but functional differences in *nef* sequences increased.

We also analyzed the Env V1 region, Nef and Int amino acid sequences for mutations in important functional domains. The average Env V1 region length and number of O-linked glycosylations, as well as the presence of a six-amino acid insertion, increased over time in the CNS and lymph nodes. For Nef, the prevalence of mutations increased over time in the basic region and N-proximal Y residues, but the frequency of mutations declined in the acidic region. The proportion of mutations in the Nef thioesterase and AP interaction sites increased over time only in the CNS.

Compartmentalization, Tissue-Specific Selection and Mutation of Envelope V1 Region, Nef and Integrase of Neuropathogenic SIVsmmFGb in the Central Nervous System and Lymph Nodes of Infected Pigtailed Macaques at One Week and Two Months Post-Infection

By

Aaron Bruce Reeve
B.Sc., University of Calgary, 2004

Advisor: Francis J. Novembre, Ph.D.

A dissertation submitted to the Faculty of the
James T. Laney School of Graduate Studies of Emory University
in partial fulfillment of the requirements for the degree of Doctor of Philosophy in the
Graduate Division of Biological and Biomedical Science
Immunology and Molecular Pathogenesis
2010

Acknowledgments

I dedicate this dissertation to my parents, Ron and Julie Reeve. Without their love and support, I would not be where I am today.

I would like to thank my advisor, Dr. Frank Novembre, for having me as a member of his laboratory and providing guidance that has been, and will continue to be, invaluable in my scientific career. I would also like to thank Nicholas Pearce and Kalpana Patel for all of the training, hands-on assistance and camaraderie they provided.

In addition, I would like to thank Drs. Rama Amara, Arash Grakoui, Paul Rota and Bill Tyor for their valuable input as members of my thesis committee.

Table of Contents

Introduction

Epidemiology of HIV/AIDS

As of 2007, 30 – 36 million people worldwide were living with HIV, including 1.2 million people in the United States (1). Also in that year, approximately 2.7 million new HIV infections and two million HIV-related deaths are estimated to have occurred (1). Roughly two million of those living with HIV in 2007 were infants and over 500 000 children were born HIV-infected due to vertical transmission from infected mothers (1). Approximately 67% of all HIV cases worldwide, and 75% of AIDS-related deaths, are in sub-Saharan Africa (1).

HIV-Associated Neurological Disorders

Beyond the systemic immunological effects of infection, HIV is also associated with neurological pathology. The HIV-associated neurocognitive disorders (HAND), a group of neurological complications caused by direct or indirect viral mechanisms, affect one- to two-thirds of AIDS patients (2-4). Though neurological symptoms are rare during the early stages of infection, some patients present with aseptic meningitis or meningoencephalitis during the acute phase (2). The most common HIV-associated peripheral neuropathy is distal symmetrical polyneuropathy, which causes pain in the lower extremities and appears in approximately 30% of infected patients (5, 6). Neurological signs of this disorder, which are found at autopsy in virtually 100% of brains from AIDS patients, include macrophage activation and degeneration of the axons of sensory neurons (5, 6). Minor cognitive/motor disorder (MCMD) is another HIV-associated neuropathology that presents in approximately 30 – 50% of patients following progression to AIDS (7, 8). Symptoms of this disorder, which include slowed thinking,

attention defects and motor defects in the extremities, usually have little or no impact on patient functioning (9, 10). Although a mild neurological disorder, MCMD is predictive for the development of HIV-associated dementia (HAD) and encephalitis, as well as a worse prognosis for AIDS (7, 11, 12). Inflammatory demyelinating polyneuropathy is a rare neurological complication that causes weakness in the extremities (6). This disorder may become chronic and may arise during the acute stages of HIV infection (6, 13). Diffuse infiltrative lymphocytosis syndrome may result from HIV-induced infiltration of activated CD8+ T cells, leading to axonal neuropathy of the peripheral nerves (14).

HIV-Associated Dementia

HAD is one of the most common syndromes in the HAND spectrum and the predominant cause of dementia among young adults in the United States (15). HAD usually develops late in HIV infection, following immunosuppression, and is rare during the acute phase (16, 17). However, even in the late stages of disease, not all AIDS patients will develop HAD and this variability may be due to a combination of host- and virus-specific factors (18). The incidence of HAD has an inverse correlation with CD4+ T cell levels and a positive correlation with levels of viral RNA in the cerebrospinal fluid (CSF) (16, 19, 20). Prior to the HAART era, and in patients without access to HAART, the six-month mortality of HAD patients is approximately 67%, higher than for opportunistic infections such as *Pneumocystis carinii* and cerebral toxoplasmosis, but comparable to the death rate from central nervous system (CNS) lymphoma (17). Progressive encephalopathy, a similar disorder in HIV-infected children, affects 20 – 60% of pediatric HIV patients (21).

HAD is a progressive disorder, with six stages of cognitive and motor symptoms (9, 18, 22): In stage 0, patients have apparently normal levels of functioning and no obvious clinical symptoms. Normal function continues through stage 0.5, with only slight motor impairments in the extremities. Symptoms in stage 1 are comparable to MCMD or fatigue in uninfected individuals, with reduced ability to perform complex mental tasks, slowed thinking and minor impairments in fine motor control. Stage 2 is a moderate disorder with impaired memory and cognition, slowed thought processes and notable motor defects. At this stage, patients can take care of themselves but cannot work or walk without support. In stage 3, patients have frank dementia, with significant impairments in memory and cognitive function, as well as severe deficits in fine motor control. By the end stage, patients suffer paralysis and enter a vegetative state, with minimal cognitive function remaining. The rates of symptom presentation and disease progression can vary greatly between HAD patients (18).

The diagnosis and progression of HAD can also be affected by a number of external factors. Both MCMD and early-stage HAD symptoms bear some resemblance to clinical depression, complicating proper diagnosis in patients with pre-existing mental illness (18). Ethanol can induce similar pathological mechanisms in the CNS as HIV and both alcohol and cocaine may affect HAD progression (23, 24). However, other studies have demonstrated no difference in the presentation of behavioral symptoms or pathological lesions between cocaine treated and untreated controls in a SCID mouse model (25). Use of injection drugs accounts for 16% of cases of HIV transmission in the United States and drug users represent a significant proportion of the HIV-infected population in this country (26). Injection drug use is associated with an increased rate of

HAD progression, as well as increased turnover of microglia in the brains of HAD patients (27). Opiate drugs, specifically, may significantly alter the phenotype of brain microglia and astrocytes and synergize with damaging viral proteins and neurotoxic mediators to damage neurons (28-30).

HAART and HIV-Associated Dementia

The availability of highly-active antiretroviral therapy (HAART) has shown a dramatic impact on the presence and progression of HAD. In the United States, HAD presents in approximately 10% of adult late-stage AIDS patients, but occurs in over 30% of patients where access to HAART is limited (22). The advent of HAART has resulted in a 50 – 75% decline in the incidence of HAD from the early 1990s to the year 2000 (22, 31, 32). HAART has increased the median survival time from approximately one year to over four years for patients with any HAND disorder and from five months to 3.5 years for HAD patients (31). Some studies suggest that reductions in plasma viral load by HAART may correlate with improvements in the psychological and neurological symptoms of HAD (21, 27, 33), but this correlation does not appear in all studies (34). Specific HAART drugs, particularly zidovudine, can improve memory, attention and cognitive function, as well as reducing the risk of developing HAD by up to 40% (35-40). HAART treatment has also halved the incidence of HIV-associated distal symmetrical polyneuropathy (32).

However, in the presence of HAART, the prevalence of HAND disorders is beginning to increase. While the frequency of new HAD cases per year declined from the early 1990s to the year 2000, the total number of people with HAD increased by 50% during the same period of time (31, 32). HAND syndromes, including HAD and MCMD,

are also beginning to present in patients with CD4+ T cell counts > 500 cells/uL, whereas, prior to the advent of HAART, this disorder would rarely appear until CD4+ T cell levels dropped below 200 cells/uL (32, 41). The prevalence of MCMD has remained largely unchanged and the prevalence of distal symmetrical polyneuropathy has increased (32, 42). As HAART increases the length of time patients can live with chronic HIV, more patients may be surviving long enough to develop HAD (43).

While HAART effectively targets HIV replication and reduces viral loads, these drugs do not affect the inflammatory and neurotoxic cascades induced by the virus (44). HAART compounds also may not adequately penetrate the CNS, which can then become a reservoir for virus replication and may re-establish infection in the periphery (45). A typical HAART regimen consists of pairing two nucleoside reverse transcriptase inhibitors (NRTIs) with either a non-nucleoside reverse transcriptase inhibitor (NNRTI) or a protease inhibitor (46). In general, antisense oligonucleotides and antiviral nucleosides penetrate the brain tissues poorly, although the latter compounds may be present at higher levels in the CSF (47-49). Zidovudine reaches high concentrations in the CNS, but still less than the dose needed to be effective against even drug-sensitive virus strains (39, 40, 47). NRTIs are generally effective at entering the CNS, but are actively removed from the brain by efflux transport and may cause distal symmetrical polyneuropathy (6, 50, 51). The most commonly used NNRTI accumulates to effective concentrations in the CNS, and some other NNRTIs are capable of penetrating the blood-brain barrier (BBB) (52). However, the ability of NNRTIs to penetrate the brain varies and these compounds may have neurological side effects (45, 47, 53). Most protease inhibitors penetrate the CNS poorly, are actively removed from the brain and have been

shown to cause distal symmetrical polyneuropathy in some studies (51, 54-57), but do not appear to be harmful in others (58).

Lesions in HIV and SIV Neuropathogenesis

Although not all infected individuals develop a HAND disorder, 90% of AIDS patients not receiving HAART treatment show some pathological changes to the brain upon autopsy (59). CNS imaging of live patients often detects cerebral atrophy and enlargement of the brain ventricles, with a direct correlation between these gross pathological changes and HAD severity (60). Although not present in all patients, one of the most common lesions in the HIV-infected CNS is the multinucleated giant cell, arising from the fusion of infected monocyte-lineage cells, with viral Env proteins on their surface, and uninfected neighboring cells that express CD4 and CCR5 (61, 62). Other common lesions include monocyte-lineage cell proliferation in the CNS, migration of peripheral monocytes into the CNS and reactive gliosis, increasing the number and size of astrocytes (63). Other lesions that appear in some HAD patients include foamy macrophage, pallor of the subcortical white matter and infiltration of peripheral lymphocytes (59, 61, 64). Microglial nodules, associations of monocyte-lineage cells with infiltrating lymphocytes, are often present (59). The level of monocyte infiltration and monocyte-lineage cell activation in the CNS correlates directly with the extent and severity of dementia (64-67). In one study, the type of CNS lesion was shown to correlate with the severity of HAD, as patients with mild disease had gliosis and pallor, while multinucleated giant cell lesions were associated with severe dementia (9).

Productively infected cells and lesions are distributed throughout the CNS in SIV-infected pigtailed macaques and HIV-infected human patients (3, 68, 69). In HAD

patients, astrocytosis, neuronal loss, high viral loads and productively-infected cells are most common in the hippocampus, basal ganglia, brain stem and subcortical regions, while lesions in the cortex are rare (59, 61, 64, 68, 69). Viral loads, lesions and productively infected cells are generally higher in the hippocampus, cerebrum and midfrontal cortex of SIV-infected macaques (70, 71). As the basal ganglia and hippocampus are involved in memory and motor functions, lesions in these areas may explain some of the symptoms of HAD (72-76). Damage to the cerebellum, which coordinates fine motor processes, is associated with ataxia, a common symptom of neuropathogenesis in SIV-infected macaques (77). During the later stages of HAD, neurons are destroyed in the midfrontal cortex and the involvement of this region of the brain in cognition and motor control may also account for some symptoms (78).

Pathways of Virus Entry into the CNS

The generally accepted hypothesis for HIV and SIV entry into the CNS is a "Trojan Horse" mechanism, similar to that used by visna virus (79-81). In this model, the virus infects bone marrow-derived monocytes in the periphery (82). While circulating monocytes have limited susceptibility to infection, those that are infected can traffic to, and seed, the CNS (83, 84). These infected monocytes differentiate into perivascular macrophages and serve as reservoirs of active virus replication (79, 85-88). Some infected monocytes may also replace parenchymal microglia, forming another cellular reservoir of virus production (89, 90). Infected circulating monocytes may also assemble HIV virions into late endosomal compartments for later release, allowing cells infected in the periphery to spread virus into the CNS (91-93).

The process of monocyte entry into the CNS likely parallels extravasation of circulating monocytes into the peripheral tissues (90, 94, 95). The BBB consists of brain microvascular endothelial cells (BMVECs) connected by tight junctions and associated with a basement membrane, Pericytes, perivascular macrophages and the foot processes of astrocytes and microglia (90, 94). The BBB screens out most large and polar molecules, as well as producing an electrical gradient by controlling ion traffic (90, 94). Pinocytosis by BMVEC is limited, but unidirectional transport mechanisms allow these cells to shuttle specific molecules to and from the CNS (90, 94). Infection, inflammation and brain injury can induce cytokines such as TNF-alpha and IL1-beta, which increase adhesion molecule expression on the BMVEC, weaken tight junctions and stimulate the production of chemokines and matrix metalloproteinases (MMPs) (90, 94-97). MMPs then increase the permeability of the BBB, while MCP1 and MIP1-alpha recruit additional monocytes to the CNS (90, 94, 95). In HIV, viral Tat protein produced by infected monocytes both promotes rolling of circulating cells by increasing production of the vasodilator nitric oxide (NO) and increases adhesion molecule expression on BMVEC (98). Tat may promote migration of peripheral monocytes into the CNS by stimulating the production of chemokines, such as MCP-1, or by acting directly as a chemokine (99-102). Infected monocytes can also produce increased levels of NO and enzymes that degrade the extracellular matrix, increasing monocyte migration through the BBB (103). A positive feedback loop may then be established, resulting in the mass infiltration of the CNS by monocytes during AIDS (90, 94, 95).

Other mechanisms of viral entry into the CNS have also been proposed. HIV can establish productive infection in BMVECs, although it is not known whether these cells

express CD4 (104-109). These cells do express CCR5 and CXCR4 and virus binding to these receptors may increase BMVEC adhesion molecule expression (107-109). Lentiviruses may enter the BMVEC through CD4-independent macropinocytosis, but most viruses taken up in this manner are degraded in the lysosomes (105, 106, 110, 111). However, some virions may survive to infect the BMVEC or transmigrate through these cells into the CNS (111, 112). While HIV may access the CNS through gaps in the BBB, this mechanism is unlikely to contribute to virus entry (113). T lymphocytes are known to patrol the CNS (114, 115) and infected CD4+ T cells may also traffic virus into the brain.

Virus Target Cells in the CNS

Contributing to the inability of the host immune system to completely clear HIV, the virus can exist as a latent, integrated provirus in a number of cell types, including quiescent CD4+ T cells, dendritic cells and macrophages (116-118). Macrophages are a particularly important reservoir, as they are permissive to virus replication and can store virus particles in multivesicular bodies for later exocytosis (93, 119, 120). Tissue macrophages have a long lifespan, ranging from months to decades, and can release infectious HIV particles for long periods without suffering cytopathic effects (83, 84, 121). HIV also cannot be cleared from infected monocyte-lineage cells, such as macrophages, by HAART and these cells will remain a persistent reservoir even during treatment (83).

Most cells in the CNS that are productively infected with HIV and SIV are the monocyte-lineage parenchymal microglia and perivascular macrophages (70, 104, 113, 122-125). Perivascular macrophages are located within the basal lamina and perivascular

cuffs of the BBB, while microglia localize to the brain parenchyma (126, 127). Both cell types are involved in CNS immune responses and damage repair, performing phagocytosis of pathogens, debris and apoptotic cells (113, 126). Perivascular macrophages play a significant role in antigen presentation, while parenchymal microglia only become effective antigen presenting cells (APCs) upon activation (87, 128, 129). Perivascular macrophages have a lifespan of two to three months and are replaced by circulating monocytes, while parenchymal microglia have a slow turnover rate and are replaced by homeostatic proliferation (127, 129-131). During infection and inflammation, the microglia population can also be rapidly replaced through recruitment of circulating monocytes (129).

Both of these monocyte-lineage cell types express CD4 and CCR5, but also have CXCR4 and other minor co-receptors for HIV and SIV (132-138). Monocyte-lineage cells are permissive to virus replication even when not actively dividing, but must possess at least some proliferative potential for establishment of viral infection (139-142). Virus replication in non-proliferating monocyte-lineage cells is generally low, possibly due to low levels of nucleosides (140, 141). Activated monocyte-lineage cells accumulate in the perivascular cuffs during sustained virus replication, leading to an increase in numbers of potential target cells and infected perivascular macrophages (67, 125). Parenchymal microglia are known to extend foot processes into the BBB (143) and this may be the avenue through which these cells are exposed to the virus and subsequently infected.

In SIV, perivascular macrophages are the cells most frequently infected and give rise to multinucleated giant cells, with the parenchymal microglia having a minor contribution to the infected cell population (79, 123, 125). In some HIV studies, the virus

replicates well in microglia and multinucleated giant cell lesions arise from microglia syncytia (138, 144-146). However, most of these analyses were conducted on cultured microglia, which easily become activated and susceptible to virus infection (86). Other studies suggest that perivascular macrophages are the main cell population infected with HIV (147). In some cases, HIV appears only in the perivascular macrophages and in others only in the microglia, so the predominant cell type infected may vary between virus strains or hosts (148).

Astrocytes, the most common cell type in the CNS, are spread throughout the brain and provide structure to the intercellular network, as well as managing the microenvironment of neurons (113, 149, 150). Astrocytes guide axon growth and regulate extracellular concentrations of ions, solutes and neurotransmitters (149, 151). Astrocytes also maintain the BBB and are involved in cytokine, chemokine and immune responses to pathogens in the CNS (113, 149). A heterogeneous population, different astrocyte subsets may perform specific functions (152). Viral proteins, RNA and DNA have been detected in astrocytes from HIV patients, suggesting these cells are permissive to infection (149, 153-155). Virus entry into astrocytes may be an endocytic process independent of CD4 and chemokine receptors (113, 156-158). Active viral replication in astrocytes is transient, followed by downregulation of virus production and establishment of persistent infection (159, 160). However, despite transient acute replication, astrocytes are not likely a source of virus production, with only limited expression of structural proteins and genomic viral RNA (149, 159). Astrocytes may produce significant levels of early viral proteins, including Tat, Rev and possibly Nef (159, 161). Limited virus

replication in these cells may be due to inhibition of reverse transcription, viral gene translation and nuclear export of early viral mRNA (158, 161, 162).

Neurons and oligodendrocytes, which form the myelin sheath around axons, have been shown to harbor HIV nucleic acids in some studies, but not in others (113, 163-166). Some virus strains may infect oligodendrocytes, primary cultured neurons and neural cell lines, but the mechanism of infection is unknown, as these cells do not express CD4 (113, 167-169). Any productive infection in oligodendrocytes is extremely limited, but infection persists throughout the life of the cell (113, 168, 169). Infection of neurons and oligodendrocytes is not believed to be an important phenomenon in neuropathogenesis.

Virus Replication in the CNS

Virus infection of the CNS can be detected as early as one week post-infection (wpi) in SIV-infected macaques (81, 123, 124, 170). Viral antigens appear in the CNS by one wpi and actively replicating virus can be detected in perivascular cells in the frontal lobe, temporal lobe and white matter (79, 123). The virus can also be harvested from the CSF within one wpi (171-173). Viral RNA and integrated proviral DNA can be harvested from the basal ganglia, parietal cortex, thalamus and cerebellum by one wpi (79, 174). By three wpi, SIV RNA can no longer be detected in most CNS regions, and actively replicating virus remains undetectable beyond 7 wpi (79, 174). However, proviral DNA is present in multiple regions of the brain at one, two, three and seven wpi, indicating that the virus remains latent in the CNS and infected cells are not cleared by the antiviral immune response (79, 174). Actively replicating virus can once again be detected in the CNS between 8 and 12 wpi (174, 175).

The following mechanism for suppression of virus replication in the CNS is commonly accepted (176, 177): In monocyte-lineage cells, the host transcriptional activator LAP interacts with the LTR of integrated lentiviruses, increasing the transcription of viral genes (178-180). LIP, a dominant negative isoform of LAP, can also be expressed and interacts with the LTR to inhibit transcription (178-181). During the acute phase of infection, IFN-beta is induced in response to virus infection in the CNS and stimulates monocyte-lineage cells to increase LIP expression (181-184). Levels of both IFN-beta and LIP in the CNS peak at two to three wpi, around the onset of suppression of virus replication (176). This pathway is known to suppress HIV replication in primary monocyte-derived macrophages and lung alveolar macrophages (176, 183, 185, 186). As the primary target cells for HIV in the CNS are monocyte-lineage, this type I interferon-dependent mechanism likely also suppresses HIV replication in the CNS (79). Given that LIP represses cytokine-activated genes, this may also limit activation of monocyte-lineage cells in the CNS, reducing the pool of activated target cells permissive to virus replication (177, 187). This mechanism may also limit the release of neurotoxic factors from activated macrophages, minimizing neurological damage during the early stages of infection (177, 187).

In studies with SIV, resumption of virus replication in the CNS during AIDS is associated with a renewed increase in the activation of monocyte-lineage cells (67, 79, 80, 174). It is possible that, without a properly-functioning immune system to regulate macrophage activation, virus-infected activated macrophages recruit additional monocyte-lineage cells to the CNS (80). These cells then become activated, increasing the pool of potential target cells for virus replication and recruiting additional monocyte-

lineage cells to the CNS (80). The accumulation of activated macrophages leads to a build-up of neurotoxic mediators, formation of multinucleated giant cell lesions and neuropathology (80). The presence of activated monocyte-lineage cells in the CNS directly correlates with the severity of dementia symptoms (67, 71).

Acquired Immune Responses to HIV and SIV Infection of the CNS

The emergence of HAD after progression to AIDS suggests some role for the immune system in limiting neuropathology (3, 9, 188). In human patients, deficient neutralizing antibody responses to HIV increase the risk of HAD development (189). In SIV-infected macaques, deficient neutralizing antibody responses increase the severity of encephalitis and the rate of progression to neuropathogenesis (3, 190-192). While the BBB normally impedes entry of peripheral antibodies into the CNS, Env can damage this barrier and allow extravasation of serum proteins, such as IgG (193-195). In healthy individuals, B cells comprise 20% of the lymphocytes in the brain and, in acute HIV infection, antibody production is detectable within the intrathecal region (9, 115). The early appearance of humoral responses, and their efficacy against the R5-tropic viruses which preferentially infect the brain, suggest antibodies are involved in adaptive immunity in the CNS (196-198).

In healthy individuals, CD4+ and CD8+ T cells patrol the CNS and act as important immune effectors (114). The CD4:CD8 T cell ratio in healthy subjects is higher in the CNS than in the peripheral organs and the CNS has a higher percentage of T cells, in general, than the periphery (114, 115). Studies in HIV-infected patients and in vitro models indicate that CD8+ and CD4+ T cell infiltration of the CNS increases during infection (199, 200), but these results have not been replicated and the contribution of T

cell responses is uncertain. Patients with HIV encephalitis have greater numbers of infiltrating activated and memory T cells than both healthy controls and patients without encephalitis (199). CD8+ T cell depletion triples the number of animals that develop encephalitis in SIV infections and CD8+ T cells reduce the number of SIV-infected perivascular macrophages in the macaque CNS (201, 202).

Neurotoxic Viral Factors

Even in cells that do not support infection, viral proteins may still be capable of inducing deleterious effects. Viral proteins may be released continuously from infected cells or en masse following cell lysis or apoptosis (203, 204). Viral proteins, such as Env, that are expressed on virions and infected cells may bind receptors on the surfaces of uninfected cells, potentially activating signaling pathways (204). Damaged neurons are frequently localized near infected cells, but neurotoxic factors may translocate to affect distant neurons (205, 206).

The primary mechanism by which the gp120 domain of the viral Env protein causes neuronal damage is through disruption of intracellular Ca^{2+} homeostasis. Upon exposure to gp120, astrocytes undergo Na+/H+ antiport, transporting a proton out of the cytoplasm in exchange for a sodium ion (207). The resulting pH increase in the cytoplasm causes the astrocyte to release K+ ions and glutamate (207). The increased K+ levels in the extracellular microenvironment activate voltage-dependent Ca^{2+} channels on neurons, while glutamate stimulates *n*-methyl *D*-aspartate (NMDA) channels on these cells (207, 208). Prolonged activation of these channels results in elevated intracellular Ca^{2+} levels, triggering mitochondrial production of reactive oxygen species (ROS), caspase cascades and death by apoptosis (204, 208-212). The gp120 portion of Env may

also interact directly with NMDA receptors and voltage-gated Ca^{2+} channels on neurons, making these receptors more sensitive to subsequent increases in extracellular K+ and glutamate (210, 213-216). Furthermore, gp120 may also bind CXCR4 on some neurons, triggering release of intracellular Ca^{2+} stores and further increasing cytoplasmic Ca^{2+} (217-219).

The gp120 protein may also activate monocyte-lineage cells, inducing the release of neurotoxic factors such as TNFalpha, IL-1 beta, leukotrienes, NTox, platelet activating factor and arachidonic acid pathway metabolites (220-224). In glial cells, gp120 may increase production of MMP-9 and release of IL-1 beta in response to oxidative stress, contributing to apoptosis of neurons (225, 226). Hippocampal neurons are preferentially destroyed in HAD and gp120, produced by astrocytes, damages these cells in neuron-astrocyte cell culture (227, 228). While neurotrophic factors, such as BDNF, protect neurons from the toxic effects of viral proteins, gp120 may reduce expression of BDNF by neurons and cause apoptosis by growth factor deprivation (229, 230). The gp120 domain may also bind receptors for the neurotrophic factor VIP, killing neurons through blockade of VIP receptor signaling and damaging astrocytes by reducing expression of the multifunctional glial fibrillary acidic protein (231, 232).

The Nef C-terminal domain is exposed on the outer leaflet of the plasma membrane of some cells and this protein may be incorporated in virions or released from infected cells (233, 234). A non-myristoylated version of Nef is also produced that can be released upon lysis or apoptosis of an infected cell (235). Interaction of this protein with astrocyte signaling pathways may result in glutamate release and excitotoxicity to surrounding neurons (236). In cultured astrocytes, Nef increases the expression of

CXCL10, which can bind to CXCR3 on neurons and disrupt Ca^{2+} homeostasis (237, 238). CXCL10 may also increase the replication of HIV in monocyte-lineage cells and expression of this protein is elevated in the CNS of patients with HAND spectrum disorders (237, 239). Recombinant Nef added to media is toxic to human glial cells and may disrupt the K+ channels of neural cells in culture (240, 241).

The viral Tat protein in serum may cross the BBB and Tat produced within the CNS can be transported along neuronal pathways, allowing neurotoxic activity at sites far removed from infected cells (205). Tat binding can depolarize neurons, disrupting the voltage-gated channels to allow Ca^{2+} influx, as well as cytoplasmic release of intracellular Ca^{2+} (209, 211, 212, 242-244). Tat can also bind glutamate receptors on NMDA channels, increasing both Ca^{2+} influx and the effects of subsequent glutamate binding (212, 245). Tat-induced decreases in glutamate re-uptake by HIV-infected astrocytes may further increase signaling through glutamate receptors, enhancing neuronal death (211, 246). Tat may also interact with non-NMDA receptors to cause similar excitotoxic effects (247, 248). Through different mechanisms, Tat may also kill BMVECs and induce production of TNF-alpha, leading to further apoptosis of neurons (248-250). Tat can also promote microglial migration by inducing production of MCP-1 from infected microglia and causes production of MMP-1 and MMP-2 in astrocyte/neuron co-cultures (101, 251). Additionally, Tat may induce production of quinolinic acid when expressed in infected monocyte-lineage cells (252, 253). Tat and gp120 can both disrupt lipid metabolism in neurons, leading to ceramide accumulation and subsequent apoptosis (254).

The N-terminal region of the viral Vpr protein can form cation channels in the plasma membranes of neurons, causing depolarization and Ca^{2+} influx (255). Vpr may also signal through receptors on the neural cell surface to activate pro-apoptotic caspase cascades (256). The viral Matrix protein has similarities to host IFN-gamma and may interact with IFN-gamma signaling pathways to prime HIV-infected macrophages in the CNS for subsequent activation (257, 258). In vitro, the gp41 domain of Env induces the expression of inducible nitric oxide synthase (iNOS) in glial cells and release of IL-1 beta by microglia, triggering NO production by astrocytes (259, 260). Alone, gp41 may also induce production of MMP-2 from glia and neurons in culture, while whole HIV virions stimulate release of MMP-2 and MMP-9 (261, 262). While both Rev and Vpu have neurotoxic potential, neither has been found in the extracellular space in HIV-infected CNS tissue (204, 263, 264). In addition to the actions of the viral proteins themselves, antibodies to gp41, Nef and Matrix may cross-react with epitopes on astrocytes, leading to potential autoimmune responses (265-267).

Neurotoxic Factors Released by Host Cells

Uninfected cells in the CNS may also produce additional neurotoxic molecules in response to viral proteins or host cellular factors released by infected cells. Activated HIV-infected macrophages release a number of potentially neurotoxic mediators, including TNF-alpha, IL-1 beta, platelet-activating factor (PAF), quinolinic acid, NO and prostaglandins (216). The neurotoxic effects of these molecules have been studied extensively in tissue culture and elevated levels of these mediators have been detected in the CNS of HAD patients (268, 269). HIV-infected macrophages express increased levels of MIP-1alpha and MIP-1beta (270). Astrocytes and microglia in the brains of

HAND patients also express high levels of MIP-1alpha and MIP-1beta mRNA, directly correlating with the severity of dementia (270). Monocytes and lymphocytes recruited to the CNS by these chemokines may become additional targets for virus replication.

At high enough levels, TNF-alpha binding to TNF receptors on oligodendrocytes and neurons may trigger apoptosis of these cells (271-274). In conjunction with glutamate, which may be increased in the extracellular space by Tat and gp120, TNF-alpha activates AMPA glutamate receptor channels on neurons, disrupting Ca^{2+} homeostasis (275). In astrocytes, TNF-alpha alters Na+/H+ transport, causing neurotoxic effects similar to gp120, and can prevent glutamate re-uptake by these cells (276, 277). TNF-alpha can also synergize with Tat to increase oxidative stress and subsequent neuronal apoptosis (278). In the brain, ceramide may be produced in response to TNF-alpha, contributing to neuronal apoptosis under conditions of oxidative stress (279, 280). TNF-alpha can also stimulate astrocytes to produce potentially neurotoxic cytokines, such as IL6, IL8, MCP-1, RANTES, GM-CSF and M-CSF (281, 282). In addition, TNF-alpha may promote increased CCR5, CXCR4 and CCR3 expression, increasing the susceptibility of target cells to viral infection (282). However, TNF-alpha also promotes expression of Bcl-2 and other protective factors in neurons, reducing the impact of excitotoxic stimulation and disruption of Ca^{2+} homeostasis (283, 284).

IL1-beta can alter Na+/H+ transport in astrocytes, disrupting Ca^{2+} homeostasis in neurons, similar to the effects of TNF-alpha and gp120 (276). This cytokine can also lead to proliferation of astrocytes, potentially causing the astrocytosis and gliosis seen in the brains of HAD patients (285). IL1-beta, as well as TGF-beta, can induce iNOS production by microglia and astrocytes, an effect that is enhanced in the presence of

TNF-alpha or IFN-gamma (286-288). TNF-alpha and IL1-beta can also act synergistically to induce oligodendrocyte apoptosis (216). Like TNF-alpha, IL1-beta can stimulate astrocytes to release potentially neurotoxic cytokines, such as IL6, IL8, MCP-1, RANTES, GM-CSF and M-CSF, and can upregulate cellular expression of CXCR4, CCR5 and CCR3 (281, 282).

In the uninfected CNS, GM-CSF and M-CSF promote the activation and proliferation of microglia (289-291). Both GM-CSF and M-CSF stimulate HIV-infected microglia to produce beta-chemokines, which recruit peripheral monocytes to the CNS, further increasing the pool of virus target cells (290). While beta-chemokines generally inhibit HIV replication by competing for CCR5 and other co-receptors, at high concentrations these chemokines form aggregates that stimulate potential virus target cells and make them more susceptible to HIV infection (290, 292, 293). M-CSF can activate monocytes in circulation and recruit these cells to the CNS, further increasing accumulation of macrophage and activated target cells that support HIV replication (294). M-CSF may also increase expression of CD4 and CCR5, and inhibit LIP, in macrophage, making these cells more susceptible to productive infection (295-297). GM-CSF alone also increases HIV replication in cells of the CNS (291).

A number of other cytokines are also involved in HIV neuropathogenesis. IFN-gamma is produced at increased levels by activated macrophage in the HIV-infected CNS (298, 299). This cytokine activates astrocytes and promotes the release of TNF-alpha, IL1-beta and quinolinic acid from astrocytes and monocyte-lineage cells in the CNS (300-302). IL8 can impair long-term potentiation in neurons and may recruit and activate peripheral monocytes and T lymphocytes, increasing the pool of potential virus target

cells (303, 304). SDF-1 signals through the CXCR4 chemokine receptor to directly induce apoptosis of neurons (219). IL6 in the CNS may promote neuron survival and offer some protection from excitotoxic stimulation, but other data suggests this cytokine increases NMDA receptor signaling and disrupts Ca^{2+} homeostasis in neurons (305). MCP-1 can protect neurons from excitotoxic stimulation through the NMDA receptors, but may also recruit HIV-infected leukocytes to the CNS and promote expression of factors that increase BBB permeability (149, 306, 307). While IL4 reduces activation of monocyte-lineage cells in the CNS, and lowers TNF-alpha and NO production by these cells, production of this cytokine by macrophage is reduced in the HIV-infected CNS (269, 298, 308).

Quinolinic acid is a metabolite of the kynurenine pathway that may damage neurons by stimulating NMDA receptors and disrupting intracellular Ca^{2+} homeostasis (309-311). Quinolinic acid causes apoptosis of astrocytes, through lipid peroxidation and production of free radicals, and may induce these cells to produce MCP-1, RANTES and IL8 (282, 312). This molecule can also increase CXCR4, CCR5 and CCR3 expression, potentially making target cells more susceptible to HIV infection (282). Arachidonic acid is another neurotoxic mediator, released following NMDA receptor signaling, which can further increase NMDA signaling and disrupt Ca^{2+} homeostasis in a positive feedback loop (313). This may be exacerbated by arachidonic acid inhibiting glutamate re-uptake by astrocytes (314).

NO, generated by iNOS at increased levels following exposure of astrocytes and monocyte-lineage cells to gp120, is an ROS by-product of arginine metabolism that may act directly on neurons to induce apoptosis (315-319). While HIV-infected macrophage

produce increased levels of superoxide anion (SO), these cells also increase production of the SO dismutase enzyme (SOD) (318). However, SO reacts with NO faster than SOD can consume SO, forming new ROS which then interact with NMDA channels on neurons to disrupt Ca^{2+} homeostasis (257, 320). Peroxynitrite, one of the products formed by NO and SO, damages the structural support proteins of neurons, an effect that may be exacerbated by high levels of SOD (320, 321). Free radicals produced by cells during oxidative stress also modify proteins into protein carbonyls and generate highly reactive aldehydes (280). These molecules are detected at increased levels in the CNS of HAD patients and are capable of modifying proteins, as well as disrupting cellular replication, transcription and translation (280, 322, 323).

PAF is a potentially neurotoxic mediator produced during interactions between astrocytes and HIV-infected macrophages (324). This molecule disrupts Ca^{2+} homeostasis in neurons both by stimulating NMDA receptors and by inducing release of quinolinic acid, TNF-alpha and IL1-beta from monocyte-lineage cells (252, 324-326). Like many of the other potentially neurotoxic factors, the amine NTox also disrupts Ca^{2+} homeostasis in neurons by stimulating the NMDA receptors (220). HAD patients have increased levels of MMPs in the CSF and these enzymes may play a role in the disruptions of the brain extracellular matrix that are often seen in these individuals (327, 328). Besides disrupting the extracellular matrix, MMP2, specifically, can cleave SDF-1 to produce a polypeptide that is capable of killing neurons (329).

HIV and SIV Envelope V1 Region

The gp120 domain of the Env protein has five highly conserved regions, C1 – C5, and five highly variable loops, V1 – V5 (330). The binding site that recognizes CD4 on

the target cell surface spans the C3 and C4 regions, with some contribution from amino acid residues in other regions (330). Co-receptor binding is determined largely by the V3 variable loop, with the V1 and V2 variable loops also playing a vital role in viral tropism (330-337). Changes in the length of the V1 region affect co-receptor usage, as viruses with longer V1V2 regions are more likely to maintain R5-tropism over the course of infection (335, 338). Along with the other variable loops, the V1 region also determines the overall structural stability of gp120 and may affect the ability of host antibodies to bind V3 and other regions of the protein (334, 339, 340).

The V1 region is a highly immunogenic linear epitope, readily recognized by neutralizing antibodies, and may be the target of strain-specific antibodies in infected hosts (335, 339, 341-343). However, the V1 loop is also the region of gp120 that develops the greatest amount of variability over the course of infection (344-346). Due to pressure from the humoral immune response, the V1 loop undergoes increases in length and changes in glycosylation profile, resulting in viruses in the later stages of infection that are resistant to antibodies to the same virus population early in infection (335, 347, 348).

N-linked glycosylation (NLG) is the addition of a complex carbohydrate chain to an N amino acid residue in the sequence N-X-S or N-X-T, where X is any amino acid except P (349-352). A complex carbohydrate chain may also potentially be added to any structurally available S or T residue as an O-linked glycosylation (OLG) (353, 354). The V1 loop has been shown to have a number of potential sites for both NLGs and OLGs (348-351, 353). In HIV-2 and most SIV strains, the V1 region has a greater number of conserved potential OLGs than HIV-1 and related SIV strains (348, 353). In SIV

specifically, the number of OLGs in the V1 region increases over the course of infection, correlating with the development of gp120 resistance to neutralizing antibody (355). The gp120 CD4-binding site is flanked by the variable loop glycosylated regions, which may shield this highly conserved site from recognition and binding by host antibodies (330).

HIV and SIV Nef

The non-structural gene *nef* codes for a multifunctional accessory protein that is one of the first produced following establishment of infection (356-358). While there is less than 40% sequence homology overall between HIV-1 Nef proteins and those from HIV-2 and most SIV strains, most of the important functional and structural domains are highly conserved (359-361). Nef is modified by the host N-myristoyl transferase enzyme, adding myristoylic acid to the N-terminal MGxxxS domain and allowing Nef to associate with host cell plasma membranes (330, 360-363). Despite lacking catalytic activity, the conserved functional domains of Nef interact with host cellular factors to alter the function of infected cells, performing a multitude of functions important to viral replication and pathogenesis (81, 116, 359, 361-370). Nef is essential for maintenance of high viral loads and progression to AIDS, with defective *nef* genes correlating with long-term non-progression (361).

One important function of Nef is downregulating the expression of CD4 on infected cells, which aids the release of progeny virions by reducing the number of CD4 molecules that could trap new viral particles on the host cell surface (371, 372). Reduced CD4 expression may also prevent superinfection, which can result in premature cell death (372, 373). The MGxxxS, $EEEE_{62,}$ FPD_{121}, D/ExxxLL$_{165}$, EE_{154} and DD_{174} domains of the Nef protein interact with the cytoplasmic tail of CD4 and components of the host

endocytic machinery (361, 374-383). These molecules, including clathrin complex AP2 subunits, V1H subunits of the vacuolar ATPase and beta-COP coatamers, assemble with CD4 and Nef in clathrin-coated pits (330, 361, 364, 374, 378). CD4 is then internalized and targeted for lysosomal degradation at a much more rapid rate than in normal turnover (330, 361, 384). Nef may also traffic CD4 directly from the trans-Golgi network (TGN) to the endolysosomes, further reducing cell surface expression of this molecule (375, 376).

The Nef protein also interacts with the clathrin-coated pit machinery to downregulate CD28 from the surface of infected lymphocytes (361, 364, 385). The MGxxxS, D/ExxxLL$_{165}$ and other domains interact with the cytoplasmic tail of CD28 while other regions of Nef recruit the endocytosis machinery, as described (385, 386). Nef can also downregulate the expression of CD80 and CD86 on APCs by inducing actin-dependent endocytosis and trafficking of these molecules to the TGN (387, 388). Downregulation of these costimulatory molecules may reduce signaling through the T-cell receptor in activated, virus-infected lymphocytes, preventing activation-induced apoptosis (361, 364, 386, 388). Downmodulation of these molecules may also reduce the strength of interactions between lymphocytes and APCs, allowing infected T cells to traffic into the periphery more easily, increasing dissemination of the virus (361). Reduced levels of costimulatory molecules on infected APCs also prevents these cells from activating virus-specific naïve T cells, reducing antiviral immune responses (387).

The MGxxxS, PxxPxR, FPD$_{121}$, EE$_{154}$ and EEEE$_{62}$ domains of Nef can interact with the cytoplasmic tails of MHCI molecules in infected cells (389, 390). Nef recruits cellular proteins, including PI3K and PACS1, which cause endocytosis of MHCI from

the plasma membrane and accumulation of this molecule in the TGN (361, 364, 389, 391, 392). Specifically downregulating HLA-A and –B MHCI molecules protects infected cells from cytotoxic CD8+ T cells, but Nef does not affect HLA-C and –E, which guard cells from destruction by natural killer (NK) cells (361, 390, 393). In APCs, Nef can downregulate cell surface expression of MHCII and simultaneously upregulate expression of the MHCII invariant chain (Ii) (361, 364, 367, 394). This prevents infected APCs from presenting viral antigens to CD4+ T cells, reducing virus-specific immune responses (361, 364, 367, 394). The MGxxxS, PxxPxR, D/ExxxLL$_{165}$ and EEEE$_{62}$ domains of Nef interact with the cytoplasmic tail of MHCII and the mechanism of downregulation may be similar that for MHCI (361, 367, 394). The Ii upregulation function is genetically separable from MHCII internalization, involves the D/ExxxLL$_{165}$ motif and may overlap with downregulation of CD4 and CD28 (361, 386).

Nef can reduce cell surface expression of CCR5, CXCR4, CCR3, CCR2 and CCR1, which may allow evasion of virus-specific immune responses by making infected cells less responsive to chemokines (395). Downregulation of CCR5 and CXCR4 may also prevent superinfection (373, 386, 396, 397). The mechanism of chemokine receptor internalization involves the intracellular loops of the chemokine receptor, as well as the PxxPxR, EEEE$_{62}$ and PACS-interaction domains of Nef (373, 397).

Nef can interact with a number of signaling molecules, including Hck, Lyn, LAT, Lck, PAK1/2, PKC, PI3K, Vav, and Raf1, to co-opt the NFkB and MAPK pathways, closely replicating signaling through the T-cell receptor (TCR) (361, 398-407). This may also sensitize infected cells to exogenous TCR stimulation, allowing these cells to become activated more easily and enhancing virus replication (359, 361). A number of

these signaling molecules are Src family tyrosine kinases, which have SH3 domains that can interact with the PxxPxR domain of Nef (404, 405, 408). The MGxxxS, PxxPxR, FPD_{121} and RR_{105} domains of Nef may recruit PAK1/2 into a complex with PI3K and Vav, inducing signals that lead to cell proliferation, rearrangement of the cytoskeleton and protection from apoptosis (359, 361). Nef can also prevent apoptosis in infected cells by associating with cellular factors that block ASK1 and by repressing signaling by pro-apoptotic Bcl-2 family proteins (361).

In HIV-2 and most SIV strains, Nef interacts with the cytoplasmic tail of the TCR zeta chain to downregulate cell surface expression of CD3, a function absent in HIV-1 and some SIV strains (366, 409). Downregulation of CD3 may prevent continuous signaling through the TCR from leading to activation-induced apoptosis, while Nef interaction with TCR signaling pathways provides the cell with survival signals (366, 386, 409-411). Interaction between Nef and the TCR zeta chain may also increase expression of Fas L on the surface of infected cells, which can then trigger apoptosis in virus-specific CD8+ T cells (361, 400).

HIV and SIV Integrase

Integrase is a structural protein that coordinates insertion of the reverse transcribed, linear, double-stranded viral DNA into the host chromosome (330, 358). During this process, Int removes a dinucleotide from each strand of the viral DNA, yielding 5' strand overhangs (412-415). Int then cleaves target sites in the host chromosome and ligates the resulting free 5' ends to the free 3' ends of the double-stranded, linear viral DNA molecule; Int can also perform 'disintegration', reversing this process (412-415). All three of these functions require specific interaction of Int with the

LTR sequence of a double-stranded, linear viral DNA molecule and a number of cellular proteins may also be involved (416, 417).

Both the section of the genome coding for Int, and the protein itself, are highly conserved, with Int from HIV-1, HIV-2, SIV, ASV, FIV, and RSV and other retroviruses having a high degree of similarity (418-424). The most highly conserved region of Int is the core domain, which is indispensable for all enzymatic functions of the protein (418-427). The core domain functions as a dimer and may associate with divalent cations (428, 429). The core alone is capable of disintegration, but the other domains of Int are required for strand transfer and DNA processing (422, 425, 430). The N-terminal domain is also highly conserved, containing a zinc-finger motif that may be involved in Int multimerization and DNA binding (330, 415, 417, 425, 426, 431). The C-terminal domain, which non-specifically binds DNA and may be involved in Int dimerization, is the least conserved region of the protein (330, 415, 417, 421).

The SIV-Macaque Animal Model of HIV Neuropathogenesis

Macaques infected with SIV show CNS lesions similar to HIV patients, with multinucleated giant cells, gliosis, monocyte infiltration, microglial nodules and microglial activation (432-435). Besides accurately reflecting the course of neuropathogenic lentiviral disease in a primate host, the SIV-macaque model of HIV pathogenesis has a number of other benefits over study of HIV in humans. The SIV-macaque model allows study of early events in the acute stage of infection, while it is difficult to know precisely when human patients have been inoculated. It is also difficult to sample the brains of human patients early in infection, whereas SIV-infected macaques can be sacrificed to analyze the CNS in acute infection (64). The genetic composition of

the inoculating virus in human patients cannot be known ahead of time, and is difficult to determine after infection, while macaques can be infected with specific strains (64). Also, the route of virus infection can affect the complexity of the transmitted quasispecies, with intravenous (i.v.) inoculation yielding a more diverse virus population (436). In humans, the exact route of transmission may not be known in many cases. Finally, it is easier to take longitudinal fluid and tissue samples from macaques, as some tissues are difficult to sample in humans and patients may drop out of studies (64). Because of these factors, SIVsmm infection of macaques is considered an excellent model of lentiviral pathogenesis and neurological disease in a primate host.

The simplest method to study lentiviral neuropathogenesis is to infect macaques with a primary SIV strain and then analyze the results. However, most SIV strains do not consistently induce neuropathogenesis in enough animals for efficient study. Studies analyzing animals infected with SIV, both naturally and under experimental conditions, found 25 – 50% of animals develop neurological lesions and SIV neuropathogenesis (70, 123, 124, 437-439). While the reason for the limited development of SIV neuropathogenesis is unknown, there are likely host-specific factors, as some animals inoculated with the same virus, under the same conditions, develop neurological disease and others do not (170). Although the percentage of animals developing SIV neuropathology is similar to the percentage of HIV patients that develop HAD, this is not a reliable model for research. Most refinements to the SIV-macaque model have focused on increasing the percentage of experimental animals that develop neuropathology.

In one model, animals were infected with SIVmac239, which does not normally infect the CNS (440). The bone marrow from these animals was then mixed with

macaque brain homogenate and the cellular mixture inoculated directly into the brain of another macaque. Bone marrow cells from this macaque produced CNS virus replication and neuropathogenic infection when inoculated directly into the brains of subsequent macaques. The virus was then isolated and could induce neuropathogenic infection when inoculated directly into the brains of subsequent animals. However, when animals were inoculated via a peripheral route, the virus did not replicate in the periphery or invade the CNS. As HIV is usually transmitted via a mucosal route, and successfully invades the CNS, this model does not accurately reflect the natural transmission and seeding of a neuropathogenic lentivirus.

In another model, a macaque was inoculated with SIVmac251 and microglia from this animal were then injected i.v. into another macaque (122). While the original macaque showed no neuropathogenic effects, the macaque inoculated with microglia demonstrated neurological symptoms and developed the classic pathology of CNS infection. These results were repeated when microglia from the second animal were harvested and inoculated into other macaques. However, although model has proven valuable for investigations of lentiviral neuropathogenesis, transfer of microglia does not accurately represent natural transmission of HIV. In addition, the authors did not discuss systemic infection, viral loads or CD4+ T cell counts. It is also unknown how the injection of virus infected microglia establishes subsequent infection in the CNS.

Another study used a pathogenic SHIV that was passaged through rhesus macaques and harvested from the CSF (441). In pigtailed macaques infected with this virus, proviral DNA was found in multiple regions of the CNS. However, the characteristic lesions of lentiviral neuropathogenesis were not detected and CNS lesions

only arose in animals with secondary infections. Results were similar in rhesus macaques, with proviral DNA and actively replicating virus detected in the CNS, but lesions only from secondary infections. While capable of neuroinvasion, and establishing productive infection when administered through peripheral inoculation, this virus did not induce the primary neuropathology necessary to be a good model of HIV.

In another model, researchers depleted CD8+ T cells, and then infected macaques with a pathogenic SIV strain (202, 442). In this system, 80% of animals developed neuropathogenesis and CNS lesions were comparable to infected animals that had not been CD8+ T cell-depleted. Although this model increased the frequency of neurological infection, it does not represent natural HIV infection, where CD8+ T cell responses in the CNS would exert selective pressure on the virus.

Another group harvested a neurovirulent SIV strain that was able to induce neuropathology, but was not neuroinvasive and could not successfully enter the CNS (440). This strain was paired with an infectious, but not neurovirulent, primary SIV quasispecies and subsequently induced neuropathogenesis in 80% of co-infected animals (443). This study also demonstrated genetic compartmentalization, with the neuropathogenic virus infecting the CNS and the primary quasispecies establishing infection in the periphery. This model, containing a viral quasispecies with one genotype that successfully infects the CNS, is closer to a natural HIV infection. However, rather than a single neurovirulent genotype, we would expect a natural HIV quasispecies to contain many different strains with a range of neuropathogenic potential. While this system may induce neuropathogenesis with increased reliability, the virus inoculum does not fully represent the genetic variety expected in a natural HIV quasispecies.

SIVsmmFGb Virus Isolation and Characteristics

Our lab has been able to isolate a novel SIV strain, which was found to reliably induce neuropathogenic infection in 90 – 100% of infected pigtailed macaques (444). In the course of other studies, sooty mangabey FGb at the Yerkes National Primate Research Center was found to be infected with both SIV and STLV. At sacrifice, SIV-infected cells were detected in the lymph node of this animal, but no infected cells appeared in the CNS and FGb did not present with neurological symptoms. As part of a study analyzing dual SIV/STLV infection, blood from FGb was transfused into two pigtailed macaques, two rhesus macaques and two sooty mangabeys. While the sooty mangabeys showed no signs of disease, the pigtailed and rhesus macaques progressed to simian AIDS within 5 months and 1 year, respectively. At sacrifice, both pigtailed macaques and one rhesus macaque presented with SIV-infected multinucleated giant cells in the CNS and neurological symptoms characteristic of SIV neuropathogenesis. Based on the clinical severity of symptoms and CD4+ T cell counts at the time of sacrifice, ROn2 was the most highly infected rhesus macaque, while PGm was the most highly infected pigtailed macaque. To obtain stocks of this SIV strain, human PBMCs were cultured with cells obtained from the mesenteric lymph node of PGm or with CSF from ROn2. Supernatants from both cultures were found to be free of STLV, ensuring that only the SIV strain was carried forward, and were used as stocks for PGm- and ROn2-derived SIV viruses.

In vitro studies with the two virus stocks demonstrated that the ROn2-derived virus replicated to 2 x 10^6 cpm/mL by one wpi in pigtailed macaque PBMCs, while the PGm-derived virus replicated to 1.5 x 10^6 cpm/mL by 10 days post-infection (dpi). In

rhesus macaque PBMCs, the ROn2-derived virus also replicated to 2.0 x10^6 cpm/mL by one wpi, while the PGm-derived virus replicated to 1.0 x 10^6 cpm/mL by 7 dpi. By two wpi, the PGm-derived virus replicated to 3.9 x 10^5 cpm/mL in pigtailed macaque macrophages, while the ROn2-derived virus replicated to 2.3 x 10^5 cpm/mL. In rhesus macaque macrophages, the PGm-derived virus replicated to 1.3 x 10^4 cpm/mL by two wpi, while the ROn2-derived virus replicated to 1.7 x 10^5 cpm/mL.

Subsequently, 12 macaques were infected with the ROn2 and PGM virus stocks, with three rhesus macaques and three pigtailed macaques receiving each virus. All of the pigtailed macaques progressed to simian AIDS, with signs of SIV encephalitis and SIV-infected cells in the CNS. While all three pigtailed macaques infected with the PGm-derived virus died within five months post-infection (mpi), two animals infected with the ROn2-derived virus survived until 8 mpi. All of the rhesus macaques progressed to simian AIDS, but symptoms were less severe than in pigtailed macaques and only a single animal infected with ROn2-derived virus developed encephalitis. The mean survival time for infected rhesus macaques was 16.5 months and there was no correlation between survival time and whether the animals received ROn2- or PGm-derived virus. The number of CD4+ T cells declined rapidly in pigtailed macaques, with these cells virtually absent in some animals at sacrifice. In rhesus macaques, CD4+ T cell numbers declined gradually and all animals had > 250 cells/uL at sacrifice. All 12 animals had detectable levels of SIV RNA in the lymph nodes, with the highest levels of viral replication in the pigtailed macaque lymph nodes.

Clinical symptoms of SIV neuropathogenesis, including tremors, ataxia, head-tilt and behavioral changes, developed in two pigtailed macaques infected with PGm-derived

virus, but only one animal infected with the ROn2-derived virus; development of neurological symptoms correlated inversely with survival time. None of the rhesus macaques, including the animal with SIV encephalitis, developed clinical symptoms characteristic of SIV-associated neuropathogenesis. Infected multinucleated giant cells, perivascular macrophages and microglia were distributed throughout the CNS, in both the white and grey matter, as well as in the brain parenchyma, meninges and associated with the BBB around the vasculature. Given these results, the SIV virus stocks produced by co-culture of human PBMCs with cells from the PGm mesenteric lymph node were reclassified as SIVsmmFGb and used for all subsequent experiments.

In subsequent infections of pigtailed macaques with SIVsmmFGb (3), the median survival time for infected animals was five mpi, with a maximum survival time of 40 mpi. Animals with a higher percentage of CD4+ T cells, lower percentage of CD8+ T cells and higher CD4:CD8 ratios prior to infection progressed more rapidly, but CD4:CD8 ratios and CD4+ T cell counts after infection did not correlate with the rate of progression. Infected animals presented with decreased CD4+ T cell percentage and absolute numbers of CD4+ and CD8+ T cells, but increased CD8+ T cell percentage, over time. Increased plasma viral loads at two mpi correlated inversely with survival time and rapid progressors had a median plasma viral load of 8.11 $\log_{10}$ RNA copies/mL at necropsy, compared to 5.68 $\log_{10}$ RNA copies/mL in slow progressors.

All rapidly progressing animals had high numbers of SIV neuropathogenic lesions in the CNS and infected cells were detected in every sample taken from every region of the brain. Multinucleated giant cells, macrophage accumulation and other lesions typical of SIV neuropathogenesis were distributed throughout the gray and white matter of the

CNS and appeared in the midfrontal cortex, cerebellum, hippocampus, choroid plexus and caudate nucleus. Only 60% of slow progressors had infected cells and lesions in the CNS, and these lesions were generally few in number. The severity of lesions was highest in rapid progressors, intermediate in slow progressors with SIV encephalitis and lowest in slow progressors without signs of SIV encephalitis. SIVsmmFGb replicated only in monocyte-lineage cells in the CNS, with the number of macrophages correlating directly with the number of SIV-infected cells and rate of disease progression. Virus burden was moderate to high in the brain tissues, particularly the midfrontal cortex and hippocampus, of rapid progressors but was low in the CNS of slow progressors. This shows some similarity to human patients, where viral RNA levels in the CNS may correlate with the severity of infection (445).

In another cohort of pigtailed macaques infected with SIVsmmFGb, all animals progressed to simian AIDS and most presented with neurological symptoms characteristic of SIV neuropathogenesis (173). During the acute phase of infection, productive replication was noted in the periphery, with 10 – 1000 cells per million PBMCs infected by two wpi. From one mpi until sacrifice, animals had 10 – 100 infected cells per million PBMCs, indicating productive infection of lymphocytes throughout infection. Most animals had rapid declines in absolute CD4+ T cell numbers and CD4/CD8 ratios in the first 1 – 2 mpi, after which these numbers remained stable. After two wpi, the mean CSF viral load was 2.5×10^4 equivalents per mL; roughly 230 times lower than the mean plasma viral load of 6×10^6 RNA equivalents per mL. Although the mean CSF viral load remained stable, plasma viral loads declined to between $10^3 – 4 \times 10^6$ equivalents per mL.

Proviral DNA was detected at high levels in the lymph nodes, GALT and brain in all animals sacrificed at two to four wpi, although levels were 100 times lower in the CNS. In animals without neurological disease, proviral DNA levels in the CNS were similar to those in the lymphoid tissues. While some animals with neuropathology had higher proviral DNA levels in the CNS, others had similar levels of proviral DNA in the brain and lymph nodes. Integrated proviral DNA appeared in the frontal lobe, parietal lobe, motor cortex, temporal lobe, thalamus, basal ganglia, cerebellum, brainstem, cervical cord, lumbar cord and thoracic cord regions of the CNS at these early time points. Proviral DNA was detected in many of these regions of the CNS, regardless of whether the animal presented with neurological symptoms.

At two to four wpi, viral RNA appeared at high levels in the lymphoid tissues and at 100 times lower levels in some regions of the brain, indicating that the virus is actively replicating in both the CNS and periphery, but that levels of replication are far lower in the CNS. Neuropathology correlated directly with viral replication in the CNS, as viral RNA could be detected at high levels in the majority of brain regions in animals with neurological symptoms. Increases in proviral DNA, viral RNA and viral protein expression in the CNS also correlated directly with the development of neurological disease.

During these studies, attempts were made to produce an infectious, biologically active, full-length molecular clone of SIVsmmFGb from the PGm-derived virus stocks (444). One successful clone, PGm5.3, was produced and tested for replicative potential in similar analyses as those used to study the original PGm-derived virus. PGm5.3 only replicated to 10^6 cpm/mL in pigtailed macaque PBMCs by 10 dpi and to 5.0 x10^5

cpm/mL by two wpi in rhesus macaque PBMCs, with significantly delayed kinetics compared to the PGm-derived virus stock. In pigtailed macaque macrophages, PGm5.3 only replicated to 2.7 x 10^5 cpm/mL and was unable to replicate at all in primary macrophages derived from rhesus macaques. Following inoculation into pigtailed macaques, PGm5.3 could be isolated from the CNS at early time points but had low pathogenicity and did not induce neuropathology in long-term infections.

Subsequent analysis of SIVsmmFGb determined that the virus was largely R5-tropic, but also demonstrated some limited X4-tropism and usage of minor co-receptors. This suggested that SIVsmmFGb is a quasispecies, composed of multiple genotypes with different co-receptor usage, rather than a single genetic isolate. PGm5.3 may be derived from a genotype that was inefficient at viral replication, target cell entry or other processes, which may explain the reduced pathogenesis of this molecular clone. Given the quasispecies nature of SIVsmmFGb, it may not be possible to produce a molecular clone that recapitulates the full pathogenic effects of the original swarm. Indeed, the pathogenic capability of SIVsmmFGb may require multiple genotypes exerting different effects on host cells. Even producing a molecular clone of the most common genotype in the population may not reproduce the full neuropathogenic effects of SIVsmmFGb.

Lentiviral Compartmentalization

A viral quasispecies is a group of genetically distinct viral genotypes that are closely related, often arising from a common progenitor strain (446, 447). In HIV and SIV, the viral reverse transcriptase lacks 3' – 5' exonuclease proofreading activity, introducing mutations at a rate of 0.3 nucleotide changes per genome per replication (448, 449). The result is a genetically diverse population of viral genotypes arising

within a single host, with variants that differ in co-receptor usage, pathogenesis and other factors important to disease (450, 451).

One potential result of infection by a viral quasispecies is compartmentalization, the development of distinct quasispecies within different tissues in a single host (452-455). This can be significant when levels of drug penetrance into one compartment, such as the CNS, are not sufficient to limit virus replication, allowing the development of drug-resistant mutant strains (456). If genotypes can traffic between compartments, these mutant strains may then establish a drug-resistant population in tissues with greater exposure to the antiretroviral compound (456). Compartmentalization may also cause divergence in virus function between compartments. For instance, HIV viruses isolated from the CNS tend to be less capable of infecting T cell lines, less cytopathic and less capable of regulating CD4 expression on infected cells, but are also less sensitive to neutralizing antibody and replicate more efficiently in macrophages (457).

Co-receptor usage, target cell tropism and replicative potential in different cell types or tissues are virus-specific factors involved in the development of genetic compartmentalization (456, 458). Compartmentalization may also result from factors intrinsic to a particular tissue, such as innate and adaptive immune responses, heterogeneity in target cell function and the availability of viral co-receptors or target cells (456, 458). For instance, compartmentalization of viral genes in the CNS, relative to the blood and peripheral tissues, may result from differences in selective pressures and viral replication kinetics between the brain and periphery (459). The brain is also unique in that it is an immunologically privileged site, with the BBB limiting traffic of genotypes between the CNS and the periphery, further promoting compartmentalization (459).

For HIV, compartmentalization of the *env* gene occurs between sequences derived from the brain and those from the lymph nodes (460). SIV *env* compartmentalization has also been demonstrated between the cerebrum, cerebellum, spinal cord and brain ventricle, as well as between each of these CNS regions and the lymph nodes, lung and colon (461). The C2 and C3 regions of HIV *env* compartmentalize separately between the CNS and PBMCs, as well as between PBMCs and the pleural space of the lung (462, 463). The region of *env* spanning the V1 – V5 loops also formed separate compartments within the CNS, segregating between the basal ganglia, frontal lobe, medial temporal lobe and non-medial temporal lobe (458). Compartmentalization of the HIV *env* V4 region also occurred between sequences harvested from the CNS and the PBMCs (464).

A number of studies have focused on compartmentalization of the *env* V3 loop specifically, as this region determines cell tropism in HIV-1 (216). The *env* V3 loop compartmentalizes between bronchoalveolar lavage cells and PBMCs, as well as between the CNS and spleen (465, 466). Focusing on the CNS, the *env* V3 loop formed separate compartments between the frontal, parietal, occipital lobes and the PBMCs, with the frontal lobes segregating the most from the other tissues (467). In HIV encephalitis patients, the *env* V3 loop formed separate compartments between the spleen and precentral or postcentral gyrus of the brain (468). HIV *env* V3 region sequences from the CNS also compartmentalized from blood-derived sequences in the majority of HAD patients (459). In addition, the V3 loops of brain-derived *env* sequences differed between HAD patients and HIV-infected patients without dementia (469, 470). Segregation of HIV *env* V3 region sequences between the blood and CSF increased over the course of infection and was more pronounced after progression to AIDS (471).

As with the *env* V3 loop, gp41 also segregates between the blood and CSF, with compartmentalization increasing over the course of infection (472). HIV LTR sequences form separate compartments between the brain dorsal root ganglion and the lung, spleen and lymph node, as well as between the grey and white matter within the CNS (473, 474). The HIV *nef* gene compartmentalized between PBMCs and a number of peripheral tissues, including the esophagus, stomach, duodenum and colorectum (475). While the HIV RT gene did not compartmentalize to the same degree as *nef*, there was notable segregation of sequences between the stomach and esophagus (475). Finally, HIV *pol* sequences compartmentalized in the brain, relative to the spleen and lymph nodes (476).

Given that SIVsmmFGb is a quasispecies population, we might expect that some of the genes of this virus could form separate compartments between different tissues in infected pigtailed macaques. Of particular interest is whether SIVsmmFGb genes form separate compartments between the CNS and the peripheral lymph nodes or between different regions within the CNS. In this study, we characterize the genetic diversity of Env V1 region, Nef and Int amino acid sequences within the SIVsmmFGb quasispecies and determine how this diversity changes over the course of infection in pigtailed macaques. We also investigate whether the *env*, *nef* and *int* genes form separate compartments between the CNS tissues and lymph nodes, as well as between different regions within the CNS, and how this compartmentalization develops over time. Finally, we begin to analyze SIVsmmFGb Env V1 region, Nef and Int amino acid sequences for mutations that may be involved in the neuropathogenic phenotype of this virus.

Materials and Methods

Adapted from Reeve, et al. ARHR. 2009. 25(6):583-601, Reeve, et al. In Press and Reeve, et al. Unpublished Data.

SIVsmmFGb Stock Virus Isolation and PCR Amplification

SIVsmmFGb stock virus, produced as described (444), was used for animal inoculations. Viral RNA was isolated using a QIAmp Viral RNA Minikit (Qiagen) according to the manufacturer's protocol and serial diluted 10-, 100- and 1000-fold. Along with undiluted RNA, these dilutions were used for RT-PCR with a SuperScript III RNase H Reverse Transcriptase kit (Invitrogen), with random hexamer primers for the initial RT step. DNA obtained from these reactions was serial diluted 10-, 100- and 1000-fold, for 16 total DNA templates (RNA diluted 1:10/DNA diluted 1:10, RNA diluted 1:100/DNA diluted 1:10, etc). Each template was used for nested PCR of *env*, *nef* and *int* genes, using the primers described in Table 1.

Pigtailed Macaque Inoculation and SIVsmmFGb-Infected Tissue Harvesting

Twelve juvenile pigtailed macaques, from the Yerkes National Primate Research Center colony, were inoculated i.v. with 100 $TCID_{50}$ of the SIVsmmFGb stock virus. Animals were inoculated and necropsied individually, using a triaging protocol that was designed to reduce variability and ensure tissue collection from matching anatomic sites in each test subject. All animals were euthanized by i.v. barbiturate overdose. Two of the macaques were euthanized at five dpi, and four animals 7 dpi, for the one wpi cohort. The remaining 6 animals were sacrificed at two mpi. Blood and CSF were harvested prior to sacrifice, to perform viral load analysis and other studies. All animals were extensively perfused with saline prior to tissue collection to prevent contamination of CNS samples by the blood. Tissue specimens that were collected from each animal for sequence analysis included the axillary lymph node, mesenteric lymph node, basal ganglia, midfrontal cortex, hippocampus and cerebellum; these were quick-frozen on dry

ice and stored at -80^{o}C. These tissue samples, and those from other anatomic sites, were also harvested at one wpi for in situ hybridization (ISH) and determination of viral loads. The tissue samples for ISH were submitted to the O'Neil group and the ISH procedure was performed as described (444). At two mpi, tissue samples were harvested for determination of viral loads, but ISH was not performed at this time point.

SIVsmmFGb Proviral DNA Extraction and Preparation from Infected Pigtailed Macaque Tissues

Using sterile scalpels, and working on ice to avoid tissue damage, small tissue segments were excised and placed in cell lysis buffer containing 0.1 M NaCl. 10 mM Tris pH 8.0, 25 mM EDTA, 0.5% SDS and ddH_2O, then homogenized with a 1.0 mL syringe plunger. Homogenates were treated with 50 ug proteinase K and incubated overnight at 55^{o}C, with periodic vortexing. Samples were brought to room temperature and DNA was harvested via a sequential extraction with Tris-saturated phenol, phenol: chloroform: isoamyl alcohol (25:24:1), chloroform and 100% ethanol. DNA was pelleted by 15,000-rpm centrifugation for 30 minutes at 4^{o}C, washed thrice with 70% ethanol, air-dried and resuspended in ddH_2O. DNA concentration was quantified using a UV spectrophotometer and samples were frozen at -20^{o}C.

PCR Amplification of SIVsmmFGb Genes from Tissue-Derived Proviral DNA

The *nef*, *env* and *int* genes were amplified from proviral DNA by nested PCR, using an Expand High Fidelity PCR System kit (Roche), according to the manufacturer's protocol. After some difficulty PCR amplifying viral genes from the CNS tissues of macaques PQo1 and PQq1, the primers in Table 1 were analyzed and found to contain

hairpins and dimers. Thus, new primers were designed for *env*, *nef* and *int* as described in Table 2.

SIVsmmFGb Gene Cloning Strategy

The PCR products were purified on 0.9% (*env*) or 1.2% (*nef*, *int*) agarose gels and were extracted with a QIAquick Gel Extraction Kit (Qiagen), according to the manufacturer's protocol. As restriction sites were not added to the primers, the purified PCR products were ligated using a pGEM-T Vector System I (Promega), following the manufacturers' protocol. After incubating for 24 hours at 4^{o}C, the ligations were transformed into Invitrogen ElectroMAX DH10B *E. coli* (*recA1*, *endA1*) cells, according to the manufacturer's protocol. Single bacterial colonies were used for preparation of plasmid DNA containing the inserts, according to standard techniques. Approximately 2 ug of each p-GEM-T vector/gene insert-positive sample was sent to MWG Biotech for sequencing (MWG Sequencing, Huntsville, Alabama). Sequencing was performed using pGEM-T vector-specific sequencing primers, each yielding approximately 800 to 900 bp of usable sequence: p-GEM-T forward primer 026 5'GTAAAACGACGGCCAGT3'-2961; p-GEM-T reverse primer 025 5'TAACAATTTCACACAGG3'-2827.

DNA Sequence Analysis

Sequences were analyzed with EditSeq in the DNAStar v7.1.0 software package (Laser-Gene) and the following sequences discarded: Poor reads; junk sequence; incomplete *nef* and *int* sequences; *nef* and *int* sequences with deletions or insertions; and *env* sequences that did not span the complete V1 region. The resulting valid sequences were copied into MegAlign in DNAStar v7.10 (Laser-Gene) for translation into Env, Nef and Int amino acid sequences and all clones with premature stop codons were discarded;

at least 20 valid clones were recovered for each gene, from each tissue, from each experimental animal. At least 20 valid clones were also collected of each gene from each of 16 stock virus dilution templates.

SIVsmmFGb Stock Virus Amino Acid Sequence Grouping

The valid amino acid sequences for Env, Nef and Int from the SIVsmmFGb stock virus dilutions were pooled in MegAlign and were aligned by the Clustal W method. A distance-based, neighbor-joining phylogenetic tree was produced for all stock virus sequences of each gene, in PAUP* 4.0b10 (145). Based on visual inspection of the phylogenetic clade structure of the resulting tree, the stock virus sequences for each gene were divided into subgroups. Sequences in each subgroup were aligned in MegAlign, via Clustal W method, and a consensus sequence was generated for each subgroup of each gene. The subgroup consensuses were then aligned in MegAlign, via Clustal W method, and a new distance-based, neighbor-joining phylogenetic tree was produced in PAUP* 4.0b10. This tree was subjected to a bootstrapping analysis, using heuristic search methods, and 1000 bootstrap replicates were produced. Subgroup consensuses for each gene were then grouped based on bootstrap support: Clades of subgroup consensuses with a bootstrap support of greater than 50% were counted as a unique group, while subgroup consensuses that did not fall into a clade with greater than 50% bootstrap support were pooled into a separate group.

Tissue-Isolated SIVsmmFGb Viral Amino Acid Sequence Alignment and Grouping

Valid amino acid sequences for Env, Nef and Int, from each tissue in each experimental animal, were aligned in MegAlign, via Clustal W method, with the stock virus subgroup consensuses for that gene. These alignments were exported to PAUP*

4.0b10 and neighbor-joining phylogenetic trees were generated, using both distance- and parsimony-based analysis, with no obvious differences noted between the two methods (data not shown). Visual inspection of the cladistic, phylogenetic distribution of tissue-isolated sequences, in relation to the stock virus subgroup consensuses, was used to sort tissue-isolated sequences into the groups defined by the stock virus analysis. The percentage of sequences in each group was determined for each tissue in each animal and then averaged for each time point to determine the mean prevalence of each sequence group in each tissue, at both one wpi and two mpi. The mean prevalence of each sequence group in each tissue at each time point was then compared to the prevalence of that group in the SIVsmmFGb stock virus, using the Mann-Whitney Rank-Sum test in SigmaStat Demo 2.03 software (Systat). The prevalence of each sequence group in all brain tissues and all lymph node tissues were collected into separate pools at each time point and then averaged to determine the mean prevalence of each group in the brain and each group in the lymph nodes at both one wpi and two mpi. The mean lymph node prevalence and the mean brain prevalence for each group were compared at each time point, and to the group prevalence in the SIVsmmFGb stock virus, using the Mann-Whitney Rank-Sum test. The Mann-Whitney Rank-Sum test was chosen due to the non-normal distribution of group prevalence between animals and the unequal variance between the sequence groups from the stock virus and those from the tissues. Those Mann-Whitney comparisons with a p-value less than, or equal to, 0.05 were considered evidence of statistically significant differences between tissues.

Phylogenetic and Phenetic Compartmentalization Analyses of SIVsmmFGb Amino Acid and Nucleotide Sequences

The phylogenetic compartmentalization of Env V1 region, Nef and Int amino acid sequences between each of the six tissues, at both one wpi and two mpi, was compared using a modified Slatkin-Maddison test, as described elsewhere (452, 461). The global mean bootstrap s and global mean random s values for each two-tissue comparison, where s is the least number of evolutionary steps for "tissue of origin", obtained from this procedure were used to calculate the ratio of bootstrap s to random s values; the standard error of this ratio was then determined using the formulas described elsewhere (477). As described (452, 461), if the ratio of global mean bootstrap s to global mean random s is two standard errors less than 1, significant compartmentalization between tissues is present (461, 463). The above procedures were repeated for every possible two-tissue comparison for each of the three viral genes at both time points. To analyze phylogenetic compartmentalization of sequences within a tissue between time points, all sequences for each gene harvested from a tissue at two mpi were aligned via Clustal W, in MegAlign, with all sequences harvested from the same tissue at one wpi. A modified Slatkin-Maddison test was then performed on each of these alignments as described (452, 461). Compartmentalization of sequences within a tissue over time was considered significant if the ratio of the mean bootstrap s value, where s is the least number of evolutionary steps for a "time point" character, to the mean random s value was two standard errors less than 1 (461, 463).

The phenetic compartmentalization of *env* V1 region, *nef* and *int* nucleotide sequences between each of the six tissues, at both one wpi and two mpi, was compared

using Mantel's Test, as described (452, 461, 463). Using XLSTAT-Pro (Addinsoft), the Pearson's correlation coefficient, r, was calculated and an estimated p-value was generated from 1000 permutations. The null hypothesis, of no compartmentalization between tissues, was rejected for all p-values less than, or equal to, 0.05. Due to the limitations of the software, and the number of nucleotide sequences involved, we were unable to perform a Mantel's test to analyze phenetic compartmentalization of sequences within each tissue between one wpi and two mpi.

Synonymous and Nonsynonymous Substitution Analyses of SIVsmmFGb Nucleotide Sequences

Analysis of selective pressure in each tissue compartment was performed by analysis of synonymous (d_S) and nonsynonymous (d_N) substitution rates, as well as the d_S / d_N ratio. All DNA sequences from the SIVsmmFGb stock virus for *env* V1 region, *nef* and *int* were aligned via Clustal W, in MegAlign, and consensus sequences were produced for each gene. These consensus sequences were then aligned via Clustal W, in MegAlign, with SIVsmmFGb viral gene sequences obtained from the experimental tissues at both one wpi and two mpi; the resulting alignments were then exported to MEGA4. For each gene in each tissue in each animal, the pairwise distance between each sequence and the stock virus consensus for that gene was used to calculate the d_S and d_N values, using the Nei-Gojobori p-distance method in MEGA4. For each gene, results from all experimental animals at one wpi or two mpi were pooled to generate mean d_S and mean d_N values for each tissue at each time point. The Mann-Whitney Rank-Sum test was used to compare mean d_S and mean d_N values for each gene within a tissue at each time point. Mean d_S and mean d_N values were used to generate the d_S / d_N

ratio for each gene, in each tissue, at each time point. The Mann-Whitney Rank-Sum test was also used to compare the d_S / d_N ratios between tissues at each time point for each gene. Those Mann-Whitney comparisons with a p-value less than, or equal to, 0.05 were considered statistically significant.

Determination of the Average Pairwise Distances of SIVsmmFGb Nucleotide Sequences from Pigtailed Macaque Tissues

For *env* V1 region, *nef* and *int*, all nucleotide sequences from a pair of tissues in each animal were aligned via Clustal W in MegAlign. These alignments were exported to MEGA4 and the Kimura two-parameter method was used to calculate the pairwise distance between each sequence in one tissue and each sequence in the other tissue. For each of these two-tissue comparisons, the pairwise distances were pooled across all animals at each time point and the average calculated, providing the mean pairwise distance between sequences from the two tissues at that time point. This procedure was repeated for every possible two-tissue comparison at both one wpi and two mpi. The Mann-Whitney Rank Sum test was used to compare the average pairwise distance between sequences in each two-tissue comparison at one wpi to the average pairwise distance between sequences in the same two-tissue comparison at two mpi. The Mann-Whitney test was also used to compare the average pairwise distance between sequences in each two-tissue comparison at each time point to every other two-tissue comparison at both time points. Any p-values less than, or equal to, 0.05 were considered to demonstrate a statistically significant difference between average pairwise distances.

In addition, for each gene in each animal, all of the nucleotide sequences from each tissue were aligned via Clustal W in MegAlign and then exported to MEGA4. The

Kimura two-parameter method was used to determine the pairwise distance between sequences within each tissue. For each tissue, these pairwise distances were pooled across all animals at each time point to calculate the average pairwise distance between sequences within a particular tissue at each time point. This procedure was repeated for all six of the experimental tissues at both one wpi and two mpi. For statistical analysis, the Mann-Whitney Rank Sum test was used to compare the average pairwise distance between sequences within each tissue at one wpi to the average pairwise distance between sequences within the same tissue at two mpi. The Mann-Whitney test was also used to compare the average pairwise distance between sequences within each tissue at each time point to every other tissue at both one wpi and two mpi. Any p-values less than, or equal to, 0.05 were considered to demonstrate a statistically significant difference between the average pairwise distances being compared.

Calculation of the Prevalence of Amino Acid Mutations in Functional Domains of SIVsmmFGb Env V1 Region, Nef and Int

A literature search was performed to determine known functional domains for Env V1 region, Nef and Int in HIV and other SIV strains. The positions of these motifs and amino acid residues were then located in the SIVsmmFGb stock virus amino acid consensus sequences for Env V1 region, Nef and Int by visual inspection. For each gene, the amino acid sequences obtained from the SIVsmmFGb stock virus were aligned by Clustal W, in MegAlign, with the stock virus consensus amino acid sequence for that gene. The percentage of stock virus sequences with one or more amino acid mutations in each functional domain, relative to the stock virus consensus sequence, was then determined. If a sequence had more than one mutation in a particular functional domain,

it was counted as one sequence with one or more mutations, rather than counting each mutation separately. At each time point, all sequences for each gene from the lymph nodes were grouped into one pool and all sequences for each gene from the CNS were grouped into another pool. The percentage of sequences with one or more mutations in each functional domain was then determined for each pool at one wpi and two mpi. The Mann-Whitney Rank Sum test was used to statistically compare the percentage of sequences with mutations in each functional domain in each pool with the percentage in every other sequence pool. Any p-values less than, or equal to, 0.05 were considered indicative of statistically significant differences in the prevalence of mutation in a particular domain.

Determination of the Frequency of Amino Acid Changes at Each Position of SIVsmmFGb Env V1 Region, Nef and Int

For Env V1 region, Nef and Int, all amino acid sequences obtained from the SIVsmmFGb stock virus were aligned in MegAlign by the Clustal W method. From these alignments, an amino acid consensus sequence was determined for each gene in the SIVsmmFGb stock virus. The presence of insertions in some sequences in the stock virus created gaps in the Env V1 region stock virus consensus sequence. These gaps were retained for subsequent analysis and gap positions were accounted for in the numbering of the Env V1 region amino acid positions. The stock virus amino acid consensus sequences for Nef and Int were contiguous, with no insertions or deletions. For each gene, the sequences in the stock virus were aligned via Clustal W, in MegAlign, with the consensus sequence to determine the percentage of sequences in the stock virus with amino acid mutations at each position, relative to the consensus. For Nef and Int, as

deletions and insertions were screened out in the clone selection process, any amino acid change was counted as a mutation. For the Env V1 region, mutations included amino acid changes, as well as novel deletions and the insertion of amino acids in gap positions. For each gene, at both one wpi and two mpi, all sequences from the lymph nodes were pooled into one group and all sequences from the CNS regions were pooled into another group. The lymph node and CNS pools for each gene at each time point were aligned with the stock virus consensus sequence for that gene by the Clustal W method in MegAlign. The percentage of sequences in each pool with mutations at each position was determined for all three genes at both one wpi and two mpi. For residues that fell within certain functional domains, the Mann-Whitney Rank Sum test was used to statistically compare the percentage of sequences with mutations in each of these positions in each pool with the percentage in every other sequence pool. Any p-values less than, or equal to, 0.05 were considered indicative of statistically significant differences in the frequency of mutations at a given site.

Sequence Data

The nucleotide sequences referenced in this study are available in the GenBank database under the accession numbers FJ396520 – FJ396665, FJ397088 – FJ398271 and FJ399865 – FJ4022403.

Chapter 1

Reduced Genetic Diversity in Lymphoid and Central Nervous System Tissues and Selection-Induced Tissue-Specific Compartmentalization of Neuropathogenic SIVsmmFGb during Acute Infection

Adapted from Reeve, et al. ARHR. 2009. 25(6):583-601

Results

SIVsmmFGb Stock Virus Grouping

The consensus sequences for Env V1 region amino acid clades were divided into four groups (Fig. 1A): Group 1 consisted of four stock virus Env V1 consensus sequences, representing 50 stock virus sequences (Fig. 2A), with 88% bootstrap support. Group 3 encompassed two stock virus Env V1 consensus sequences, representing 54 stock virus sequences (Fig. 2A), with 58% bootstrap support. Group 4 consisted of 10 stock virus Env V1 consensus sequences, representing 276 stock virus sequences (Fig. 2A), as part of a superclade with 64% bootstrap support. Group 2 consisted of the remaining three consensuses, representing 25 stock virus sequences (Fig. 2A), falling outside any bootstrap-supported clade. For Nef (Fig. 1B), the stock virus consensus sequences were divided into two groups: Group 1 consisted of 20 stock virus Nef consensus sequences, representing 354 stock virus sequences (Fig. 2B), with 64% bootstrap support. The remaining two stock virus Nef consensus sequences, representing 38 stock virus sequences and falling outside the bootstrap-supported clade (Fig. 2B), were collected into group 2. For Int (Fig. 1C), the stock virus consensus sequences were separated into three groups: Group 2 contained four stock virus Int consensus sequences, representing 78 stock virus sequences (Fig. 2C), with 58% bootstrap support. The group 3 clade had 64% bootstrap support and was composed of two stock virus Int consensus sequences (Fig. 2C), representing 31 stock virus sequences. The remaining stock virus Int consensus sequences, falling outside the bootstrap-supported clades and representing 279 stock virus sequences (Fig. 2C), were organized into group 1.

ISH of SIVsmmFGb in Brain and Peripheral Tissues of Infected Pigtailed Macaques

Of the animals sacrificed at five dpi (Table 3), PQq1 had high numbers of SIV-infected cells in both the inguinal lymph node and spleen, as well as in all gastrointestinal tissues. Comparable numbers of productively infected cells were detected in the inguinal lymph node of animal PQo1, but few infected cells were noted in the spleen and gastrointestinal tissues. Neither animal sacrificed at five dpi had SIV RNA-positive cells in the bone marrow or brain tissues. PCR amplification of genes from proviral DNA were successful in the lymph node and CNS tissues of animal PQq1 (data not shown) but we were unable to PCR amplify the following genes from animal PQo1: *env* from the basal ganglia, midfrontal cortex and cerebellum; *nef* from the basal ganglia and midfrontal cortex; and *int* from the basal ganglia and cerebellum. The remaining four animals were sacrificed at 7 dpi and all demonstrated high numbers of SIV-positive cells in the inguinal lymph node and spleen, as well as some degree of productive SIV infection in the bone marrow. Three of these animals had high numbers of infected cells in the gastrointestinal tract, while PKo1 showed moderate levels of virus in these tissues. The presence of viral RNA in the CNS varied between animals, with productive infection in 4/5 and 3/3 of the brain tissues from animals PGt1 and PFp1, respectively. SIV RNA-positive cells could not be detected in the CNS samples from PKo1 and were only present at low levels in medulla from animal PHs1. The low level of SIV RNA in the CNS of most animals undoubtedly represents genotypes introduced by early, initial seeding. We successfully PCR amplified *env*, *nef* and *int* genes from all lymph node and CNS tissue samples taken from PFp1, PGt1, PHs1 and PKo1 (data not shown). Because of the relatively low levels of SIVsmmFGb viral RNA present in some of the CNS samples

from these animals, we used proviral DNA as a substrate for PCR amplification to maintain consistency through all tissues.

Diversity of Env V1 Region, Nef and Int Amino Acid Sequences Isolated from Pigtailed Macaque Brain and Lymph Node Tissues Compared to Stock Virus

Amino acid sequences for Env V1 region, Nef and Integrase were harvested from the tissues of SIVsmmFGb-infected pigtailed macaques, were screened and were grouped as described in the Materials and Methods section. For Env V1 (Fig. 3), the prevalence of group 1 decreased significantly in the axillary lymph node, basal ganglia, hippocampus and midfrontal cortex. Prevalence of this group did not change significantly in the cerebellum and mesenteric lymph node. The prevalence of the other three Env V1 groups in any of the tissues was not found to differ significantly from prevalence of those groups in the SIVsmmFGb stock virus. The prevalence of Nef group 1 increased significantly in the basal ganglia, while group 2 showed a significant decrease (Fig. 4). In contrast, the prevalence of Nef group 1 decreased significantly in the midfrontal cortex, while the prevalence of group 2 increased in this tissue. No significant differences in Nef group prevalence, compared to the stock virus, were noted in the remaining four tissues. The prevalence of Int group 1 decreased significantly in the basal ganglia and both lymph nodes, relative to the stock virus (Fig. 5). The prevalence of Int group 3, meanwhile, increased significantly in both lymph nodes, the basal ganglia and the cerebellum. Significant decreases in Int group 2 prevalence, relative to the stock virus, appeared in all tissues and this group was absent from the basal ganglia, the midfrontal cortex and both lymph nodes.

We also compared the mean prevalence of each Env V1, Nef and Int group across all brain tissues to the mean prevalence of each group in the lymph nodes, as well as the SIVsmmFGb stock virus. The prevalence of Env V1 group 1 in both the CNS and lymph nodes decreased significantly compared to the stock virus, but no significant difference in the prevalence of this group was noted between the CNS and lymph nodes (Fig. 6A). The prevalence of the other Env V1 groups did not differ between the SIVsmmFGb stock virus, the lymph nodes and the CNS. There was also no significant difference between the stock virus, CNS and lymph nodes in the prevalence of either group of Nef sequences (Fig. 6B). Int group 1 prevalence decreased significantly in the lymph node compared to the stock virus, but no other significant changes in the prevalence of this Int group were noted (Fig. 6C). The prevalence of Int group 2 decreased significantly in the CNS and the lymph nodes compared to the stock virus, but there was no significant difference between the CNS and the lymph nodes. The prevalence of Int group 3 increased significantly in the CNS and the lymph nodes compared to the SIVsmmFGb stock virus, but there was no difference between the CNS and the lymph nodes.

The prevalence of each Env V1, Nef and Int sequence group in each tissue was also analyzed in each animal individually. The most prevalent Env V1 region group was group 4, although group 2 predominated in one tissue for three of the six animals and group 3 was the most prevalent in one tissue for two of the six animals (Fig. 7). Group 1 was the most prevalent Nef group in all animals across all tissues, except for in the hippocampus and mesenteric lymph node of PKo1 (Fig. 8). Group 3 was the most prevalent of the Int groups, but all of the animals had at least one tissue where the prevalence of group 1 was greater than, or equal to, that of group 3 (Fig. 9).

Phylogenetic Analysis of Compartmentalization of Env V1 Region, Nef and Int Amino Acid Sequences Isolated from Pigtailed Macaque Brain and Lymph Node Tissues

To determine whether SIVsmmFGb Env V1 region, Nef or Int formed distinct genetic compartments in any CNS or lymph node tissue, a modified Slatkin-Maddison test was used, as described in the Materials and Methods section. The Env V1 region sequences obtained from all of the CNS tissues compartmentalized separately from both of the lymph nodes; the formation of distinct compartments between CNS tissues was also noted (Fig. 10A). However, no significant Env V1 region sequence compartmentalization appeared between the lymph nodes. Similar results were observed for Nef (Fig. 10B), with Nef sequences from each CNS tissue forming distinct compartments from the other CNS tissues and both of the lymph nodes. However, significant compartmentalization of Nef sequences was seen between the axillary and mesenteric lymph nodes. The degree of compartmentalization was greater for Nef than for Env V1 region sequences, with average s ratios of 0.32 (range ~ 0.16 to 0.67) and 0.60 (range ~ 0.40 to 0.81), respectively. The Int sequences obtained from each of the CNS tissues also formed separate compartments from those Int sequences from the other CNS regions and those from the lymph nodes (Fig. 10C). There was no significant Int compartmentalization noted between the basal ganglia and cerebellum or between the axillary and mesenteric lymph nodes. Int sequences had the weakest level of compartmentalization, with an average s ratio of 0.70 (range ~ 0.51 to 0.94).

Phenetic Analysis of the Compartmentalization of SIVsmmFGb *env* V1 Region, *nef* and *int* Sequences Isolated from Pigtailed Macaque CNS and Lymph Node Tissues

To bolster the results of the phylogenetic compartmentalization analysis, and provide a degree of quantification, a Mantel's test was used, as described in the Materials and Methods section, to analyze the phenetic structure of each two-tissue comparison in each of the experimental animals. Due to the size of the data sets, the full results, including the Pearson's correlation coefficients and p-values, for the Mantel's tests on the *env* V1 region, *nef* and *int* proviral DNA sequences can be found in Tables 4 – 6, respectively.

As summarized in Table 7, the *env* V1 region sequences compartmentalized separately between most of the CNS tissues and both lymph nodes in the majority of the experimental animals. The only exceptions were the *env* V1 region sequences obtained from the midfrontal cortex, which did not compartmentalize separately from either lymph node in most animals. The *env* V1 region sequences also did not form separate compartments between the axillary and mesenteric lymph nodes in most animals. The compartmentalization of *env* V1 region sequences varied between animals, with the basal ganglia-mesenteric lymph node comparison the only one in which all animals demonstrated significant compartmentalization. For both *nef* and *int*, most animals showed independent compartmentalization of sequences between all tissues within the CNS. As with *env*, the *nef* and *int* sequences did not form separate compartments between lymph nodes in most animals.

d_S and d_N Values for SIVsmmFGb *env* V1 Region, *nef* and *int* Sequences Isolated from Pigtailed Macaque CNS and Lymph Node Tissues

Though the modified Slatkin-Maddison and Mantel's tests suggest compartmentalization of SIVsmmFGb *env* V1 region, *nef* and *int* sequences, it was left undetermined whether this was due to tissue-specific selection or the replication of limited founder genomes. To test for selective pressure, d_S and d_N values were determined as described in the Materials and Methods section. The *env* V1 region sequences harvested from the experimental animals demonstrated mean d_N values significantly higher than the d_S values in all six tissues (Fig. 11A). While the d_S / d_N ratio values for the *env* V1 region sequences from all six tissues were less than 1, 1 fell within the standard error range of the mean d_S / d_N ratio of the *env* V1 region sequences from the midfrontal cortex (Fig. 12A). The *nef* and *int* sequences derived from all six experimental tissues had significantly higher d_S values than d_N values (Figs. 11B and 11C), as well as d_S / d_N ratios greater than 1 (Figs. 12B and 12C).

Comparing the d_N, d_S and d_S / d_N ratio values between tissues can allow for the analysis of differences in selective pressure between tissues. While the mean d_S values of the *env* V1 region sequences obtained from the basal ganglia and midfrontal cortex did not differ from each other (Fig. 11A and Table 8), both had mean d_S values significantly higher than the mean d_S values of the *env* V1 region sequences collected from the axillary lymph node and hippocampus. The mean d_S value of the *env* V1 region sequences from the basal ganglia was also found to be significantly higher than those sequences from the mesenteric lymph node. The highest mean d_N value was noted in *env* V1 region sequences from the cerebellum. The mean d_N value of midfrontal cortex-derived *env* V1

region sequences did not differ from the mean d_N value of the lymph node-derived sequences, but was significantly lower than the mean d_N values of sequences from the other three brain tissues. Cerebellum-derived *nef* sequences had the lowest mean d_S value (Fig. 11B and Table 8), although this was not significantly different from the d_S values of *nef* sequences collected from the basal ganglia and hippocampus. Mesenteric lymph node-derived *nef* sequences had the highest mean d_S value, though this value did not differ significantly from the d_S value of *nef* sequences from the basal ganglia or midfrontal cortex. The highest mean d_S value for *int* was found in sequences obtained from the axillary lymph node (Fig. 11C and Table 8). The next highest mean d_S value was for *int* sequences from the mesenteric lymph node, although this value was only statistically higher than the d_S value for *nef* sequences obtained from the midfrontal cortex and hippocampus. In addition, basal ganglia-derived *nef* sequences were found to have a higher mean d_S value than those sequences collected from the hippocampus. The mean d_N values of *int* sequences from the cerebellum and mesenteric lymph node were both significantly lower than the mean d_N values of sequences from the axillary lymph node and hippocampus.

The highest mean d_S / d_N ratio values for *env* V1 regions were found in sequences derived from the basal ganglia and midfrontal cortex (Fig. 12A and Table 9), while the d_S / d_N ratios of *env* V1 region sequences obtained from the other four tissues did not differ from each other significantly. For *nef* (Fig. 12B and Table 9), sequences from the cerebellum, hippocampus and axillary lymph node had significantly lower mean d_S / d_N ratio values than those *nef* sequences obtained from the basal ganglia, midfrontal cortex and mesenteric lymph node. The *int* sequences collected from the hippocampus had a

significantly lower mean d_S / d_N value than those from the cerebellum and lymph nodes, while the midfrontal cortex and axillary lymph node-derived *int* sequences had lower mean d_S / d_N values than those sequences obtained from the mesenteric lymph node.

Discussion

Although prior studies have investigated the pathogenesis of SIVsmmFGb, this is the first to comprehensively analyze the genetic characteristics of the virus in the CNS and lymph nodes of pigtailed macaques during initial tissue seeding. Prior research has demonstrated that SIVsmmFGb is a swarm (173), but the genetic make-up of the quasispecies had yet to be determined. We analyzed three SIVsmmFGb genes: *int*, a highly conserved gene that is resistant to mutations which impact protein function (478, 479), integrates reverse-transcribed viral DNA into the host chromosome (415); *nef*, which has been shown to be involved in HIV and SIV neuropathogenesis (161, 237, 480-482); and *env*, a rapidly evolving and highly variable gene essential for target cell entry (343, 483) and with demonstrated functions in neuropathogenesis (216, 484).

For *env*, we focused on the V1 variable loop of gp120 (485), a major target of neutralizing antibody (343, 486) and the predominant region of SIV *env* sequence variation (487). Our results indicate that the Env V1 regions present within our SIVsmmFGb stock virus form four groups, with group 4 being predominant. Meanwhile, the Int sequences in our stock virus separate into three groups and the Nef sequences into two, with group 1 being dominant in both Int and Nef. While we expected Env V1 region sequences to be the most variable, we did not expect a greater diversity of Int sequences over Nef. Using a less stringent method of grouping sequences, such as lowering bootstrap support required for significant clades, or basing groupings on visual

inspection of phylogenetic trees, may increase the number of Nef groups, revealing additional diversity of this gene. Another possibility is considering each stock virus consensus sequence for each gene to be a separate group, rather than aligning them to form super-groups. However, the resulting number of groups, over 20 for Nef alone, would have been overly difficult to analyze and represent clearly. In addition, because the SIVsmmFGb stock virus was grown in PBMC culture, we would not expect any selective pressure to restrict Int diversity or promote Nef diversification.

Given the total number of sequences analyzed, we expect that our results accurately represent the genetic diversity of the SIVsmmFGb stock virus. We obtained at least 20 sequences from each of 16 different dilutions of the RNA and DNA templates used for RT-PCR and PCR, for a balance of statistical significance and feasibility (488); few other SIV or HIV studies have analyzed this volume of data. Template dilutions were used to minimize the over-amplification of common sequences, the non-amplification of rare sequences and other factors in PCR and RT-PCR, which could introduce bias. While DH10B bacterial subcloning may induce mutations or select against some genomes, the procedure has been used extensively and we would expect this bias to be low. Another potential bias with our protocol is that PCR amplification of proviral DNA presents a 'history' of virus infection: Rather than only assessing actively replicating virus, any virus that was capable of reverse transcription and integration will be amplified, regardless of subsequent replicative fitness. Over time, replication-competent viruses with selective advantages should expand more than weak or defective viruses and come to represent the greatest proportion of the proviral DNA population. While defective viruses may be sampled in our procedure, the number of sequences

harvested for each tissue should be significant enough to accurately reflect the proviral DNA population, of which defective strains would be a very small part. In addition, we screened all sequences and discarded any clones with in-frame stop codons and frame shift mutations (all three genes) or insertions and deletions (*nef* and *int*), which were unlikely to code functional proteins. By not considering these defective sequences in our analysis, we would expect to screen out most integrated, non-replicating genotypes, reducing this potential bias.

Due to the complexity of the SIVsmmFGb stock virus, some rare genomes may not have been characterized, even with the amount of sequences collected. However, the amount of sequencing required to be certain of having characterized the entire quasispecies would be prohibitively difficult, if not impossible. With the amount of sequences collected for each gene from the stock virus, we expect the possibility of missing a rare, important strain to be low. Using an inoculum composed of a mixture of SIVsmmFGb molecular clones may have eased subsequent analysis, but would introduce bias in choosing which molecular clones to use and what proportion of the inoculum each clone would comprise. In that method, rare constituents of the SIVsmmFGb quasispecies, or sequences that are difficult to clone, could be artificially unrepresented. A less complex inoculum virus could have been used instead, but may not have been as representative of a highly complex quasispecies like HIV-1 (463, 489).

We were interested in determining the effect of the initial seeding of the pigtailed macaque CNS and lymphoid tissues on the genetic profile of our SIVsmmFGb stock virus. We believe the SIVsmmFGb quasispecies is representative of HIV-1 swarms (463, 489) and is a strong model of virus seeding that is unique from studies using single,

molecularly cloned isolates. An i.v. inoculation was used, as this route of infection is known to preserve the diversity of an SIV population better than mucosal infection (436, 490). ISH results coincided with our expectations of highly active viral replication in the lymph nodes and gastrointestinal tissues, but limited actively replicating virus in the CNS (173). While the low numbers of SIVsmmFGb RNA-positive cells detected in the CNS may not be strongly convincing of active infection, our previous studies lead us to expect productive CNS infection at early time points; even by five or seven dpi (3, 173, 444). In fact, detection of only low levels of SIVsmmFGb RNA in the CNS confirms that we are assessing the very earliest stages of initial CNS colonization, before extensive viral replication and accumulation of mutations, validating our choice of sampling at five or seven dpi. As we expect only limited, diffuse, replication of SIVsmmFGb in the CNS so early in infection (3), it is possible the samples used for ISH simply did not contain any productively infected cells or levels of actively replicating virus were below the threshold of detection. The isolation of proviral DNA from brain tissues of most of the experimental animals also confirms SIVsmmFGb replication in the CNS, despite the lack of ISH support. The CNS tissues sampled in this study were chosen from anatomical sites known to be important for neuropathogenic replication in HIV (basal ganglia and hippocampus (68, 69)) and SIV (cerebellum and midfrontal cortex (3, 70)) infections. The mesenteric lymph node was chosen from the gut-associated lymphoid tissues, a major area of SIV replication in early infection (436), while the axillary lymph node was selected to represent non-intestinal lymphoid tissues.

We were unable to amplify some viral genes from three of the CNS tissues harvested from animal PQo1, which was euthanized at five dpi, when we expected that

proviral DNA would be present in the CNS. PQo1 was noted to have unusually low numbers of productively-infected cells in the lymph node and gastrointestinal tissues by ISH; similarly reduced levels of active virus replication in the CNS could explain the difficulty harvesting proviral DNA from those tissues. While SIVsmmFGb replicates well in most pigtailed macaques (444), PQo1 may have been a rare host in which the virus was unable to initiate rapid dissemination. From each of the midfrontal cortex and cerebellum of PQo1, we were eventually able to amplify one viral gene but, by the time we were successful, tissue supplies were exhausted and the remaining two genes could not be amplified. Although there was no difficulty in amplifying viral genes from PQq1, which was also sacrificed at five dpi, we chose to sacrifice the remaining four animals at seven dpi, to ensure the virus would have sufficient time to begin colonization of the CNS and reduce the likelihood of difficulty harvesting proviral DNA.

The adaptive immune system is not expected to play a role in host responses to SIVsmmFGb at five or seven dpi. The innate immune response, while presenting a challenge to virus replication, would not be expected to specifically target any subset of the quasispecies. Thus, we suspect that any advantage a gene group has at five or seven dpi is due to some intrinsic replicative advantage. Our results suggested that there was selective pressure against Env V1 region group 1 regardless of tissue, but no significant pressure on the other Env V1 region groups. In general, changes in the Env V1 region have been shown to negatively impact SIV replication in macrophages (491). As the Env V1 region is primarily involved in binding CD4 (492), it is possible that the Env V1 regions in group 1 possess mutations reducing their capacity to bind CD4. In the CNS, where the target cells for virus infection are primarily macrophage-related and express

low levels of CD4, a subset of viruses with diminished CD4-binding capacity would be expected to face a disadvantage (493). Unexpectedly, there appeared to be selective pressure against both group 1 and group 2 Int sequences in all tissues, while selection favored Int group 3. Viruses with Int sequences from groups 1 and 2 may replicate well in the human PBMC tissue culture used to produce the SIVsmmFGb stock virus but not in pigtailed macaques, due to species-specific host factors. Conversely, group 3 Int sequences may have advantageous changes that improve in vivo replication, although this is unlikely given the low mutation rate of *int* (478, 479) and the general tendency of any mutation to impair protein function. Our results suggested tissue-specific variation in the fitness of the two Nef groups in the CNS, but Nef diversity appears to be largely unaffected by seeding of the pigtailed macaque host. HIV and SIV naturally trigger apoptotic pathways in infected cells (361, 494) but Nef protects cells, including macrophages, from these deleterious effects (361, 495). If a mutation hampering this function was present in one of the Nef groups, this could lead to the death of cells infected with those Nefs and limit the spread of viruses in that group. Similarly. Nef increases virion infectivity (361), and a Nef group with mutations in this function may also see reduction in the spread of the virus.

We expected that SIVsmmFGb *env*, *int* and *nef* sequences harvested from the CNS would compartmentalize separately from those obtained from the lymph nodes due to differences in available target cells. While the lymph nodes provide ample lymphocytes and macrophages for virus infection, virus infecting the CNS is largely restricted to replication in macrophages and related cells (79, 122, 144, 145, 450, 496). In addition, while the peripheral lymphoid tissues may be exposed to infectious virus in

the blood and plasma, the BBB minimizes exposure of the brain to cell-free virus, leaving traffic of infected monocytes or direct BBB infection as the primary routes of CNS seeding (94, 105, 123). While HIV and SIV *env* genes have been shown to form separate compartments between the CNS and lymph nodes, and even between CNS tissues (459, 461, 477, 497), no similar research could be found for *int* and *nef*. We expected *nef* and *int* would face the same pressures as *env* in terms of target cell availability and restricted seeding of the CNS. However, we presumed that the reduced variability of *nef* and *int* would limit the compartmentalization of these two genes. We did not expect to see any of the three genes form separate compartments between the axillary and mesenteric lymph nodes due to similarities in seeding and target cell availability between these two tissues. We used two unique statistical analyses to test for compartmentalization, the modified Slatkin-Maddison test and the more stringent Mantel's test (452, 461, 463), in order to strengthen our findings (488). The results of both statistical tests supported our hypotheses for *env* V1 region, except that the Mantel's test indicated that *env* V1 region sequences from the midfrontal cortex did not compartmentalize independently from those obtained from the lymph nodes in most animals. This discrepancy may be due to the different stringencies of the tests; accounting for standard error, the s ratio values for the midfrontal cortex-lymph node comparisons in the modified Slatkin-Maddison test are very close to 1. There may also be similarities between viruses seeding the midfrontal cortex and those seeding the lymph nodes or the midfrontal cortex and lymph nodes may exert similar selective pressures on the *env* V1 region. We thus concluded that *env* V1 region sequences from the basal ganglia, cerebellum and hippocampus formed separate compartments from each other, the midfrontal cortex and the lymph nodes. The results of

both statistical analyses also largely supported our hypotheses for *nef*. However, *nef* sequences from the axillary and mesenteric lymph nodes formed separate compartments from each other and, in the modified Slatkin-Maddison test, *nef* had a greater degree of compartmentalization overall than *env* V1 region. The results of the more stringent Mantel's test suggests that *nef* sequences from the lymph nodes do not compartmentalize separately from each other and, accounting for standard error, the modified Slatkin-Maddison s ratio value for this comparison is close to 1. However, further data will be required to analyze compartmentalization between these two tissues. We thus conclude that *nef* sequences compartmentalize separately between CNS tissues and between the CNS tissues and the lymph nodes. The results for *int* met most of our expectations, except that sequences derived from the basal ganglia and cerebellum did not compartmentalize separately from each other in the modified Slatkin-Maddison test, suggesting seeding of virus between these tissues or similar selective pressures on the *int* within these tissues. However, compartmentalization of *int* between the basal ganglia and cerebellum was detected by Mantel's test in all animals and the modified Slatkin-Maddison s ratio value for this comparison is close to 1, accounting for standard error.

There are two likely causes of inter-tissue compartmentalization of virus gene sequences (461, 463): First, while host tissues may all be seeded by the same or similar components of the quasispecies, selective pressures unique to each tissue may have different effects on swarm evolution in each tissue. The second possibility is that tissue seeding represents a genetic bottleneck for the virus, with a limited subset of the quasispecies forming the founder population that infects a given tissue. The latter possibility appeared most likely, given the restricted seeding and diffuse infection of the

CNS by SIVsmmFGb during acute phase (3, 444), as well as the lack of an adaptive immune response at five or seven dpi. Analysis of d_S and d_N values for *env* V1, *nef* and *int* sequences from each tissue was performed to analyze for the presence of selective pressure (498), although such analysis does not completely rule out the possibility of a founder effect. While the SIVsmmFGb swarm is primarily CCR5-tropic (173), which should allow efficient infection of macrophage-related cells in the CNS (79, 122, 144, 145, 450, 496), a small subset of the quasispecies uses alternate co-receptors. We expected this non-CCR5-tropic subset would face a selective disadvantage in the CNS and positive selection would favor mutation of these *env* V1 regions to CCR5 tropism. The results of our d_S / d_N tests suggest that *env* V1 region sequences in all six experimental tissues compartmentalized due to positive selection, although results from the midfrontal cortex were less convincing. Similar d_S / d_N ratio values for *env* V1 sequences from the basal ganglia and midfrontal cortex suggest similar selective pressures on the *env* V1 region in these tissues. These results also argue against a founder effect being responsible for *env* V1 region selection in at least some of the CNS tissues. With a genetic bottleneck in the CNS, we would expect to see stronger selection in these tissues compared to the lymph nodes, but our results indicate the strength of positive selection in the cerebellum and hippocampus is similar to that in the lymph nodes. However, the level of active virus replication is much higher in the lymph nodes than in the CNS, which may result in increased selective pressure comparable to that of a genetic bottleneck in the CNS tissues. Significant differences in *env* V1 region mean d_S and/or d_N values were noted in most comparisons between tissues, suggesting some functional variance in V1 regions between most tissues.

We expected to find negative selection on *nef* sequences, as the product of this gene has multiple, conserved functional domains (359, 361). Results of the d_S / d_N analysis supported our hypothesis, as *nef* sequences appeared to undergo negative selection in all six tissues. Based on the significant differences in mean d_S / d_N ratio values, the hippocampus, cerebellum and axillary lymph node all exert similar selective pressures on the *nef* gene. The basal ganglia, midfrontal cortex and mesenteric lymph node also all exert similar selective pressures on *nef* sequences, but these pressures are distinct from the other trio of tissues. Given that *nef* sequences from all of the CNS tissues experienced a degree of selective pressure similar to one of the lymph nodes, this suggests a founder effect is not responsible for differences in selection between tissues. As *nef* is not expected to be under the same evolutionary pressure as the *env* V1 region, increased virus replication in the lymph nodes is less likely to obscure a possible founder effect in the CNS tissues. While we cannot rule out a founder effect causing negative selection on *nef* sequences in the CNS, tissue-specific selective pressures appear to be a more likely explanation. Significant differences between the mean d_S values of *nef* sequences in some inter-tissue comparisons suggests there may be functional differences between viruses harvested from these tissues. The mechanism of these functional differences is currently unknown.

We expected, and our results confirmed, negative selection of *int* sequences in all tissues, as the functional importance of this gene reduces the likelihood of amino acid changes (478, 479). As most genotypes with mutations in *int* would be expected to be replication defective, they should be rapidly out-competed by those genotypes with a functional version of this gene. Our results indicated that the effect of negative selection

on integrase in most of the CNS tissues is similar to that in the lymph nodes, which suggests that a founder effect plays little role in *int* selection. As *int* would be expected to face very little selective pressure compared to *env* V1 region and *nef*, increased levels of virus replication in the lymph nodes should not obscure a founder effect in the CNS tissues. However, we cannot rule out a genetic bottleneck on *int* in the CNS tissues and, indeed, our results suggest this may be an important factor on *int* selection in the hippocampus. Based on differences in the mean d_S / d_N values of the *int* sequences, tissue specific selective pressures on this gene appear to be strongest in the hippocampus, though differences were also present between the two lymph nodes, and between the midfrontal cortex and one lymph node. Most of the inter-tissue comparisons of *int* sequences had differences in the mean d_S and/or d_N value, suggesting some functional differences between genes from each tissue. However, most of the differences were between *int* sequences from the CNS and the lymph nodes, rather than from one CNS tissue to another.

Our study focused only on the V1 region of *env*, due to difficulties we encountered constructing nested, full-length sequencing primers for this gene. Once the primers are refined, we will fully sequence *env* and determine whether the results for the V1 region represent those for the complete gene. Alternatively, we will sequence and analyze the other *env* variable loops. We are currently analyzing the replication of SIVsmmFGb viruses, harvested from the experimental tissues from this study, in primary pigtailed macaque macrophage cultures. These experiments may help reveal functional differences in the *env* V1 region, *nef* and *int* genes of the SIVsmmFGb viruses after five to seven dpi. Experiments are also underway analyzing *env* V1 region, *nef* and *int*

sequences harvested from SIVsmmFGb-infected pigtailed macaques sacrificed at two mpi, during the clinically latent stage of infection. That study will allow analysis of the results of long-term infection on the genetic diversity of SIVsmmFGb genes in various CNS and lymphoid tissues, as well as changes in compartmentalization and selection after onset of the adaptive immune response.

Chapter 2

Neuropathogenic SIVsmmFGb Genetic Diversity and Selection-Induced Tissue-Specific Compartmentalization during Chronic Infection and Temporal Evolution of Viral Genes in Lymphoid and Central Nervous System Tissues

Adapted from Reeve, et al. In Press.

Results

Diversity of Env V1 Region, Nef and Int Amino Acid Sequences Isolated from Pigtailed Macaque Brain Regions and Lymph Node Tissues at Two Months Post-Infection

In our previous study, we determined that four groups of Env V1 region, two groups of Nef and three groups of Int amino acid sequences were present in our SIVsmmFGb stock virus (499). We also analyzed how the prevalence of each group of each gene changed after one wpi in the pigtailed macaque host (499). Here, we were interested in determining how the prevalence of those amino acid sequence groups, harvested from infected pigtailed macaques at two mpi, compared to the prevalence of those groups in the SIVsmmFGb stock virus. For the Env V1 region (Fig. 13), the prevalence of sequence groups 1 and 2 decreased in the basal ganglia, compared to the SIVsmmFGb stock virus, while group 4 saw an increase in prevalence in this region of the brain. The hippocampus had a reduced prevalence of Env V1 region sequence groups 2 and 3, compared to the stock virus. An increase in the prevalence of Nef sequence group 1, and decrease in the prevalence of group 2, was noted in the axillary lymph node, midfrontal cortex and hippocampus (Fig. 14). The Int sequence group 1 prevalence increased in the basal ganglia, midfrontal cortex and hippocampus, compared to the stock virus (Fig. 15). The prevalence of Int sequence group 2 decreased in the cerebellum, midfrontal cortex and hippocampus, while the prevalence of group 3 decreased in the basal ganglia.

We also compared the average group prevalence for Env V1 region, Nef and Int in pooled CNS region sequences to mean group prevalence in the stock virus and the

pooled lymph node tissue sequences. Env V1 region sequence group 4 demonstrated an increased prevalence in the pooled CNS sequences, while groups 1 – 3 decreased, compared to the SIVsmmFGb stock virus (Fig. 16A). Env V1 region sequence groups 1 and 2 prevalence was lower in the CNS than the lymph nodes, while the presence of group 4 was higher in the CNS. For Nef, the presence of sequence group 1 was lower in the pooled CNS sequences, compared to the stock virus, with a corresponding increase in the prevalence of group 2 (Fig. 16B). The prevalence of Nef group 1 increased in the pooled lymph node sequences, compared to the stock virus, while the prevalence of group 2 declined. Int sequence groups 2 and 3 had a lower prevalence in the pooled CNS sequences, compared to the SIVsmmFGb stock virus, but the prevalence of group 1 was higher in the CNS pool (Fig. 16C). The level of Int group 2 was lower in the lymph node pool relative to the stock virus. There was no significant difference seen in Nef or Int sequence group prevalence between the CNS and lymph node sequence pools.

The prevalence of each sequence group, for each gene in each tissue, was also analyzed in the experimental animals individually. Five of the six animals sacrificed at two mpi had group 4 as the predominant Env V1 region group in all tissues analyzed, while the most prevalent group in animal PHt1 varied between tissues (Fig. 17). For Nef, group 1 sequences were predominant in the lymph nodes, the midfrontal cortex and the hippocampus of all six animals, as well as in the basal ganglia and cerebellum of most animals (Fig. 18). Although Int group 1 was generally the most prevalent sequence group, four animals had group 3 dominant, or at similar levels to group 1, in at least one lymphoid tissue or brain region (Fig. 19).

Phylogenetic Compartmentalization Analysis of Env V1 Region, Nef and Int Amino Acid Sequences Isolated from Pigtailed Macaque Brain Regions and Lymphoid Tissues Two Months Post-Infection

We utilized two methods of analysis to examine the compartmentalization of Env V1 region, Nef and Int sequences obtained from the various tissues. The first test, the modified Slatkin-Maddison test, is a phylogenetic method of compartmentalization analysis. Based on the results of this analysis, the Env V1 region amino acid sequences from each region of the brain compartmentalized separately from all other CNS regions and from the lymph nodes, but compartmentalization between the lymph nodes did not appear (Fig. 20A). Similar results were found for the Nef (Fig. 20B) and Int (Fig. 20C) sequences. The Env V1 and Int sequences had a similar degree of compartmentalization, with average s ratio values of 0.61, while Nef sequences had the strongest compartmentalization, with an average s ratio of 0.42.

Phenetic Compartmentalization Analysis of *env* V1 Region, *nef* and *int* Nucleotide Sequences Isolated from Pigtailed Macaque Brain Regions and Lymphoid Tissues Two Months Post-Infection

The second test we used to investigate the compartmentalization of envelope V1 region, nef and integrase sequences was the Mantel's test, a phenetic method of analysis. Table 10 summarizes the Mantel's test results on each of fifteen two-tissue comparisons of *env* V1 region, *nef* and *int* nucleotide sequences from all experimental animals. This summary table indicates the number of animals in the cohort that had statistically significant compartmentalization of *env* V1 region, *nef* or *int* by Mantel's test in each of the inter-tissue comparisons. Due to the size of the data sets, a full listing of Pearson's

correlation coefficients and p-values for the *env* V1 region, *nef* and *int* nucleotide sequences can be found in Tables 11 – 13. The *env* V1 region sequences obtained from each region of the CNS compartmentalized separately from the other brain regions, and from lymph node-derived sequences, in a majority of animals. However, the *env* V1 region sequences from the basal ganglia only compartmentalized separately from the axillary lymph node and hippocampus in half of the experimental animals. Compartmentalization of the *env* V1 region sequences between the lymph nodes appeared in only one test animal. For both *nef* and *int*, the sequences compartmentalized separately between CNS regions, as well as between the CNS and the lymph nodes, in a majority of animals. While none of the experimental animals demonstrated compartmentalization of *nef* between the lymph nodes, the axillary and mesenteric lymph nodes of one subject did have compartmentalization of *int* sequences.

Synonymous and Nonsynonymous Nucleotide Substitution Rates of SIVsmmFGb *env* V1 Region, *nef* and *int* Sequences Isolated from Pigtailed Macaque Brain Regions and Lymph Node Tissues Two Months Post-Infection

In order to determine whether the *env* V1 region, *nef* and *int* genes were undergoing positive or negative selection at two mpi, we next analyzed d_S and d_N for all of the sequences, as well as the ratio of d_S to d_N. The *env* V1 region sequences harvested from all six of the experimental tissues had significantly higher d_N values than d_S values (Fig. 21A and Table 14), as well as d_S /d_N ratio values of less than 1 (Fig. 22A and Table 15). The basal ganglia-derived *env* V1 region sequences had the lowest mean d_S value, while the sequences obtained from the cerebellum had a lower average d_S value than those from the midfrontal cortex and mesenteric lymph node (Figs. 21A and D, Table

14). The average d_S values of *env* V1 region sequences from the mesenteric lymph node and midfrontal cortex were significantly higher than the d_S values of sequences from the axillary lymph node and the other brain regions. The lowest mean d_N value appeared for the *env* V1 region sequences from the hippocampus. While the average d_N value of *env* V1 region sequences from the basal ganglia was higher than those in the hippocampus, it was lower than in both lymph nodes and the remaining two regions of the CNS. The *env* V1 region sequences from the basal ganglia had the lowest mean d_S/d_N ratio value, while sequences from the cerebellum, axillary lymph node and hippocampus all had average d_S/d_N values lower than those sequences from the midfrontal cortex (Figs. 22A and D, Table 15). The average d_S/d_N value of *env* V1 region sequences from the mesenteric lymph node was higher than the mean d_S/d_N values of sequences from the basal ganglia, cerebellum and axillary lymph nodes.

For the *nef* sequences, the mean d_S values were significantly higher than mean d_N values in all tissues and all tissues had an average *nef* d_S/d_N ratio value greater than 1 (Figs. 21B and 22B, Tables 14 and 15). The basal ganglia-derived *nef* sequences had the lowest mean d_S value, while the mean d_S value for *nef* sequences from the hippocampus was only higher than the mean d_S value in the axillary lymph node (Figs. 21B and D, Table 14). The highest mean d_S value was for those *nef* sequences from the midfrontal cortex. Those *nef* sequences obtained from the cerebellum had the highest mean d_N value, while the sequences from the hippocampus and lymph nodes had the lowest mean d_N values. The *nef* sequences from the basal ganglia had the lowest average d_S/d_N ratio, while sequences from the cerebellum had a mean d_S/d_N ratio lower than the lymph nodes

and the remaining regions of the CNS. The highest mean d_S /d_N value appeared in the *nef* sequences from the midfrontal cortex (Figs. 22B and D, Table 15).

The *int* sequences also had significantly higher mean d_S values than mean d_N values in all six tissues, and average d_S /d_N ratios greater than 1 (Figs. 21C and 22C, Tables 14 and 15), but no differences in mean d_S values between tissues were noted (Figs. 21C and 21D, Table 14). The midfrontal cortex-derived *int* sequences had a mean d_N value higher than those from the axillary lymph node, but lower than sequences from the basal ganglia. The mean d_N value of *int* sequences from the hippocampus was significantly higher than the cerebellum and the lymph nodes, while sequences from the basal ganglia had a mean d_N value higher than that of all other tissues except the hippocampus. The average d_S /d_N values for *int* sequences obtained from the hippocampus and basal ganglia were significantly lower than the mean d_S /d_N values of sequences from all other tissues.

Phylogenetic Analysis of Temporal Compartmentalization of Envelope V1 Region, Nef and Integrase Amino Acid Sequences between Pigtailed Macaque Brain and Lymph Node Tissues Harvested at One Week and Two Months Post-Infection

We were also interested in determining whether SIVsmmFGb sequences compartmentalized within a particular tissue over time. Thus, we performed a modified Slatkin-Maddison test, comparing sequences obtained from a tissue at one wpi (499) with sequences obtained from the same tissue at two mpi. Env V1 region amino acid sequences compartmentalized separately within each tissue, between time points, in all tissues studied (Fig. 23A). While Env V1 region sequences from the basal ganglia had the lowest degree of temporal segregation of all the CNS regions, all brain tissues

demonstrated stronger temporal compartmentalization of Env V1 region than either lymph node. Similar results were obtained for Nef, with temporal compartmentalization of this gene in all tissues, but a higher degree of segregation in the CNS over time (Fig. 23B). Nef sequences from the basal ganglia appeared to have the strongest intra-tissue temporal compartmentalization of all the CNS regions, while sequences from the midfrontal cortex had the weakest degree of temporal segregation. All tissues demonstrated temporal compartmentalization of Int (Fig. 23C). The Int sequences from the midfrontal cortex, cerebellum and lymph nodes had similar degrees of intra-tissue temporal compartmentalization, while basal ganglia-derived Int sequences had the highest degree of temporal segregation over time. The sequences with the lowest degree of temporal segregation were the Env V1 region samples, with an average s ratio value of 0.71, while the Nef sequences had the highest, with a mean s ratio value of 0.40. The Int sequences fell in between, with an average s ratio value of 0.60.

Discussion

While we have previously studied SIVsmmFGb neuropathogenesis and genetic diversity at one wpi (3, 444, 499), this follow-up study explores the genetic diversity and evolution of SIVsmmFGb at two mpi. In studies with SIV infection of the CNS, viral replication has been detected in multiple regions of the brain for a period of up to two wpi (79, 499). Subsequently, viral RNA within the CNS becomes undetectable by three wpi and active replication, as measured by viral RNA, does not become elevated again until 8 – 12 wpi (174, 202, 481). The exact mechanism that suppresses SIV RNA expression within the CNS from 3 – 8 wpi has yet to be determined, however, research suggests that beta-interferon induces production of LIP, a dominant negative isoform of

the transcription activator LAP, in macrophages and related cells (181-183). Interaction of LIP with the proviral LTR may then block viral transcription, preventing replication and inducing a latent infection in macrophages (176, 178-180, 185, 186). Based on these SIV models, we would expect SIVsmmFGb replication in the CNS to be completely suppressed before two mpi. Analyzing SIVsmmFGb genes at two mpi allows us to assess the virus population that emerges following completion of the initial burst of replication and evolution during the early weeks of infection. The choice to sample at two mpi was balanced between choosing a time point late enough for the initial round of viral replication in the CNS to be complete, but early enough that the virus would not have emerged from suppression in most animals.

Prior studies of SIVsmmFGb have shown that rapid progressors do not demonstrate symptoms until at least three mpi (3), so we did not specifically monitor the animals in this study for overt clinical symptoms of lentiviral neuropathogenesis. Still, none of the animals in this study were noted to have gross clinical signs of SIVsmmFGb neuropathogenesis at sacrifice. Although research has not specifically addressed suppression of SIVsmmFGb replication in the CNS, based on the studies of other SIV strains discussed above, we would expect actively replicating SIVsmmFGb in the CNS to be present at low or undetectable levels in most animals at two mpi. Our rationale for focusing on the SIVsmmFGb *env* V1 region, *nef* and *int* genes, as well as our choice of tissues to sample, is discussed above. To elaborate on our choice of tissues, prior studies with SIVsmmFGb have shown development of lesions in the midfrontal cortex, cerebellum and hippocampus of rapidly-progressing animals, indicating these regions of the brain are involved in neuropathogenesis (3).

A number of potential issues with our methodology, and the steps we undertook to minimize these biases, are described above. One other potential flaw is that the tissue samples we harvested likely contain a number of different cell types that may support SIV infection. The majority of SIV-infected cells in the CNS are of the monocytic cell lineage (macrophages and microglia), which harbor productive viral infection when replication is not suppressed (70, 104, 113, 122-125). However, astrocytes and oligodendrocytes may also be infected with SIV (149, 153-155, 163, 167), yielding only a transient productive infection, followed by long-term viral latency (113, 159, 160). Given the limited replication of the virus in non-macrophage-related cells, we would expect limited selective pressure on SIVsmmFGb viruses infecting these cell types. Thus, infection of oligodendrocytes and astrocytes would not be expected to contribute significantly to evolution of the SIVsmmFGb genes analyzed in this study. In macrophage-related cells, where virus replicates extensively during the early weeks of infection, viral genes should face increased selective pressure, contributing to the majority of SIVsmmFGb sequence evolution. However, the methods used in our studies do not allow us to determine from which cells our gene sequences were obtained. Given that we would expect most infected cells in the CNS to be macrophage-related, we would then expect the majority of our sequences to originate from these cell types, with astrocyte- or oligodendrocyte-derived sequences representing a much smaller proportion of our sample. Future studies using techniques such as laser capture microdissection could allow us to collect specific cell types for use in isolating proviral DNA from the CNS.

Other longitudinal studies of HIV and SIV genetic diversity have focused on samples from the peripheral blood lymphocytes, plasma or CSF (452, 500), allowing collection of samples at multiple time points from the same animal. However, this type of sampling does not address viral genetic diversity and evolution in tissues such as the brain, which are difficult to sample in a longitudinal manner. Thus, we utilized two pigtailed macaque cohorts: One sacrificed after one wpi, described above, and the other after two mpi. Variation between host animals may introduce biases not present in longitudinal samples from the same animal, but our procedure is more ethical and feasible. Though longitudinal analyses of SIV *env* sequence compartmentalization have been conducted in prior research (452), this investigation is unique in studying compartmentalization, evolution and genetic diversity in multiple CNS and lymphoid tissues.

Selection against Env V1 region sequence group 1 was noted across all experimental tissues at one wpi, likely due to lower fitness of sequences in this group relative to the other three groups (499). We expected that the less-fit Env V1 region group 1 sequences would contribute to a smaller proportion of the proviral DNA population over time and the prevalence of these sequences would decline over the course of infection. However, Env V1 region group 1 increased in prevalence in the lymph nodes and hippocampus at two mpi. One possibility is that group 1 Env V1 region sequences possess mutations that provide a replicative advantage with the onset of host adaptive immunity (501-503). Preliminary analyses indicate that group 1 sequences have an increased number of amino acid changes compared to sequences from the other three groups (data not shown), which could allow escape from neutralizing antibody (501-503).

However, the increased presence of group 1 sequences may reflect a decline in the proportion of the other Env V1 region groups in the virus population. Given the increased prevalence of Env V1 region group 4 sequences at one wpi (499), we expected more virions with these Env V1 regions would be produced as infection continued. This could lead to increased pressure on these sequences from the adaptive immune response and a decline in their prevalence as infection progressed. However, while group 4 sequences did face a selective disadvantage in the lymph nodes at two mpi, this group was selected for in the CNS over the course of infection. Preliminary analyses of the Env V1 region group 4 sequences obtained in these studies indicate that the number of sequences in this group with an insertion in the V1 loop, which may affect the capability of the virus to enter target cells or allow viral escape from neutralizing antibody (501-503), increases at two mpi (data not shown).

Tissue-specific variation in the fitness of Nef group 1 and 2 sequences was noted in the CNS samples harvested at one wpi, with group 1 the most prevalent in all tissues (499). In the midfrontal cortex, hippocampus and lymph nodes, the prevalence of group 1 Nef sequences increased by two mpi compared to the SIVsmmFGb stock virus. Nef is capable of selectively downmodulating MHCI molecules (390, 504) and, if this function were defective in group 2 Nef sequences, this group may face a selective disadvantage in the CNS, where cytotoxic T cells may play some role in the immune response (199). However, Nef sequences from the basal ganglia and cerebellum had an increased prevalence of group 2 and decreased prevalence of group 1 by two mpi compared to the stock virus, suggesting selective pressure on Nef varies between regions of the brain.

At one wpi, selection favored Int group 3 (499). We expected this trend could continue through two mpi, although the increased prevalence of group 3 Int sequences at one wpi could result in increased adaptive immune pressure on this group. Consistent with this, Int group 3 prevalence was lower at two mpi in all tissues, compared to one wpi (499). Increases in the prevalence of groups 1 and 2 at two mpi could result from an advantage of these sequences or merely be a proportional increase, due to selection against group 3. In the CNS, the prevalence of Int groups 1 and 3 was higher at two mpi, while the prevalence of group 2 declined, compared to the SIVsmmFGb stock virus. The decreased prevalence of group 3 Int sequences in the CNS from one wpi to two mpi suggests selection against this group over time.

The *env* V1 region sequences formed separate compartments between most tissues at one wpi (499). We expected that *env* V1 region sequence compartmentalization would increase at two mpi, given continued replication of the virus and selective pressures unique to each microenvironment. The results supported our expectations, showing segregation of *env* V1 region sequences between all tissues except the axillary and mesenteric lymph nodes at two mpi. Compartmentalization of *env* V1 region sequences was weaker in a slight majority of inter-tissue comparisons at two mpi than at one wpi (499), suggesting a mixture of convergent and divergent evolution of *env* V1 region sequences between compartments over time.

At one wpi, *nef* sequences formed distinct genetic compartments in all tissues (499). Given our expectation of differences in virus replication and selective pressures between each microenvironment, we expected increases in *nef* compartmentalization over time. The results confirmed our expectations, showing that *nef* sequences form separate

compartments between different regions of the CNS, and between the CNS regions and the lymph nodes, at two mpi. Axillary and mesenteric lymph node-derived *nef* sequences did not compartmentalize separately from each other at two mpi, perhaps due to the ease of virus transfer between lymph nodes. The degree of *nef* compartmentalization was largely weaker at two mpi than one wpi (499), suggesting convergent evolution of *nef* sequences between most tissue compartments.

The formation of distinct *int* sequence compartments between most tissues was noted at one wpi (499). Given the resistance of *int* to mutation (479), we expected the inter-tissue *int* sequence compartments to remain stable over time. At two mpi, *int* sequences formed distinct genetic compartments between all regions of the CNS and between the CNS regions and the lymph nodes, confirming our expectations. In most two-tissue comparisons, the strength of *int* compartmentalization increased by two mpi, compared to one wpi (499), suggesting divergent evolution of *int* sequence populations. However, all inter-tissue comparisons involving sequences from the hippocampus showed weaker compartmentalization at two mpi than one wpi (499), suggesting convergent evolution of *int* between the hippocampus and the lymph nodes, as well as between the hippocampus and the other regions of the CNS.

We expected sequences from each tissue at two mpi to compartmentalize separately from those obtained at one wpi, reflecting additional virus evolution and exposure to selective pressure prior to the suppression of replication. Intra-tissue temporal compartmentalization was seen for all three genes in all tissues, suggesting that sequences within a tissue diverge over time. For Nef and Env V1, temporal segregation was strongest within each region of the CNS, suggesting greater divergence of sequences

in these regions over time, compared to the lymph nodes. Temporal compartmentalization of Int was similar in most of the tissues, suggesting little difference between divergence of Int in the CNS and lymph nodes over time. Genetic divergence of Env V1 region and Nef in the brain may be necessary to allow efficient viral replication in target cells or escape from immune pressures specific to the CNS. As the highly conserved function of Int does not play a role in virus entry into target cells or avoidance of the immune system, this gene would not be expected to diverge in the CNS relative to the lymph nodes. Preliminary genetic analysis of the SIVsmmFGb Nef amino acid sequences in our studies indicate that amino acid changes in the basic region, N-proximal Y residues and PAK binding site increase over time in both lymph nodes and all regions of the CNS (data not shown). Nef sequences from the CNS appear to accumulate an increased number of amino acid changes in the AP interaction site over time, compared to sequences from the lymph nodes. These changes suggest that a number of Nef functional motifs adapt to enhance the replicative potential of the virus in the CNS and that Nef may plays an important role in driving SIVsmmFGb compartmentalization. Analysis of intra-tissue temporal compartmentalization by Mantel's test was not feasible given the number of sequences and software limitations.

At one wpi, negative selection contributed to *nef* and *int* compartmentalization, while positive selection was a factor in *env* V1 region segregation (499). We expected that positive selection on the *env* V1 region sequences would increase over time, with selection for increased co-receptor usage and adaptive immune pressure selecting for escape mutants. Given the conserved functions of *nef* (364-367), we expected the resistance of this gene to mutation would overcome selective pressures for escape

mutants, and that negative selection would continue. Similarly, given the tendency of *int* to evolve slowly and resist amino acid changes (479), we expected negative selection on that gene to continue. The d_S /d_N values for sequences harvested at two mpi confirmed that positive selection of *env* V1 region, and negative selection of *nef* and *int*, continued over the course of infection. The strength of positive selection on *env* V1 region sequences increased over time in most tissues, based on lower mean d_S /d_N values at two mpi compared to one wpi (499). Conversely, the strength of negative selection on *nef* and *int* sequences increased over time in most tissues, based on increased mean d_S /d_N values at two mpi compared to one wpi (499). Although preliminary analysis suggests that *nef* accumulates mutations in certain functional motifs (data not shown), there may be enough purifying selection on other domains to cause an overall increase in negative selection.

Changes in the mean d_S value are affected by the frequency of silent synonymous mutations, while d_N is affected more by the nonsynonymous substitutions induced by selective pressure (505, 506). If both the mean d_S and mean d_N value are highest at two mpi, this suggests the general rate of mutation of a gene increases over the course of infection, likely resulting from external selective pressures, such as the immune response, and factors intrinsic to the virus, such as generation time and replication fidelity. Increases in both mean d_S and mean d_N from one wpi to two mpi occurred for *env* V1 regions from the midfrontal cortex and lymph nodes, *nef* sequences from the cerebellum and hippocampus and *int* sequences from the basal ganglia and cerebellum (499). If sequences have a higher mean d_S value and lower mean d_N value at two mpi than one wpi, this indicates that silent mutations increase over the course of infection, with

reduced accumulation of amino acid changes. This suggests that evolution is influenced more by factors intrinsic to the virus than external selective pressure. This pattern appeared for *env* V1 region sequences in the hippocampus; *nef* sequences in the axillary lymph node and midfrontal cortex; and *int* sequences in the midfrontal cortex, hippocampus and mesenteric lymph node (499). A higher mean d_N value at two mpi compared to one wpi, but lower mean d_S, suggests an increased rate of amino acid substitutions over time, while the rate of silent mutation declines. In this situation, which occurred in basal ganglia-derived *env* V1 region sequences (499), evolution is influenced more by external selective pressure. Finally, decreased mean d_S and d_N values at two mpi, compared to one wpi, indicate evolution is due to a combination of intrinsic and extrinsic factors, but the general rate of mutation is lower. Decreases in both d_S and d_N occurred in *env* V1 region sequences from the cerebellum, *int* sequences from the axillary lymph node and *nef* sequences from the basal ganglia and mesenteric lymph node (499).

We also expected an increase in functional differences between *env* V1 regions harvested from the CNS and the lymph nodes, given expected variance in selective pressures between the CNS regions and the lymph nodes. At two mpi, most inter-tissue comparisons had some variation in mean d_S or d_N, suggesting functional differences between *env* V1 regions from different tissues. The number of inter-tissue comparisons with a significant difference in mean d_S, d_N or both increased at two mpi, compared to one wpi (499), suggesting that *env* V1 regions in the various compartments gained functional differences as infection progressed. At two mpi, most inter-tissue comparisons of *nef* sequences had differences in either d_S or d_N, suggesting variations in *nef* function between tissues. Compared with the results at one wpi (499), this suggests differences in

nef function between compartments develop over the course of infection. At two mpi, variations in mean d_N were noted in the majority of *int* inter-tissue comparisons, suggesting functional differences between certain tissues. An overall net loss of functional differences in *int* between tissues was noted by two mpi, compared to one wpi (499).

While our study did not specifically analyze the immune responses of the infected animals to SIVsmmFGb, the host adaptive immune response may potentially have some role in the evolution of the viral genes analyzed in this study. In studies with other SIV and HIV strains, CD8+ T cells are known to infiltrate the CNS (199) and can respond to Nef and Int proteins (507), as well as epitopes within the Env V1 region (508). Relative to protein length, Nef elicits the greatest CTL response of the three genes considered in this study, while responses to Int and the Env V1 region are comparatively moderate and low, respectively (507, 508). The high mutation rate and variability of the *env* gene can alter Env CTL epitopes, making the CD8+ T cell response less effective, over time, than against less variable proteins such as Nef and Int (509). If CD8+ T cells play a similar role in the response to SIVsmmFGb in the CNS, then we might expect the evolution and compartmentalization of all three genes analyzed in this study to be partly due to differences in CTL activity in different regions of the brain. Unlike Int and Nef, however, the Env protein also induces neutralizing antibodies (196, 509, 510), particularly the V1 region (343, 486). Although the BBB normally blocks antibody entry into the CNS, Env can damage this barrier (195) and allow extravasation of serum proteins, including IgG (193, 194). While prior studies have demonstrated that plasma levels of anti-SIV p27 antibody have a negative correlation with SIVsmmFGb viral load

in the CNS upon progression to neurological disease (3), it is currently unknown what role Env-specific antibodies might play in SIVsmmFGb neuropathogenesis. The early appearance of humoral responses to other SIV strains (196, 197), and the efficacy of these responses against other macrophage-tropic viral strains (198), suggest antibodies may be involved in adaptive immunity in the CNS. If SIVsmmFGb elicits similar antibody responses to other SIV strains, we might expect the humoral response to play a role in *env* V1 region evolution in the CNS. Future studies may be necessary to analyze the cellular and humoral immune responses to SIVsmmFGb in the CNS and determine how these responses correlate with the evolution and compartmentalization of viral genes. Of particular interest would be to compare immune responses and sequence evolution between SIVsmmFGb-infected animals with different rates of disease progression, as well as the rare animals that do not develop neuropathogenesis. This may allow for the determination of host- or virus-specific factors that influence the development and progression of SIVsmmFGb neuropathogenesis.

Chapter 3

Pairwise Distances Between SIVsmmFGb *env* V1 Region, *nef* and *int* Nucleotide Sequences and Mutations in Functional Domains of Env V1 Region, Nef and Integrase Amino Acid Sequences from the Central Nervous System and Lymph Nodes of Infected Pigtailed Macaques at One Week and Two Months Post-Infection Adapted from Reeve, et al. Unpublished Data.

Results

Comparison of Pairwise Distances of SIVsmmFGb *env* V1 Region, *nef* and *int* Sequences Between and Within Lymph Node Tissues and CNS Regions from Infected Pigtailed Macaques at One Week and Two Months Post-Infection

We calculated the average pairwise distance between sequences from each possible pair of tissues to determine the degree of relation between *env* V1 region, *nef* and *int* sequences. The average pairwise distance for each two-tissue comparison at one wpi was then compared to the same two-tissue comparison at two mpi. For the *env* V1 region, the average pairwise distance between sequences from the axillary lymph node and each region of the CNS increased over time (Fig. 24). Similar results were noted when comparing *env* V1 regions between the axillary and mesenteric lymph nodes, as well as between the mesenteric lymph node and each region of the CNS. When comparing areas of the CNS to each other, the average pairwise distance between *env* V1 regions decreased from one wpi to two mpi. The average pairwise distance between *nef* sequences decreased over time in most two-tissue comparisons (Fig. 25). The exception was the comparison of the cerebellum and mesenteric lymph node, where the mean pairwise distance increased from one wpi to two mpi. Between *int* sequences, the average pairwise distance increased over time in most two-tissue pairs, except the comparison of the basal ganglia and hippocampus (Fig. 26). Across all two-tissue comparisons, *env* V1 region sequences had the greatest average mean pairwise distance at both one wpi (0.049) and two mpi (0.048). The mean average pairwise distance was lowest for *int*, with values of 0.018 and 0.019 at one wpi and two mpi, respectively. We performed all possible statistical comparisons of all the average two-tissue pairwise

distance values at both one wpi and two mpi and found statistically significant differences between most of the values for all three genes (Tables 16 – 18).

We also compared the average pairwise distance of the *env* V1 region, *nef* and *int* nucleotide sequences within each experimental tissue, at one wpi and two mpi, to determine the distance between sequences in each tissue and whether sequences within a tissue become more or less distant over time. For the *env* V1 region, the average pairwise distance between sequences increased over time in the hippocampus and both lymph nodes but decreased in the remaining three regions of the CNS (Figs. 27A and B). The average pairwise distance between *nef* sequences decreased over the course of infection in all tissues except the mesenteric lymph node (Figs. 27C and D). For *int*, the average pairwise distance between sequences decreased from one wpi to two mpi in all tissues except the hippocampus (Figs. 27E and F). The *env* V1 region had the highest mean average pairwise distance value within tissues at one wpi (0.032) and two mpi (0.035), while *int* had the lowest average mean pairwise distance within tissues at both time points (0.014). We performed all possible statistical comparisons of all average intra-tissue pairwise distances, finding significant differences between most of the values for all three genes (Table 19).

Prevalence of Sequences with Mutations in Functional Domains of SIVsmmFGb Env V1 Region, Nef and Int Amino Acid Sequences from the Lymph Nodes and Central Nervous System of Infected Pigtailed Macaques at One Week and Two Months Post-Infection

We also analyzed the Env V1 region, Nef and Int amino acid sequences for changes in the prevalence of mutations in known functional domains. We performed

literature searches to determine important functional motifs in each protein and calculated the percentage of sequences in the SIVsmmFGb stock virus with mutations in these domains. We then determined the proportion of sequences from the lymph node and CNS sequences pools, at both time points, with mutations at these sites.

The Env V1 region stock virus consensus sequence was 57 amino acids long and contained 13 potential OLGs (Fig. 28); we chose to study changes in both sequence length and the total number of OLGs. The stock virus consensus sequence also had three potential NLGs, at positions 39 – 41, 49 – 51 and 64 – 66. We analyzed for any mutations removing an NLG, S-to-T mutations that could change an NLG while leaving it intact and an N49S/T mutation that could shift the second NLG to positions 47 – 49. We also evaluated sequences for an I10S/T mutation, which could potentially produce a new NLG at positions 8 – 10. While most insertions in the Env V1 region consisted of one or more T residues, we also noted a six-amino acid insertion in a number of sequences. This insertion consisted of the residues K-S-P-K-A-E, taking up positions 26 – 31 and flanked by V32A and A33I mutations on the C-terminal end.

The average Env V1 region sequence length and number of OLGs increased over the course of infection in both the lymph node and CNS (Figs. 31A and B, Tables 20 and 21). Both the average sequence length and mean number of OLGs were greatest in the CNS at two mpi, with 58.6 amino acids and 14 OLGs, respectively. The prevalence of the K-S-P-K-A-E insertion also increased over time in the CNS and lymph nodes (Fig. 31C, Table 22). The greatest frequency of K-S-P-K-A-E was in the CNS at two mpi, occurring in 37% of sequences, compared to 22% of sequences in the lymph nodes at that time. The prevalence of mutations removing the NLG at positions 39 – 41 declined in

both sequence pools at one wpi, compared to the stock virus (Fig. 31D, Table 23). By two mpi, the proportion of sequences in the CNS with these mutations returned to levels similar to the stock virus. The proportion of sequences with the first NLG removed was highest in the lymph nodes at two mpi. The prevalence of mutations moving the second NLG decreased in the CNS at two mpi, compared to the lymph node at both time points and the stock virus (Fig. 31E, Table 24). No significant prevalence changes, relative to the stock virus, were noted for I10S/T mutations, mutations removing the second or third NLGs or S-to-T mutations modifying any NLG (data not shown).

Potentially important functional domains and residues in Nef are shown in Fig. 29. Mutations in the basic region increased in the CNS and lymph nodes at one wpi and two mpi, relative to the stock virus, but no differences were noted between the lymph node and CNS pool at or between time points (Fig. 32A, Table 25). The prevalence of mutations in the N-proximal Y residues increased in both pools at one wpi and remained stable in the CNS, but increased further in the lymph nodes from one wpi to two mpi (Fig. 32B, Table 26). The proportion of sequences with one or more mutations in the acidic region decreased from stock virus levels in the CNS and lymph nodes at both time points (Fig. 32C, Table 27). While the proportion of sequences with changes in this region remained stable in the CNS, these mutations declined in the lymph nodes over time. By one wpi, the prevalence of sequences with mutated thioesterase binding sites increased in the CNS and lymph node, compared to the stock virus (Fig. 32D, Table 28). While the proportion of sequences in the CNS with these mutations increased further by two mpi, the frequency declined in the lymph node. The proportion of sequences with mutations in the AP interaction site increased by one wpi in both the CNS and lymph

nodes (Fig. 32E, Table 29). By two mpi, the prevalence of mutations in this domain declined in the lymph nodes, but continued to increase in the CNS. No significant difference in the frequency of mutations, relative to the stock virus, was noted in the myristoylation, CD4 downregulation, P-rich, PAK-binding, V1H or MHC-1 downregulation sites (data not shown).

Potentially important residues and domains of the Int protein are noted in Fig. 30. The flexible loop in the active site saw a decreased frequency of mutations by one wpi in the CNS and lymph node, relative to the stock virus (Fig. 33, Table 30). The proportion of these mutations was stable over time in the lymph node, but continued to decline in the CNS. No significant changes in the prevalence of mutations, relative to the stock virus, were noted in any other Int domain (data not shown).

Prevalence of Specific Mutations in Functional Domains of SIVsmmFGb Env V1 Region, Nef and Int Amino Acid Sequences in the Central Nervous System and Lymph Nodes of Infected Pigtailed Macaques at One Week and Two Months Post-Infection

After determining which Env V1 region, Nef and Int functional domains had a significant change in mutation prevalence, we analyzed for which residues were mutated in these domains. For all three genes, we determined the percentage of sequences in the lymph node and CNS sequence pools at one wpi and two mpi, as well as the stock virus, with mutations at each residue, relative to the stock virus consensus sequence. For the Env V1 region, sequence variation clustered mostly around the K-S-P-K-A-E insertion but other peaks of mutation prevalence appeared at positions 13, 24, 46 and 62 (Fig. 34). Most residues in Nef had a low frequency of mutation in all five sequence pools (Fig.

35). The basic region had a number of peaks of mutation frequency, particularly positions 9, 13, 14 and 19. Peaks also appeared at position 28 in the N-proximal Y-residues, position 153 in the thioesterase binding site and position 193 in the AP interaction site. Other peaks of sequence variation, most not associated with any functional motif, appeared at positions 43, 55, 101, 104, 136, 144, 181, 200, 222, 229, 250 and 254. Most residues in Int demonstrated little variation in all five sequence pools (Fig. 36). No peaks of mutation frequency appeared in the flexible loop in the active site, but residues with a relatively high proportion of mutations appeared at positions 52, 59, 60, 202, 260 and 377.

A mutation in N39 or S41 could potentially remove the first NLG in the Env V1 region. While no significant changes in the prevalence of mutations at N39 were noted (data not shown), mutations to S41 were more common in both pools at two mpi, compared to one wpi and the stock virus, with changes most frequent in the lymph node (Fig. 37A, Table 31). The most common amino acid substitution at this site was S41N/Y (Table 51). The proportion of mutations at N49 in the CNS at one wpi was similar to the stock virus, but decreased by two mpi (Fig. 37B and Table 32). In the lymph node, variation at this site remained similar to the stock virus over time. All substitutions shifting the second NLG were N49S, with no N49T mutations noted (Table 51).

Analyzing specific amino acid residues in the Nef basic region demonstrated no significant change in the frequency of mutations at positions 7, 8, 10, 11 and 16 – 18 (data not shown). The percentage of mutations at R13, G14 and K19 increased over the course of infection in the lymph node and CNS (Figs. 38C, D and F, Tables 35, 36 and 38). Mutations in Q9 also increased over time in the lymph nodes, relative to the stock

virus, but remained stable in the CNS after an increase at one wpi (Fig. 38A and Table 33). Mutations in Q12 and G15 increased from the stock virus to one wpi in both sequence pools, but declined again by two mpi (Figs. 38B and E, Tables 34 and 37). The most prevalent mutations were Q9R, Q12R, R13Q, G14R, G15R/K and K19R (Table 51). In the Nef N-proximal Y residues, variation at H28 increased in both the lymph node and CNS over time (Fig. 39A, Table 39). At Y39, the frequency of mutations declined in the CNS and lymph node by one wpi, relative to the stock virus (Fig. 39B, Table 40). By one wpi, the percentage of these mutations in the CNS remained low, but recovered to stock virus levels in the lymph nodes. The most common mutations at these sites were H28Y and Y39C (Table 51).

In the Nef acidic region, no significant changes were noted at position 90 (data not shown), but variation at D89 declined in both the CNS and lymph nodes over time, relative to the stock virus (Fig. 40A, Table 41). The percentage of mutations in D91 and D94 declined in the lymph nodes over time (Figs. 40B and E, Tables 42 and 45). The frequency of mutations at these sites in the CNS declined by one wpi, and then increased somewhat by two mpi. At D92 and E96, the percentage of mutations increased in the CNS by one wpi, but returned to levels below the stock virus by two mpi (Figs. 40C and G, Tables 43 and 47). The proportion of mutations at these sites decreased over time in the lymph nodes. The variation at D93 and D95 declined in both pools by one wpi, followed by slight increases by two mpi (Figs. 40D and F, Tables 44 and 46). The most common changes were E96K and D-to-N mutations at positions 89 and 91 – 95 (Table 51).

In the Nef thioesterase binding site, the prevalence of mutations to I153 increased over time in the CNS, relative to the stock virus (Fig. 41A, Table 48). In the lymph nodes, variation at position 153 increased by one wpi, followed by a decline to below stock virus levels at two mpi. The most common mutation at this site was I153V (Table 51). No significant changes were noted in the proportion of mutations at P154, D155 or positions 190 – 192 and 194 in the AP interaction site (data not shown). At Y193, the prevalence of mutations increased over time in the CNS and by one wpi in the lymph nodes, followed by a decline back to stock virus levels in the lymph nodes by two mpi (Fig. 41B, Table 49). In the CNS, the proportion of the changes to V195 declined by one wpi, and then increased to levels beyond the stock virus by two mpi (Fig. 41C, Table 50). By one wpi, variation in this site in the lymph node was similar to the stock virus, with a slight decline by two mpi. The most common changes at these sites were Y193C and V195M (Table 51).

Discussion

We found that the mean pairwise distance of *env* V1 region sequences increased from one wpi to two mpi between all lymph nodes and the CNS regions, suggesting that *env* V1 regions in the CNS become less closely related to sequences in the lymphoid tissues over time. As productive infection is suppressed after three wpi in the CNS, but not the periphery (79, 174), the *env* V1 region should face more exposure to selective pressure in the lymph nodes, driving nucleotide changes that increase the pairwise distance between these tissues and the CNS. Conversely, the average pairwise distance of *env* V1 regions decreased between regions of the CNS, suggesting that sequences from different areas of the brain become more closely related as infection progresses. Similar

selective pressures on the *env* V1 region may be present throughout the CNS during replication from one to three wpi, causing the *env* V1 regions in different brain areas to evolve in a similar manner. The average pairwise distance of *env* V1 regions increased over time between the axillary and mesenteric lymph nodes. As the rate of virus replication should be high in both lymph nodes (444), we might expect rapid evolution of the *env* V1 region populations in each of these tissues. Minor differences in selective pressure between lymph nodes could then result in populations becoming less related over time, even with similar rates of virus replication and the potential for exchange of viruses between lymph nodes.

For *nef* sequences, the mean pairwise distance decreased between most tissues over the course of infection. This coincides with our expectations, as mutated *nef* genes should generally have decreased fitness and be selected against, causing the *nef* populations in each tissue to become more closely related over time. These results also fit with our previously reported data showing that negative selection on *nef* increases over the course of infection (499). Purifying selection should drive *nef* sequences towards a consensus sequence, resulting in populations in different tissues that are more closely related over time.

Against our expectations, the average pairwise distance between *int* sequences from most tissues increased over the course of infection, suggesting that *int* genes from different tissues become less related over time. As this gene is highly conserved and resistant to mutation (478, 479), we might expect the average pairwise distance of *int* sequences to decrease between tissues over time. Our previous results, demonstrating increased purifying selection on the *int* gene over time (499), further indicate these

sequences should develop towards a similar sequence in all tissues. However, certain regions of *int*, particularly the C-terminal domain, are somewhat more variable than the rest of the protein (415, 511). Given the conservation of the rest of *int*, a small number of mutations in this area may cause significant changes in the average pairwise distance between tissues. Our previous studies indicated that *int* has a much higher d_S than d_N, and that d_S increases in most tissues over time (499). Synonymous substitutions could alter the *int* nucleotide sequence, and increase the pairwise distance between tissues, while not affecting the amino acid sequence or selection on the protein (505). Of the three genes studied, *int* has the lowest average mean pairwise distance between tissues at both time points, as well as the least amount of change in average pairwise distance from one wpi to two mpi for any given two-tissue comparison. Therefore, between any two tissues, the *int* sequences remain the most closely related of the three genes studied.

Our analyses of the average pairwise distances between nucleotide sequences within the same tissue demonstrated that *env* V1 regions within each lymph node become less related over time. This may be expected, as the high levels of viral replication in these tissues, and continued exposure to host immune responses, should lead to increased changes in nucleotide sequence over time. Conversely, *env* V1 regions within most of the individual CNS regions became more closely related over time, suggesting that selective pressures in each region of the CNS vary little from one wpi until the suppression of replication. In this case, it would be advantageous for the *env* V1 region to evolve towards a consensus sequence that can avoid these selective pressures until the onset of suppression. For *nef*, the average pairwise distance between sequences within each tissue decreases over the course of infection in the majority of tissues. Once again,

this is likely due to less fit, mutated *nef* genes being out-competed by genes with fewer mutations. The mean pairwise distances between *nef* sequences within a tissue are lower than for the *env* V1 region, suggesting that *nef* genes are generally more closely related than *env* V1 region genes in the same tissue. For *int*, the mean pairwise distance between sequences within each tissue decreased over time in most tissues, suggesting these sequences become more closely related within a tissue over time. This may be due to increased negative selection, as detected in our previous studies, with mutated sequences out-competed by wild-type genes. Over time, sequences within each tissue may converge towards a consensus sequence that is slightly different from that in other tissues, perhaps leading to *int* genes from different tissues becoming less related. The average pairwise distance between *int* sequences within a tissue is the lowest out of all three genes studied, coinciding with our expectations that *int* sequences should remain much more closely related than *nef* or the *env* V1 region.

Our results demonstrated an increase in the average length, and number of OLGs, in the Env V1 region over time, with the greatest length and number of OLGs present in the CNS at two mpi. As increased Env V1 region length and glycosylation can allow for evasion of neutralizing antibody responses (335, 338, 348, 355), these changes may be the result of viral adaptations to host immune responses. Additionally, increased Env V1 region length increases R5-tropism and selects against utilization of alternate co-receptors (335, 338). As most target cells in the CNS are monocyte-lineage (70, 104, 113, 122-125), CCR5 is the primary viral co-receptor in the brain and highly R5-tropic strains should have a selective advantage. We also found a K-S-P-K-A-E insertion that lengthens the V1 loop by six amino acids, which may reduce recognition of this region by

neutralizing antibody and improve binding to CCR5. The S residue in this motif may also be an OLG, potentially increasing glycosylation and improving escape from neutralizing antibody, which could prove beneficial to replication in the lymph nodes. The P residue in this motif may significantly affect the V1 loop structure (512, 513), which could contribute further to escape from antibody recognition.

We also found the prevalence of mutations removing the first NLG decreased by one wpi in the lymph nodes and CNS, and then rebounded by two mpi. N-linked glycosylation can allow the Env V1 region to avoid antibody recognition (335, 347), so removal of the first NLG may initially be selected against to allow evasion of the early neutralizing antibodies. However, as host responses adapt, the first NLG may become a target for antibody recognition and viruses with mutations that remove this site may have a selective advantage. The increased presence of neutralizing antibody responses in the lymph nodes, compared to the CNS, may explain the higher proportion of mutations removing the first NLG in the lymph nodes at two mpi. The increase in mutations at this site was likely due to S41N/Y substitutions. As N and Y are both hydrophilic-neutral (514), replacing S with either of these amino acids could abrogate the NLG while still preserving the Env V1 region structural stability. The frequency of mutations moving the second NLG decreased in the CNS at two mpi, relative to all other sequence pools, suggesting that N49S is selected against in the CNS. One possibility is that moving the second NLG may negatively impact Env V1 region loop stability or co-receptor binding. As this mutation also changes the protein glycosylation profile, the selective pressure from high levels of antibody in the periphery may allow these mutations to persist in the

lymph nodes. However, no selective benefit would be present with the limited antibody responses in the CNS and strains with this mutation could be at a disadvantage.

Although not within any of the structural domains we studied, the frequency of mutations at position 24 in the Env V1 region declined by one wpi in both the CNS and lymph node but rebounded to levels greater than in the stock virus by two mpi. The most common mutation is I24T, potentially adding an OLG, which may allow evasion of host immune responses (355). Mutations at positions 13, 46 and 62 increased over the course of infection, suggesting selection for mutations at these sites. The T residue at position 13 is a potential OLG, but perhaps glycosylation at this site may be selected against due to negatively impacting structural stabilities or co-receptor binding. The most common mutation at this site is T13P (data not shown), and the addition of a P residue may alter the structure of the Env V1 loop sufficiently to allow escape from immune responses. The mutation E46S exchanges a hydrophilic charged amino acid for a hydrophilic neutral amino acid, while the K62R mutation exchanges two basic, charged amino acids (data not shown) (514). Both of these positions are proximal to an NLG site and mutations may alter recognition of the NLG by host antibody.

The percentage of Nef sequences with mutations in the basic region is elevated in all experimental sequence pools, relative to the stock virus. This is likely due to changes in multiple sites, as mutations in positions 9, 13, 14 and 19 increased in both the CNS and lymph nodes over time. The Q9R, R13Q and G14R mutations yield a net gain of one basic residue, while the K19R mutation introduces an R side chain, which has an increased pKa compared to K. The basic region is required for Nef association with cellular membranes, possibly by interacting with acidic phospholipids in the inner leaflet

of the membrane (515). Increased basicity of this region may strengthen the interaction of Nef with cellular membranes, perhaps improving the efficiency of Nef functions. However, the frequency of mutations at other sites in the basic region generally decreased over time, likely balancing out the increase in mutations at positions 9, 13, 14 and 19, causing the overall prevalence of sequences with at least one mutation in this region to remain stable from one wpi to two mpi. The Q12R and G15R mutations should also increase the basicity of the basic region, and are more prevalent in both the CNS and lymph node by one wpi, but appear to be selected against by two mpi. The percentage of mutations at positions 7, 8, 10, 11 and 16 – 18 also declined in the lymph node and CNS after one wpi (data not shown). Mutations at these sites may potentially be deleterious to the structure of Nef, off-setting any gain in function provided by increased basicity.

The proportion of Nef sequences with at least one mutation in the N-proximal Y residues increased over time in both the CNS and lymph node, peaking in the lymph node at two mpi; a similar pattern appeared for the H28Y mutation. This substitution makes the region spanning amino acids 28 – 42 resemble the canonical sequence of an ITAM, YXXL/I(X_{6-8})YXXL/I (516), potentially allowing the protein to interact with cell signaling pathways more efficiently and improving Nef function. Mutations generating an ITAM in Nef may be particularly important in the lymph nodes, where most target cells are T lymphocytes (517). An ITAM could allow the virus to more efficiently hijack T cell signaling pathways, improving viral replication in these cells. The prevalence of a Y39C mutation, making the region less similar to an ITAM and potentially reducing Nef function, was at or below stock virus levels in all pools.

The prevalence of sequences with one or more mutations in the Nef acidic region declined from the stock virus to one wpi in both the CNS and lymph nodes. While the frequency of these mutations then increased slightly in the CNS, they continued to decrease in the lymph nodes. Mutations in positions 89, 91, 92, 94 and 96 declined over time in the lymph nodes, offset by slight increases in the frequency of mutations in positions 93 and 95 at two mpi. In the CNS, decreases in the proportion of mutations in positions 91 and 93 – 95 at one wpi were followed by slight increases in the mutation rate at these sites by two mpi. Mutations in the acidic region are likely selected against, given the number of Nef functions that involve this region. However, the proportion of sequences with one or more mutations in the acidic region is higher than expected, with over 30% of sequences having at least one. Most sequences with acidic region changes only had one residue mutated (data not shown), which suggests SIVsmmFGb Nef may tolerate single mutations in this region without significant loss of function. The most common mutation at positions 89 and 91 – 95 was D-to-N, exchanging a hydrophilic charged amino acid for a hydrophilic uncharged amino acid which is structurally similar. Perhaps only one of these substitutions does not significantly disrupt the acidic region structure or function.

The proportion of sequences with one or more mutations in the thioesterase binding site increased over time in the CNS, but declined by two mpi in the lymph nodes, following an initial increase at one wpi. This was likely the result of an I153V mutation at position 153. The thioesterase binding site may interact with the intracellular domains of CD4 and MHCI, facilitating endocytosis and downregulation of these molecules (518, 519). This region also represents a hydrophobic domain important for oligomerization of

Nef (518). The main functional residue is a D123 in HIV-1, or D155 in our SIVsmmFGb consensus sequence, but the nearby residues also contribute (518). In HIV-1, an F residue is typically present at site 121, suggesting any hydrophobic amino acid is sufficient at this position (518). Therefore, an I153V mutation, exchanging structurally similar hydrophobic amino acid residues (514), may not be expected to impact the function of this motif. However, the declining prevalence of I153V in the lymph nodes from one wpi to two mpi suggests selection against this mutation. While V is slightly less hydrophobic than I, F is even less non-polar (514, 520), so selection against the V mutation is not likely due to decreasing hydrophobicity. Strains with the I153V mutation may potentially be less efficient at downregulation of MHCI or CD4, allowing detection by CD8+ T cells or superinfection, respectively. With continued replication in the lymph nodes through two mpi, viruses with the consensus sequence would out-compete the mutants, reducing the prevalence of these strains in those tissues. In the CNS, the amount of replication may be insufficient to select against these mutants and reduce their prevalence prior to suppression.

The frequency of sequences with at least one mutation in the AP interaction site increased over time in the CNS. In the lymph nodes, the percentage of sequences with these mutations rose by one wpi, but returned to levels similar to the stock virus by two mpi. A similar pattern appeared for the percentage of sequences with the Y193C mutation. While a Y residue is present at position 193 in SIVmac239, a number of HIV-1, HIV-2 and other SIV strains have a C residue at this site (361, 386). As this site does not specifically interact with the adaptor proteins (386), the functional significance of any particular residue at this location is unknown. Structurally, Y is a more bulky side chain,

which may interfere with Nef binding to the adaptor proteins (514). The prevalence of a V195M mutation in the AP interaction site declined in the lymph nodes over time but increased by two mpi in the CNS, following a slight decline by one wpi. This site interacts directly with the adaptor proteins and mutations could reduce the efficacy of Nef downregulation of cell surface receptors (386). The AP interaction site merely requires a hydrophobic residue at position 195, so M may be sufficient to allow some activity (521). However, V is much more hydrophobic and may be required for the most efficient function (520). In the CNS, virus replication is limited even prior to viral suppression, so sequences with a partially functional thioesterase binding site may still accumulate in the population, rather than being entirely out-competed. Another possibility is that V195M may be beneficial in monocyte-lineage cells, providing an advantage in the CNS, but may be deleterious in T cells, leading to selection against these sequences in the lymph nodes.

As expected, little variation was noted for Int, as the only motif with a significant change in variation compared to the stock virus consensus was the flexible loop in the active site. In this domain, the percentage of sequences with mutations declined over time in the CNS, and from the stock to one wpi in the lymph nodes, indicating selection against changes in the flexible loop. No specific residue in the flexible loop saw a significant decline in the frequency of mutations over time, suggesting the overall reduction in flexible loop variation was a cumulative effect of lower variability in all residues in this domain. Unexpectedly, a large increase in mutations at residue 377, relative to the stock virus, appeared in all lymph node-derived sequences, and most CNS-derived sequences, at one wpi. Variation at this site had decreased by two mpi, but remained elevated relative to the stock virus. Virtually all changes at this site are S377P.

As P can significantly alter protein structure (512, 513), this mutation may introduce some structural benefit that improved replication at one wpi. However, if this site is within a T-cell epitope, the mutation may have been selected against by host adaptive immune responses, accounting for the decline at two mpi. Alternatively, as this residue is in the more variable C-terminus of the protein (415, 511), it may simply be an epicenter of variation.

While these results indicate residues that are commonly mutated and changes in prevalence of mutations over time, future studies will be needed to determine the functional effects of these mutations. For Env V1 region, we are interested in performing functional assays to determine the effect of the K-S-P-K-A-E insertion, S41N/Y and N49S mutations on co-receptor usage and target cell entry in lymphocyte- and monocyte-lineage cell lines, as well as primary macaque lymphocytes, macrophage and microglia. We would also analyze changes in the sensitivity of our Env V1 regions to neutralizing antibody. It would not be feasible to select full-length SIVsmmFGb *env* clones for further study based solely on the V1 region sequence, as there may be functionally significant changes to other sites in the *env* sequence that do not appear in our current analyses. Sequencing full-length *env* genes for all clones in our studies would overcome this obstacle and is being planned in our laboratory. Alternatively, we could insert our *env* V1 regions into a defined *env* background, such as SIVmac239, to study the function of the SIVsmmFGb Env V1 region alone. We aim to study the function of the SIVsmmFGb stock virus consensus *env* V1 region, as well as sequences from clones harvested from the lymph node and CNS at one wpi and two mpi. In addition, site-directed mutagenesis could allow us to specifically introduce the K-S-P-K-A-E insertion,

S41N/Y, N49S and/or other mutations into the SIVsmmFGb Env V1 region consensus sequence to study the effect of these changes.

For Nef, we are most interested in analyzing the effect of mutations on the downregulation of cell surface receptors and interaction with cell signaling pathways. A number of Nef expression vectors are available into which we could clone the SIVsmmFGb stock virus *nef* consensus sequence. Site-directed mutagenesis could then be used to introduce one or more of the mutations discussed above, after which the function of these mutants could be compared to that of the SIVsmmFGb stock consensus *nef* sequence. By this method, we could determine the specific residues responsible for beneficial or deleterious changes in the Nef functional domains discussed here. Of particular interest is comparing the function of SIVsmmFGb Nef mutants in lymphocyte- and monocyte-derived cell lines, as well as primary macaque lymphocytes, macrophage and microglia. This would allow us to determine whether certain Nef mutations have varying effects on function in lymphocytes as opposed to monocyte-lineage cells. Not only would this analysis explain selection for and against certain mutations in the CNS, but it may also reveal mutations that are potentially important for inducing neuropathogenesis.

Conclusions

In the first of our studies, we confirmed the quasispecies nature of the highly neuropathogenic primate lentivirus SIVsmmFGb and provided valuable characterization of the *env* V1 region, *nef* and *int* genes. We demonstrated that virus seeding of the CNS and lymph nodes at one wpi decreases Env V1 region and Int diversity in the pigtailed macaque host. We have shown that the *env* V1 region compartmentalizes separately in different areas of the CNS compared to the lymph nodes, partially due to selective pressure. We also illustrated that *nef* and *int* compartmentalize in most experimental tissues due to negative selection. These results, with a neuropathogenic SIV swarm in a primate host, provided insight into viral genetics during seeding of the CNS and may be a valuable model of a comparable process in HIV neuropathogenesis.

In our second study, our results revealed the effect of replication and evolution on diversity and compartmentalization of the SIVsmmFGb swarm in the pigtailed macaque lymph nodes and CNS. Our data suggest that viruses evolving in different regions of the CNS may vary in their potential to induce neuropathogenesis or escape immune responses. In particular, Nef function and diversity differs between areas of the CNS and between the CNS and lymph nodes, suggesting that Nef determines the presence and severity of neuropathogenesis in a given region of the brain. We also found convergent evolution for both *env* V1 region and *nef* between compartments, decreased differences in *env* V1 region and *int* function, as well as evolution of all three genes within CNS regions over time. These results suggest that selective pressure drives SIVsmmFGb strains in all areas of the CNS towards a common phenotype necessary to induce full neuropathogenesis. It is reasonable to expect that HIV may also follow a similar course

of evolution during replication in the brain, and these results may provide insight into that process in human infection with a neuropathogenic lentivirus.

In our third study, we built on our previous results and investigated amino acid changes to SIVsmmFGb Env V1 region, Nef and Int sequences in the CNS and lymph nodes over time. We found *env* V1 regions in the CNS become less related to lymph node-derived sequences over time, but more related to other sequences within the CNS. The *env* V1 regions within each lymph node also became less related, while sequences within each CNS area became more related over time. The average length and number of OLGs, as well as prevalence of a K-S-P-K-A-E insertion, increased in the Env V1 region over time. The *nef* genes between and within tissues became more related over time, with variation in the prevalence of a number of mutations in various functional domains. The *int* sequences became less related between tissues, but more related within each tissue, over time. These results suggest the functions of Env V1 region and Nef change over time in the CNS and lymph nodes. Further study will be required to determine if these mutations truly affect Env V1 and Nef function or interaction with the immune system. These functional changes may be involved in development of SIVsmmFGb neuropathogenesis and could represent alterations in Nef and the Env V1 region in HAD patients. If specific mutations can be linked to neuropathology, studies could screen patient quasispecies for these mutations to determine those at risk of severe or early neuropathogenesis. Mutations within immune epitopes could also potentially be considered for vaccines focused on preventing or ameliorating HIV neuropathology.

Index of Figures[1]

[1] All Figures are based on data generated by the Ph.D. candidate.

Figure 1. SIVsmmFGb stock virus sequence grouping strategy. Amino acid sequences of (A) Env V1, (B) Nef and (C) Int obtained from the stock virus were grouped as described in the Materials and Methods section. Group breakdowns, and clades with greater than 50% bootstrap support, are indicated.

*, Group 1; **, Group 2; ***, Group 3; ****, Group 4.

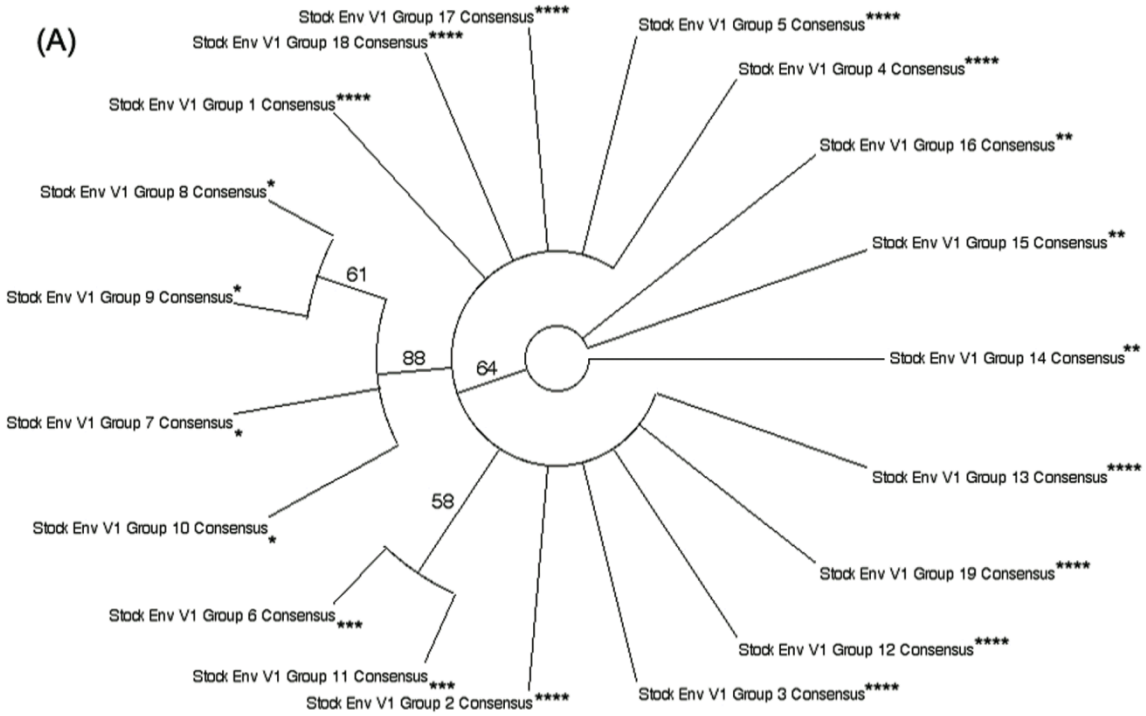

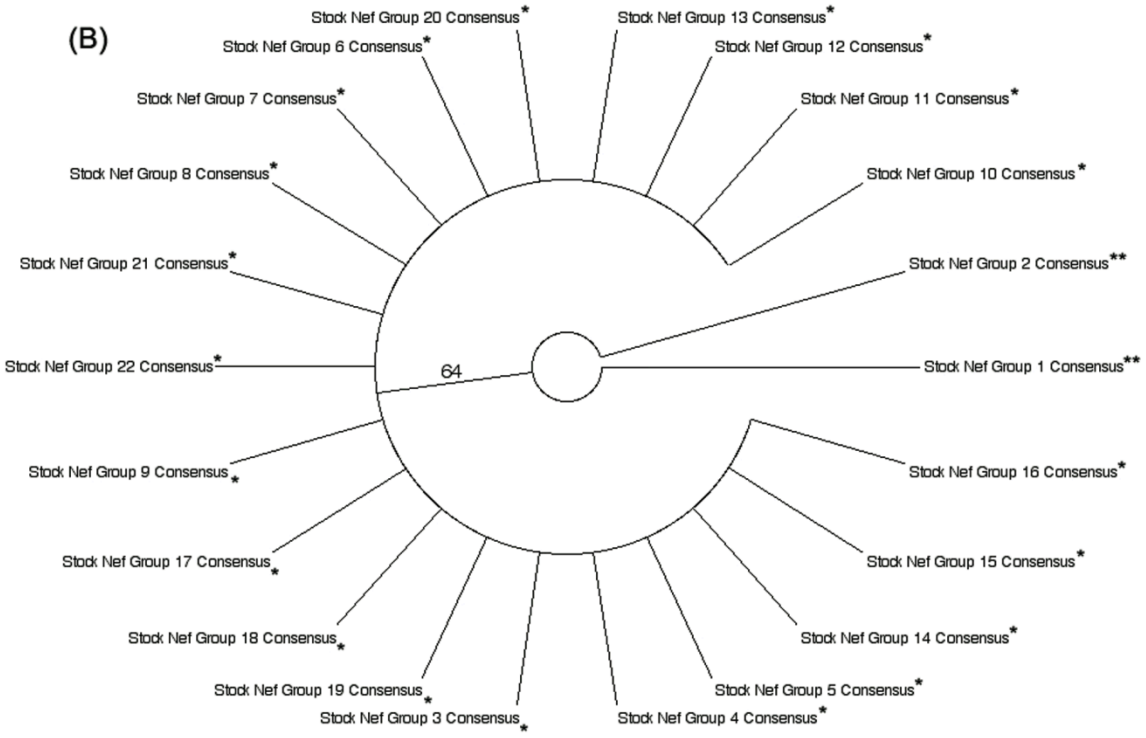
(B)
Stock Nef Group 20 Consensus*
Stock Nef Group 13 Consensus*
Stock Nef Group 6 Consensus*
Stock Nef Group 12 Consensus*
Stock Nef Group 7 Consensus*
Stock Nef Group 11 Consensus*
Stock Nef Group 8 Consensus*
Stock Nef Group 10 Consensus*
Stock Nef Group 21 Consensus*
Stock Nef Group 2 Consensus**
Stock Nef Group 22 Consensus*
64
Stock Nef Group 1 Consensus**
Stock Nef Group 9 Consensus*
Stock Nef Group 16 Consensus*
Stock Nef Group 17 Consensus*
Stock Nef Group 15 Consensus*
Stock Nef Group 18 Consensus*
Stock Nef Group 14 Consensus*
Stock Nef Group 19 Consensus*
Stock Nef Group 5 Consensus*
Stock Nef Group 3 Consensus*
Stock Nef Group 4 Consensus*

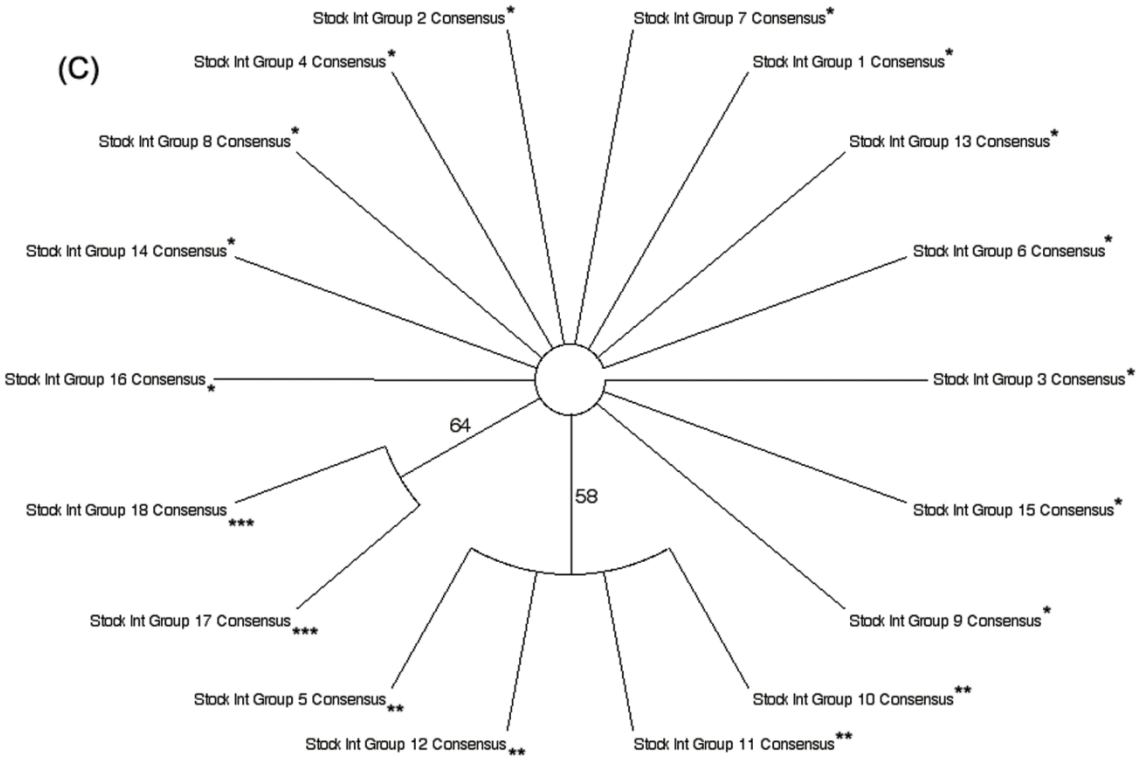
(C)
Stock Int Group 2 Consensus*
Stock Int Group 7 Consensus*
Stock Int Group 4 Consensus*
Stock Int Group 1 Consensus*
Stock Int Group 8 Consensus*
Stock Int Group 13 Consensus*
Stock Int Group 14 Consensus*
Stock Int Group 6 Consensus*
Stock Int Group 16 Consensus*
Stock Int Group 3 Consensus*
64
58
Stock Int Group 18 Consensus***
Stock Int Group 15 Consensus*
Stock Int Group 17 Consensus***
Stock Int Group 9 Consensus*
Stock Int Group 5 Consensus**
Stock Int Group 10 Consensus**
Stock Int Group 12 Consensus**
Stock Int Group 11 Consensus**

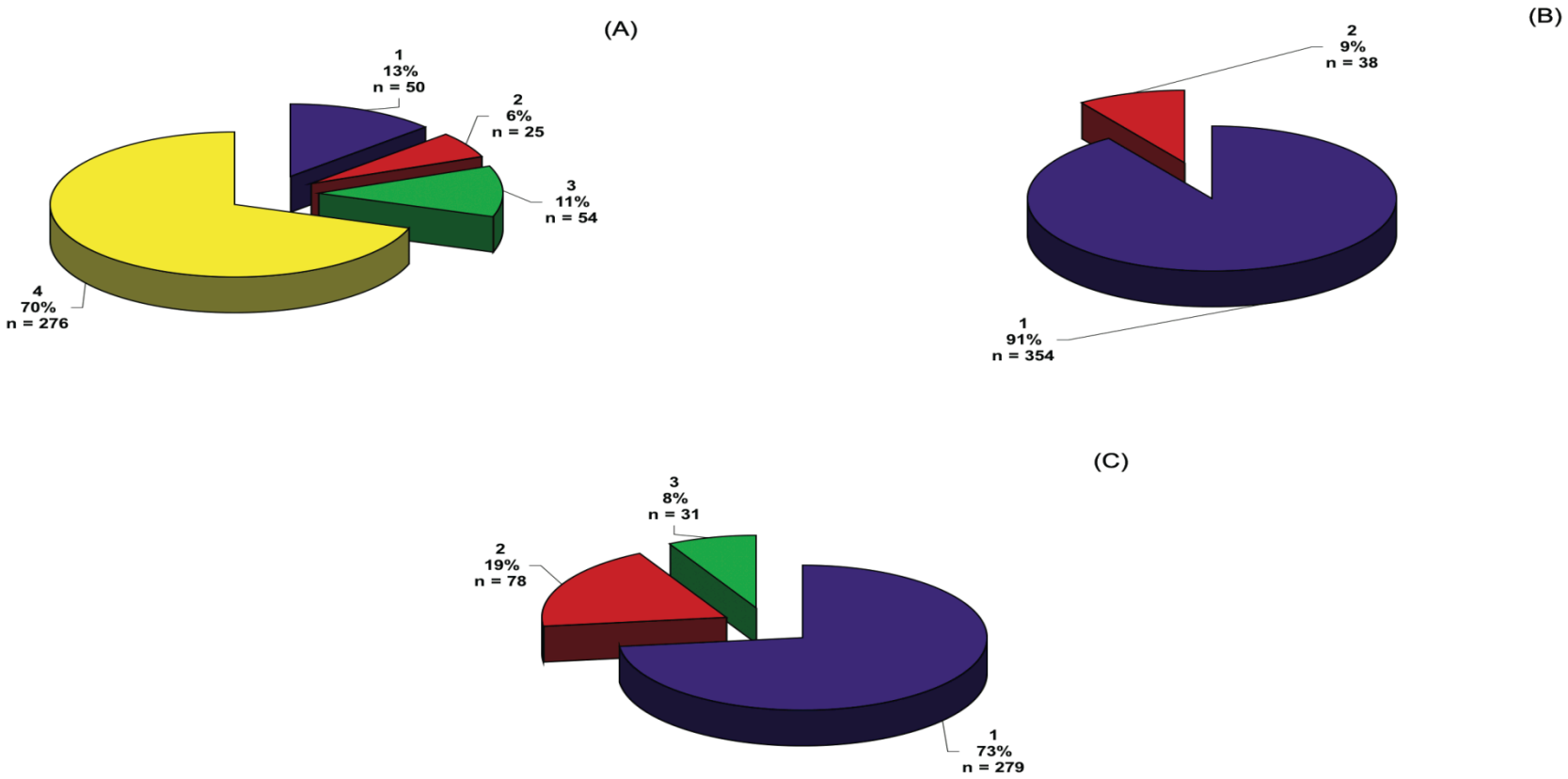

Figure 2. SIVsmmFGb stock virus sequence group composition. Sequences were grouped as described in Figure 1. The number (n) and percentage of amino acid sequences in each group for (A) Env V1 region, (B) Nef and (C) Int are shown.

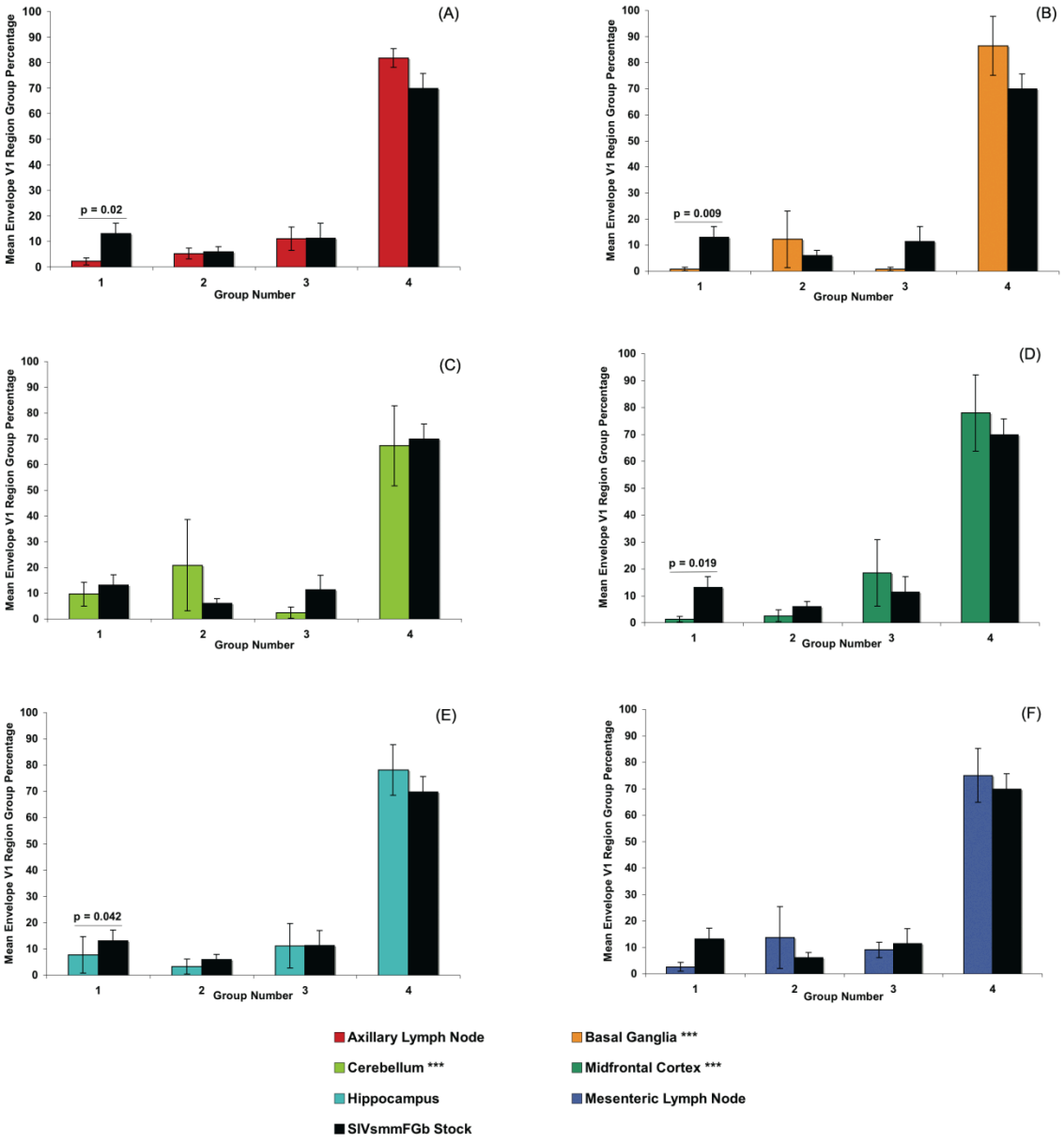

Figure 3. Comparison of Env V1 region group percentages between tissues harvested from infected pigtailed macaques at one wpi and the SIVsmmFGb stock virus. (A) axillary lymph node, (B) basal ganglia, (C) cerebellum, (D) midfrontal cortex, (E) hippocampus and (F) mesenteric lymph node. Statistically significant differences ($p < 0.05$) in the percentage of sequences in each group are noted. Error bars represent one standard error.

***, No Env V1 region sequences obtained from this tissue in animal PQo1.

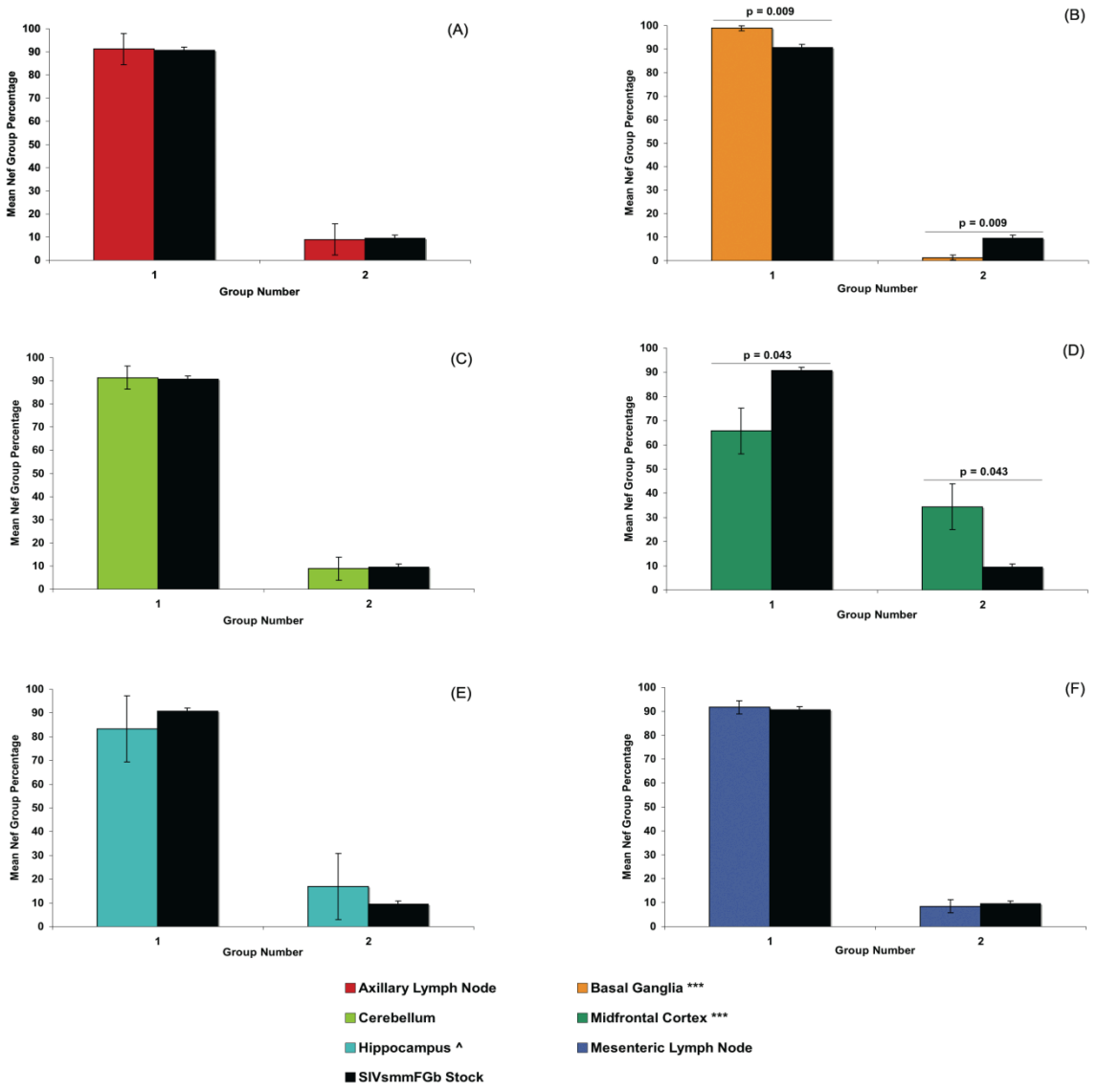

Figure 4. Comparison of Nef group percentages between tissues harvested from infected pigtailed macaques at one wpi and the SIVsmmFGb stock virus. (A) axillary lymph node, (B) basal ganglia, (C) cerebellum, (D) midfrontal cortex, (E) hippocampus and (F) mesenteric lymph node. Statistically significant differences ($p < 0.05$) in the percentage of sequences in each group are noted. Error bars represent one standard error.

***, No Nef sequences obtained from this tissue in animal PQo1.

^, Only 19 Nef sequences obtained from this tissue in animal PQo1.

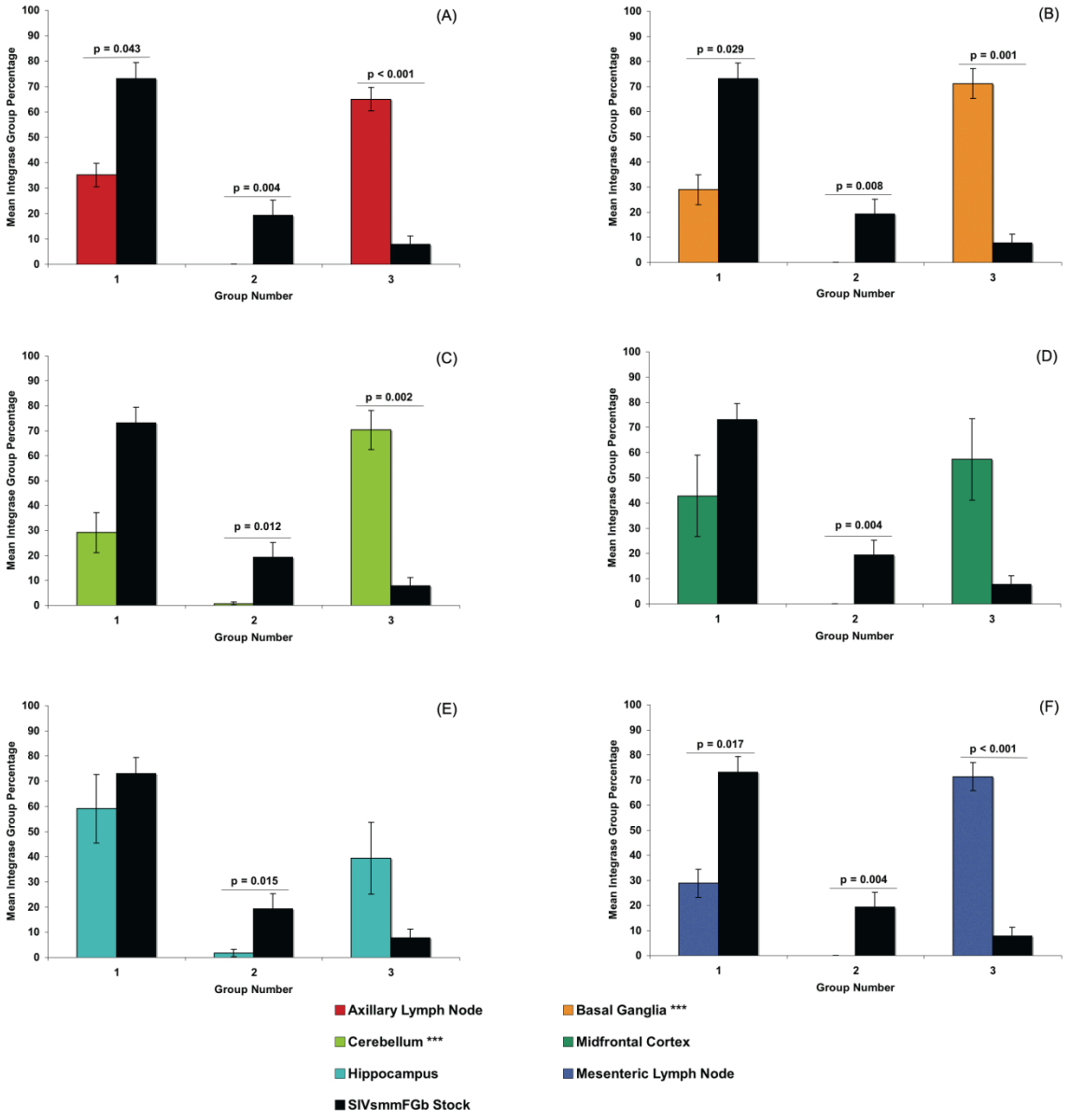

Figure 5. Comparison of Int group percentages between tissues harvested from infected pigtailed macaques at one wpi and the SIVsmmFGb stock virus. (A) axillary lymph node, (B) basal ganglia, (C) cerebellum, (D) midfrontal cortex, (E) hippocampus and (F) mesenteric lymph node. Statistically significant differences ($p < 0.05$) in the percentage of sequences in each group are noted. Error bars represent one standard error. ***, No Int sequences obtained from this tissue in animal PQo1.

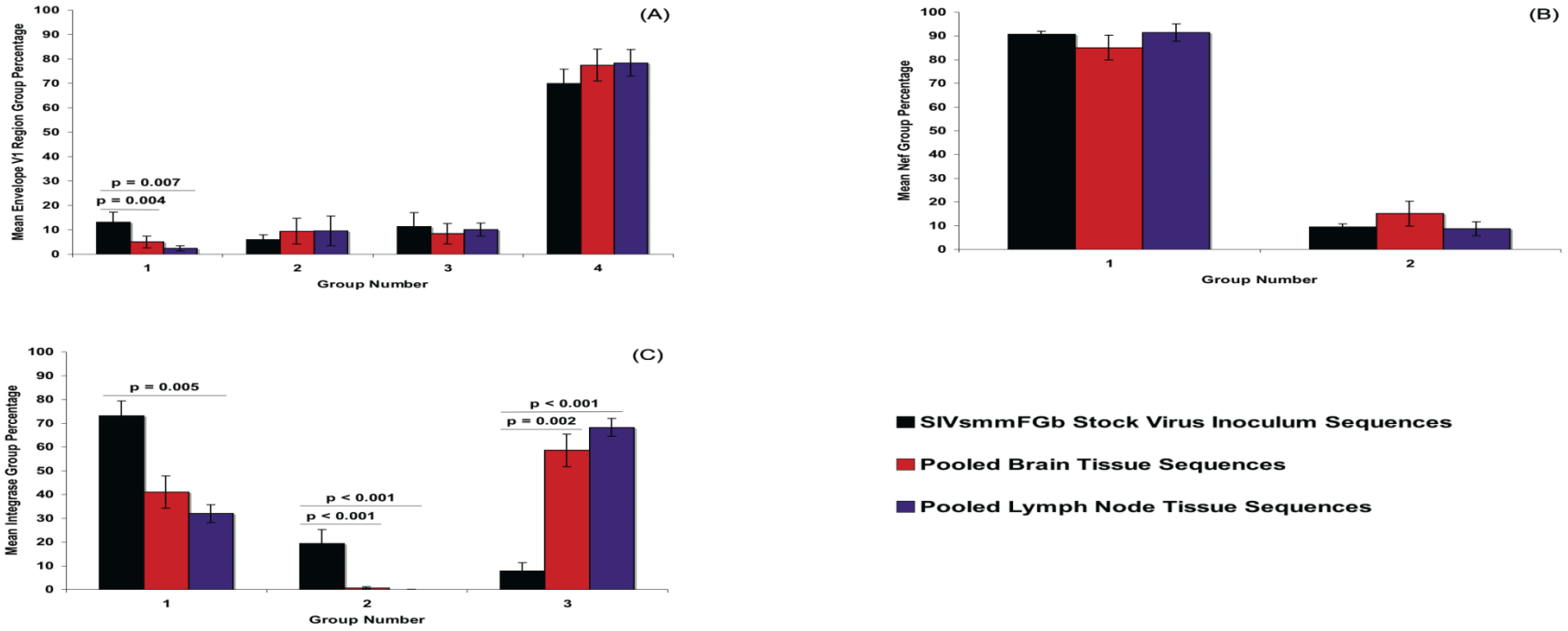

Figure 6. Comparison of sequence group percentages between CNS and lymph node tissues harvested from infected pigtailed macaques at one wpi and the SIVsmmFGb stock virus. Amino acid sequences for (A) Env V1 region, (B) Nef and (C) Int were pooled based on their origin in either the CNS or the lymph nodes. Statistically significant differences ($p < 0.05$) in the percentage of sequences in each group are noted. Error bars represent one standard error. Data is absent from one or more PQo1 central nervous system tissues and only 19 *nef* sequences were amplified from PQo1 hippocampus.

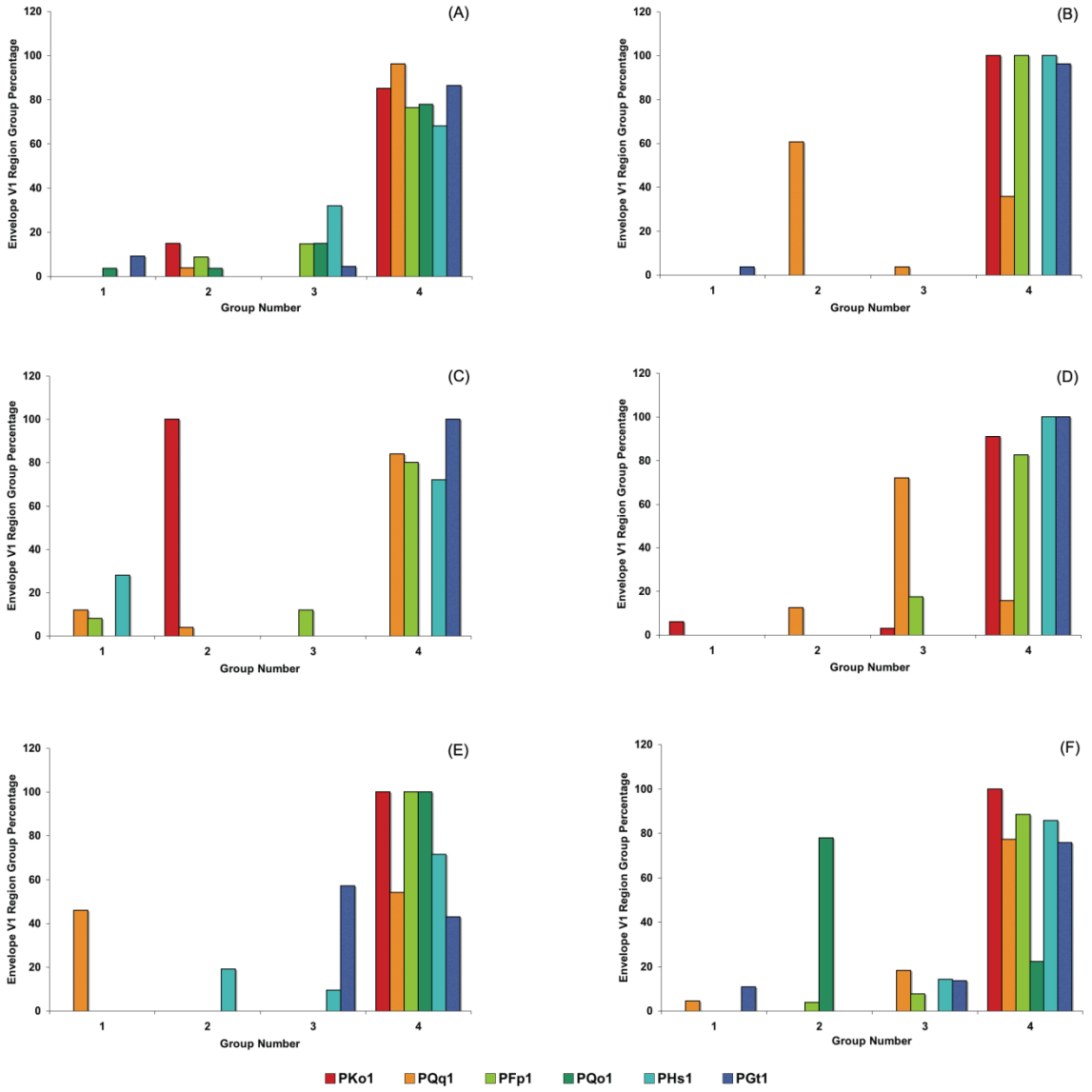

Figure 7. Percentage of Env V1 region amino acid sequences in each sequence group in each SIVsmmFGb-infected pigtailed macaque at one wpi. (A) Axillary lymph node, (B) basal ganglia, (C) cerebellum, (D) midfrontal cortex, (E) hippocampus and (F) mesenteric lymph node. Basal ganglia, cerebellum and midfrontal cortex lack data from PQo1.

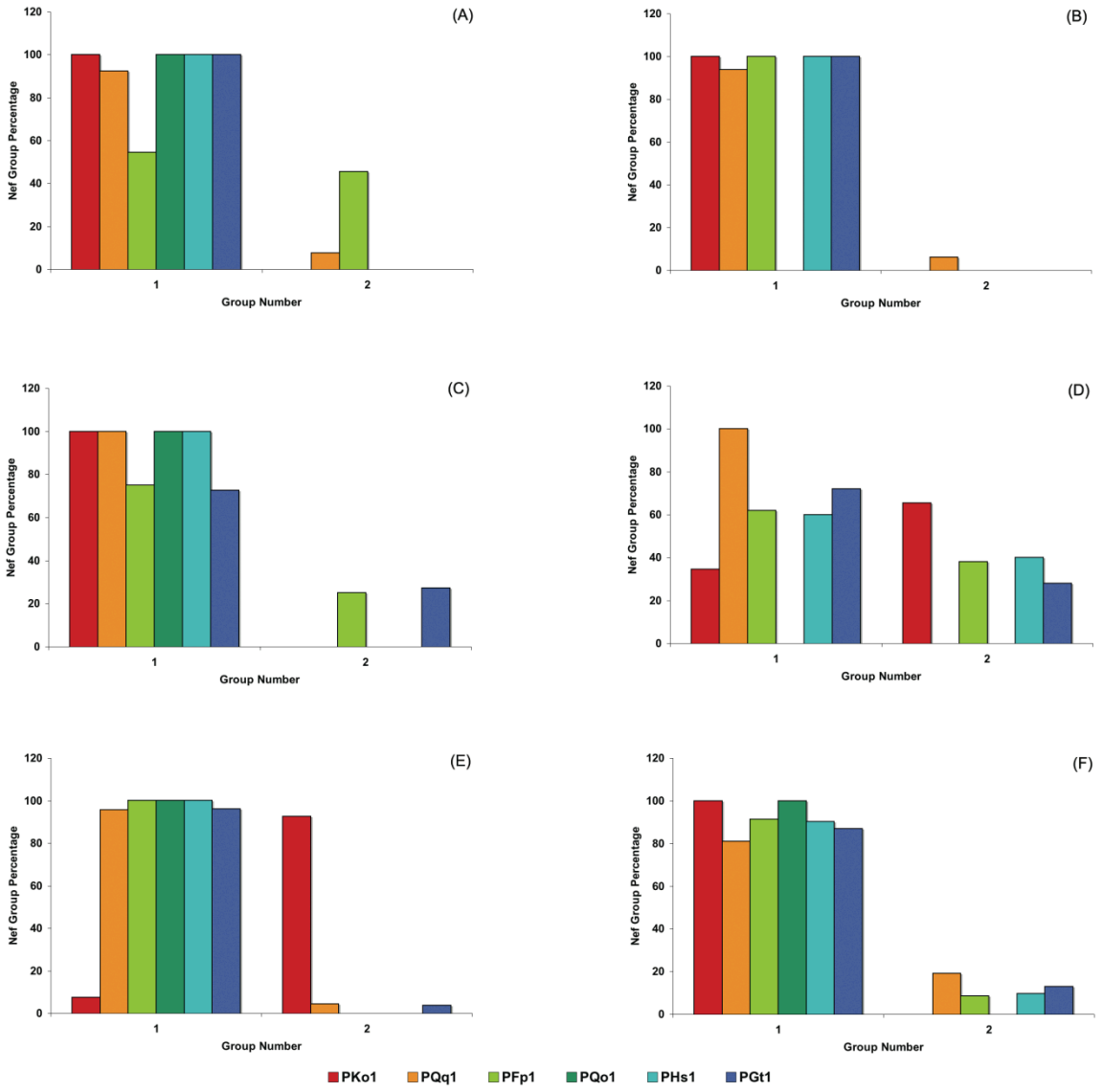

Figure 8. Percentage of Nef amino acid sequences in each sequence group in each SIVsmmFGb-infected pigtailed macaque at one wpi. (A) Axillary lymph node, (B) basal ganglia, (C) cerebellum, (D) midfrontal cortex, (E) hippocampus and (F) mesenteric lymph node. Basal ganglia and midfrontal cortex lack data from PQo1. Only 19 nef sequences were amplified from the hippocampus of PQo1.

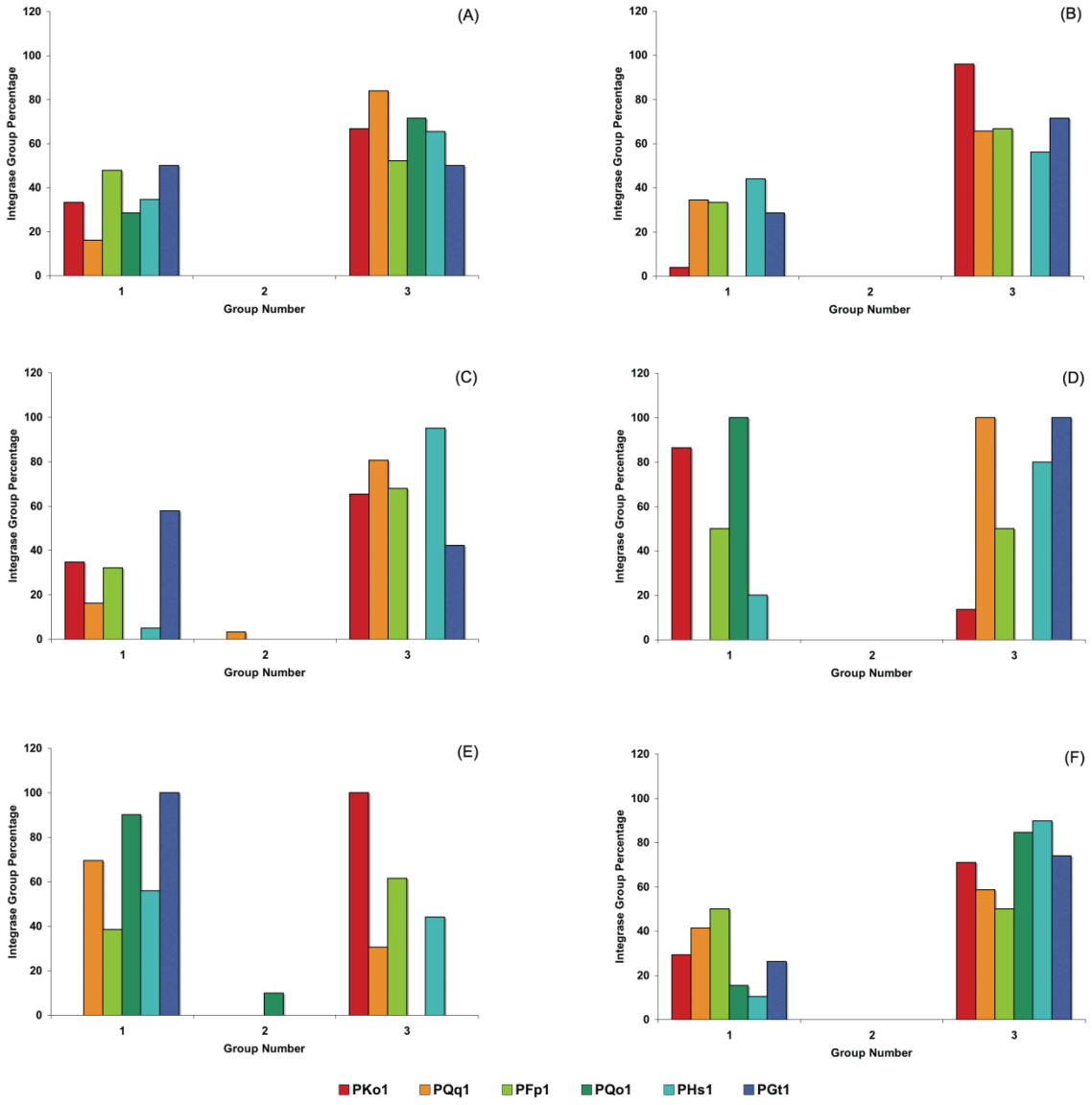

Figure 9. Percentage of Int amino acid sequences in each sequence group in each SIVsmmFGb-infected pigtailed macaque at one wpi. (A) Axillary lymph node, (B) basal ganglia, (C) cerebellum, (D) midfrontal cortex, (E) hippocampus and (F) mesenteric lymph node. Basal ganglia and cerebellum lack data from PQo1.

Figure 10. Phylogenetic analysis of SIVsmmFGb compartmentalization between tissues harvested from infected pigtailed macaques at one wpi. Results of the modified Slatkin-Maddison test for compartmentalization of (A) Env V1 region, (B) Nef and (C) Int amino acid sequences between pairs of tissues are shown. Error bars represent two standard errors of the *S* ratio; significant compartmentalization between tissues is indicated by *S* ratio values more than two standard errors less than 1.

*, Data is absent from one or more PQo1 central nervous tissues.

^, Only 19 Nef sequences amplified from PQo1 hippocampus.

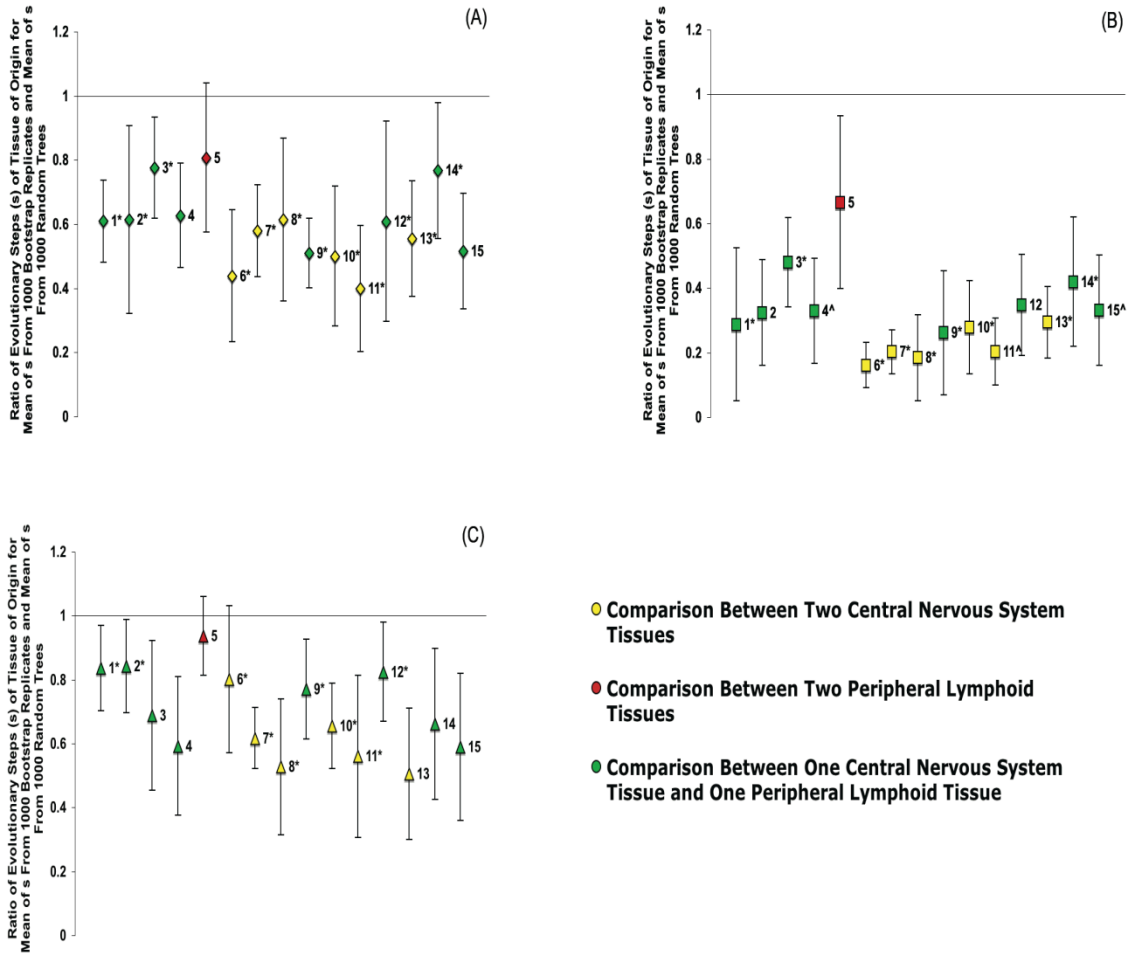

Tissue Comparisons Key	
1	Axillary Lymph Node and Basal Ganglia
2	Axillary Lymph Node and Cerebellum
3	Axillary Lymph Node and Midfrontal Cortex
4	Axillary Lymph Node and Hippocampus
5	Axillary Lymph Node and Mesenteric Lymph Node
6	Basal Ganglia and Cerebellum
7	Basal Ganglia and Midfrontal Cortex
8	Basal Ganglia and Hippocampus
9	Basal Ganglia and Mesenteric Lymph Node
10	Cerebellum and Midfrontal Cortex
11	Cerebellum and Hippocampus
12	Cerebellum and Mesenteric Lymph Node
13	Midfrontal Cortex and Hippocampus
14	Midfrontal Cortex and Mesenteric Lymph Node
15	Hippocampus and Mesenteric Lymph Node

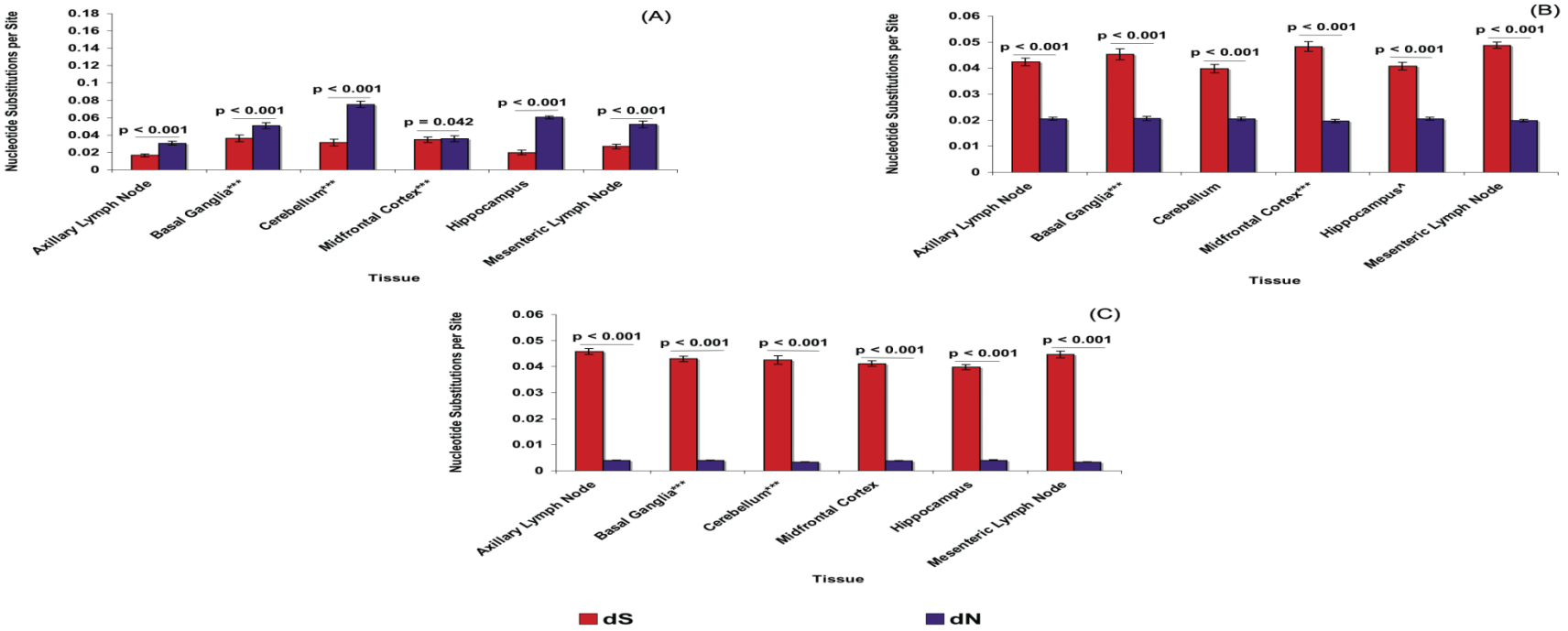

Figure 11. Mean d_S and d_N values for *env* V1 region, *nef* and *int* sequences isolated from tissues of SIVsmmFGb infected pigtailed macaques at one wpi. Average d_S and d_N values of (A) *env* V1 region, (B) *nef* and (C) *int* sequences were determined for each tissue. Error bars represent one standard error. Statistically significant differences ($p < 0.05$) between mean d_S and d_N values within a tissue are noted. The p-values for statistical comparisons of the mean d_S or d_N values between tissues are noted in Table 8.

***, Data is absent from one or more PQo1 brain tissues.

^, Only 19 nef sequences amplified from PQo1 hippocampus.

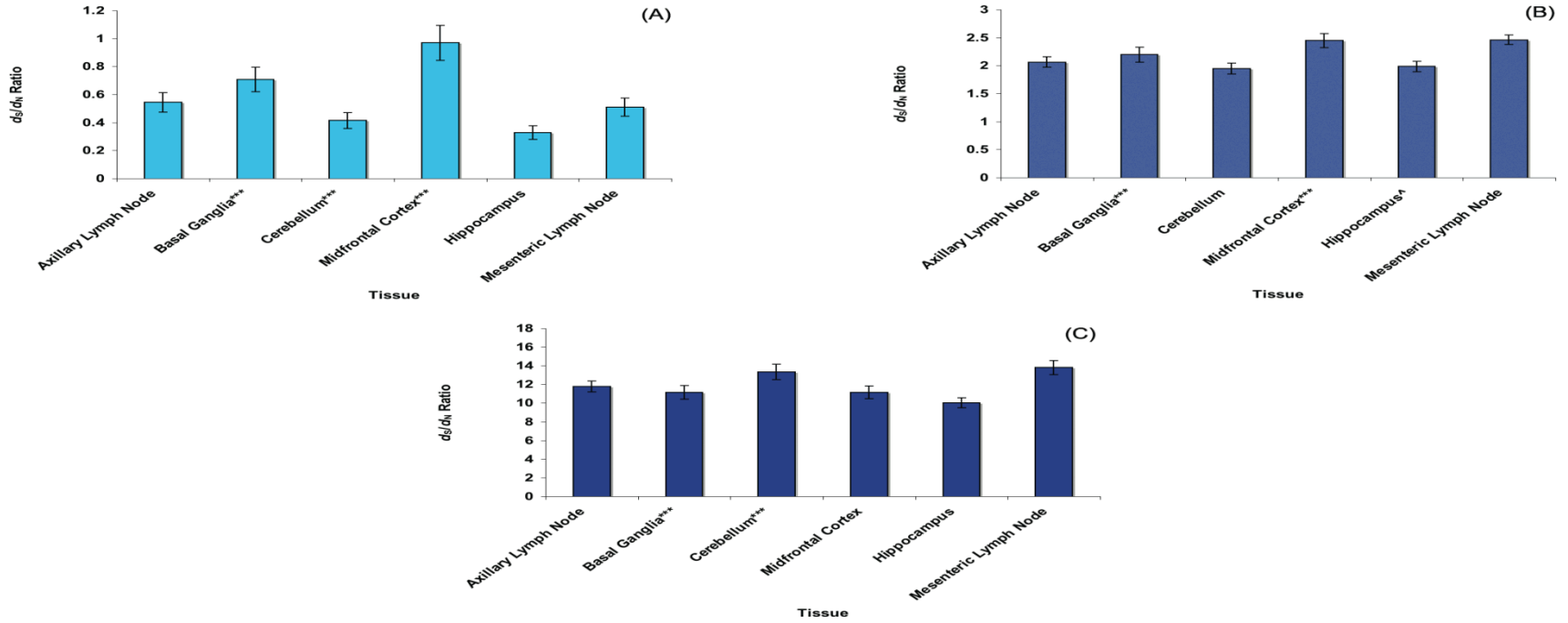

Figure 12. Average d_S/d_N values for *env* V1 region, *nef* and *int* sequences isolated from tissues of SIVsmmFGb-infected pigtailed macaques at one wpi. Mean d_S/d_N values for (A) *env* V1 region, (B) *nef* and (C) *int* were determined for each tissue. Error bars represent one standard error. The p-values for statistical comparisons of the mean d_S/d_N ratio values between tissues are noted in Table 9.

***, Tissues lack data from PQo1.

^, Only 19 nef sequences amplified from PQo1 hippocampus.

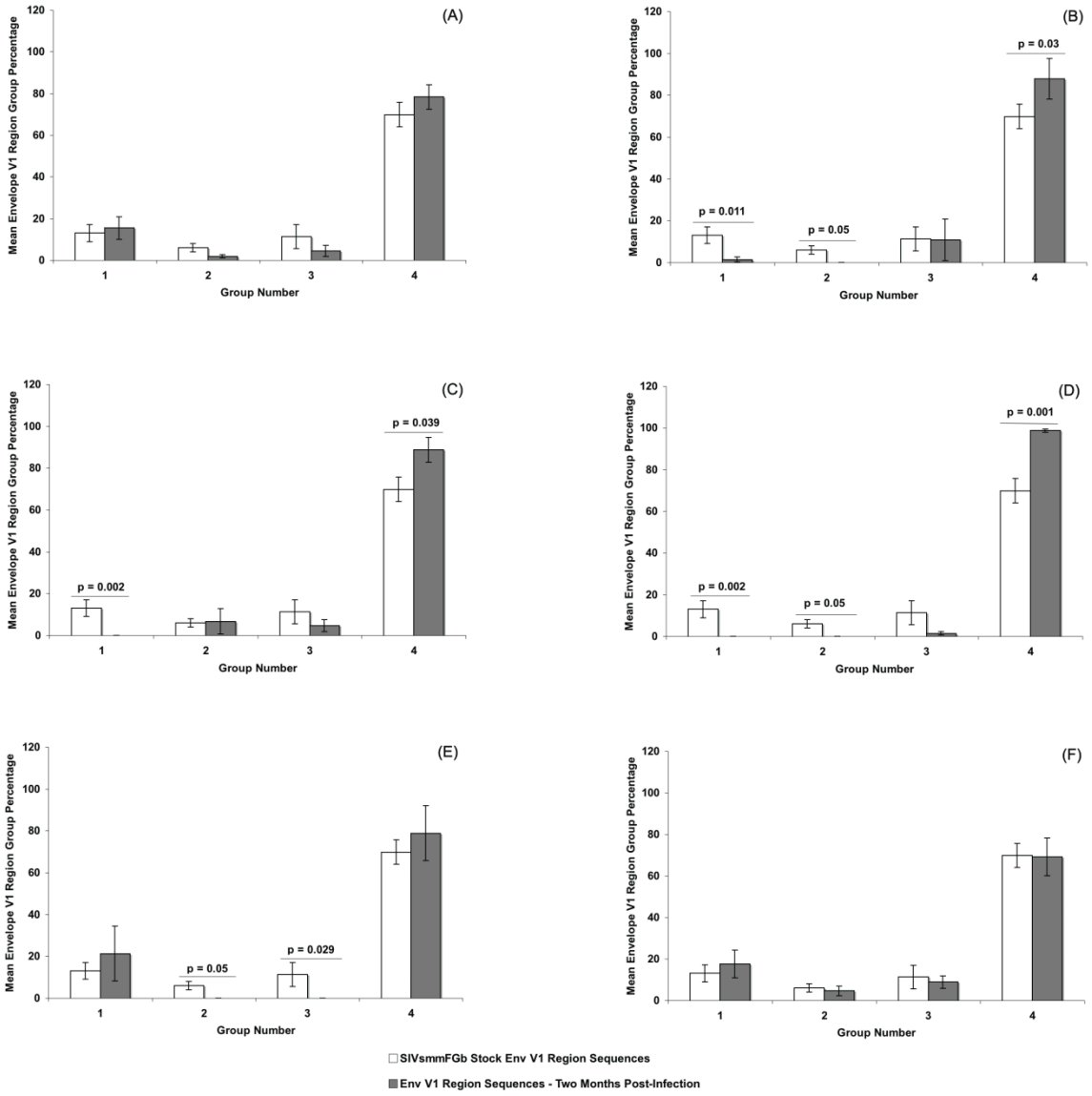

Figure 13. Comparison of Envelope V1 region group percentages between SIVsmmFGb stock virus and tissues harvested from pigtailed macaques at two mpi. (A) Axillary lymph node, (B) basal ganglia, (C) cerebellum, (D) midfrontal cortex, (E) hippocampus and (F) mesenteric lymph node. Statistically significant differences ($p < 0.05$) are noted. Error bars represent one standard error.

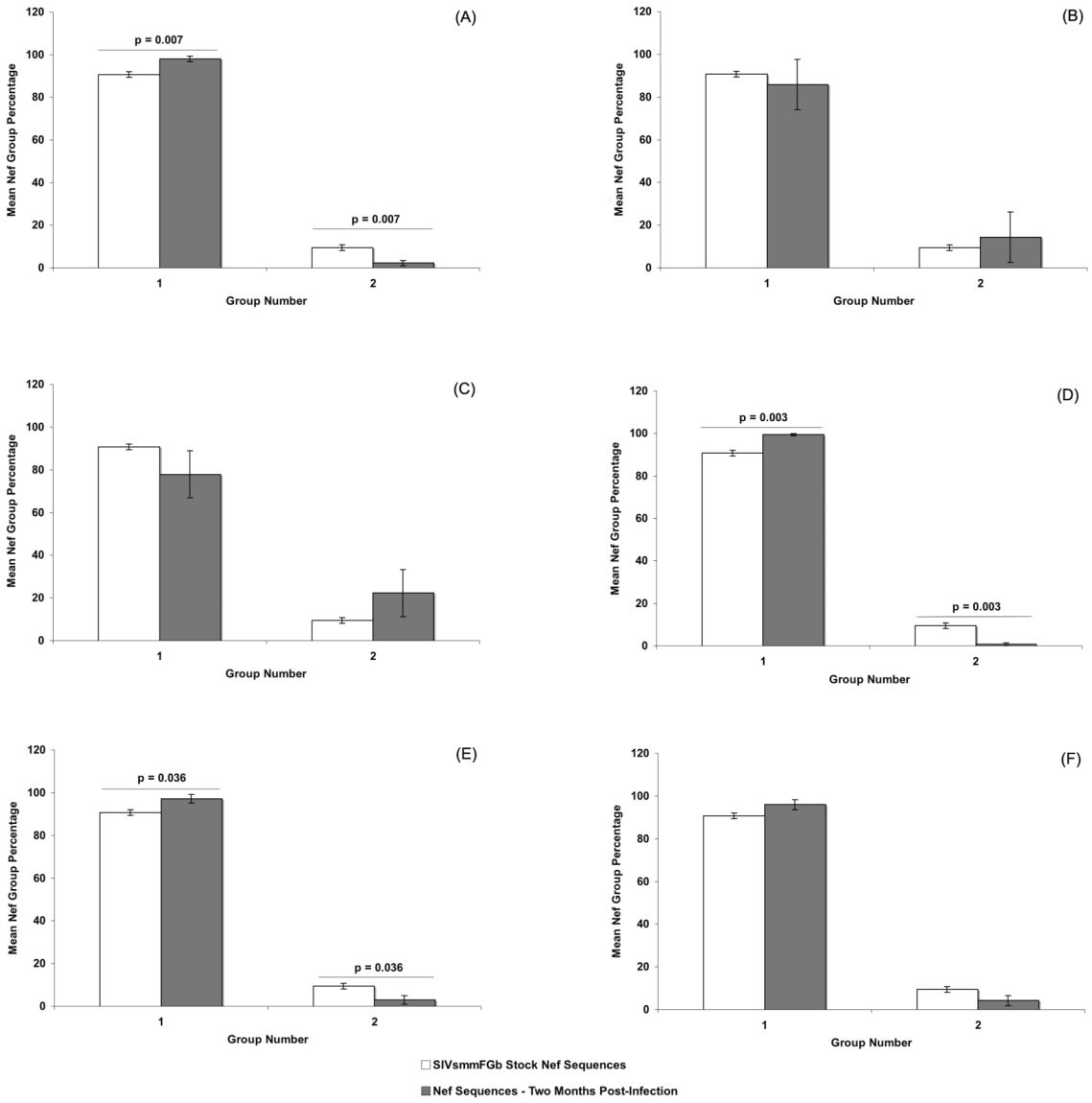

Figure 14. Comparison of Nef group percentages between SIVsmmFGb stock virus and tissues harvested from pigtailed macaques at two mpi. (A) Axillary lymph node, (B) basal ganglia, (C) cerebellum, (D) midfrontal cortex, (E) hippocampus and (F) mesenteric lymph node. Statistically significant differences ($p < 0.05$) are noted. Error bars represent one standard error.

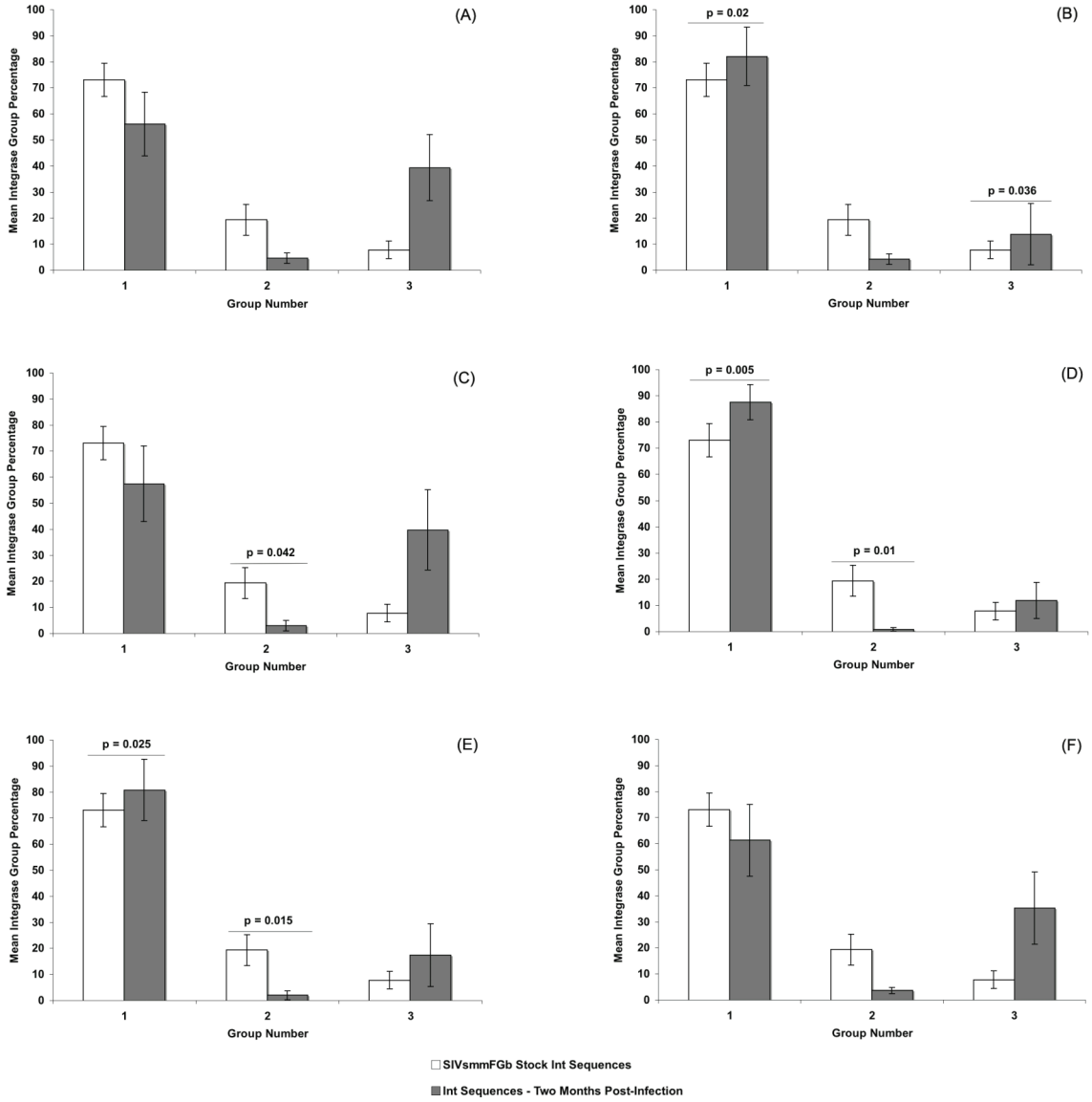

Figure 15. Comparison of Int group percentages between SIVsmmFGb stock virus and tissues harvested from pigtailed macaques at one wpi or two mpi. (A) Axillary lymph node, (B) basal ganglia, (C) cerebellum, (D) midfrontal cortex, (E) hippocampus and (F) mesenteric lymph node. Statistically significant differences ($p < 0.05$) are noted. Error bars represent one standard error.

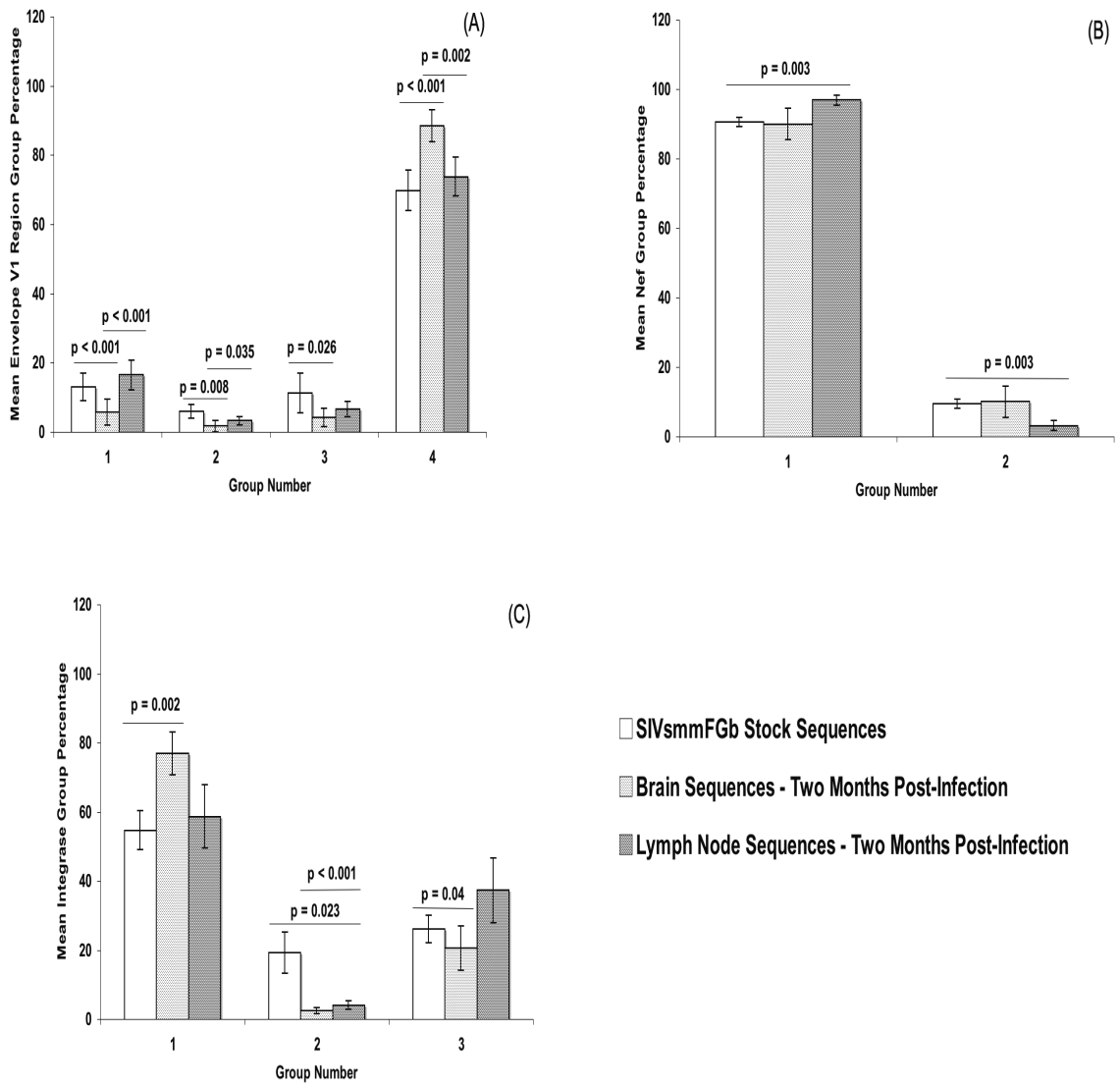

Figure 16. Comparison of sequence group percentages between the SIVsmmFGb stock virus and sequences harvested from the CNS and lymph node at two mpi. (A) Env V1 region, (B) Nef and (C) Int amino acid sequences. Error bars represent one standard error of the mean.

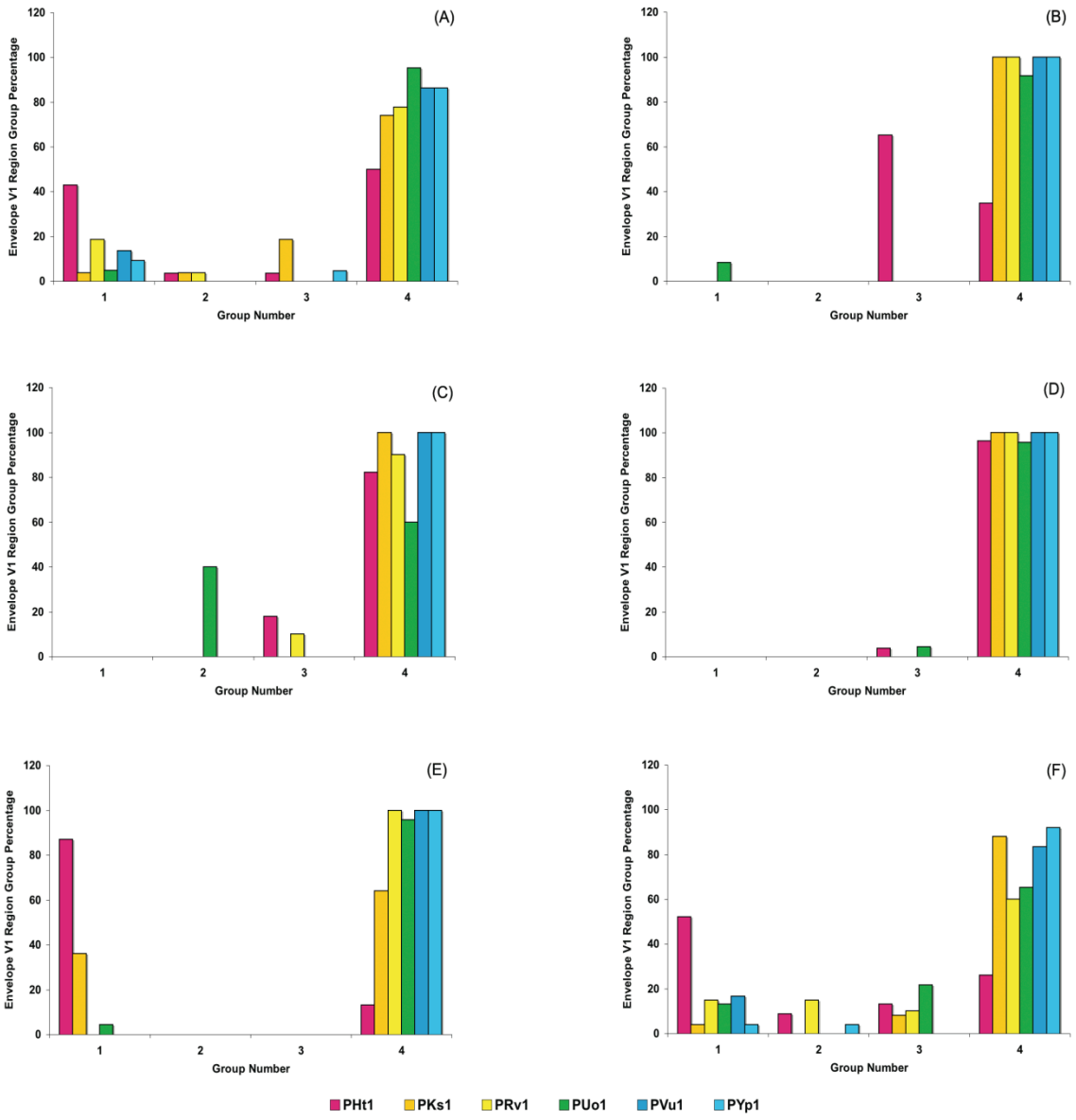

Figure 17. Comparison of Env V1 region amino acid sequence group percentages obtained from tissues harvested from each SIVsmmFGb-infected pigtailed macaque at two mpi. (A) Axillary lymph node, (B) basal ganglia, (C) cerebellum, (D) midfrontal cortex, (E) hippocampus and (F) mesenteric lymph node.

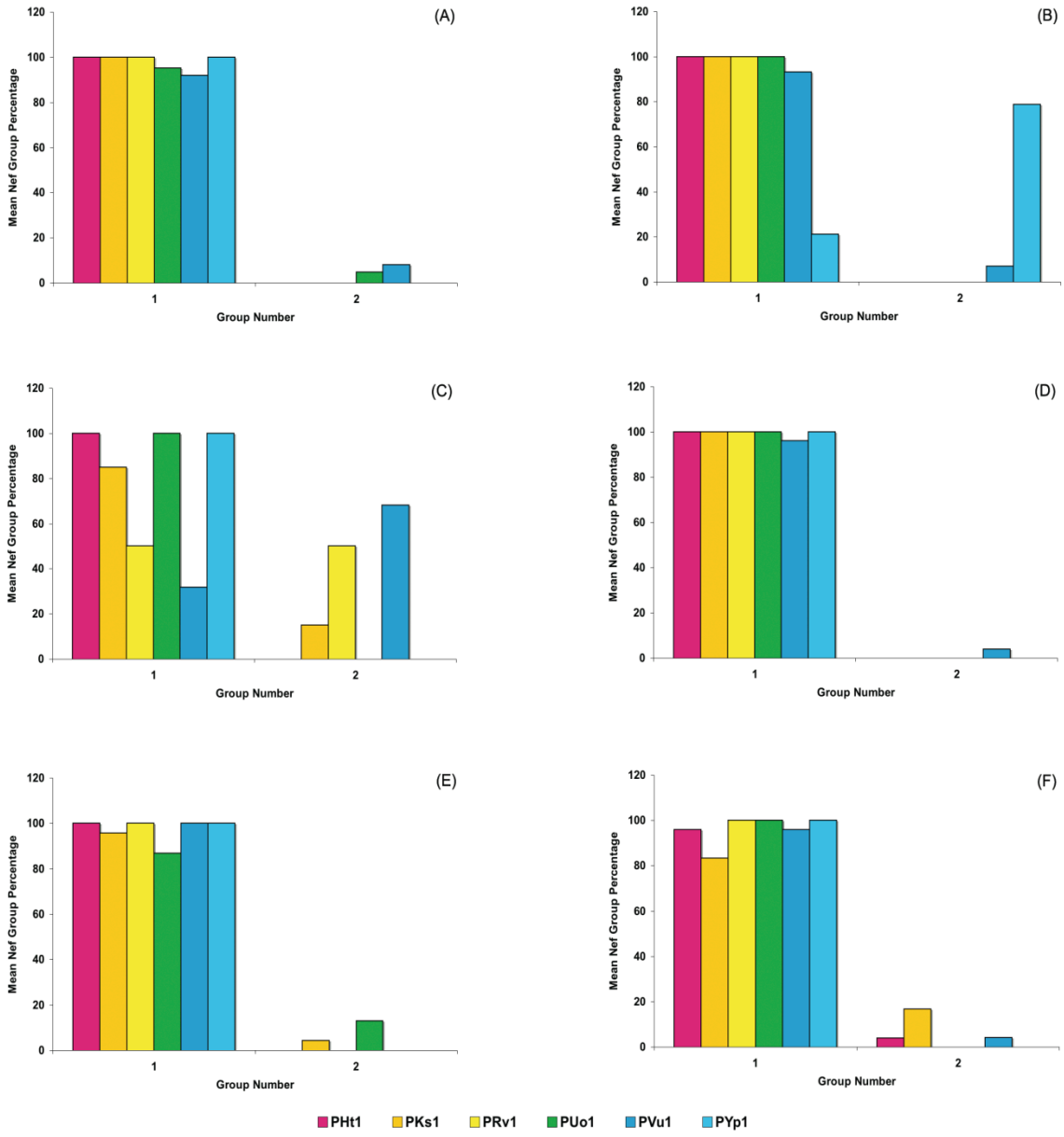

Figure 18. Comparison of Nef amino acid sequence group percentages obtained from tissues harvested from each SIVsmmFGb-infected pigtailed macaque at two mpi. (A) Axillary lymph node, (B) basal ganglia, (C) cerebellum, (D) midfrontal cortex, (E) hippocampus and (F) mesenteric lymph node.

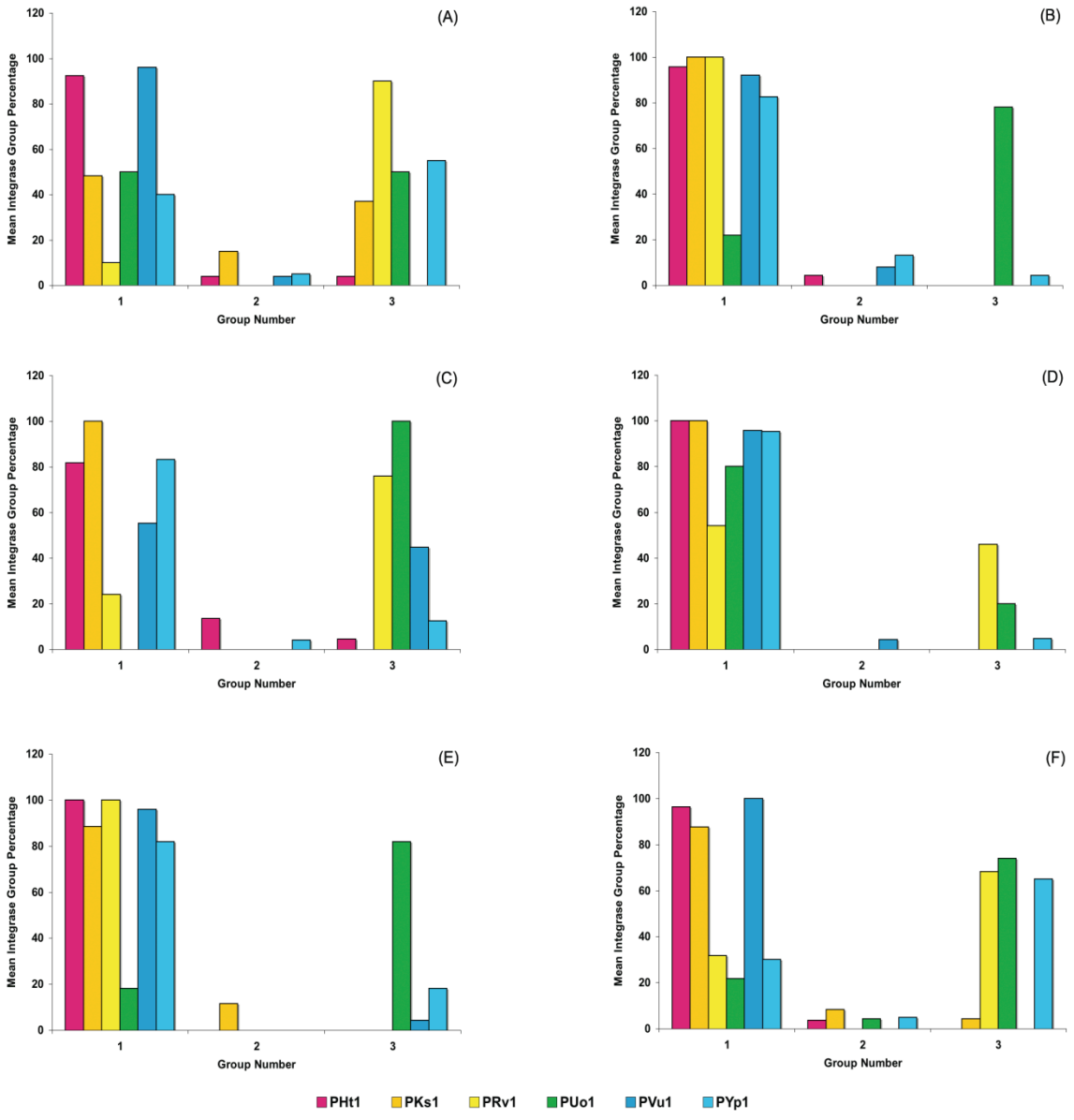

Figure 19. Comparison of Int amino acid sequence group percentages obtained from tissues harvested from each SIVsmmFGb-infected pigtailed macaque at two mpi. (A) Axillary lymph node, (B) basal ganglia, (C) cerebellum, (D) midfrontal cortex, (E) hippocampus and (F) mesenteric lymph node.

Figure 20. Phylogenetic analysis of SIVsmmFGb compartmentalization between tissues harvested from pigtailed macaques at two mpi. (A) Env V1 region, (B) Nef and (C) Int amino acid sequences. Error bars represent two standard errors of the *S* ratio; significant compartmentalization between tissues is indicated by ratios more than two standard errors less than 1.

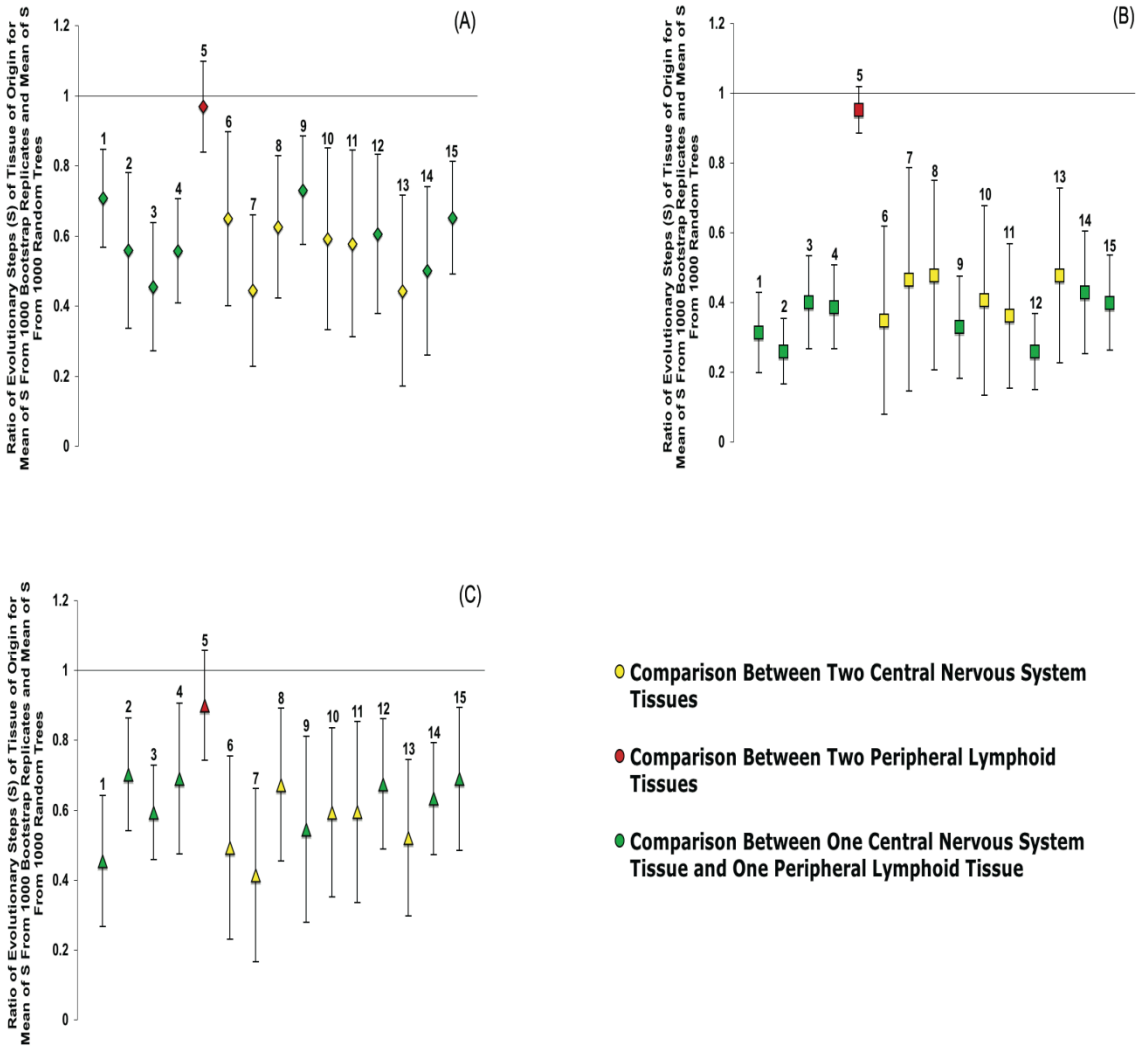

Modified Slatkin-Maddison Test **Tissue Comparisons Key**	
1	Axillary Lymph Node and Basal Ganglia
2	Axillary Lymph Node and Cerebellum
3	Axillary Lymph Node and Midfrontal Cortex
4	Axillary Lymph Node and Hippocampus
5	Axillary Lymph Node and Mesenteric Lymph Node
6	Basal Ganglia and Cerebellum
7	Basal Ganglia and Midfrontal Cortex
8	Basal Ganglia and Hippocampus
9	Basal Ganglia and Mesenteric Lymph Node
10	Cerebellum and Midfrontal Cortex
11	Cerebellum and Hippocampus
12	Cerebellum and Mesenteric Lymph Node
13	Midfrontal Cortex and Hippocampus
14	Midfrontal Cortex and Mesenteric Lymph Node
15	Hippocampus and Mesenteric Lymph Node

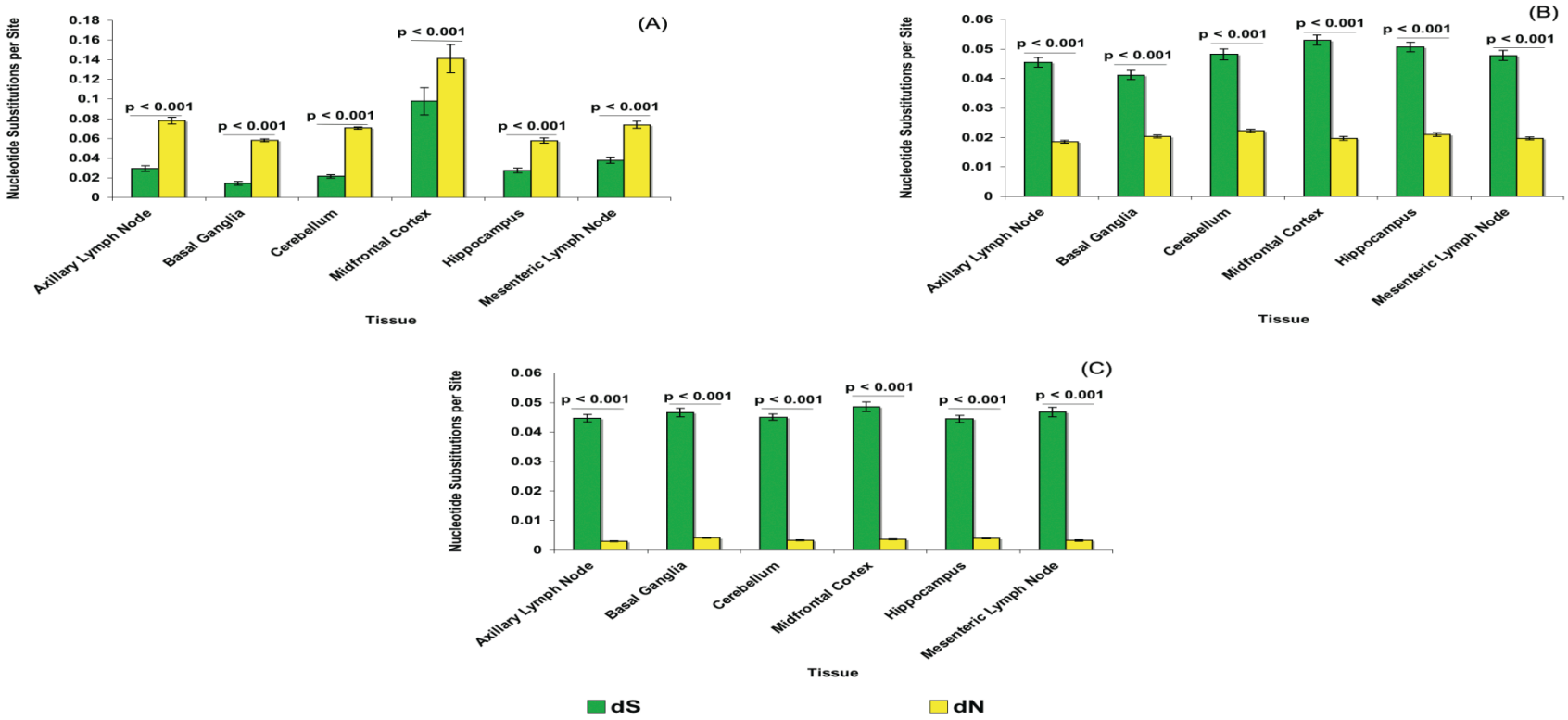

Figure 21. Average d_S and d_N values for sequences isolated from tissues of SIVsmmFGb-infected pigtailed macaques at two mpi. (A) *env* V1 region, (B) *nef* and (C) *int*. Statistically significant differences ($p < 0.05$) in d_S and d_N within a tissue are noted. Error bars represent one standard error. The p-values, obtained from statistical comparisons of d_S and d_N between tissues, are provided for all three genes in Table 14.

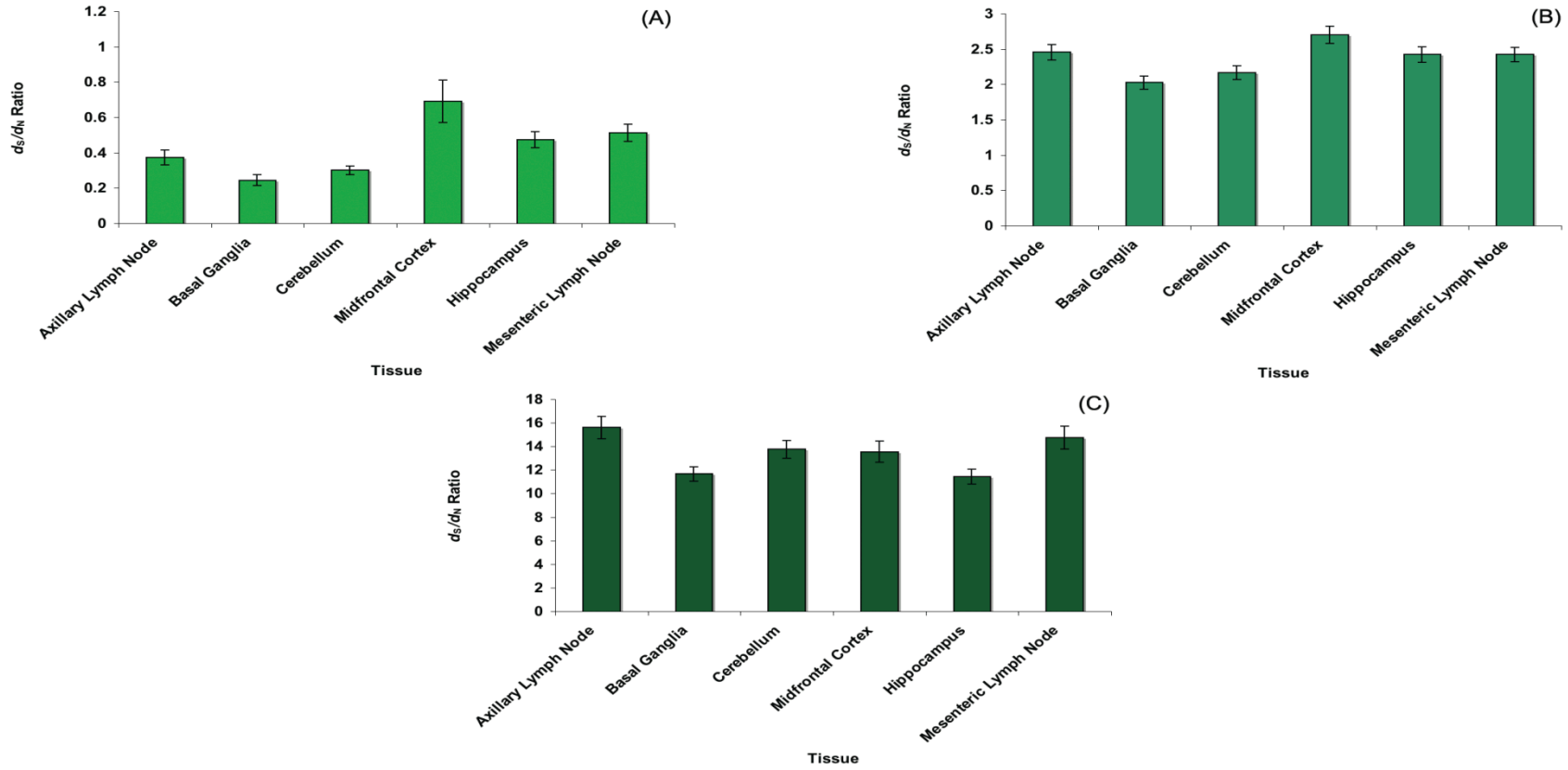

Figure 22. Average d_S / d_N values for sequences isolated from tissues of SIVsmmFGb-infected pigtailed macaques at two mpi. (A) *env* V1 region, (B) *nef* and (C) *int*. Error bars represent one standard error. The p-values obtained from statistical comparisons of d_S / d_N ratio values between tissues for each gene are provided in Table 15.

Figure 23. Phylogenetic analysis of temporal compartmentalization of SIVsmmFGb amino acid sequences within the same tissue harvested from infected pigtailed macaques at one wpi and two mpi. (A) Env V1 region, (B) Nef and (C) Int. Error bars represent two standard errors of the determined *S* ratio; significant compartmentalization between tissues is indicated by ratios more than two standard errors less than 1. Some sequences for Env V1 region, Nef and Int could not be obtained from animal PQo1 at one wpi, as described.

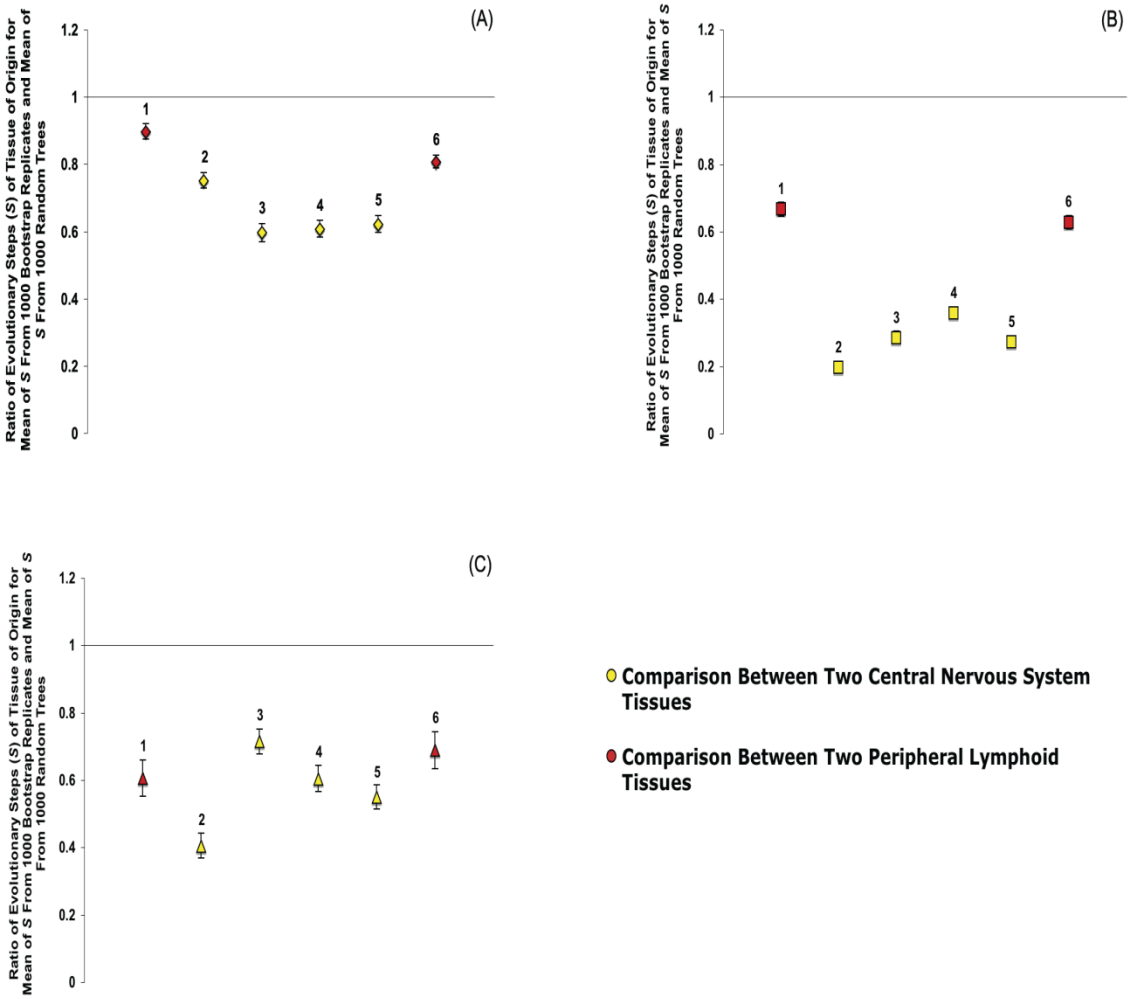

Tissue Comparisons Key		
	Tissue	**Time points**
1	Axillary Lymph Node	One Week Post-Infection
		Two Months Post-Infection
2	Basal Ganglia	One Week Post-Infection
		Two Months Post-Infection
3	Cerebellum	One Week Post-Infection
		Two Months Post-Infection
4	Midfrontal Cortex	One Week Post-Infection
		Two Months Post-Infection
5	Hippocampus	One Week Post-Infection
		Two Months Post-Infection
6	Mesenteric Lymph Node	One Week Post-Infection
		Two Months Post-Infection

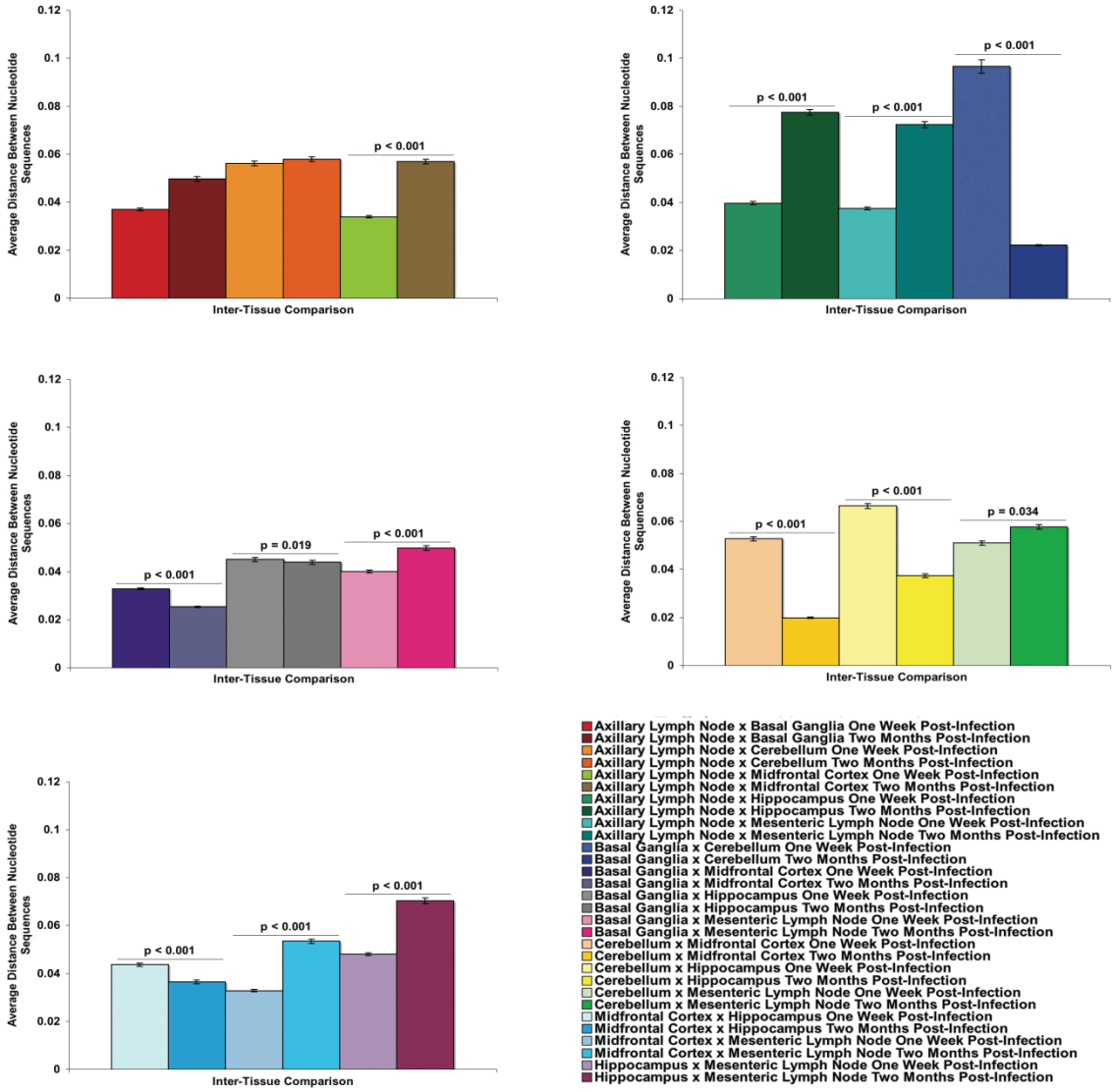

Figure 24. Comparison of average pairwise distances of SIVsmmFGb *env* V1 region nucleotide sequences between tissues of infected pigtailed macaques. Each bar represents the average pairwise distance between nucleotide sequences from the two tissues being compared, as noted in the legend. Statistically significant differences ($p <$ or $= 0.05$) between a particular two-tissue comparison at one wpi and two mpi are noted. The p-values for all possible statistical comparisons of all two-tissue comparisons at both time points are provided in Tables 16A - D.

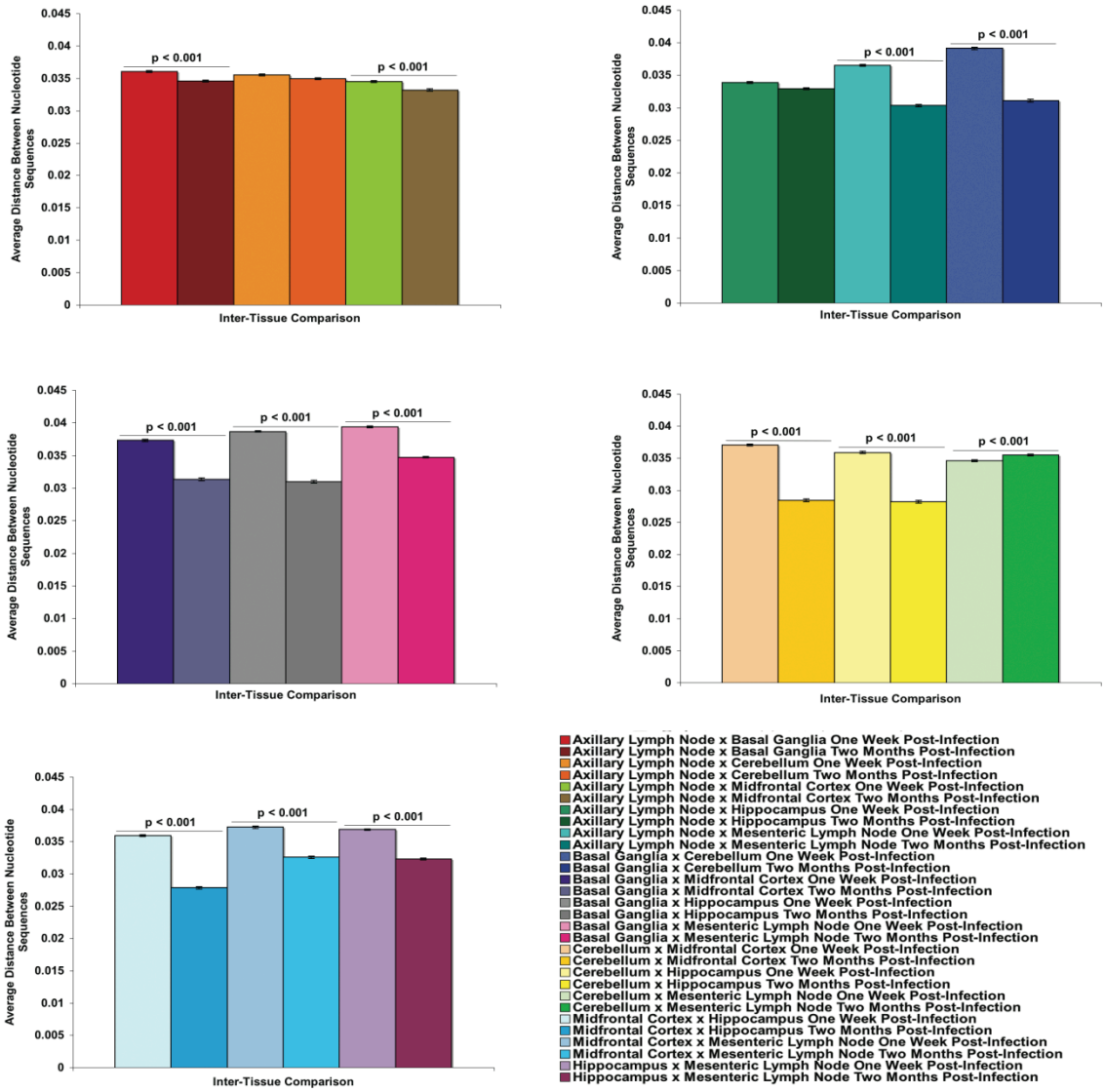

Figure 25. Comparison of average pairwise distances of SIVsmmFGb *nef* nucleotide sequences between tissues of infected pigtailed macaques. Each bar represents the average pairwise distance between nucleotide sequences from the two tissues being compared, as noted in the legend. Statistically significant differences ($p < \text{or} = 0.05$) between a particular two-tissue comparison at one wpi and two mpi are noted. The p-values for all possible statistical comparisons of all two-tissue comparisons at both time points are provided in Tables 17A - D.

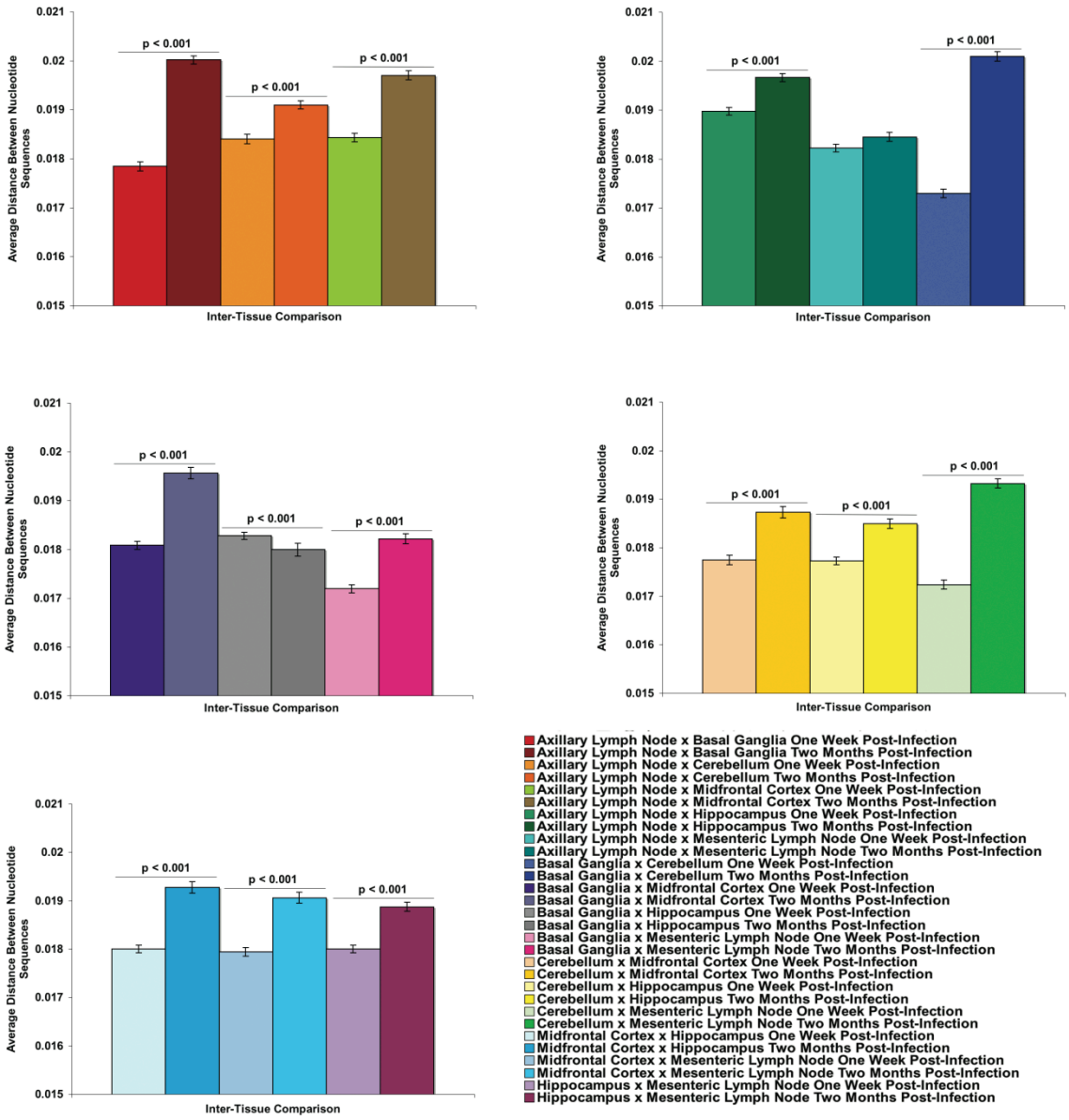

Figure 26. Comparison of average pairwise distances of SIVsmmFGb *int* nucleotide sequences between tissues of infected pigtailed macaques. Each bar represents the average pairwise distance between nucleotide sequences from the two tissues being compared. Statistically significant differences ($p < \text{or} = 0.05$) between a particular two-tissue comparison at one wpi and two mpi are noted. The p-values for all possible statistical comparisons of all two-tissue comparisons at both time points are provided in Tables 18A - D.

Figure 27. Comparison of the average pairwise distances of SIVsmmFGb nucleotide sequences within each tissue in infected pigtailed macaques. (A) and (B) *env* V1 region, (C) and (D) *nef*, (E) and (F) *int*. Each bar represents the average pairwise distance between nucleotide sequences within a particular tissue at either one wpi or two mpi. Statistically significant differences ($p < \text{or} = 0.05$) between one wpi and two mpi are noted. The p-values for all possible statistical comparisons of the intra-tissue pairwise distances at both time points are provided in Tables 19A - C.

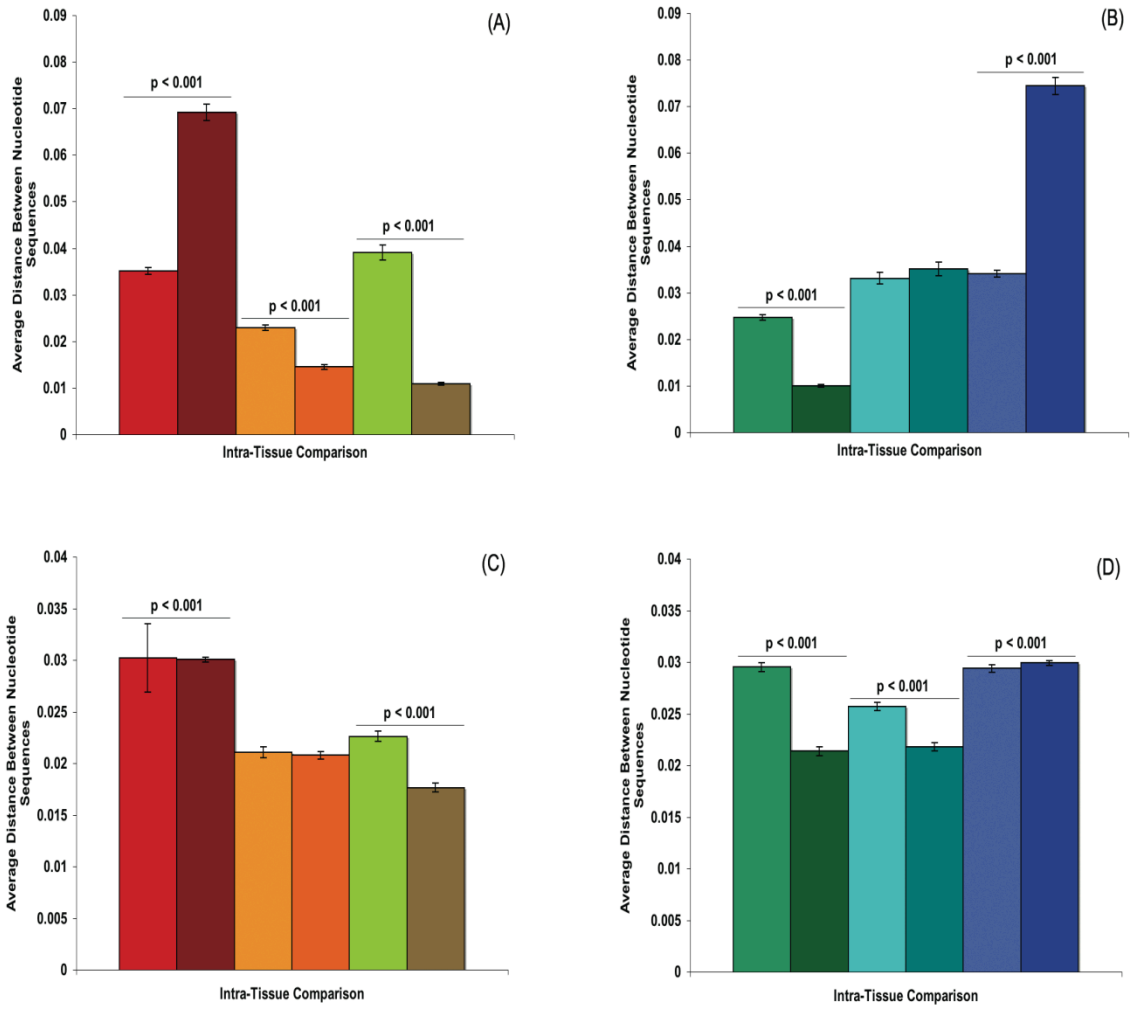

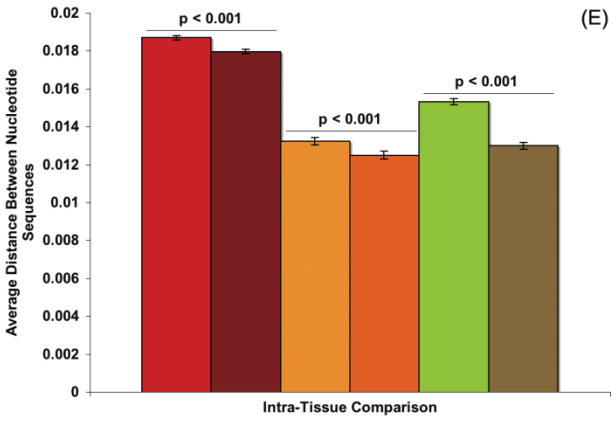
(E)
p < 0.001
p < 0.001
p < 0.001
Average Distance Between Nucleotide Sequences
0.02
0.018
0.016
0.014
0.012
0.01
0.008
0.006
0.004
0.002
0
Intra-Tissue Comparison

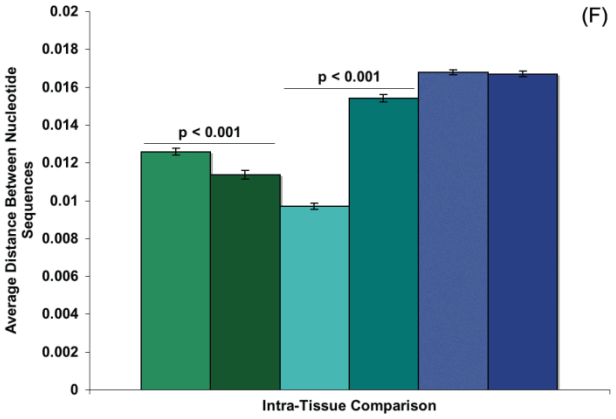
(F)
p < 0.001
p < 0.001
Average Distance Between Nucleotide Sequences
0.02
0.018
0.016
0.014
0.012
0.01
0.008
0.006
0.004
0.002
0
Intra-Tissue Comparison


Axillary Lymph Node One Week Post-Infection
Axillary Lymph Node Two Months Post-Infection
Basal Ganglia One Week Post-Infection
Basal Ganglia Two Months Post-Infection
Cerebellum One Week Post-Infection
Cerebellum Two Months Post-Infection
Midfrontal Cortex One Week Post-Infection
Midfrontal Cortex Two Months Post-Infection
Hippocampus One Week Post-Infection
Hippocampus Two Months Post-Infection
Mesenteric Lymph Node One Week Post-Infection
Mesenteric Lymph Node Two Months Post-Infection

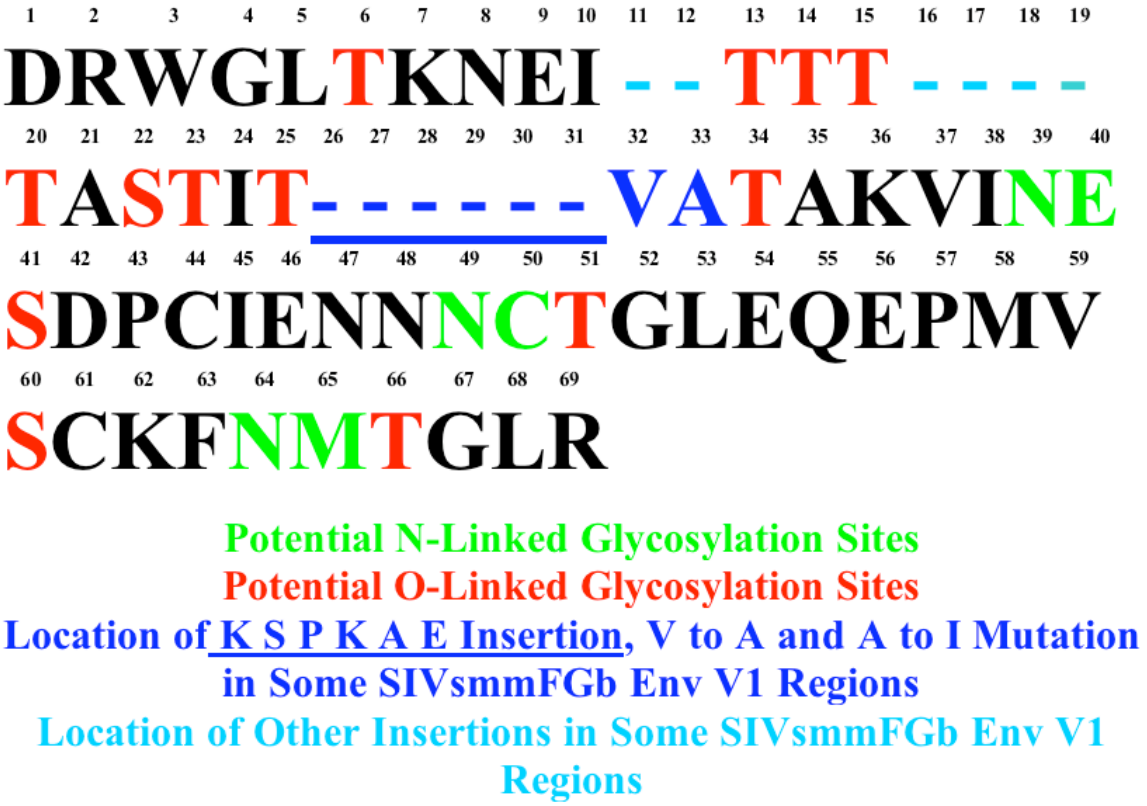

Figure 28. SIVsmmFGb stock virus Env V1 region amino acid consensus sequence. The location of potential N- and O-linked glycosylation sites are indicated, as are regions where insertions appear in Env V1 region amino acid sequences from the SIVsmmFGb stock and/or the experimental tissues.

Figure 29. SIVsmmFGb stock virus Nef amino acid consensus sequence. The locations of conserved Nef functional domains, and specific amino acid residues of interest, are noted.

Figure 30. SIVsmmFGb stock virus Int amino acid consensus sequence. The locations of conserved Int domains and amino acid residues are noted.

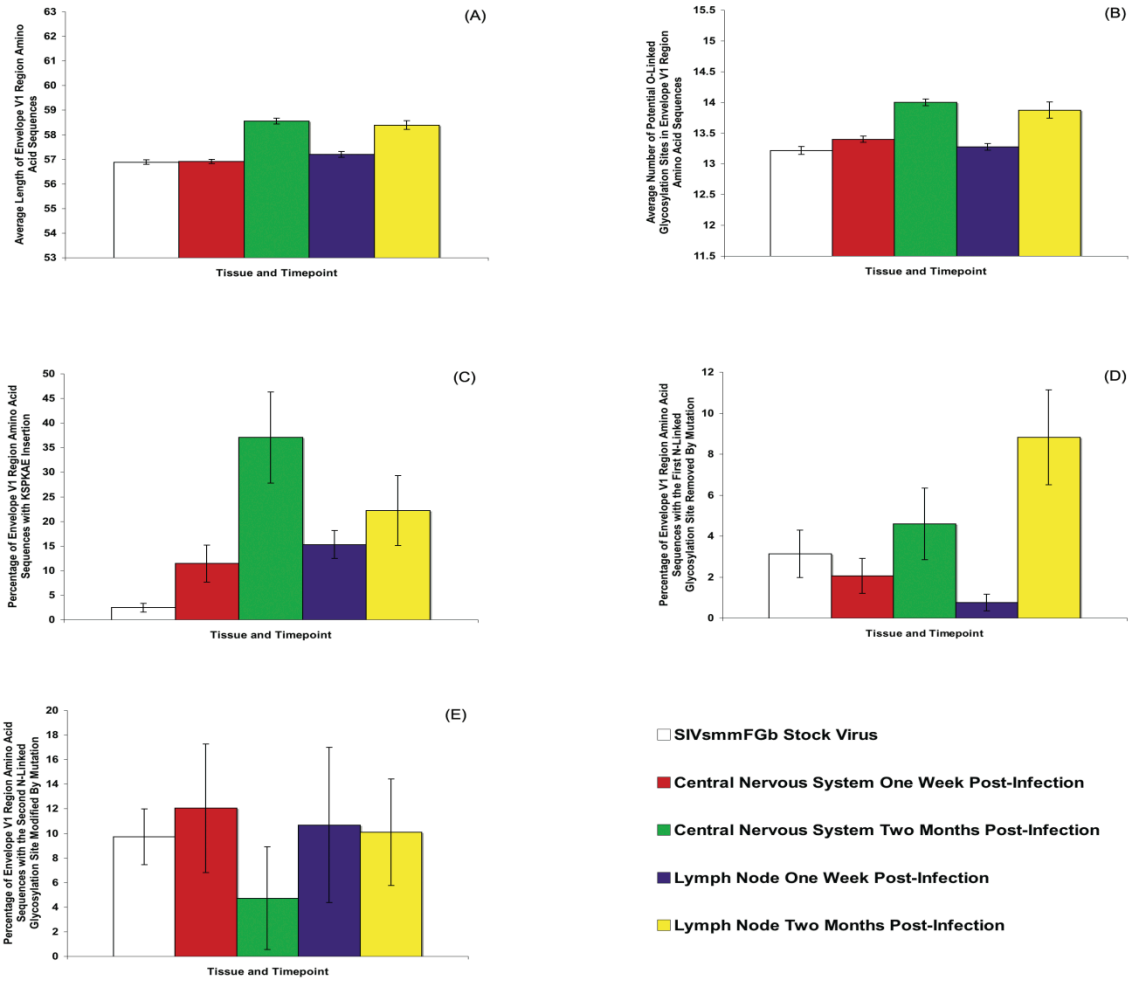

Figure 31. Prevalence of Env V1 region amino acid mutations in the SIVsmmFGb stock virus and CNS and lymph nodes of infected pigtailed macaques. (A) Average length of the Env V1 region, (B) average number of potential O-linked glycosylation sites per Env V1 region sequence, (C) percentage of Env V1 region sequences with the KSPKAE insertion, (D) percentage of Env V1 region sequences with the first N-linked glycosylation site removed by mutation and (E) percentage of Env V1 region sequences with the position of the second N-linked glycosylation site altered by mutation. The p-values for the statistical comparisons of the prevalence of each mutation in each sequence pool are provided in Tables 20 - 24.

Figure 32. Prevalence of Nef amino acid mutations in the SIVsmmFGb stock virus and CNS and lymph nodes of infected pigtailed macaques. Percentage of sequences with one or more mutations in (A) the basic region, (B) the N-proximal Y residues, (C) the acidic region, (D) the thioesterase binding site and (E) the AP interaction residues. Statistical comparisons of the prevalence of each mutation in each sequence pool are provided in Tables 25 – 29.

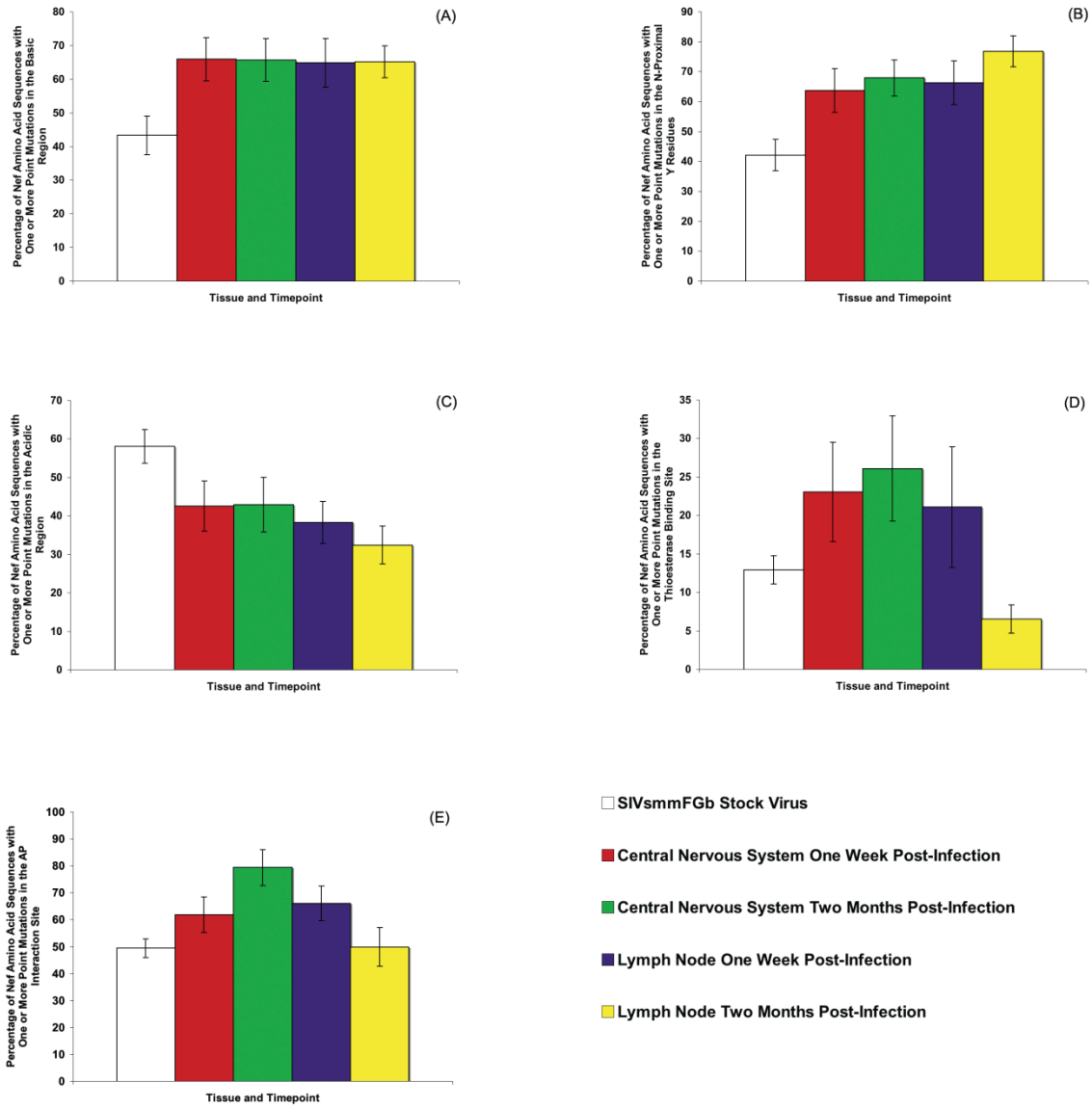

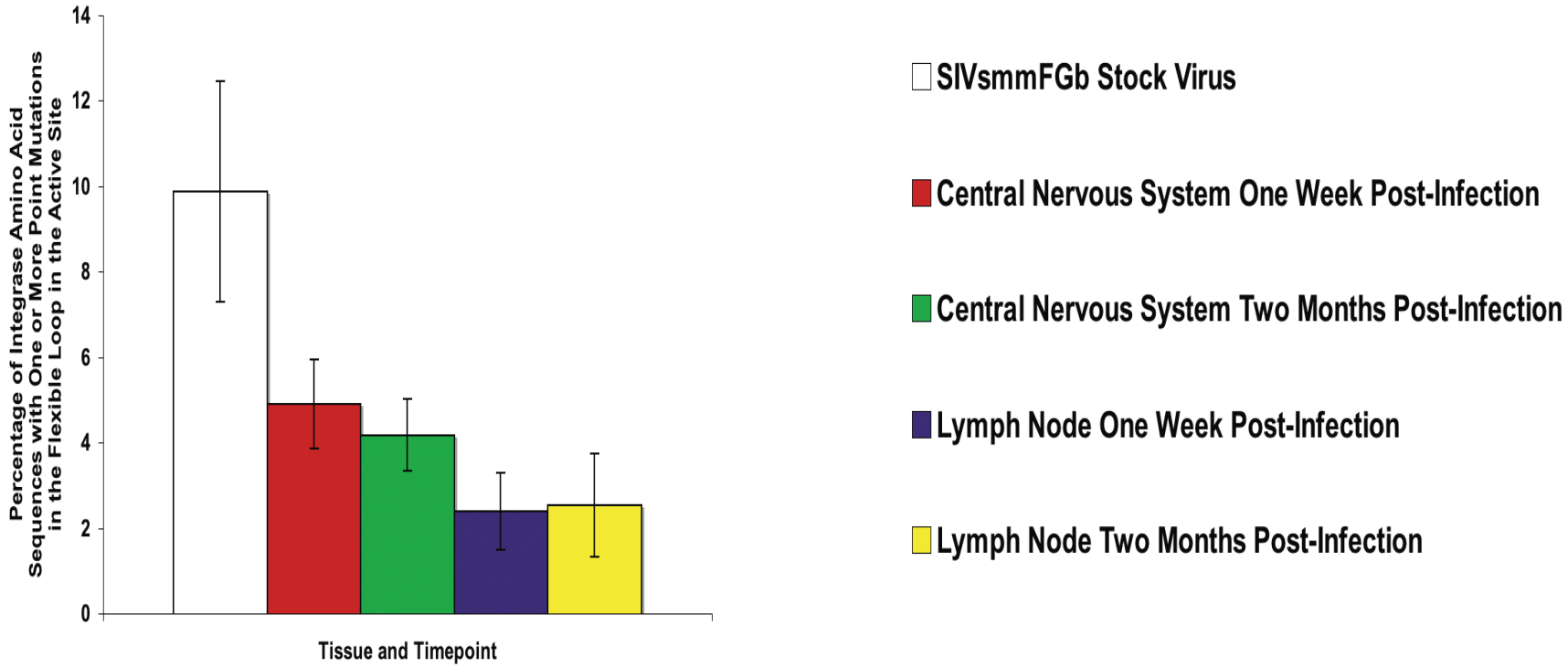

Figure 33. Prevalence of Int amino acid mutations in the SIVsmmFGb stock virus and CNS and lymph nodes of infected pigtailed macaques. Percentage of sequences with one or more mutations in the flexible loop in the active site. Statistical comparisons of the prevalence of each mutation in each sequence pool are provided in Table 30.

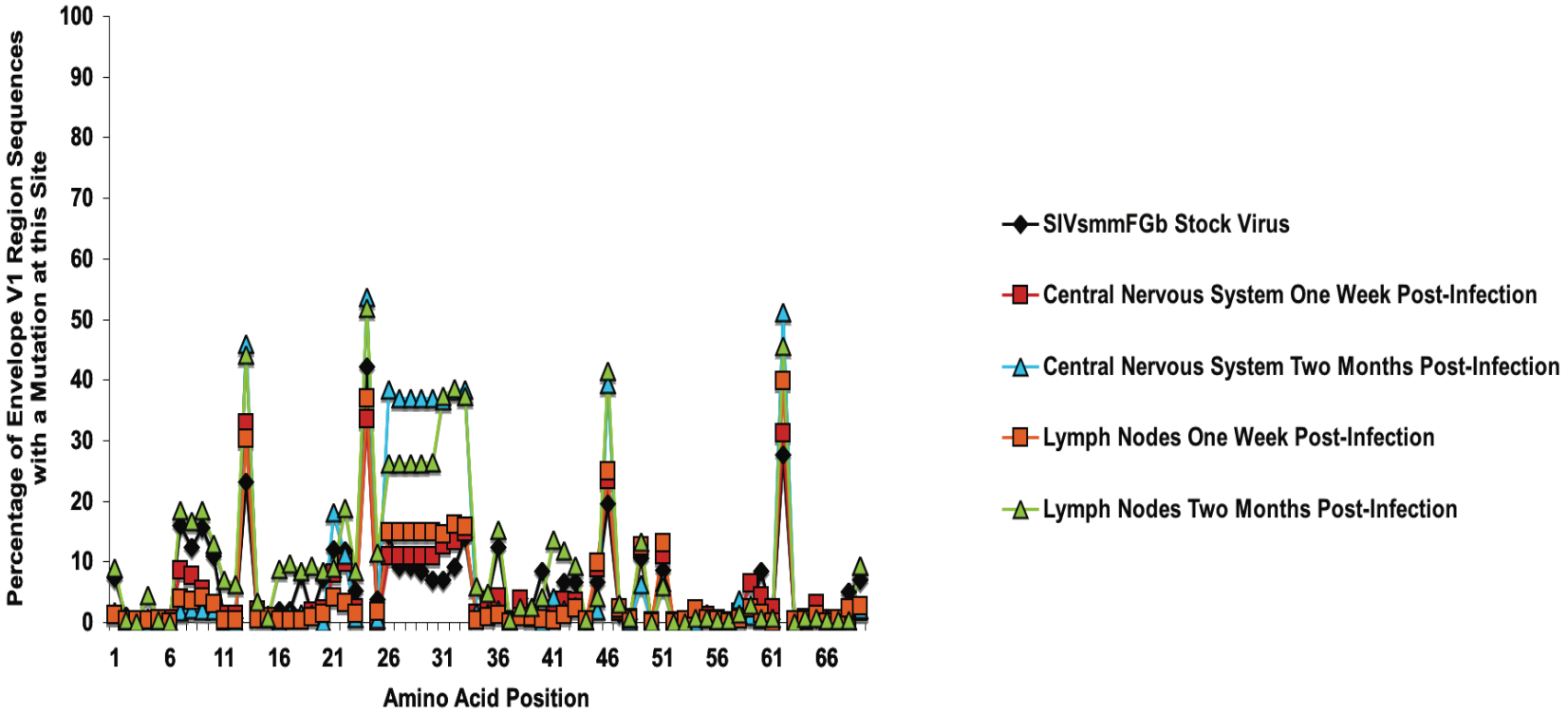

Figure 34. Percentage of SIVsmmFGb Env V1 region sequences from the stock virus and experimental tissues with an amino acid change at each site, relative to the stock virus consensus sequence. Sequences from the lymph node tissues and CNS regions at each time point were pooled to generate lymph node and CNS sequence pools at both one wpi and two mpi.

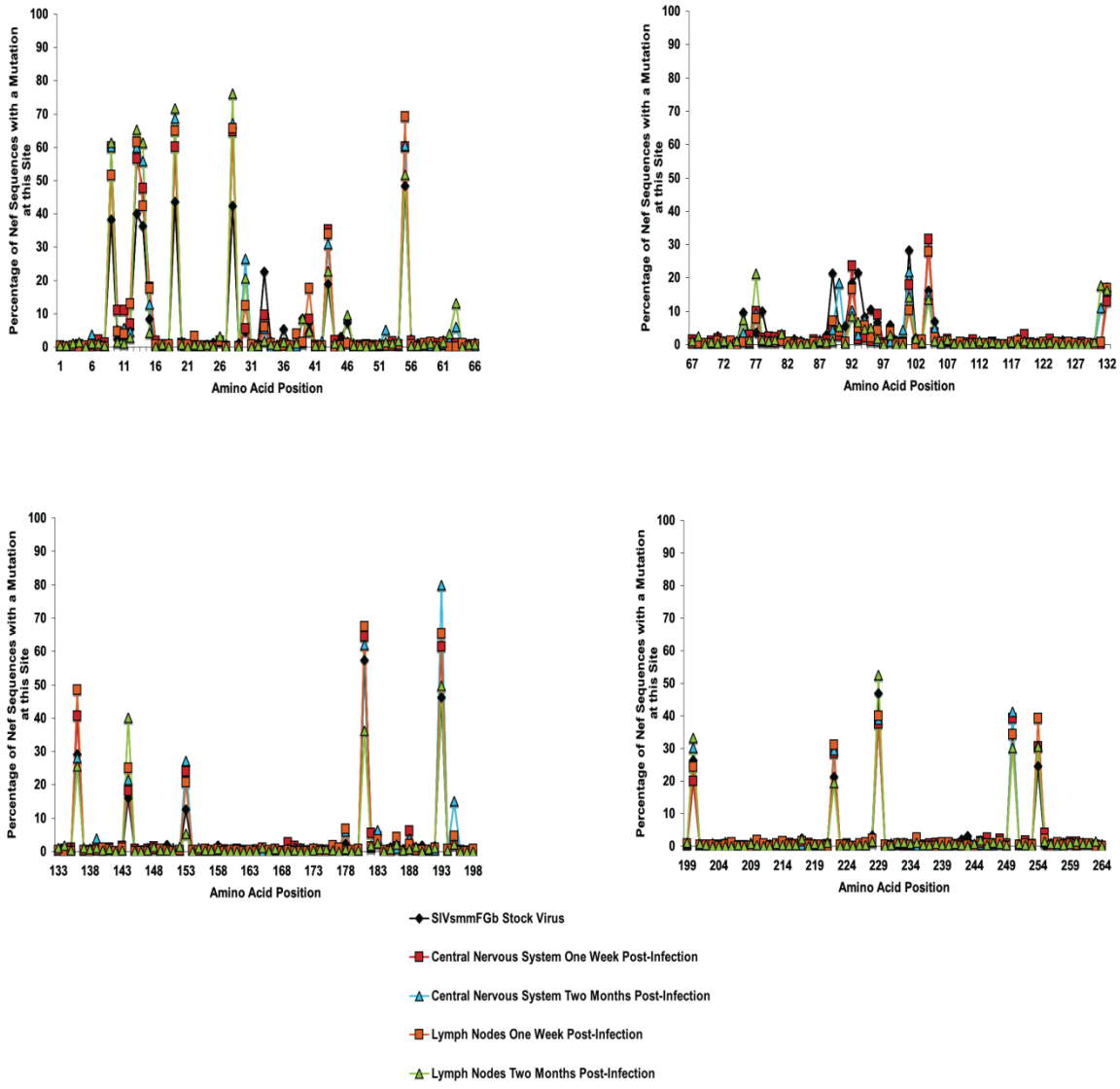

Figure 35. Percentage of SIVsmmFGb Nef sequences from the stock virus and experimental tissues with an amino acid change at each site, relative to the stock virus consensus sequence. Sequences from the lymph node tissues and CNS regions at each time point were pooled to generate lymph node and CNS sequence pools at both one wpi and two mpi.

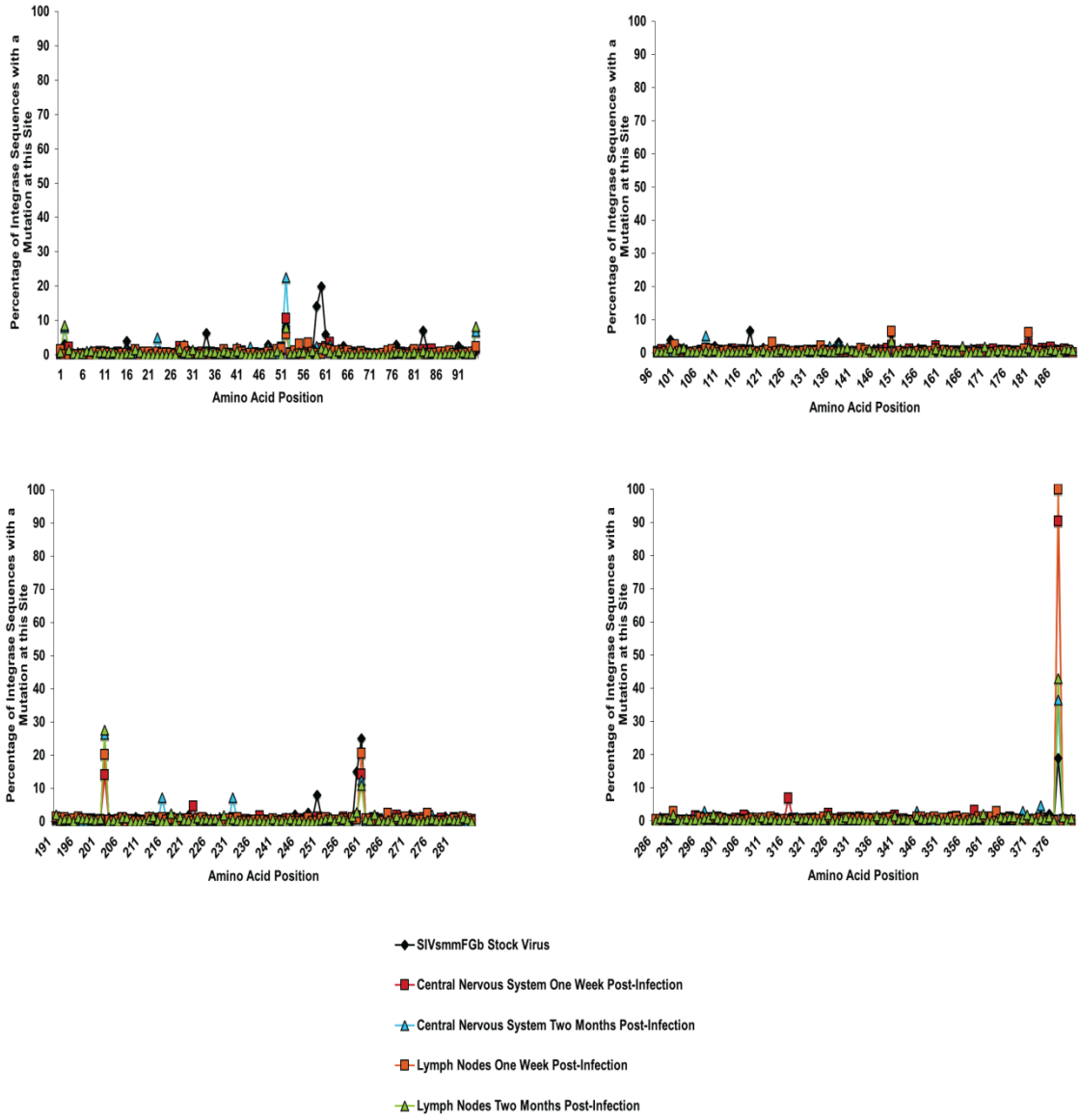

Figure 36. Percentage of SIVsmmFGb Int sequences from the stock virus and experimental tissues with an amino acid change at each site, relative to the stock virus consensus sequence. Sequences from the lymph node tissues and CNS regions at each time point were pooled to generate lymph node and CNS sequence pools at both one wpi and two mpi.

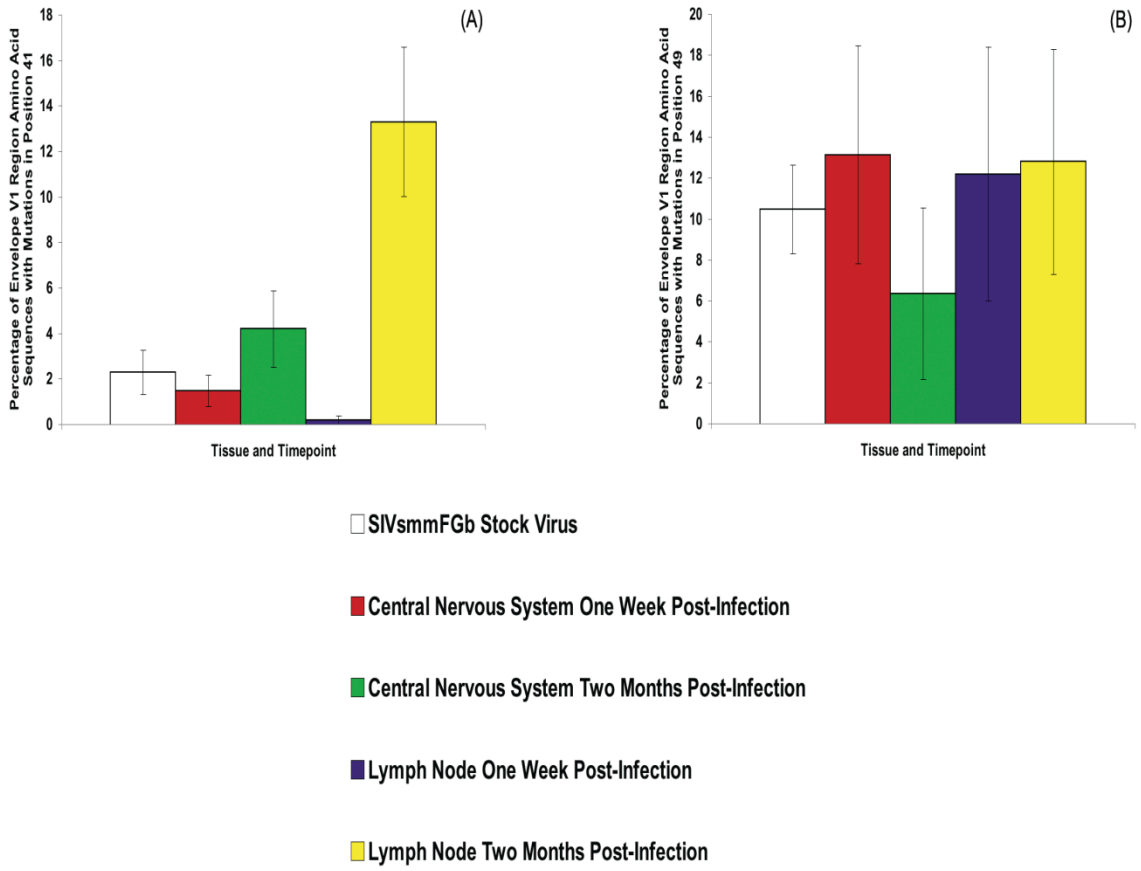

Figure 37. Prevalence of Env V1 region amino acid mutations in sequences harvested from the SIVsmmFGb stock virus, lymph node at one wpi, CNS at one wpi, lymph node at two mpi and CNS at two mpi. Percentage of sequences with amino acid mutations at positions (A) 41 and (B) 49. The p-values for the statistical comparisons of the prevalence of each mutation in each sequence pool are provided in Tables 31 – 32.

Figure 38. Prevalence of Nef basic region amino acid mutations in sequences harvested from the SIVsmmFGb stock virus, lymph node at one wpi, CNS at one wpi, lymph node at two mpi and CNS at two mpi. Percentage of sequences with mutations at positions (A) 9, (B) 12, (C) 13, (D) 14, (E) 15 and (F) 19. Statistical comparisons of the prevalence of each mutation in each sequence pool are provided in Tables 33 – 38.

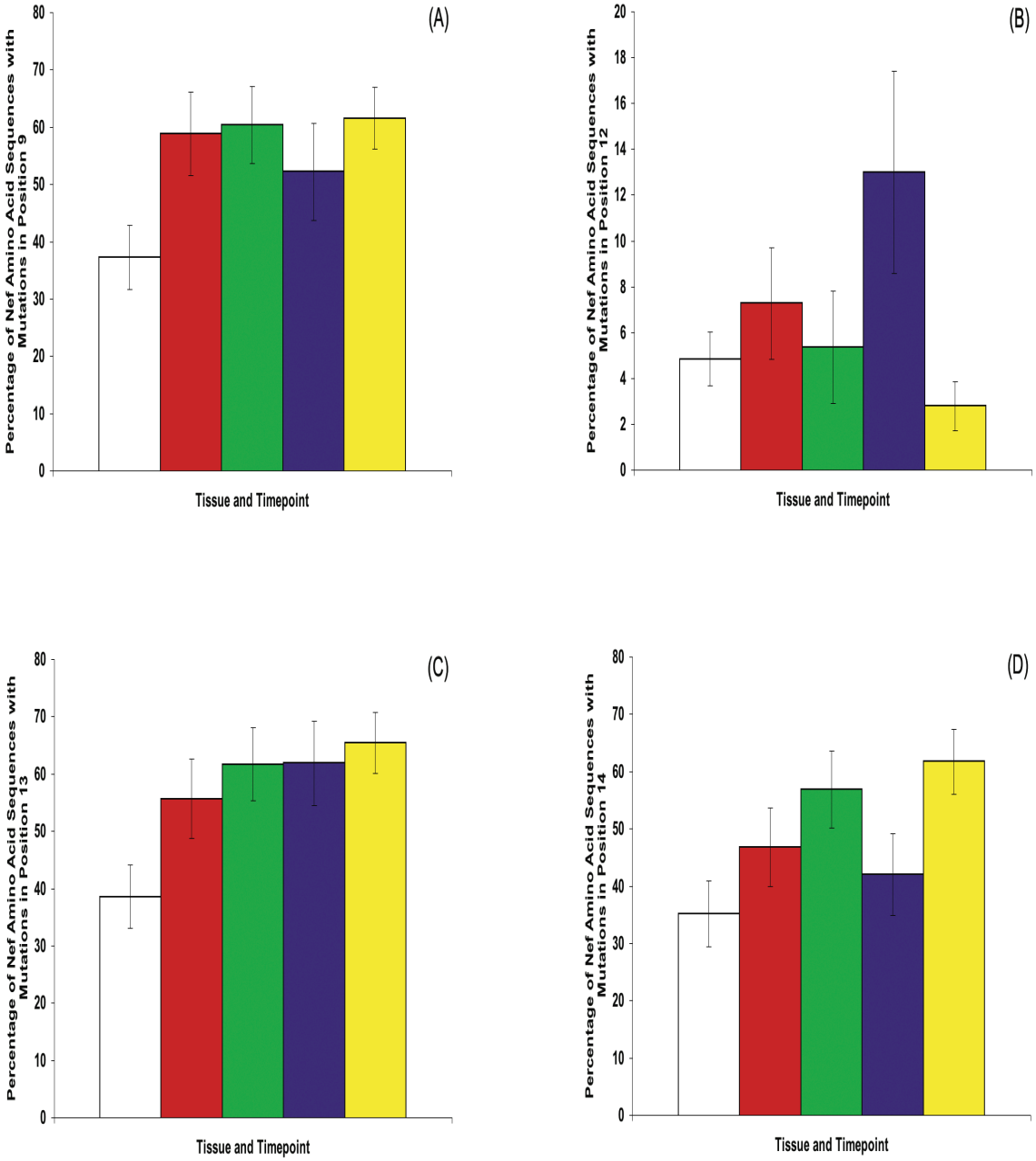

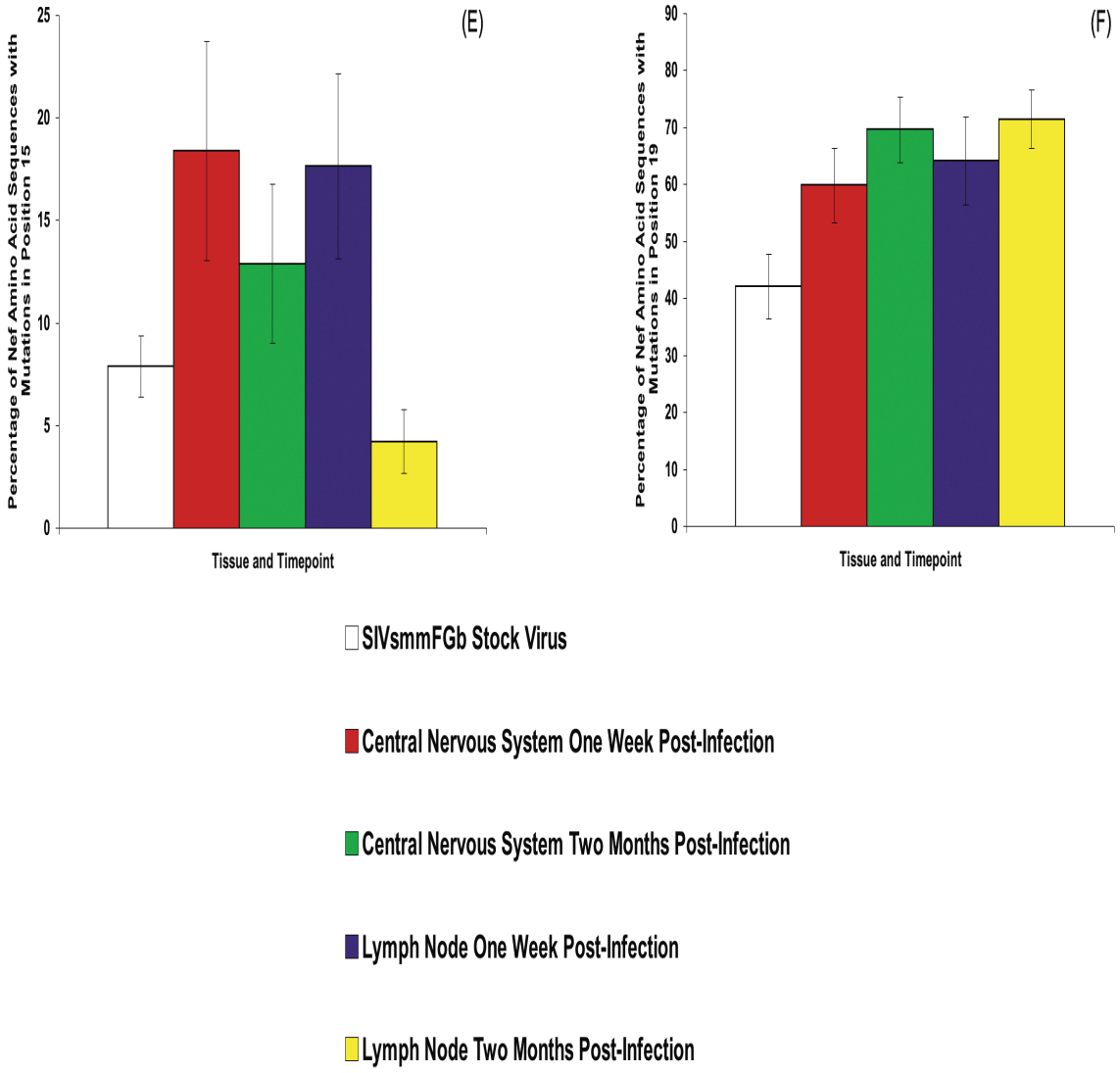
(E)
Percentage of Nef Amino Acid Sequences with Mutations in Position 15
25
20
15
10
5
0
Tissue and Timepoint
(F)
Percentage of Nef Amino Acid Sequences with Mutations in Position 19
90
80
70
60
50
40
30
20
10
0
Tissue and Timepoint
SIVsmmFGb Stock Virus
Central Nervous System One Week Post-Infection
Central Nervous System Two Months Post-Infection
Lymph Node One Week Post-Infection
Lymph Node Two Months Post-Infection

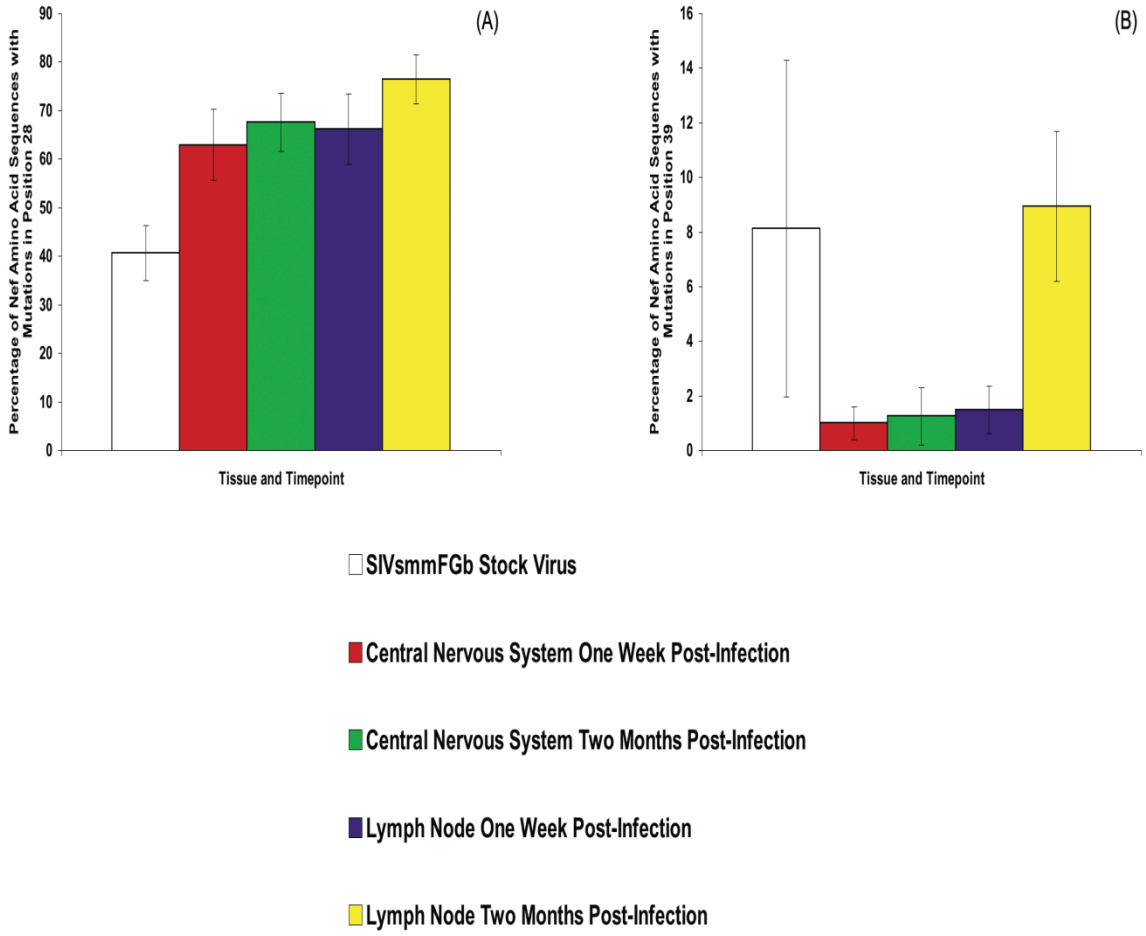

Figure 39. Prevalence of Nef N-proximal Y residue amino acid mutations in sequences harvested from the SIVsmmFGb stock virus, lymph node at one wpi, CNS at one wpi, lymph node at two mpi and CNS at two mpi. Percentage of sequences with mutations at positions (A) 28 and (B) 39. Statistical comparisons of the prevalence of each mutation in each sequence pool are provided in Tables 39 – 40.

Figure 40. Prevalence of Nef acidic region amino acid mutations in sequences harvested from the SIVsmmFGb stock virus, lymph node at one wpi, CNS at one wpi, lymph node at two mpi and CNS at two mpi. Percentage of sequences with mutations at positions (A) 89, (B) 91, (C) 92, (D) 93, (E) 94, (F) 95 and (G) 96. Statistical comparisons of the prevalence of each mutation in each sequence pool are provided in Tables 41 – 47.

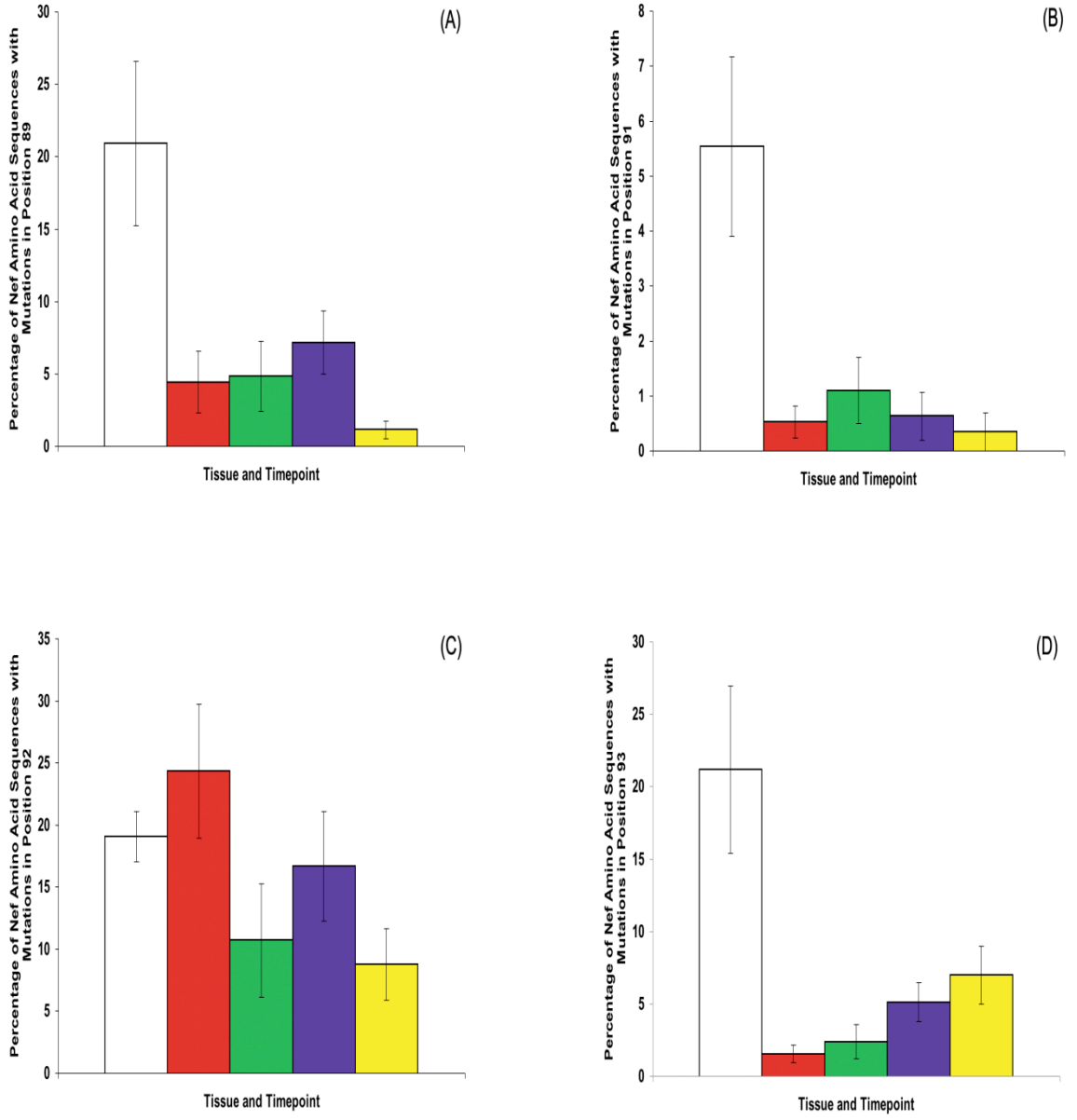

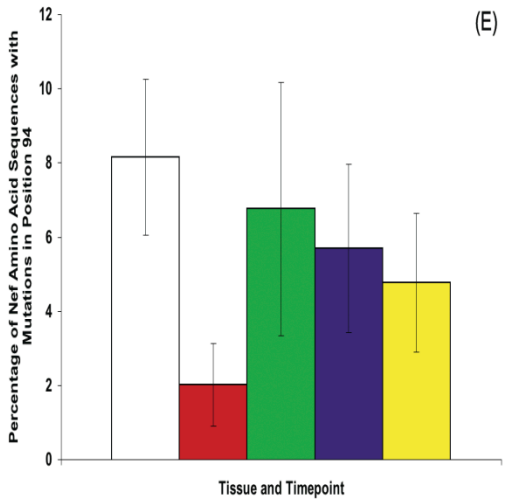
(E)
Percentage of Nef Amino Acid Sequences with Mutations in Position 94
0
2
4
6
8
10
12
Tissue and Timepoint

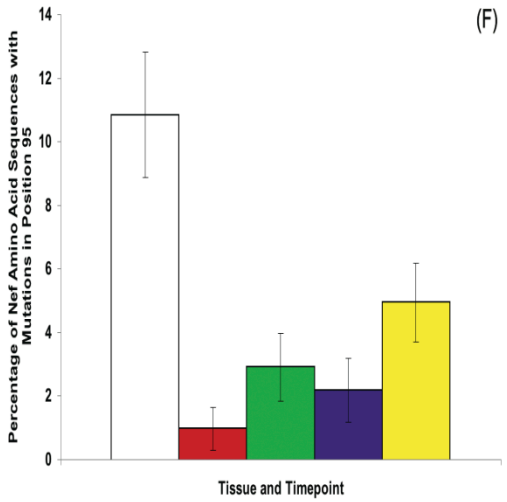
(F)
Percentage of Nef Amino Acid Sequences with Mutations in Position 95
0
2
4
6
8
10
12
14
Tissue and Timepoint

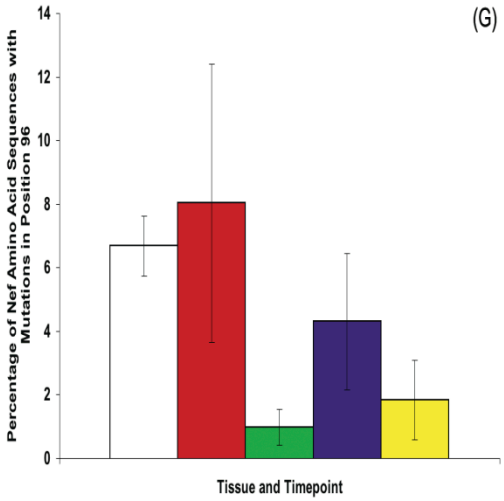
(G)
Percentage of Nef Amino Acid Sequences with Mutations in Position 96
0
2
4
6
8
10
12
14
Tissue and Timepoint

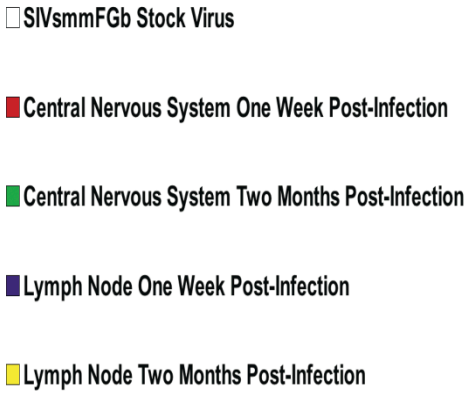
SIVsmmFGb Stock Virus
Central Nervous System One Week Post-Infection
Central Nervous System Two Months Post-Infection
Lymph Node One Week Post-Infection
Lymph Node Two Months Post-Infection

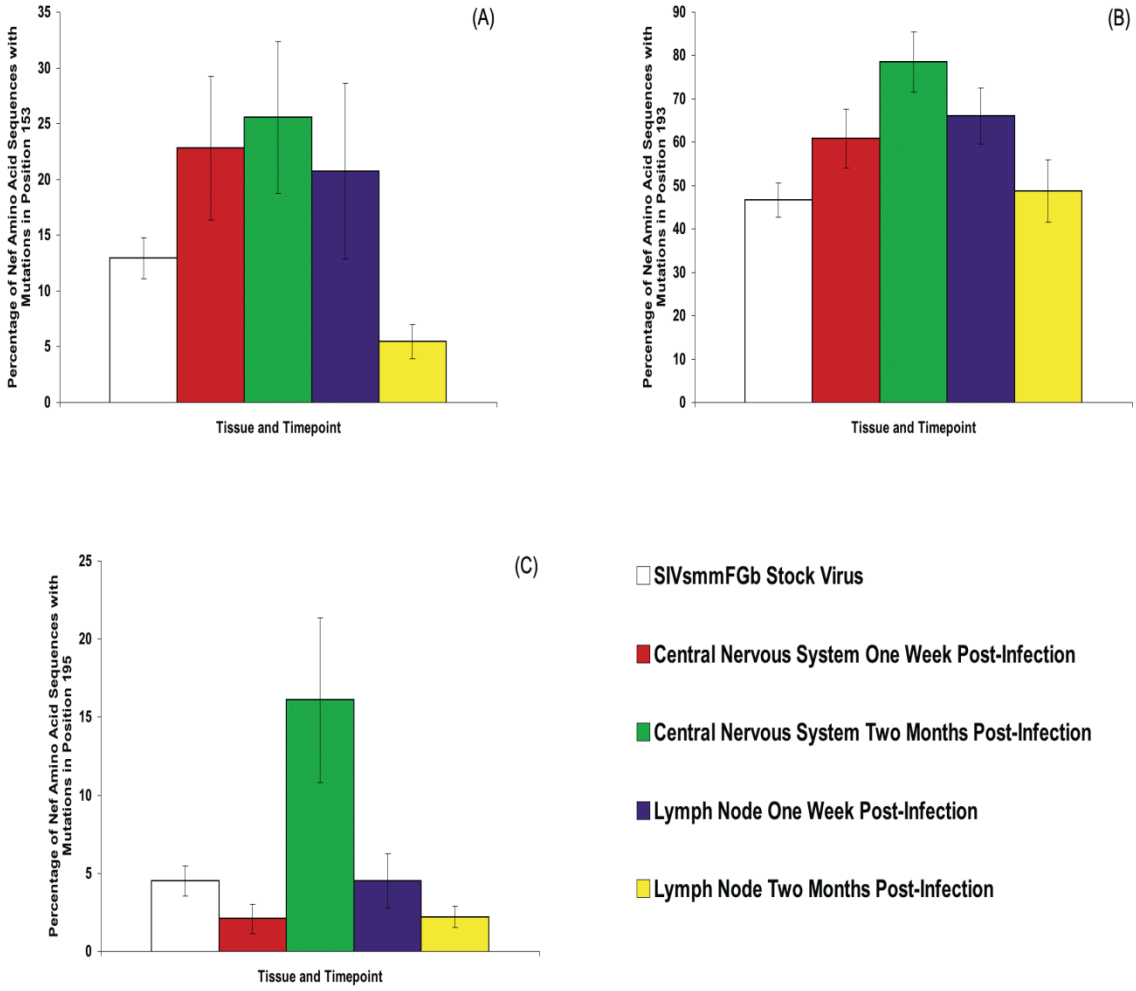

Figure 41. Prevalence of Nef thioesterase binding site and AP interaction site amino acid mutations in sequences harvested from the SIVsmmFGb stock virus, lymph node at one wpi, CNS at one wpi, lymph node at two mpi and CNS at two mpi. Percentage of sequences with mutations at positions (A) 153, (B) 193 and (C) 195. Statistical comparisons of the prevalence of each mutation in each sequence pool are provided in Tables 48 – 50.

Index of Tables[2]

[2] All Tables, except 1 and 3, are based on data generated by the Ph.D. candidate.

Table 1. Description and sequences of primers used for PCR amplification of *env*, *nef* and *int* genes from SIVsmmFGb virus stocks[3]

Primer Number	Primer Coordinates[1]	Primer Description	Primer Sequence (5' to 3')
919	6419	*env* outer forward	TCTTAAAAAGGGCTTGGG
920	9383	*env* outer reverse	AAAATGAGACATGTCTAT
922	6464	*env* inner forward	AAGAAGAACTCCGAAGAAG
923	9282	*env* inner reverse	CATCCATGTTTTGTTGTC
915	8856	*nef* outer forward	ATATTCATTTCCTGATCCGCC
916	9858	*nef* outer reverse	TCCCCAGTACCTCCCCGTAAC
917	8885	*nef* inner forward	CGCCTCTTGACTTGGCT
918	9827	*nef* inner reverse	TGGAAAGTCCCTGCTGTC
898A	4122	*int* outer forward	AAAGGCAGGCTATGTAACAG
899A	5326	*int* outer reverse	GCTATGCCACTTCTCTAGCCTCCCC
900A	4156	*int* inner forward	AAGGCAAAACCTTTGGAACAGA
901A	5295	*int* inner reverse	TTCCAAGTGGGGACCACTATCC

[1]Primer coordinates based on PGm5.3 genome[4]

[3] Primers created by F.J. Novembre.

Table 2. Description and sequences of primers used for PCR amplification of *env*, *nef* and *int* genes from tissue proviral DNA[4]

Primer Number	Primer Coordinates[1]	Primer Description	Primer Sequence (5' to 3')
952	6360	*env* outer forward	GAGGCGTGCTCTAATACAT
953	9299	*env* outer reverse	ATCATCATCATCTACATCATC
954	6474	*env* inner forward	CCGAAGAAGGCTAAGGCTAATACA
955	9210	*env* inner reverse	ATTGTCCCTCACTGTATCCCTG
959	8806	*nef* outer forward	AGACGGTGGAGACAGAGGTGG
960	9950	*nef* outer reverse	TCAATCTGCCAGCCTCTCCG
961	8947	*nef* inner forward	CCAACCAGTGTTCCAGAGGC
962	9845	*nef* inner reverse	CCCGTAACATCCCCTTTGTGG
963	4021	*int* outer forward	CCTCCCTTAGTCAGATTAGTC
964	5433	*int* outer reverse	GGGAAGATTACTCTGCTG
965	4106	*int* inner forward	GGCAATCAAGAGAAGGAAAGGC
966	5378	*int* inner reverse	CATAACAAGCCTTCTGTAGGTCC

[1]Primer coordinates based on PGm5.3 genome (444)

[4] Primers created by Ph.D. candidate, with assistance from N.C. Pearce.

Table 3. In situ hybridization results on short fixation tissue specimens harvested at necropsy from pigtailed macaques infected i.v. with SIVsmmFGb[5]

		Animal					
		PQq1	**PQo1**	**PKo1**	**PFp1**	**PGt1**	**PHs1**
	Sacrificed (dpi)	5	5	7	7	7	7
Systemic Lymphoid Tissues	**Spleen**	4[1,3]	2	4	5	5[3]	5[3]
	Inguinal Lymph Node	5	4	4	5	5[3]	5[3]
	Bone Marrow	0	0[2]	2	3	4	4
Gastrointestinal Tissues	**Stomach, Fundus**	3	1[2]	3	3	4	3
	Stomach, Pylorus	4	2	3	4	4	3
	Duodenum	4	1	3	4	5	4
	Jejunum	5	0[2]	3	4	4	4
	Ileum	4	2	4	3	3	3
	Colon	5	1	2	4	4	4
	Rectum	4	1	2	4	4	4
Brain Tissues	**Prefrontal Cortex**	0	0	0	2[4]	2	0
	Midfrontal Cortex	0	0	0	1	1	0
	Basal Ganglia	ND	ND	ND	ND	1	ND
	Hippocampus	0	0	0	ND	2	0
	Cerebellar Cortex	0	0	0	1	0	0
	Medulla	ND	ND	ND	ND	ND	1

[1]ND – Not done; 0 – No infected cells; 1 – Rare infected cells; 2 – Small numbers of infected cells; 3 – Moderate numbers of infected cells; 4 – Large numbers of infected cells; 5 – Extremely large numbers of infected cells

[2]Quality of short fixation specimen evaluated not satisfactory for proper analysis

[3]Diffuse hybridization present, indicating dendritic cell trapping of virions.

[4]SIV+ cells in parenchyma, as well as meninges.

[5] Data generated by H.G. Domingues and S.P. O'Neil.

Table 4. Mantel's test results for inter-tissue *env* V1 region compartmentalization in SIVsmmFGb-infected pigtailed macaques at one wpi

PFp1	Pearson's Correlation Coefficient	p-Value	PGt1	Pearson's Correlation Coefficient	p-Value
A x B	0.082	0.001[1]	**A x B**	0.141	0.001
A x C	0.033	0.183	**A x C**	0.201	0.001
A x F	- 0.015	0.523	**A x F**	0.040	0.201
A x H	- 0.047	0.045	**A x H**	0.037	0.221
A x M	- 0.019	0.391	**A x M**	0.016	0.515
B x C	0.105	0.001	**B x C**	0.453	0.001
B x F	0.095	0.001	**B x F**	0.270	0.001
B x H	0.265	0.001	**B x H**	0.038	0.127
B x M	0.172	0.001	**B x M**	0.222	0.001
C x F	0.019	0.543	**C x F**	0.175	0.001
C x H	- 0.019	0.571	**C x H**	0.283	0.001
C x M	0.009	0.761	**C x M**	0.067	0.005
F x H	0.057	0.087	**F x H**	0.107	0.001
F x M	0.032	0.295	**F x M**	- 0.045	0.075
H x M	- 0.029	0.333	**H x M**	0.093	0.001

Abbreviations: A, axillary lymph node; B, basal ganglia; C, cerebellum; F, midfrontal cortex; H, hippocampus; M, mesenteric lymph node.

[1]p-values < or = 0.05 noted in red.

PHs1	Pearson's Correlation Coefficient	p-Value	PKo1	Pearson's Correlation Coefficient	p-Value
A x B	0.136	0.001[1]	**A x B**	0.028	0.283
A x C	0.080	0.001	**A x C**	0.781	0.001
A x F	0.157	0.001	**A x F**	0.019	0.415
A x H	0.021	0.513	**A x H**	0.076	0.003
A x M	0.01	0.635	**A x M**	0.082	0.007
B x C	0.076	0.001	**B x C**	0.957	0.001
B x F	0.243	0.001	**B x F**	- 0.017	0.463
B x H	0.277	0.001	**B x H**	0.017	0.521
B x M	0.201	0.001	**B x M**	0.180	0.001
C x F	0.171	0.001	**C x F**	0.872	0.001
C x H	0.059	0.053	**C x H**	0.992	0.001
C x M	0.052	0.079	**C x M**	0.845	0.001
F x H	0.191	0.001	**F x H**	0.009	0.701
F x M	0.158	0.001	**F x M**	0.116	0.001
H x M	0.079	0.025	**H x M**	0.276	0.001

Abbreviations: A, axillary lymph node; B, basal ganglia; C, cerebellum; F, midfrontal cortex; H, hippocampus; M, mesenteric lymph node.

[1]p-values < or = 0.05 noted in red.

PQo1	Pearson's Correlation Coefficient	p-Value	PQq1	Pearson's Correlation Coefficient	p-Value
A x B	ND[1]	ND	**A x B**	0.191	0.001[2]
A x C	ND	ND	**A x C**	0.028	0.327
A x F	ND	ND	**A x F**	0.109	0.001
A x H	0.285	0.001	**A x H**	0.125	0.001
A x M	0.423	0.001	**A x M**	- 0.013	0.479
B x C	ND	ND	**B x C**	0.024	0.383
B x F	ND	ND	**B x F**	0.209	0.001
B x H	ND	ND	**B x H**	0.249	0.001
B x M	ND	ND	**B x M**	0.074	0.001
C x F	ND	ND	**C x F**	0.107	0.001
C x H	ND	ND	**C x H**	0.123	0.001
C x M	ND	ND	**C x M**	0.061	0.005
F x H	ND	ND	**F x H**	0.313	0.001
F x M	ND	ND	**F x M**	0.009	0.631
H x M	0.710	0.001	**H x M**	0.231	0.001

Abbreviations: A, axillary lymph node; B, basal ganglia; C, cerebellum; F, midfrontal cortex; H, hippocampus; M, mesenteric lymph node.

[1]ND = Not determined due to absence of data from one or more PQo1 tissues.

[2]p-values < or = 0.05 noted in red.

Table 5. Mantel's test results for inter-tissue *nef* compartmentalization in SIVsmmFGb-infected pigtailed macaques at one wpi

PFp1	Pearson's Correlation Coefficient	p-Value	PGt1	Pearson's Correlation Coefficient	p-Value
A x B	0.549	0.001[1]	**A x B**	0.368	0.001
A x C	0.084	0.009	**A x C**	0.082	0.009
A x F	0.139	0.001	**A x F**	0.049	0.085
A x H	0.120	0.001	**A x H**	0.091	0.003
A x M	0.027	0.389	**A x M**	0.029	0.379
B x C	0.493	0.001	**B x C**	0.397	0.001
B x F	0.473	0.001	**B x F**	0.224	0.001
B x H	0.586	0.001	**B x H**	0.387	0.001
B x M	0.394	0.001	**B x M**	0.420	0.001
C x F	0.114	0.003	**C x F**	0.084	0.003
C x H	0.115	0.005	**C x H**	0.072	0.007
C x M	0.061	0.077	**C x M**	0.068	0.013
F x H	0.147	0.001	**F x H**	0.137	0.001
F x M	0.085	0.019	**F x M**	0.082	0.003
H x M	0.112	0.001	**H x M**	0.056	0.053

Abbreviations: A, axillary lymph node; B, basal ganglia; C, cerebellum; F, midfrontal cortex; H, hippocampus; M, mesenteric lymph node.

[1]p-values < or = 0.05 noted in red.

PHs1	Pearson's Correlation Coefficient	p-Value	PKo1	Pearson's Correlation Coefficient	p-Value
A x B	0.250	0.001[1]	**A x B**	0.732	0.001
A x C	0.324	0.001	**A x C**	0.754	0.001
A x F	0.314	0.001	**A x F**	0.346	0.001
A x H	0.407	0.001	**A x H**	0.594	0.001
A x M	0.033	0.247	**A x M**	0.809	0.001
B x C	0.590	0.001	**B x C**	0.985	0.001
B x F	0.501	0.001	**B x F**	0.600	0.001
B x H	0.482	0.001	**B x H**	0.902	0.001
B x M	0.331	0.001	**B x M**	0.989	0.001
C x F	0.408	0.001	**C x F**	0.695	0.001
C x H	0.555	0.001	**C x H**	0.834	0.001
C x M	0.155	0.001	**C x M**	0.981	0.001
F x H	0.413	0.001	**F x H**	0.548	0.001
F x M	0.086	0.003	**F x M**	0.693	0.001
H x M	0.193	0.001	**H x M**	0.900	0.001

Abbreviations: A, axillary lymph node; B, basal ganglia; C, cerebellum; F, midfrontal cortex; H, hippocampus; M, mesenteric lymph node.

[1]p-values < or = 0.05 noted in red.

PQo1	Pearson's Correlation Coefficient	p-Value	PQq1	Pearson's Correlation Coefficient	p-Value
A x B	ND[1]	ND	**A x B**	0.159	0.001[2]
A x C	0.560	0.001	**A x C**	0.175	0.001
A x F	ND	ND	**A x F**	0.087	0.011
A x H	0.360	0.001	**A x H**	0.133	0.001
A x M	0.450	0.001	**A x M**	0.025	0.361
B x C	ND	ND	**B x C**	0.302	0.001
B x F	ND	ND	**B x F**	0.255	0.001
B x H	ND	ND	**B x H**	0.193	0.001
B x M	ND	ND	**B x M**	0.105	0.001
C x F	ND	ND	**C x F**	0.343	0.001
C x H	0.888	0.001	**C x H**	0.306	0.001
C x M	0.425	0.001	**C x M**	0.204	0.001
F x H	ND	ND	**F x H**	0.248	0.001
F x M	ND	ND	**F x M**	0.245	0.001
H x M	0.711	0.001	**H x M**	0.078	0.019

Abbreviations: A, axillary lymph node; B, basal ganglia; C, cerebellum; F, midfrontal cortex; H, hippocampus; M, mesenteric lymph node.

[1]ND = Not determined due to absence of data from one or more PQo1 tissues.

[2]p-values < or = 0.05 noted in red.

Table 6. Mantel's test results for *int* inter-tissue compartmentalization in SIVsmmFGb-infected pigtailed macaques at one wpi

PFp1	Pearson's Correlation Coefficient	p-Value	PGt1	Pearson's Correlation Coefficient	p-Value
A x B	0.220	0.001[1]	**A x B**	0.135	0.001
A x C	0.007	0.789	**A x C**	0.226	0.001
A x F	0.291	0.001	**A x F**	0.086	0.003
A x H	0.115	0.001	**A x H**	0.446	0.001
A x M	- 0.037	0.271	**A x M**	0.006	0.917
B x C	0.151	0.001	**B x C**	0.232	0.001
B x F	0.489	0.001	**B x F**	0.229	0.001
B x H	0.231	0.001	**B x H**	0.681	0.001
B x M	0.136	0.001	**B x M**	0.176	0.001
C x F	0.200	0.001	**C x F**	0.226	0.001
C x H	0.077	0.001	**C x H**	0.706	0.001
C x M	- 0.083	< 0.001	**C x M**	0.213	0.001
F x H	0.335	0.001	**F x H**	0.431	0.001
F x M	0.395	0.001	**F x M**	0.052	0.053
H x M	0.063	0.063	**H x M**	0.535	0.001

Abbreviations: A, axillary lymph node; B, basal ganglia; C, cerebellum; F, midfrontal cortex; H, hippocampus; M, mesenteric lymph node.

[1]p-values < or = 0.05 noted in red.

PHs1	Pearson's Correlation Coefficient	p-Value	PKo1	Pearson's Correlation Coefficient	p-Value
A x B	0.117	0.001[1]	**A x B**	0.395	0.001
A x C	0.055	0.091	**A x C**	0.248	0.001
A x F	0.087	0.005	**A x F**	0.114	0.005
A x H	0.058	0.047	**A x H**	0.640	0.001
A x M	0.040	0.093	**A x M**	0.236	0.001
B x C	0.301	0.001	**B x C**	0.484	0.001
B x F	0.289	0.001	**B x F**	0.500	0.001
B x H	0.163	0.001	**B x H**	0.922	0.001
B x M	0.133	0.001	**B x M**	0.495	0.001
C x F	0.160	0.001	**C x F**	0.322	0.001
C x H	0.095	0.001	**C x H**	0.568	0.001
C x M	0.010	0.741	**C x M**	0.365	0.001
F x H	0.097	0.003	**F x H**	0.612	0.001
F x M	0.137	0.001	**F x M**	0.348	0.001
H x M	0.040	0.143	**H x M**	0.654	0.001

Abbreviations: A, axillary lymph node; B, basal ganglia; C, cerebellum; F, midfrontal cortex; H, hippocampus; M, mesenteric lymph node.

[1]p-values < or = 0.05 noted in red.

PQo1	Pearson's Correlation Coefficient	p-Value	PQq1	Pearson's Correlation Coefficient	p-Value
A x B	ND[1]	ND	**A x B**	0.093	0.001[2]
A x C	ND	ND	**A x C**	0.121	0.001
A x F	0.504	0.001	**A x F**	0.370	0.001
A x H	0.710	0.001	**A x H**	0.280	0.001
A x M	0.052	0.075	**A x M**	0.063	0.017
B x C	ND	ND	**B x C**	0.106	0.001
B x F	ND	ND	**B x F**	0.308	0.001
B x H	ND	ND	**B x H**	0.317	0.001
B x M	ND	ND	**B x M**	0.123	0.001
C x F	ND	ND	**C x F**	0.353	0.001
C x H	ND	ND	**C x H**	0.281	0.001
C x M	ND	ND	**C x M**	0.071	0.003
F x H	0.970	0.001	**F x H**	0.612	0.001
F x M	0.394	0.001	**F x M**	0.347	0.001
H x M	0.619	0.001	**H x M**	0.218	0.001

Abbreviations: A, axillary lymph node; B, basal ganglia; C, cerebellum; F, midfrontal cortex; H, hippocampus; M, mesenteric lymph node.

[1]ND = Not determined due to absence of data from one or more PQo1 tissues.

[2]p-values < or = 0.05 noted in red.

Table 7. Proportion of SIVsmmFGb-infected pigtailed macaques with compartmentalization between compared tissues, as determined by Mantel's test[1]

Tissue Comparison	*env V1*	*nef*	*int*
A x B	4/5	5/5	5/5
A x C	3/5	6/6	3/5
A x F	**2/5**[2]	4/5	6/6
A x H	4/6	6/6	6/6
A x M	**2/6**	**2/6**	**2/6**
B x C	4/5	5/5	5/5
B x F	4/5	5/5	5/5
B x H	3/5	5/5	5/5
B x M	5/5	5/5	5/5
C x F	4/5	5/5	5/5
C x H	3/5	6/6	5/5
C x M	3/5	5/6	4/5
F x H	3/5	5/5	6/6
F x M	**2/5**	5/5	5/6
H x M	5/6	5/6	4/6

Abbreviations: A, axillary lymph node; B, basal ganglia; C, cerebellum; F, midfrontal cortex; H, hippocampus; M, mesenteric lymph node.

[1]Due to absence of data from certain PQo1 tissues, some proportions represent results from only the remaining five animals.

[2]Comparisons with compartmentalization in only a minority of animals noted in **green**.

Table 8. Determined p-values for statistical comparisons of mean d_S and d_N values for *env* V1 region, *nef* and *int* nucleotide sequences harvested from SIVsmmFGb-infected pigtailed macaque tissues at one wpi

	***env* V1 Region**		***nef***		***int***	
Tissue Comparison	d_S	d_N	d_S	d_N	d_S	d_N
A x B	< 0.001[1]	< 0.001	0.443	0.356	0.028	0.298
A x C	0.077	< 0.001	0.046	0.736	0.019	0.007
A x F	0.001	0.540	0.024	0.302	0.002	0.242
A x H	0.538	< 0.001	0.344	0.963	< 0.001	0.874
A x M	0.160	0.036	< 0.001	0.186	0.254	0.007
B x C	0.181	< 0.001	0.080	0.475	0.315	0.128
B x F	0.739	0.034	0.264	0.128	0.256	0.959
B x H	0.004	0.054	0.273	0.578	0.016	0.418
B x M	0.032	0.958	0.120	0.053	0.379	0.142
C x F	0.328	< 0.001	< 0.001	0.401	0.885	0.132
C x H	0.207	< 0.001	0.217	0.747	0.509	0.016
C x M	0.711	< 0.001	< 0.001	0.544	0.132	0.904
F x H	0.005	< 0.001	0.005	0.283	0.133	0.386
F x M	0.094	0.058	0.575	0.869	0.055	0.140
H x M	0.407	0.003	< 0.001	0.226	0.003	0.012

Abbreviations: A, axillary lymph node; B, basal ganglia; C, cerebellum; F, midfrontal cortex; H, hippocampus; M, mesenteric lymph node.

[1]p-values < or = 0.05 noted in red.

Table 9. Determined p-values for statistical comparisons of mean d_S/d_N values for *env* V1 region, *nef* and *int* nucleotide sequences harvested from SIVsmmFGb-infected pigtailed macaque tissues at one wpi

Tissue Comparison	*env* V1 Region	*nef*	*int*
A x B	0.010[1]	0.015	0.821
A x C	0.456	0.283	0.185
A x F	< 0.001	< 0.001	0.780
A x H	0.762	0.856	0.045
A x M	0.512	< 0.001	0.031
B x C	< 0.001	0.009	0.347
B x F	0.191	0.318	0.604
B x H	0.002	0.036	0.055
B x M	0.011	0.706	0.074
C x F	< 0.001	< 0.001	0.085
C x H	0.578	0.259	0.001
C x M	0.099	< 0.001	0.300
F x H	< 0.001	0.009	0.079
F x M	< 0.001	0.554	0.006
H x M	0.235	0.002	< 0.001

Abbreviations: A, axillary lymph node; B, basal ganglia; C, cerebellum; F, midfrontal cortex; H, hippocampus; M, mesenteric lymph node.

[1]p-values < or = 0.05 noted in red.

Table 10. Proportion of SIVsmmFGb-infected pigtailed macaques with compartmentalization between compared tissues as determined by Mantel's test

Tissue Comparison	*env V1*	*nef*	*int*
A x B	**3/6**[1]	6/6	6/6
A x C	4/6	6/6	5/6
A x F	5/6	6/6	6/6
A x H	4/6	6/6	6/6
A x M	**1/6**[2]	**0/6**	**1/6**
B x C	5/6	5/6	5/6
B x F	5/6	4/6	6/6
B x H	**3/6**	5/6	4/6
B x M	4/6	6/6	5/6
C x F	5/6	5/6	5/6
C x H	4/6	6/6	4/6
C x M	4/6	6/6	6/6
F x H	4/6	4/6	5/6
F x M	5/6	6/6	6/6
H x M	5/6	6/6	5/6

Abbreviations: A, axillary lymph node; B, basal ganglia; C, cerebellum; F, midfrontal cortex; H, hippocampus; M, mesenteric lymph node.

[1]Comparisons with compartmentalization in only half of the animals noted in **blue**.

[2]Comparisons with compartmentalization in only a minority of animals noted in **green**.

Table 11. Mantel's test results for *env* V1 region inter-tissue compartmentalization in SIVsmmFGb-infected pigtailed macaques at two mpi

PHt1	Pearson's Correlation Coefficient	p-Value	PKs1	Pearson's Correlation Coefficient	p-Value
A x B	0.081	0.007[1]	**A x B**	0.180	0.001
A x C	0.166	0.001	**A x C**	0.029	0.299
A x F	0.121	0.001	**A x F**	0.141	0.001
A x H	0.113	0.001	**A x H**	0.206	0.001
A x M	-0.024	0.405	**A x M**	0.005	0.939
B x C	0.112	0.001	**B x C**	0.609	0.001
B x F	0.183	0.001	**B x F**	0.724	0.001
B x H	0.209	0.001	**B x H**	0.283	0.001
B x M	0.155	0.001	**B x M**	0.128	0.001
C x F	0.284	0.001	**C x F**	0.228	0.001
C x H	0.710	0.001	**C x H**	0.213	0.001
C x M	0.263	0.001	**C x M**	0.028	0.305
F x H	0.716	0.001	**F x H**	0.181	0.001
F x M	0.217	0.001	**F x M**	0.064	0.033
H x M	0.206	0.001	**H x M**	0.139	0.001

Abbreviations: A, axillary lymph node; B, basal ganglia; C, cerebellum; F, midfrontal cortex; H, hippocampus; M, mesenteric lymph node.

[1]p-values < or = 0.05 noted in red.

PRv1	Pearson's Correlation Coefficient	p-Value	PUo1	Pearson's Correlation Coefficient	p-Value
A x B	0.050	0.069	**A x B**	0.042	0.197
A x C	-0.039	0.195	**A x C**	0.370	0.001[1]
A x F	0.096	0.001	**A x F**	0.085	0.005
A x H	0.007	0.727	**A x H**	0.154	0.001
A x M	-0.010	0.717	**A x M**	-0.010	0.743
B x C	0.210	0.001	**B x C**	0.705	0.001
B x F	0.962	0.001	**B x F**	0.334	0.001
B x H	0.008	0.799	**B x H**	0.019	0.493
B x M	0.171	0.001	**B x M**	0.352	0.001
C x F	0.862	0.001	**C x F**	0.580	0.001
C x H	0.152	0.001	**C x H**	0.565	0.001
C x M	0.052	0.181	**C x M**	0.292	0.001
F x H	0.960	0.001	**F x H**	0.243	0.001
F x M	0.271	0.001	**F x M**	0.075	0.017
H x M	0.120	0.001	**H x M**	0.174	0.001

Abbreviations: A, axillary lymph node; B, basal ganglia; C, cerebellum; F, midfrontal cortex; H, hippocampus; M, mesenteric lymph node.

[1]p-values < or = 0.05 noted in red.

PVu1	Pearson's Correlation Coefficient	p-Value	PYp1	Pearson's Correlation Coefficient	p-Value
A x B	0.197	0.001[1]	**A x B**	0.036	0.271
A x C	0.598	0.001	**A x C**	0.093	0.001
A x F	0.592	0.001	**A x F**	0.052	0.105
A x H	0.631	0.001	**A x H**	0.062	0.065
A x M	0.089	0.009	**A x M**	0.007	0.793
B x C	0.233	0.001	**B x C**	0.012	0.695
B x F	0.244	0.001	**B x F**	-0.006	0.797
B x H	0.242	0.001	**B x H**	0.012	0.723
B x M	0.033	0.289	**B x M**	-0.013	0.631
C x F	0.188	0.001	**C x F**	0.003	0.935
C x H	-0.001	0.963	**C x H**	-0.011	0.725
C x M	0.293	0.001	**C x M**	0.021	0.443
F x H	0.002	0.947	**F x H**	-0.001	0.973
F x M	0.238	0.001	**F x M**	-0.004	0.899
H x M	0.240	0.001	**H x M**	-0.001	0.927

Abbreviations: A, axillary lymph node; B, basal ganglia; C, cerebellum; F, midfrontal cortex; H, hippocampus; M, mesenteric lymph node.

[1]p-values < or = 0.05 noted in red.

Table 12. Mantel's test results for *nef* inter-tissue compartmentalization in SIVsmmFGb-infected pigtailed macaques at two mpi

PHt1	Pearson's Correlation Coefficient	p-Value	PKs1	Pearson's Correlation Coefficient	p-Value
A x B	0.689	0.001[1]	**A x B**	0.144	0.001
A x C	0.301	0.001	**A x C**	0.233	0.001
A x F	0.392	0.001	**A x F**	0.178	0.001
A x H	0.374	0.001	**A x H**	0.129	0.001
A x M	0.037	0.173	**A x M**	0.004	0.919
B x C	0.586	0.001	**B x C**	0.369	0.001
B x F	0.981	0.001	**B x F**	0.393	0.001
B x H	0.983	0.001	**B x H**	0.316	0.001
B x M	0.793	0.001	**B x M**	0.228	0.001
C x F	0.513	0.001	**C x F**	0.319	0.001
C x H	0.577	0.001	**C x H**	0.208	0.001
C x M	0.390	0.001	**C x M**	0.220	0.001
F x H	0.948	0.001	**F x H**	0.228	0.001
F x M	0.410	0.001	**F x M**	0.163	0.001
H x M	0.356	0.001	**H x M**	0.244	0.001

Abbreviations: A, axillary lymph node; B, basal ganglia; C, cerebellum; F, midfrontal cortex; H, hippocampus; M, mesenteric lymph node.

[1]p-values < or = 0.05 noted in red.

PRv1	Pearson's Correlation Coefficient	p-Value	PUo1	Pearson's Correlation Coefficient	p-Value
A x B	0.160	0.001[1]	**A x B**	0.511	0.001
A x C	0.304	0.001	**A x C**	0.503	0.001
A x F	0.187	0.001	**A x F**	0.104	0.007
A x H	0.163	0.001	**A x H**	0.223	0.001
A x M	-0.020	0.561	**A x M**	-0.010	0.761
B x C	0.387	0.001	**B x C**	0.741	0.001
B x F	0.274	0.001	**B x F**	0.435	0.001
B x H	0.115	0.001	**B x H**	0.527	0.001
B x M	0.231	0.001	**B x M**	0.497	0.001
C x F	0.201	0.001	**C x F**	0.579	0.001
C x H	0.190	0.001	**C x H**	0.463	0.001
C x M	0.330	0.001	**C x M**	0.536	0.001
F x H	0.154	0.001	**F x H**	0.197	0.001
F x M	0.171	0.001	**F x M**	0.135	0.001
H x M	0.166	0.001	**H x M**	0.267	0.001

Abbreviations: A, axillary lymph node; B, basal ganglia; C, cerebellum; F, midfrontal cortex; H, hippocampus; M, mesenteric lymph node.

[1]p-values < or = 0.05 noted in red.

PVu1	Pearson's Correlation Coefficient	p-Value	PYp1	Pearson's Correlation Coefficient	p-Value
A x B	0.310	0.001[1]	**A x B**	0.364	0.001
A x C	0.340	0.001	**A x C**	0.702	0.001
A x F	0.203	0.001	**A x F**	0.667	0.001
A x H	0.216	0.001	**A x H**	0.607	0.001
A x M	0.025	0.383	**A x M**	0.045	0.105
B x C	0.434	0.001	**B x C**	-0.021	0.401
B x F	0.012	0.621	**B x F**	-0.042	0.115
B x H	0.102	0.001	**B x H**	-0.008	0.739
B x M	0.175	0.001	**B x M**	0.346	0.001
C x F	0.368	0.001	**C x F**	0.021	0.461
C x H	0.187	0.001	**C x H**	0.088	0.009
C x M	0.316	0.001	**C x M**	0.774	0.001
F x H	0.025	0.361	**F x H**	0.035	0.277
F x M	0.099	0.001	**F x M**	0.730	0.001
H x M	0.097	0.001	**H x M**	0.636	0.001

Abbreviations: A, axillary lymph node; B, basal ganglia; C, cerebellum; F, midfrontal cortex; H, hippocampus; M, mesenteric lymph node.

[1]p-values < or = 0.05 noted in red.

Table 13. Mantel's test results for *int* inter-tissue compartmentalization in SIVsmmFGb-infected pigtailed macaques at two mpi

PHt1	Pearson's Correlation Coefficient	p-Value	PKs1	Pearson's Correlation Coefficient	p-Value
A x B	0.177	0.001[1]	**A x B**	0.610	0.001
A x C	0.054	0.079	**A x C**	0.514	0.001
A x F	0.488	0.001	**A x F**	0.329	0.001
A x H	0.303	0.001	**A x H**	0.104	0.003
A x M	0.004	0.945	**A x M**	0.002	0.955
B x C	0.339	0.001	**B x C**	0.964	0.001
B x F	0.719	0.001	**B x F**	0.818	0.001
B x H	0.356	0.001	**B x H**	0.685	0.001
B x M	0.208	0.001	**B x M**	0.613	0.001
C x F	0.646	0.001	**C x F**	0.835	0.001
C x H	0.342	0.001	**C x H**	0.574	0.001
C x M	0.117	0.001	**C x M**	0.604	0.001
F x H	0.719	0.001	**F x H**	0.333	0.001
F x M	0.502	0.001	**F x M**	0.296	0.001
H x M	0.371	0.001	**H x M**	0.099	0.001

Abbreviations: A, axillary lymph node; B, basal ganglia; C, cerebellum; F, midfrontal cortex; H, hippocampus; M, mesenteric lymph node.

[1]p-values < or = 0.05 noted in red.

PRv1	Pearson's Correlation Coefficient	p-Value	PUo1	Pearson's Correlation Coefficient	p-Value
A x B	0.480	0.001[1]	**A x B**	0.188	0.001
A x C	0.182	0.001	**A x C**	0.333	0.001
A x F	0.262	0.001	**A x F**	0.438	0.001
A x H	0.545	0.001	**A x H**	0.070	0.029
A x M	0.053	0.119	**A x M**	-0.003	0.939
B x C	0.469	0.001	**B x C**	0.407	0.001
B x F	0.653	0.001	**B x F**	0.476	0.001
B x H	0.003	0.987	**B x H**	0.222	0.001
B x M	0.426	0.001	**B x M**	0.113	0.001
C x F	0.322	0.001	**C x F**	0.513	0.001
C x H	0.534	0.001	**C x H**	0.352	0.001
C x M	0.133	0.001	**C x M**	0.317	0.001
F x H	0.717	0.001	**F x H**	0.493	0.001
F x M	0.255	0.001	**F x M**	0.446	0.001
H x M	0.491	0.001	**H x M**	0.060	0.061

Abbreviations: A, axillary lymph node; B, basal ganglia; C, cerebellum; F, midfrontal cortex; H, hippocampus; M, mesenteric lymph node.

[1]p-values < or = 0.05 noted in red.

PVu1	Pearson's Correlation Coefficient	p-Value	PYp1	Pearson's Correlation Coefficient	p-Value
A x B	0.400	0.001[1]	**A x B**	0.262	0.001
A x C	0.090	0.003	**A x C**	0.504	0.001
A x F	0.106	0.001	**A x F**	0.669	0.001
A x H	0.160	0.001	**A x H**	0.362	0.001
A x M	0.383	0.001	**A x M**	0.031	0.369
B x C	0.248	0.001	**B x C**	0.046	0.121
B x F	0.088	0.003	**B x F**	0.134	0.001
B x H	0.088	0.001	**B x H**	0.024	0.439
B x M	0.001	0.957	**B x M**	0.310	0.001
C x F	0.096	0.001	**C x F**	0.011	0.735
C x H	0.049	0.590	**C x H**	0.034	0.303
C x M	0.241	0.001	**C x M**	0.528	0.001
F x H	0.035	0.291	**F x H**	0.077	0.015
F x M	0.100	0.001	**F x M**	0.719	0.001
H x M	0.067	0.011	**H x M**	0.359	0.001

Abbreviations: A, axillary lymph node; B, basal ganglia; C, cerebellum; F, midfrontal cortex; H, hippocampus; M, mesenteric lymph node.

[1]p-values < or = 0.05 noted in red.

Table 14. Determined p-values for statistical comparisons of mean d_S and d_N values for *env* V1 region, *nef* and *int* nucleotide sequences harvested from SIVsmmFGb-infected pigtailed macaque tissues at two mpi

	***env* V1 Region**		***nef***		***int***	
Tissue Comparison	d_S	d_N	d_S	d_N	d_S	d_N
A x B	< 0.001[1]	< 0.001	0.009	0.026	0.438	< 0.001
A x C	0.068	0.827	0.428	< 0.001	0.709	0.067
A x F	0.033	0.994	0.004	0.183	0.193	0.036
A x H	0.989	< 0.001	0.040	0.003	0.973	< 0.001
A x M	0.011	0.249	0.322	0.099	0.438	0.303
B x C	0.010	< 0.001	0.003	0.003	0.653	0.002
B x F	< 0.001	< 0.001	< 0.001	0.457	0.606	0.014
B x H	< 0.001	0.011	< 0.001	0.319	0.391	0.644
B x M	< 0.001	0.002	< 0.001	0.562	0.941	< 0.001
C x F	< 0.001	0.237	0.039	0.003	0.340	0.676
C x H	0.096	< 0.001	0.262	0.247	0.573	0.019
C x M	< 0.001	0.331	0.736	< 0.001	0.657	0.508
F x H	0.027	0.006	0.296	0.146	0.168	0.093
F x M	0.628	0.334	0.066	0.955	0.563	0.277
H x M	0.009	0.044	0.450	0.078	0.453	0.005

Abbreviations: A, axillary lymph node; B, basal ganglia; C, cerebellum; F, midfrontal cortex; H, hippocampus; M, mesenteric lymph node.

[1]p-values < or = 0.05 noted in red.

Table 15. Determined p-values for statistical comparisons of mean d_S/d_N values for *env* V1 region, *nef* and *int* nucleotide sequences harvested from SIVsmmFGb-infected pigtailed macaque tissues at two mpi

Tissue Comparison	***env* V1 Region**	***nef***	***int***
A x B	0.018[1]	< 0.001	< 0.001
A x C	0.857	0.010	0.199
A x F	0.020	0.047	0.244
A x H	0.234	0.538	< 0.001
A x M	0.010	0.649	0.398
B x C	0.023	0.043	0.011
B x F	< 0.001	< 0.001	0.003
B x H	0.001	< 0.001	0.821
B x M	< 0.001	< 0.001	0.005
C x F	< 0.001	< 0.001	0.821
C x H	0.123	0.001	0.008
C x M	0.003	0.039	0.727
F x H	0.041	0.144	0.002
F x M	0.812	0.022	0.862
H x M	0.116	0.299	0.003

Abbreviations: A, axillary lymph node; B, basal ganglia; C, cerebellum; F, midfrontal cortex; H, hippocampus; M, mesenteric lymph node.

[1]p-values < or = 0.05 noted in red.

Table 16A. Determined p-values for statistical comparisons of average pairwise distances of SIVsmmFGb *env* V1 region nucleotide sequences between SIVsmmFGb-infected pigtailed macaque lymph nodes and CNS regions

		One Week Post-Infection									
		A x C	**A x F**	**A x H**	**A x M**	**B x C**	**B x F**	**B x H**	**B x M**	**C x F**	**C x H**
One Week Post-Infection	**A x B**	< 0.001[1]	< 0.001	0.007	0.348	< 0.001	< 0.001	0.013	< 0.001	< 0.001	< 0.001
	A x C		< 0.001	< 0.001	< 0.001	< 0.001	< 0.001	< 0.001	< 0.001	0.003	< 0.001
	A x F			0.355	< 0.001	< 0.001	0.145	0.38	< 0.001	< 0.001	< 0.001
	A x H				0.026	< 0.001	0.921	0.728	< 0.001	< 0.001	< 0.001
	A x M					< 0.001	< 0.001	0.024	< 0.001	< 0.001	< 0.001
	B x C						< 0.001	< 0.001	< 0.001	< 0.001	< 0.001
	B x F							0.695	< 0.001	< 0.001	< 0.001
	B x H								< 0.001	< 0.001	< 0.001
	B x M									< 0.001	< 0.001
	C x F										< 0.001

Abbreviations: A, axillary lymph node; B, basal ganglia; C, cerebellum; F, midfrontal cortex; H, hippocampus; M, mesenteric lymph node.

[1]p-values < or = 0.05 noted in red.

Table 16B. Determined p-values for statistical comparisons of average pairwise distances of SIVsmmFGb *env* V1 region nucleotide sequences between SIVsmmFGb-infected pigtailed macaque lymph nodes and CNS regions (continued)

		One Week Post-Infection					Two Months Post-Infection				
		C x M	**F x H**	**F x M**	**H x M**		**A x B**	**A x C**	**A x F**	**A x H**	**A x M**
One Week Post-Infection	**A x B**	< 0.001[1]	0.168	< 0.001	< 0.001		0.153	< 0.001	< 0.001	< 0.001	< 0.001
	A x C	< 0.001	< 0.001	< 0.001	< 0.001		< 0.001	0.138	0.601	< 0.001	< 0.001
	A x F	< 0.001	< 0.001	< 0.001	< 0.001		0.154	< 0.001	< 0.001	< 0.001	< 0.001
	A x H	< 0.001	< 0.001	< 0.001	< 0.001		0.652	< 0.001	< 0.001	< 0.001	< 0.001
	A x M	< 0.001	0.015	< 0.001	< 0.001		0.211	< 0.001	< 0.001	< 0.001	< 0.001
	B x C	< 0.001	< 0.001	< 0.001	< 0.001		< 0.001	< 0.001	< 0.001	< 0.001	0.01
	B x F	< 0.001	< 0.001	< 0.001	< 0.001		0.249	< 0.001	< 0.001	< 0.001	< 0.001
	B x H	< 0.001	< 0.001	0.002	< 0.001		0.044	< 0.001	< 0.001	< 0.001	< 0.001
	B x M	0.836	0.005	< 0.001	< 0.001		< 0.001	< 0.001	< 0.001	< 0.001	< 0.001
	C x F	0.024	< 0.001	< 0.001	0.969		< 0.001	0.147	< 0.001	< 0.001	< 0.001
	C x H	< 0.001	< 0.001	< 0.001	< 0.001		< 0.001	< 0.001	< 0.001	0.01	< 0.001
	C x M		0.007	< 0.001	< 0.001		< 0.001	< 0.001	< 0.001	< 0.001	< 0.001
	F x H			< 0.001	< 0.001		0.002	< 0.001	< 0.001	< 0.001	< 0.001
	F x M				< 0.001		< 0.001	< 0.001	< 0.001	< 0.001	< 0.001
	H x M						< 0.001	0.033	0.002	< 0.001	< 0.001
Two Months Post-Infection	**A x B**							< 0.001	< 0.001	< 0.001	< 0.001
	A x C								0.275	< 0.001	< 0.001
	A x F									< 0.001	0.006
	A x H										< 0.001

Abbrev.: A, axillary lymph node; B, basal ganglia; C, cerebellum; F, midfrontal cortex; H, hippocampus; M, mesenteric lymph node.

[1]p-values < or = 0.05 noted in red.

Table 16C. Determined p-values for statistical comparisons of average pairwise distances of SIVsmmFGb *env* V1 region nucleotide sequences between SIVsmmFGb-infected pigtailed macaque lymph nodes and CNS regions (continued)

		Two Months Post-Infection									
		B x C	**B x F**	**B x H**	**B x M**	**C x F**	**C x H**	**C x M**	**F x H**	**F x M**	**H x M**
One Week Post-Infection	**A x B**	< 0.001[1]	< 0.001	< 0.001	0.709	< 0.001	< 0.001	< 0.001	< 0.001	< 0.001	< 0.001
	A x C	< 0.001	< 0.001	< 0.001	< 0.001	< 0.001	< 0.001	0.014	< 0.001	0.015	< 0.001
	A x F	< 0.001	< 0.001	0.096	0.006	< 0.001	< 0.001	< 0.001	< 0.001	< 0.001	< 0.001
	A x H	< 0.001	< 0.001	0.005	0.077	< 0.001	< 0.001	< 0.001	< 0.001	< 0.001	< 0.001
	A x M	< 0.001	< 0.001	< 0.001	0.97	< 0.001	< 0.001	< 0.001	< 0.001	< 0.001	< 0.001
	B x C	< 0.001	< 0.001	< 0.001	< 0.001	< 0.001	< 0.001	< 0.001	< 0.001	< 0.001	0.548
	B x F	< 0.001	< 0.001	0.051	0.051	< 0.001	< 0.001	< 0.001	< 0.001	< 0.001	< 0.001
	B x H	< 0.001	< 0.001	0.019	0.003	< 0.001	< 0.001	< 0.001	0.007	< 0.001	< 0.001
	B x M	< 0.001	< 0.001	< 0.001	< 0.001	< 0.001	< 0.001	< 0.001	< 0.001	0.002	< 0.001
	C x F	< 0.001	< 0.001	< 0.001	< 0.001	< 0.001	< 0.001	0.967	< 0.001	0.484	< 0.001
	C x H	< 0.001	< 0.001	< 0.001	< 0.001	< 0.001	< 0.001	< 0.001	< 0.001	< 0.001	0.015
	C x M	< 0.001	< 0.001	< 0.001	< 0.001	< 0.001	< 0.001	0.034	< 0.001	< 0.001	< 0.001
	F x H	< 0.001	< 0.001	< 0.001	0.065	< 0.001	< 0.001	< 0.001	< 0.001	< 0.001	< 0.001
	F x M	< 0.001	0.169	0.397	< 0.001	< 0.001	< 0.001	< 0.001	0.667	< 0.001	< 0.001
	H x M	< 0.001	< 0.001	< 0.001	< 0.001	< 0.001	< 0.001	0.504	< 0.001	0.357	< 0.001

Abbreviations: A, axillary lymph node; B, basal ganglia; C, cerebellum; F, midfrontal cortex; H, hippocampus; M, mesenteric lymph node.

[1]p-values < or = 0.05 noted in red.

Table 16D. Determined p-values for statistical comparisons of average pairwise distances of SIVsmmFGb *env* V1 region nucleotide sequences between SIVsmmFGb-infected pigtailed macaque lymph nodes and CNS regions (continued)

		Two Months Post-Infection									
		B x C	**B x F**	**B x H**	**B x M**	**C x F**	**C x H**	**C x M**	**F x H**	**F x M**	**H x M**
Two Months Post-Infection	**A x B**	< 0.001[1]	< 0.001	< 0.001	0.386	< 0.001	< 0.001	< 0.001	< 0.001	< 0.001	< 0.001
	A x C	< 0.001	< 0.001	< 0.001	< 0.001	< 0.001	< 0.001	0.018	< 0.001	0.015	< 0.001
	A x F	< 0.001	< 0.001	< 0.001	< 0.001	< 0.001	< 0.001	< 0.001	< 0.001	< 0.001	< 0.001
	A x H	< 0.001	< 0.001	< 0.001	< 0.001	< 0.001	< 0.001	< 0.001	< 0.001	< 0.001	< 0.001
	A x M	< 0.001	< 0.001	< 0.001	< 0.001	< 0.001	< 0.001	< 0.001	< 0.001	< 0.001	0.836
	B x C		< 0.001	< 0.001	< 0.001	< 0.001	< 0.001	< 0.001	< 0.001	< 0.001	< 0.001
	B x F			0.052	< 0.001	< 0.001	< 0.001	< 0.001	0.005	< 0.001	< 0.001
	B x H				< 0.001	< 0.001	< 0.001	< 0.001	0.939	< 0.001	< 0.001
	B x M					< 0.001	< 0.001	< 0.001	< 0.001	< 0.001	< 0.001
	C x F						< 0.001	< 0.001	< 0.001	< 0.001	< 0.001
	C x H							< 0.001	< 0.001	< 0.001	< 0.001
	C x M								< 0.001	0.576	< 0.001
	F x H									< 0.001	< 0.001
	F x M										< 0.001

Abbreviations: A, axillary lymph node; B, basal ganglia; C, cerebellum; F, midfrontal cortex; H, hippocampus; M, mesenteric lymph node.

[1]p-values < or = 0.05 noted in red.

Table 17A. Determined p-values for statistical comparisons of average pairwise distances of SIVsmmFGb *nef* nucleotide sequences between SIVsmmFGb-infected pigtailed macaque lymph nodes and CNS regions

		One Week Post-Infection									
		A x C	**A x F**	**A x H**	**A x M**	**B x C**	**B x F**	**B x H**	**B x M**	**C x F**	**C x H**
One Week Post-Infection	**A x B**	0.168	< 0.001[1]	< 0.001	< 0.001	< 0.001	< 0.001	< 0.001	< 0.001	< 0.001	0.397
	A x C		< 0.001	< 0.001	< 0.001	< 0.001	< 0.001	< 0.001	< 0.001	< 0.001	0.999
	A x F			< 0.001	< 0.001	< 0.001	< 0.001	< 0.001	< 0.001	< 0.001	< 0.001
	A x H				< 0.001	< 0.001	< 0.001	< 0.001	< 0.001	< 0.001	< 0.001
	A x M					< 0.001	< 0.001	< 0.001	< 0.001	0.006	< 0.001
	B x C						< 0.001	0.256	0.004	< 0.001	< 0.001
	B x F							< 0.001	< 0.001	0.04	< 0.001
	B x H								< 0.001	< 0.001	< 0.001
	B x M									< 0.001	< 0.001
	C x F										< 0.001

Abbreviations: A, axillary lymph node; B, basal ganglia; C, cerebellum; F, midfrontal cortex; H, hippocampus; M, mesenteric lymph node.

[1]p-values < or = 0.05 noted in red.

Table 17B. Determined p-values for statistical comparisons of average pairwise distances of SIVsmmFGb *nef* nucleotide sequences between SIVsmmFGb-infected pigtailed macaque lymph nodes and CNS regions (continued)

		One Week Post-Infection					Two Months Post-Infection				
		C x M	**F x H**	**F x M**	**H x M**		**A x B**	**A x C**	**A x F**	**A x H**	**A x M**
One Week Post-Infection	**A x B**	< 0.001[1]	0.34	< 0.001	< 0.001		< 0.001	0.009	< 0.001	< 0.001	< 0.001
	A x C	< 0.001	0.558	< 0.001	< 0.001		0.009	0.208	< 0.001	< 0.001	< 0.001
	A x F	0.159	< 0.001	< 0.001	< 0.001		< 0.001	< 0.001	< 0.001	< 0.001	< 0.001
	A x H	< 0.001	< 0.001	< 0.001	< 0.001		< 0.001	< 0.001	0.25	0.213	< 0.001
	A x M	< 0.001	< 0.001	0.09	0.006		< 0.001	< 0.001	< 0.001	< 0.001	< 0.001
	B x C	< 0.001	< 0.001	< 0.001	< 0.001		< 0.001	< 0.001	< 0.001	< 0.001	< 0.001
	B x F	< 0.001	< 0.001	< 0.001	0.002		< 0.001	< 0.001	< 0.001	< 0.001	< 0.001
	B x H	< 0.001	< 0.001	< 0.001	< 0.001		< 0.001	< 0.001	< 0.001	< 0.001	< 0.001
	B x M	< 0.001	< 0.001	< 0.001	< 0.001		< 0.001	< 0.001	< 0.001	< 0.001	< 0.001
	C x F	< 0.001	< 0.001	0.324	0.527		< 0.001	< 0.001	< 0.001	< 0.001	< 0.001
	C x H	< 0.001	0.805	< 0.001	< 0.001		0.005	0.247	< 0.001	< 0.001	< 0.001
	C x M		< 0.001	< 0.001	< 0.001		0.002	< 0.001	< 0.001	< 0.001	< 0.001
	F x H			< 0.001	< 0.001		< 0.001	0.065	< 0.001	< 0.001	< 0.001
	F x M				0.326		< 0.001	< 0.001	< 0.001	< 0.001	< 0.001
	H x M						< 0.001	< 0.001	< 0.001	< 0.001	< 0.001
Two Months Post-Infection	**A x B**							0.211	< 0.001	< 0.001	< 0.001
	A x C								< 0.001	< 0.001	< 0.001
	A x F									0.809	< 0.001
	A x H										< 0.001

Abbrev.: A, axillary lymph node; B, basal ganglia; C, cerebellum; F, midfrontal cortex; H, hippocampus; M, mesenteric lymph node.

[1]p-values < or = 0.05 noted in red.

Table 17C. Determined p-values for statistical comparisons of average pairwise distances of SIVsmmFGb *nef* nucleotide sequences between SIVsmmFGb-infected pigtailed macaque lymph nodes and CNS regions (continued)

		Two Months Post-Infection									
		B x C	**B x F**	**B x H**	**B x M**	**C x F**	**C x H**	**C x M**	**F x H**	**F x M**	**H x M**
One Week Post-Infection	**A x B**	< 0.001[1]	< 0.001	< 0.001	< 0.001	< 0.001	< 0.001	0.752	< 0.001	< 0.001	< 0.001
	A x C	< 0.001	< 0.001	< 0.001	0.008	< 0.001	< 0.001	0.265	< 0.001	< 0.001	< 0.001
	A x F	< 0.001	< 0.001	< 0.001	< 0.001	< 0.001	< 0.001	< 0.001	< 0.001	< 0.001	< 0.001
	A x H	0.15	0.108	< 0.001	< 0.001	< 0.001	< 0.001	< 0.001	< 0.001	0.006	< 0.001
	A x M	< 0.001	< 0.001	< 0.001	< 0.001	< 0.001	< 0.001	< 0.001	< 0.001	< 0.001	< 0.001
	B x C	< 0.001	< 0.001	< 0.001	< 0.001	< 0.001	< 0.001	< 0.001	< 0.001	< 0.001	< 0.001
	B x F	< 0.001	< 0.001	< 0.001	< 0.001	< 0.001	< 0.001	< 0.001	< 0.001	< 0.001	< 0.001
	B x H	< 0.001	< 0.001	< 0.001	< 0.001	< 0.001	< 0.001	< 0.001	< 0.001	< 0.001	< 0.001
	B x M	< 0.001	< 0.001	< 0.001	< 0.001	< 0.001	< 0.001	< 0.001	< 0.001	< 0.001	< 0.001
	C x F	< 0.001	< 0.001	< 0.001	< 0.001	< 0.001	< 0.001	< 0.001	< 0.001	< 0.001	< 0.001
	C x H	< 0.001	< 0.001	< 0.001	0.002	< 0.001	< 0.001	0.329	< 0.001	< 0.001	< 0.001
	C x M	< 0.001	< 0.001	< 0.001	0.004	< 0.001	< 0.001	< 0.001	< 0.001	< 0.001	< 0.001
	F x H	< 0.001	< 0.001	< 0.001	< 0.001	< 0.001	< 0.001	0.614	< 0.001	< 0.001	< 0.001
	F x M	< 0.001	< 0.001	< 0.001	< 0.001	< 0.001	< 0.001	< 0.001	< 0.001	< 0.001	< 0.001
	H x M	< 0.001	< 0.001	< 0.001	< 0.001	< 0.001	< 0.001	< 0.001	< 0.001	< 0.001	< 0.001

Abbreviations: A, axillary lymph node; B, basal ganglia; C, cerebellum; F, midfrontal cortex; H, hippocampus; M, mesenteric lymph node.

[1]p-values < or = 0.05 noted in red.

Table 17D. Determined p-values for statistical comparisons of average pairwise distances of SIVsmmFGb *nef* nucleotide sequences between SIVsmmFGb-infected pigtailed macaque lymph nodes and CNS regions (continued)

		Two Months Post-Infection									
		B x C	**B x F**	**B x H**	**B x M**	**C x F**	**C x H**	**C x M**	**F x H**	**F x M**	**H x M**
Two Months Post-Infection	**A x B**	< 0.001[1]	< 0.001	< 0.001	0.99	< 0.001	< 0.001	< 0.001	< 0.001	< 0.001	< 0.001
	A x C	< 0.001	< 0.001	< 0.001	0.169	< 0.001	< 0.001	0.008	< 0.001	< 0.001	< 0.001
	A x F	0.122	0.402	< 0.001	< 0.001	< 0.001	< 0.001	< 0.001	< 0.001	0.103	< 0.001
	A x H	0.105	0.523	< 0.001	< 0.001	< 0.001	< 0.001	< 0.001	< 0.001	0.216	0.003
	A x M	< 0.001	< 0.001	< 0.001	< 0.001	0.254	< 0.001	< 0.001	< 0.001	< 0.001	< 0.001
	B x C		0.115	0.144	< 0.001	< 0.001	< 0.001	< 0.001	< 0.001	0.53	0.226
	B x F			0.002	< 0.001	< 0.001	< 0.001	< 0.001	< 0.001	0.957	0.086
	B x H				< 0.001	< 0.001	< 0.001	< 0.001	< 0.001	0.005	0.298
	B x M					< 0.001	< 0.001	< 0.001	< 0.001	< 0.001	< 0.001
	C x F						0.012	< 0.001	< 0.001	< 0.001	< 0.001
	C x H							< 0.001	0.032	< 0.001	< 0.001
	C x M								< 0.001	< 0.001	< 0.001
	F x H									< 0.001	< 0.001
	F x M										0.114

Abbreviations: A, axillary lymph node; B, basal ganglia; C, cerebellum; F, midfrontal cortex; H, hippocampus; M, mesenteric lymph node.

[1]p-values < or = 0.05 noted in red.

Table 18A. Determined p-values for statistical comparisons of average pairwise distances of SIVsmmFGb *int* nucleotide sequences between SIVsmmFGb-infected pigtailed macaque lymph nodes and CNS regions

		One Week Post-Infection									
		A x C	**A x F**	**A x H**	**A x M**	**B x C**	**B x F**	**B x H**	**B x M**	**C x F**	**C x H**
One Week Post-Infection	**A x B**	< 0.001[1]	< 0.001	< 0.001	0.011	< 0.001	0.746	0.035	< 0.001	0.048	0.011
	A x C		0.99	< 0.001	0.257	< 0.001	< 0.001	0.07	< 0.001	< 0.001	< 0.001
	A x F			< 0.001	0.246	< 0.001	< 0.001	0.09	< 0.001	< 0.001	< 0.001
	A x H				< 0.001	< 0.001	< 0.001	< 0.001	< 0.001	< 0.001	< 0.001
	A x M					< 0.001	0.015	0.549	< 0.001	< 0.001	< 0.001
	B x C						< 0.001	< 0.001	0.001	0.278	0.492
	B x F							0.034	< 0.001	0.01	< 0.001
	B x H								< 0.001	< 0.001	< 0.001
	B x M									< 0.001	< 0.001
	C x F										0.713

Abbreviations: A, axillary lymph node; B, basal ganglia; C, cerebellum; F, midfrontal cortex; H, hippocampus; M, mesenteric lymph node.

[1]p-values < or = 0.05 noted in red.

Table 18B. Determined p-values for statistical comparisons of average pairwise distances of SIVsmmFGb *int* nucleotide sequences between SIVsmmFGb-infected pigtailed macaque lymph nodes and CNS regions (continued)

		One Week Post-Infection					Two Months Post-Infection				
		C x M	**F x H**	**F x M**	**H x M**		**A x B**	**A x C**	**A x F**	**A x H**	**A x M**
One Week Post-Infection	**A x B**	< 0.001[1]	0.708	0.881	0.649		< 0.001	< 0.001	< 0.001	< 0.001	< 0.001
	A x C	< 0.001	< 0.001	< 0.001	< 0.001		< 0.001	< 0.001	< 0.001	< 0.001	0.664
	A x F	< 0.001	< 0.001	< 0.001	< 0.001		< 0.001	< 0.001	< 0.001	< 0.001	0.657
	A x H	< 0.001	< 0.001	< 0.001	< 0.001		< 0.001	0.68	< 0.001	< 0.001	< 0.001
	A x M	< 0.001	0.012	0.008	0.016		< 0.001	< 0.001	< 0.001	< 0.001	0.105
	B x C	0.006	< 0.001	< 0.001	< 0.001		< 0.001	< 0.001	< 0.001	< 0.001	< 0.001
	B x F	< 0.001	0.988	0.681	0.986		< 0.001	< 0.001	< 0.001	< 0.001	< 0.001
	B x H	< 0.001	0.025	0.016	0.041		< 0.001	< 0.001	< 0.001	< 0.001	0.051
	B x M	0.879	< 0.001	< 0.001	< 0.001		< 0.001	< 0.001	< 0.001	< 0.001	< 0.001
	C x F	< 0.001	0.007	0.032	0.007		< 0.001	< 0.001	< 0.001	< 0.001	< 0.001
	C x H	< 0.001	< 0.001	0.007	< 0.001		< 0.001	< 0.001	< 0.001	< 0.001	< 0.001
	C x M		< 0.001	< 0.001	< 0.001		< 0.001	< 0.001	< 0.001	< 0.001	< 0.001
	F x H			0.672	0.984		< 0.001	< 0.001	< 0.001	< 0.001	< 0.001
	F x M				0.69		< 0.001	< 0.001	< 0.001	< 0.001	< 0.001
	H x M						< 0.001	< 0.001	< 0.001	< 0.001	< 0.001
Two Months Post-Infection	**A x B**							< 0.001	< 0.001	< 0.001	< 0.001
	A x C								< 0.001	< 0.001	< 0.001
	A x F									0.293	< 0.001
	A x H										< 0.001

Abbrev.: A, axillary lymph node; B, basal ganglia; C, cerebellum; F, midfrontal cortex; H, hippocampus; M, mesenteric lymph node.

[1]p-values < or = 0.05 noted in red.

Table 18C. Determined p-values for statistical comparisons of average pairwise distances of SIVsmmFGb *int* nucleotide sequences between SIVsmmFGb-infected pigtailed macaque lymph nodes and CNS regions at one wpi and two mpi

		Two Months Post-Infection									
		B x C	**B x F**	**B x H**	**B x M**	**C x F**	**C x H**	**C x M**	**F x H**	**F x M**	**H x M**
One Week Post-Infection	**A x B**	< 0.001[1]	< 0.001	< 0.001	0.002	< 0.001	< 0.001	< 0.001	< 0.001	< 0.001	< 0.001
	A x C	< 0.001	< 0.001	0.001	0.72	0.116	0.025	< 0.001	< 0.001	0.001	< 0.001
	A x F	< 0.001	< 0.001	< 0.001	0.754	0.116	0.017	< 0.001	< 0.001	0.001	< 0.001
	A x H	< 0.001	< 0.001	0.637	< 0.001	0.027	0.012	0.022	< 0.001	0.33	0.89
	A x M	< 0.001	< 0.001	< 0.001	0.409	0.006	< 0.001	< 0.001	< 0.001	< 0.001	< 0.001
	B x C	< 0.001	< 0.001	< 0.001	< 0.001	< 0.001	< 0.001	< 0.001	< 0.001	< 0.001	< 0.001
	B x F	< 0.001	< 0.001	< 0.001	0.009	< 0.001	< 0.001	< 0.001	< 0.001	< 0.001	< 0.001
	B x H	< 0.001	< 0.001	< 0.001	0.338	0.008	< 0.001	< 0.001	< 0.001	< 0.001	< 0.001
	B x M	< 0.001	< 0.001	< 0.001	< 0.001	< 0.001	< 0.001	< 0.001	< 0.001	< 0.001	< 0.001
	C x F	< 0.001	< 0.001	< 0.001	< 0.001	< 0.001	< 0.001	< 0.001	< 0.001	< 0.001	< 0.001
	C x H	< 0.001	< 0.001	< 0.001	< 0.001	< 0.001	< 0.001	< 0.001	< 0.001	< 0.001	< 0.001
	C x M	< 0.001	< 0.001	< 0.001	< 0.001	< 0.001	< 0.001	< 0.001	< 0.001	< 0.001	< 0.001
	F x H	< 0.001	< 0.001	< 0.001	0.004	< 0.001	< 0.001	< 0.001	< 0.001	< 0.001	< 0.001
	F x M	< 0.001	< 0.001	< 0.001	0.002	< 0.001	< 0.001	< 0.001	< 0.001	< 0.001	< 0.001
	H x M	< 0.001	< 0.001	< 0.001	0.004	< 0.001	< 0.001	< 0.001	< 0.001	< 0.001	< 0.001

Abbreviations: A, axillary lymph node; B, basal ganglia; C, cerebellum; F, midfrontal cortex; H, hippocampus; M, mesenteric lymph node.

[1]p-values < or = 0.05 noted in red.

Table 18D. Determined p-values for statistical comparisons of average pairwise distances of SIVsmmFGb *int* nucleotide sequences between SIVsmmFGb-infected pigtailed macaque lymph nodes and CNS regions (continued)

		Two Months Post-Infection									
		B x C	**B x F**	**B x H**	**B x M**	**C x F**	**C x H**	**C x M**	**F x H**	**F x M**	**H x M**
Two Months Post-Infection	**A x B**	0.007[1]	0.088	< 0.001	< 0.001	< 0.001	< 0.001	< 0.001	< 0.001	< 0.001	< 0.001
	A x C	< 0.001	< 0.001	0.873	< 0.001	0.006	0.016	0.029	< 0.001	0.26	0.781
	A x F	< 0.001	0.13	< 0.001	< 0.001	< 0.001	< 0.001	0.093	0.57	< 0.001	< 0.001
	A x H	< 0.001	0.296	< 0.001	< 0.001	< 0.001	< 0.001	0.004	0.281	< 0.001	< 0.001
	A x M	< 0.001	< 0.001	0.017	0.47	0.141	0.114	< 0.001	< 0.001	0.003	< 0.001
	B x C		< 0.001	< 0.001	< 0.001	< 0.001	< 0.001	< 0.001	< 0.001	< 0.001	< 0.001
	B x F			< 0.001	< 0.001	< 0.001	< 0.001	0.002	0.029	< 0.001	< 0.001
	B x H				0.009	0.549	0.161	0.007	< 0.001	0.26	0.56
	B x M					0.02	0.03	< 0.001	< 0.001	< 0.001	< 0.001
	C x F						0.698	< 0.001	< 0.001	0.131	0.044
	C x H							< 0.001	< 0.001	0.108	0.01
	C x M								0.266	0.004	0.037
	F x H									< 0.001	0.001
	F x M										0.398

Abbreviations: A, axillary lymph node; B, basal ganglia; C, cerebellum; F, midfrontal cortex; H, hippocampus; M, mesenteric lymph node.

[1]p-values < or = 0.05 noted in red.

Table 19A. Determined p-values for statistical comparisons of average pairwise distances of SIVsmmFGb *env* V1 region nucleotide sequences within SIVsmmFGb-infected pigtailed macaque lymph nodes and CNS regions

		One Week Post-Infection					Two Months Post-Infection					
		B x B	**C x C**	**F x F**	**H x H**	**M x M**	**A x A**	**B x B**	**C x C**	**F x F**	**H x H**	**M x M**
One Week Post-Infection	**A x A**	< 0.001[1]	< 0.001	< 0.001	< 0.001	< 0.001	< 0.001	< 0.001	< 0.001	< 0.001	< 0.001	< 0.001
	B x B		0.935	< 0.001	0.266	< 0.001	< 0.001	< 0.001	< 0.001	< 0.001	0.034	< 0.001
	C x C			< 0.001	0.01	< 0.001	< 0.001	< 0.001	< 0.001	< 0.001	0.026	< 0.001
	F x F				< 0.001	< 0.001	< 0.001	< 0.001	< 0.001	< 0.001	< 0.001	< 0.001
	H x H					< 0.001	< 0.001	< 0.001	< 0.001	< 0.001	0.634	< 0.001
	M x M						< 0.001	< 0.001	< 0.001	< 0.001	< 0.001	< 0.001
Two Months Post-Infection	**A x A**							< 0.001	< 0.001	< 0.001	< 0.001	0.195
	B x B								< 0.001	0.784	< 0.001	< 0.001
	C x C									0.002	< 0.001	< 0.001
	F x F										< 0.001	< 0.001
	H x H											< 0.001

Abbreviations: A, axillary lymph node; B, basal ganglia; C, cerebellum; F, midfrontal cortex; H, hippocampus; M, mesenteric lymph node.

[1]p-values < or = 0.05 noted in red.

Table 19B. Determined p-values for statistical comparisons of average pairwise distances of SIVsmmFGb *nef* nucleotide sequences within SIVsmmFGb-infected pigtailed macaque lymph nodes and CNS regions

		One Week Post-Infection					Two Months Post-Infection					
		B x B	**C x C**	**F x F**	**H x H**	**M x M**	**A x A**	**B x B**	**C x C**	**F x F**	**H x H**	**M x M**
One Week Post-Infection	**A x A**	< 0.001[1]	< 0.001	0.835	< 0.001	0.645	< 0.001	< 0.001	< 0.001	< 0.001	< 0.001	< 0.001
	B x B		0.001	< 0.001	< 0.001	< 0.001	< 0.001	0.329	< 0.001	0.026	0.007	< 0.001
	C x C			< 0.001	< 0.001	< 0.001	< 0.001	< 0.001	< 0.001	0.61	0.274	< 0.001
	F x F				< 0.001	0.854	< 0.001	< 0.001	< 0.001	< 0.001	< 0.001	0.002
	H x H					< 0.001	< 0.001	< 0.001	< 0.001	< 0.001	< 0.001	< 0.001
	M x M						< 0.001	< 0.001	< 0.001	< 0.001	< 0.001	< 0.001
Two Months Post-Infection	**A x A**							< 0.001	< 0.001	< 0.001	< 0.001	0.879
	B x B								< 0.001	0.003	< 0.001	< 0.001
	C x C									< 0.001	< 0.001	< 0.001
	F x F										0.541	< 0.001
	H x H											< 0.001

Abbreviations: A, axillary lymph node; B, basal ganglia; C, cerebellum; F, midfrontal cortex; H, hippocampus; M, mesenteric lymph node.

[1]p-values < or = 0.05 noted in red.

Table 19C. Determined p-values for statistical comparisons of average pairwise distances of SIVsmmFGb *int* nucleotide sequences within SIVsmmFGb-infected pigtailed macaque lymph nodes and CNS regions

		One Week Post-Infection					Two Months Post-Infection					
		B x B	**C x C**	**F x F**	**H x H**	**M x M**	**A x A**	**B x B**	**C x C**	**F x F**	**H x H**	**M x M**
One Week Post-Infection	**A x A**	< 0.001[1]	< 0.001	< 0.001	< 0.001	< 0.001	< 0.001	< 0.001	< 0.001	< 0.001	< 0.001	< 0.001
	B x B		< 0.001	0.022	< 0.001	< 0.001	< 0.001	< 0.001	0.317	< 0.001	< 0.001	< 0.001
	C x C			< 0.001	< 0.001	< 0.001	< 0.001	< 0.001	< 0.001	< 0.001	0.181	< 0.001
	F x F				< 0.001	< 0.001	< 0.001	0.082	0.172	< 0.001	< 0.001	< 0.001
	H x H					< 0.001	< 0.001	< 0.001	< 0.001	< 0.001	< 0.001	< 0.001
	M x M						< 0.001	< 0.001	< 0.001	< 0.001	0.003	0.738
Two Months Post-Infection	**A x A**							< 0.001	< 0.001	< 0.001	< 0.001	< 0.001
	B x B								0.002	0.019	< 0.001	< 0.001
	C x C									< 0.001	< 0.001	< 0.001
	F x F										< 0.001	< 0.001
	H x H											0.003

Abbreviations: A, axillary lymph node; B, basal ganglia; C, cerebellum; F, midfrontal cortex; H, hippocampus; M, mesenteric lymph node.

[1]p-values < or = 0.05 noted in red.

Table 20. Determined p-values for statistical comparisons of the average amino acid sequence length of Env V1 region sequences in the SIVsmmFGb stock virus and infected pigtailed macaque lymph nodes and CNS regions at one wpi and two mpi

			Central Nervous System Tissues			Lymph Node Tissues	
			One Week Post-Infection	Two Months Post-Infection		One Week Post-Infection	Two Months Post-Infection
	Stock		0.703	< 0.001[1]		0.192	< 0.001
Central Nervous System Tissues	**One Week Post-Infection**			< 0.001		0.087	< 0.001
	Two Months Post-Infection					< 0.001	0.562
Lymph Node Tissues	**One Week Post-Infection**						< 0.001

[1]p-values < or = 0.05 noted in red.

Table 21. Determined p-values for statistical comparisons of the average number of potential O-linked glycosylation sites of Env V1 region sequences in the SIVsmmFGb stock and infected pigtailed macaque lymph nodes and CNS one wpi and two mpi

			Central Nervous System Tissues			Lymph Node Tissues	
			One Week Post-Infection	Two Months Post-Infection		One Week Post-Infection	Two Months Post-Infection
	Stock		< 0.001[1]	< 0.001		0.05	< 0.001
Central Nervous System Tissues	**One Week Post-Infection**			< 0.001		0.194	0.042
	Two Months Post-Infection					< 0.001	< 0.001
Lymph Node Tissues	**One Week Post-Infection**						0.006

[1]p-values < or = 0.05 noted in red.

Table 22. Determined p-values for statistical comparisons of the prevalence of the KSPKAE insertion in Env V1 region sequences in the SIVsmmFGb stock virus and infected pigtailed macaque lymph nodes and CNS regions at one wpi and two mpi

			Central Nervous System Tissues			Lymph Node Tissues	
			One Week Post-Infection	Two Months Post-Infection		One Week Post-Infection	Two Months Post-Infection
	Stock		0.136[1]	0.18		< 0.001	< 0.001
Central Nervous System Tissues	**One Week Post-Infection**			0.509		0.069	0.049
	Two Months Post-Infection					0.737	0.638
Lymph Node Tissues	**One Week Post-Infection**						0.931

[1]p-values < or = 0.05 noted in red.

Table 23. Determined p-values for statistical comparisons of the prevalence of mutations removing the first N-linked glycosylation site in Env V1 region sequences in the SIVsmmFGb stock virus and infected pigtailed macaque lymph nodes and CNS regions at one wpi and two mpi

			Central Nervous System Tissues			Lymph Node Tissues	
			One Week Post-Infection	Two Months Post-Infection		One Week Post-Infection	Two Months Post-Infection
	Stock		0.325[1]	0.989		0.133	0.026
Central Nervous System Tissues	**One Week Post-Infection**			0.405		0.51	0.003
	Two Months Post-Infection					0.201	0.04
Lymph Node Tissues	**One Week Post-Infection**						0.001

[1]p-values < or = 0.05 noted in red.

Table 24. Determined p-values for statistical comparisons of the prevalence of mutations modifying the second N-linked glycosylation site in Env V1 region sequences in the SIVsmmFGb stock virus and infected pigtailed macaque lymph nodes and CNS regions at one wpi and two mpi

			Central Nervous System Tissues			Lymph Node Tissues	
			One Week Post-Infection	Two Months Post-Infection		One Week Post-Infection	Two Months Post-Infection
	Stock		0.237	< 0.001[1]		0.255	0.39
Central Nervous System Tissues	**One Week Post-Infection**			0.056		0.294	0.339
	Two Months Post-Infection					< 0.001	0.003
Lymph Node Tissues	**One Week Post-Infection**						0.862

[1]p-values < or = 0.05 noted in red.

Table 25. Determined p-values for statistical comparisons of the prevalence of Nef sequences with basic region mutations in the SIVsmmFGb stock virus and infected pigtailed macaque lymph node tissues and CNS regions at one wpi and two mpi

			Central Nervous System Tissues			Lymph Node Tissues	
			One Week Post-Infection	Two Months Post-Infection		One Week Post-Infection	Two Months Post-Infection
	Stock		0.017[1]	0.03		0.015	0.007
Central Nervous System Tissues	**One Week Post-Infection**			0.904		0.692	0.494
	Two Months Post-Infection					0.675	0.557
Lymph Node Tissues	**One Week Post-Infection**						0.862

[1]p-values < or = 0.05 noted in red.

Table 26. Determined p-values for statistical comparisons of the prevalence of Nef sequences with N-proximal Y residue mutations in the SIVsmmFGb stock virus and infected pigtailed macaque lymph node tissues and CNS regions one wpi and two mpi

			Central Nervous System Tissues			Lymph Node Tissues	
			One Week Post-Infection	**Two Months Post-Infection**		**One Week Post-Infection**	**Two Months Post-Infection**
	Stock		0.017[1]	0.012		0.005	< 0.001
Central Nervous System Tissues	**One Week Post-Infection**			0.709		0.773	0.46
	Two Months Post-Infection					0.725	0.557
Lymph Node Tissues	**One Week Post-Infection**						0.299

[1]p-values < or = 0.05 noted in red.

Table 27. Determined p-values for statistical comparisons of the prevalence of Nef sequences with acidic region mutations in the SIVsmmFGb stock virus and infected pigtailed macaque lymph node tissues and CNS regions at one wpi and two mpi

			Central Nervous System Tissues			Lymph Node Tissues	
			One Week Post-Infection	Two Months Post-Infection		One Week Post-Infection	Two Months Post-Infection
	Stock		0.044[1]	0.19		0.004	< 0.001
Central Nervous System Tissues	**One Week Post-Infection**			0.93		0.914	0.601
	Two Months Post-Infection					0.867	0.546
Lymph Node Tissues	**One Week Post-Infection**						0.507

[1]p-values < or = 0.05 noted in red.

Table 28. Determined p-values for statistical comparisons of the prevalence of Nef sequences with thioesterase binding site mutations in the SIVsmmFGb stock virus and infected pigtailed macaque lymph node tissues and CNS regions one wpi and two mpi

			Central Nervous System Tissues			Lymph Node Tissues	
			One Week Post-Infection	**Two Months Post-Infection**		**One Week Post-Infection**	**Two Months Post-Infection**
	Stock		0.894	0.868		0.516	0.023[1]
Central Nervous System Tissues	**One Week Post-Infection**			0.775		0.759	0.367
	Two Months Post-Infection					0.687	0.214
Lymph Node Tissues	**One Week Post-Infection**						0.061

[1]p-values < or = 0.05 noted in red.

Table 29. Determined p-values for statistical comparisons of the prevalence of Nef sequences with AP interaction site mutations in the SIVsmmFGb stock virus and infected pigtailed macaque lymph node tissues and CNS regions one wpi and two mpi

			Central Nervous System Tissues			Lymph Node Tissues	
			One Week Post-Infection	Two Months Post-Infection		One Week Post-Infection	Two Months Post-Infection
	Stock		0.152	0.001[1]		0.033	0.275
Central Nervous System Tissues	**One Week Post-Infection**			0.023		0.773	0.241
	Two Months Post-Infection					0.041	0.014
Lymph Node Tissues	**One Week Post-Infection**						0.094

[1]p-values < or = 0.05 noted in red.

Table 30. Determined p-values for statistical comparisons of the prevalence of Int sequences with mutations in the active site flexible loop in the SIVsmmFGb stock virus and infected pigtailed macaque lymph nodes and CNS regions one wpi and two mpi

			Central Nervous System Tissues			Lymph Node Tissues	
			One Week Post-Infection	Two Months Post-Infection		One Week Post-Infection	Two Months Post-Infection
	Stock		0.071	0.03[1]		0.013	0.009
Central Nervous System Tissues	**One Week Post-Infection**			0.7		0.188	0.112
	Two Months Post-Infection					0.392	0.131
Lymph Node Tissues	**One Week Post-Infection**						0.772

[1]p-values < or = 0.05 noted in red.

Table 31. Determined p-values for statistical comparisons of the prevalence of sequences with mutations in position 41 of the Env V1 region in the SIVsmmFGb stock virus and infected pigtailed macaque lymph nodes and CNS regions one wpi and two mpi

			Central Nervous System Tissues			Lymph Node Tissues	
			One Week Post-Infection	**Two Months Post-Infection**		**One Week Post-Infection**	**Two Months Post-Infection**
	Stock		0.451	0.793		0.154	< 0.001[1]
Central Nervous System Tissues	**One Week Post-Infection**			0.332		0.417	< 0.001
	Two Months Post-Infection					0.121	0.003
Lymph Node Tissues	**One Week Post-Infection**						< 0.001

[1]p-values < or = 0.05 noted in red.

Table 32. Determined p-values for statistical comparisons of the prevalence of sequences with mutations in position 49 of the Env V1 region in the SIVsmmFGb stock virus and infected pigtailed macaque lymph nodes and CNS regions one wpi and two mpi

			Central Nervous System Tissues			Lymph Node Tissues	
			One Week Post-Infection	Two Months Post-Infection		One Week Post-Infection	Two Months Post-Infection
	Stock		0.256	0.004[1]		0.403	0.403
Central Nervous System Tissues	**One Week Post-Infection**			0.073		0.512	0.512
	Two Months Post-Infection					0.015	0.02
Lymph Node Tissues	**One Week Post-Infection**						0.751

[1]p-values < or = 0.05 noted in red.

Table 33. Determined p-values for statistical comparisons of the prevalence of sequences with mutations in position 9 of Nef in the SIVsmmFGb stock virus and infected pigtailed macaque lymph nodes and CNS regions one wpi and two mpi

			Central Nervous System Tissues			Lymph Node Tissues	
			One Week Post-Infection	Two Months Post-Infection		One Week Post-Infection	Two Months Post-Infection
	Stock		0.041[1]	0.035		0.109	0.003
Central Nervous System Tissues	**One Week Post-Infection**			0.826		0.449	0.815
	Two Months Post-Infection					0.411	1
Lymph Node Tissues	**One Week Post-Infection**						0.371

[1]p-values < or = 0.05 noted in red.

Table 34. Determined p-values for statistical comparisons of the prevalence of sequences with mutations in position 12 of Nef in the SIVsmmFGb stock virus and infected pigtailed macaque lymph nodes and CNS regions one wpi and two mpi

			Central Nervous System Tissues			Lymph Node Tissues	
			One Week Post-Infection	**Two Months Post-Infection**		**One Week Post-Infection**	**Two Months Post-Infection**
	Stock		0.544	0.109		0.15	0.201
Central Nervous System Tissues	**One Week Post-Infection**			0.396		0.08	0.759
	Two Months Post-Infection					0.01[1]	0.602
Lymph Node Tissues	**One Week Post-Infection**						0.014

[1]p-values < or = 0.05 noted in red.

Table 35. Determined p-values for statistical comparisons of the prevalence of sequences with mutations in position 13 of Nef in the SIVsmmFGb stock virus and infected pigtailed macaque lymph nodes and CNS regions one wpi and two mpi

			Central Nervous System Tissues			Lymph Node Tissues	
			One Week Post-Infection	Two Months Post-Infection		One Week Post-Infection	Two Months Post-Infection
	Stock		0.065	0.02[1]		0.01	0.003
Central Nervous System Tissues	**One Week Post-Infection**			0.545		0.639	0.449
	Two Months Post-Infection					0.827	0.893
Lymph Node Tissues	**One Week Post-Infection**						0.862

[1]p-values < or = 0.05 noted in red.

Table 36. Determined p-values for statistical comparisons of the prevalence of sequences with mutations in position 14 of Nef in the SIVsmmFGb stock virus and infected pigtailed macaque lymph nodes and CNS regions one wpi and two mpi

			Central Nervous System Tissues			Lymph Node Tissues	
			One Week Post-Infection	Two Months Post-Infection		One Week Post-Infection	Two Months Post-Infection
	Stock		0.209	0.048[1]		0.275	0.003
Central Nervous System Tissues	**One Week Post-Infection**			0.312		0.692	0.16
	Two Months Post-Infection					0.208	0.687
Lymph Node Tissues	**One Week Post-Infection**						0.061

[1]p-values < or = 0.05 noted in red.

Table 37. Determined p-values for statistical comparisons of the prevalence of sequences with mutations in position 15 of Nef in the SIVsmmFGb stock virus and infected pigtailed macaque lymph nodes and CNS regions one wpi and two mpi

			Central Nervous System Tissues			**Lymph Node Tissues**	
			One Week Post-Infection	**Two Months Post-Infection**		**One Week Post-Infection**	**Two Months Post-Infection**
	Stock		0.69	0.473		0.054	0.095
Central Nervous System Tissues	**One Week Post-Infection**			0.56		0.601	0.144
	Two Months Post-Infection					0.118	0.43
Lymph Node Tissues	**One Week Post-Infection**						0.01[1]

[1]p-values < or = 0.05 noted in red.

Table 38. Determined p-values for statistical comparisons of the prevalence of sequences with mutations in position 19 of Nef in the SIVsmmFGb stock virus and infected pigtailed macaque lymph nodes and CNS regions one wpi and two mpi

			Central Nervous System Tissues			Lymph Node Tissues	
			One Week Post-Infection	Two Months Post-Infection		One Week Post-Infection	Two Months Post-Infection
	Stock		0.058	0.008[1]		0.014	0.002
Central Nervous System Tissues	**One Week Post-Infection**			0.301		0.732	0.417
	Two Months Post-Infection					0.411	0.893
Lymph Node Tissues	**One Week Post-Infection**						0.665

[1]p-values < or = 0.05 noted in red.

Table 39. Determined p-values for statistical comparisons of the prevalence of sequences with mutations in position 28 of Nef in the SIVsmmFGb stock virus and infected pigtailed macaque lymph nodes and CNS regions one wpi and two mpi

			Central Nervous System Tissues			Lymph Node Tissues	
			One Week Post-Infection	Two Months Post-Infection		One Week Post-Infection	Two Months Post-Infection
	Stock		0.02[1]	0.012		0.004	< 0.001
Central Nervous System Tissues	**One Week Post-Infection**			0.725		0.885	0.517
	Two Months Post-Infection					0.725	0.603
Lymph Node Tissues	**One Week Post-Infection**						0.326

[1]p-values < or = 0.05 noted in red.

Table 40. Determined p-values for statistical comparisons of the prevalence of sequences with mutations in position 39 of Nef in the SIVsmmFGb stock virus and infected pigtailed macaque lymph nodes and CNS regions one wpi and two mpi

			Central Nervous System Tissues			Lymph Node Tissues	
			One Week Post-Infection	**Two Months Post-Infection**		**One Week Post-Infection**	**Two Months Post-Infection**
	Stock		0.126	0.078		0.401	0.177
Central Nervous System Tissues	**One Week Post-Infection**			0.782		0.611	0.019[1]
	Two Months Post-Infection					0.467	0.014
Lymph Node Tissues	**One Week Post-Infection**						0.064

[1]p-values < or = 0.05 noted in red.

Table 41. Determined p-values for statistical comparisons of the prevalence of sequences with mutations in position 89 of Nef in the SIVsmmFGb stock virus and infected pigtailed macaque lymph nodes and CNS regions one wpi and two mpi

			Central Nervous System Tissues			Lymph Node Tissues	
			One Week Post-Infection	Two Months Post-Infection		One Week Post-Infection	Two Months Post-Infection
	Stock		< 0.001[1]	< 0.001		0.011	< 0.001
Central Nervous System Tissues	**One Week Post-Infection**			0.938		0.077	0.842
	Two Months Post-Infection					0.057	0.84
Lymph Node Tissues	**One Week Post-Infection**						0.026

[1]p-values < or = 0.05 noted in red.

Table 42. Determined p-values for statistical comparisons of the prevalence of sequences with mutations in position 91 of Nef in the SIVsmmFGb stock virus and infected pigtailed macaque lymph nodes and CNS regions one wpi and two mpi

			Central Nervous System Tissues			Lymph Node Tissues	
			One Week Post-Infection	Two Months Post-Infection		One Week Post-Infection	Two Months Post-Infection
	Stock		< 0.001[1]	0.006		0.008	0.004
Central Nervous System Tissues	**One Week Post-Infection**			0.765		0.899	0.856
	Two Months Post-Infection					0.933	0.648
Lymph Node Tissues	**One Week Post-Infection**						0.748

[1]p-values < or = 0.05 noted in red.

Table 43. Determined p-values for statistical comparisons of the prevalence of sequences with mutations in position 92 of Nef in the SIVsmmFGb stock virus and infected pigtailed macaque lymph nodes and CNS regions one wpi and two mpi

			Central Nervous System Tissues			Lymph Node Tissues	
			One Week Post-Infection	Two Months Post-Infection		One Week Post-Infection	Two Months Post-Infection
	Stock		0.871	0.001[1]		0.186	0.011
Central Nervous System Tissues	**One Week Post-Infection**			0.007		0.46	0.044
	Two Months Post-Infection					0.014	0.4
Lymph Node Tissues	**One Week Post-Infection**						0.133

[1]p-values < or = 0.05 noted in red.

Table 44. Determined p-values for statistical comparisons of the prevalence of sequences with mutations in position 93 of Nef in the SIVsmmFGb stock virus and infected pigtailed macaque lymph nodes and CNS regions one wpi and two mpi

			Central Nervous System Tissues			Lymph Node Tissues	
			One Week Post-Infection	Two Months Post-Infection		One Week Post-Infection	Two Months Post-Infection
	Stock		< 0.001[1]	< 0.001		0.001	0.005
Central Nervous System Tissues	**One Week Post-Infection**			0.991		0.033	0.009
	Two Months Post-Infection					0.038	0.022
Lymph Node Tissues	**One Week Post-Infection**						0.751

[1]p-values < or = 0.05 noted in red.

Table 45. Determined p-values for statistical comparisons of the prevalence of sequences with mutations in position 94 of Nef in the SIVsmmFGb stock virus and infected pigtailed macaque lymph nodes and CNS regions one wpi and two mpi

			Central Nervous System Tissues			Lymph Node Tissues	
			One Week Post-Infection	Two Months Post-Infection		One Week Post-Infection	Two Months Post-Infection
	Stock		0.003[1]	0.031		0.365	0.227
Central Nervous System Tissues	**One Week Post-Infection**			0.707		0.086	0.311
	Two Months Post-Infection					0.239	0.555
Lymph Node Tissues	**One Week Post-Infection**						0.772

[1]p-values < or = 0.05 noted in red.

Table 46. Determined p-values for statistical comparisons of the prevalence of sequences with mutations in position 95 of Nef in the SIVsmmFGb stock virus and infected pigtailed macaque lymph nodes and CNS regions one wpi and two mpi

			Central Nervous System Tissues			Lymph Node Tissues	
			One Week Post-Infection	Two Months Post-Infection		One Week Post-Infection	Two Months Post-Infection
	Stock		< 0.001[1]	< 0.001		0.003	0.031
Central Nervous System Tissues	**One Week Post-Infection**			0.233		0.318	0.008
	Two Months Post-Infection					0.987	0.114
Lymph Node Tissues	**One Week Post-Infection**						0.156

[1]p-values < or = 0.05 noted in red.

Table 47. Determined p-values for statistical comparisons of the prevalence of sequences with mutations in position 96 of Nef in the SIVsmmFGb stock virus and infected pigtailed macaque lymph nodes and CNS regions one wpi and two mpi

			Central Nervous System Tissues			Lymph Node Tissues	
			One Week Post-Infection	**Two Months Post-Infection**		**One Week Post-Infection**	**Two Months Post-Infection**
	Stock		0.03[1]	< 0.001		0.033	0.008
Central Nervous System Tissues	**One Week Post-Infection**			0.089		0.986	0.286
	Two Months Post-Infection					0.098	0.8
Lymph Node Tissues	**One Week Post-Infection**						0.257

[1]p-values < or = 0.05 noted in red.

Table 48. Determined p-values for statistical comparisons of the prevalence of sequences with mutations in position 153 of Nef in the SIVsmmFGb stock virus and infected pigtailed macaque lymph nodes and CNS regions one wpi and two mpi

			Central Nervous System Tissues			Lymph Node Tissues	
			One Week Post-Infection	Two Months Post-Infection		One Week Post-Infection	Two Months Post-Infection
	Stock		0.824	0.836		0.71	0.01[1]
Central Nervous System Tissues	**One Week Post-Infection**			0.775		0.678	0.33
	Two Months Post-Infection					0.687	0.19
Lymph Node Tissues	**One Week Post-Infection**						0.03

[1]p-values < or = 0.05 noted in red.

Table 49. Determined p-values for statistical comparisons of the prevalence of sequences with mutations in position 193 of Nef in the SIVsmmFGb stock virus and infected pigtailed macaque lymph nodes and CNS regions one wpi and two mpi

			Central Nervous System Tissues			Lymph Node Tissues	
			One Week Post-Infection	Two Months Post-Infection		One Week Post-Infection	Two Months Post-Infection
	Stock		0.107	0.001[1]		0.022	0.286
Central Nervous System Tissues	**One Week Post-Infection**			0.025		0.719	0.249
	Two Months Post-Infection					0.05	0.022
Lymph Node Tissues	**One Week Post-Infection**						0.065

[1]p-values < or = 0.05 noted in red.

Table 50. Determined p-values for statistical comparisons of the prevalence of sequences with mutations in position 195 of Nef in the SIVsmmFGb stock virus and infected pigtailed macaque lymph nodes and CNS regions one wpi and two mpi

			Central Nervous System Tissues			Lymph Node Tissues	
			One Week Post-Infection	**Two Months Post-Infection**		**One Week Post-Infection**	**Two Months Post-Infection**
	Stock		0.037[1]	0.847		0.659	0.131
Central Nervous System Tissues	**One Week Post-Infection**			0.081		0.205	0.356
	Two Months Post-Infection					0.545	0.373
Lymph Node Tissues	**One Week Post-Infection**						0.524

[1]p-values < or = 0.05 noted in red.

Table 51 – The most common amino acid substitutions at residues with significant changes in the percentage of sequences with mutations in the lymph node or CNS at one wpi or two mpi, relative to the SIVsmmFGb stock virus

Gene	Position	SIVsmmFGb Stock Virus Consensus Sequence Amino Acid	Most Common Amino Acid Substitution(s)
Env V1 Region	41	Serine	Asparagine, Tyrosine
	49	Asparagine	Serine
Nef	9	Glutamine	Arginine
	12	Glutamine	Arginine
	13	Arginine	Glutamine
	14	Glycine	Arginine
	15	Glycine	Arginine, Lysine
	19	Lysine	Arginine
	28	Histidine	Tyrosine
	39	Tyrosine	Cysteine
	89	Aspartate	Asparagine
	91	Aspartate	Asparagine
	92	Aspartate	Asparagine
	93	Aspartate	Asparagine
	94	Aspartate	Asparagine
	95	Aspartate	Asparagine
	96	Glutamate	Lysine
	153	Isoleucine	Valine
	193	Tyrosine	Cysteine
	195	Valine	Methionine

References

1. UNAIDS. 2008. 2008 Report on the Global AIDS Epidemic.
2. Schacker T, Collier AC, Hughes J, Shea T, and Corey L. 1996. Clinical and Epidemiologic Features of Primary HIV Infection. *Annals of Internal Medicine* 125: 257 - 64
3. O'Neil SP, Suwyn C, Anderson DC, Niedziela G, Bradley J, Novembre FJ, Herndon JG and McClure HM. 2004. Correlation of Acute Humoral Response with Brain Virus Burden and Survival Time in Pigtailed Macaques Infected with the Neurovirulent Simian Immunodeficiency Virus SIVsmmFGb. *American Journal of Pathology* 164: 1157-72
4. Glenn AA, and Novembre FJ. 2004. A Single Amino Acid Change in gp41 is Linked to the Macrophage-Only Replication Phenotype of a Molecular Clone of Simian Immunodeficiency Virus Derived from the Brain of a Macaque with Neuropathogenic Infection. *Virology* 325: 297-307
5. So YT, Holtzman DM, Abrams DI, and Olney RK. 1988. Peripheral Neuropathy Associated with Acquired Immunodeficiency Syndrome: Prevalence and Clinical Features from a Population-Based Survey. *Arch. Neurol.* 45: 945 - 8
6. Ferrari S, Vento S, Monaco S, Cavallaro T, Cainelli F, Rizzuto N, and Temesgen Z. 2006. Human Immunodeficiency Virus-Associated Peripheral Neuropathies. *Mayo Clin. Proc.* 81: 213 - 9
7. McArthur JC, Haughey N, Gartner S, Conant K, Pardo C, Nath A and Sacktor N. 2003. Human Immunodeficiency Virus-Associated Dementia: An Evolving Disease. *Journal of Neurovirology* 9: 205 - 21

8. Ellis RJ, Calero P and Stockin MD. 2009. HIV Infection and the Central Nervous System: A Primer. *Neuropsychol. Rev.* 19: 144 - 51

9. Spencer DC, and Price RW. 1992. Human Immunodeficiency Virus and the Central Nervous System. *Annu. Rev. Microbiol.* 46: 655 - 93

10. Weisberg LA. 2001. Neurologic Abnormalities in Human Immunodeficiency Virus Infection. *Southern Medical Journal* 94: 266 - 76

11. Sacktor NC, Caellar H, Hoover DR, Nance-Sproson TE, Selnes OA, Miller EN, Dal Pan GJ, Kleeberger C, Brown A, Saah A, and McArthur JC. 1996. Psychomotor Slowing in HIV Infection. A Predictor of Dementia, AIDS and Death. *Journal of Neurovirology* 2: 404 - 10

12. Cherner M, Masliah E, Ellis RJ, Marcotte TD, Moore DJ, Grant I and Heaton RK. 2002. Neurocognitive Dysfunction Predicts Postmortem Findings of HIV Encephalitis. *Neurology* 59: 1563 - 7

13. Piette AM, Tusseau F, Vignon D, et al. 1986. Acute Neuropathy Coincident with Seroconversion for Anti-LAV/HTLV-III [Letter]. *Lancet* 1: 852

14. Gherardi RK, Chretien F, Delfau-Larue MH, et al. 1998. Neuropathy in Diffuse Infiltrative Lymphocytosis Syndrome: An HIV Neuropathy, Not A Lymphoma. *Neurology* 50: 1041 - 4

15. Janssen RS. 1992. Epidemiology of Human Immunodeficiency Virus Infection and the Neurologic Complications of the Infection. *Semin. Neurol.* 12: 10 - 7

16. Bacellar H, Munoz A, Miller EN, Cohen BA, Besley D, Selnes OA, Becker JT, and McArthur JC. 1994. Temporal Trends in the Incidence of HIV-1-Related

Neurologic Diseases: Multicenter AIDS Cohort Study, 1985 - 1992. *Neurology* 44: 1892 - 900

17. Neaton JD, Wentworth DN, Rhame F, Hogan C, Abrams DI, and Deyton L. 1994. Considerations in Choice of a Clinical Endpoint for AIDS Clinical Trials. Terry Beirn Community Programs for Clinical Research on AIDS (CPCRA). *Stat. Med.* 13: 2107 - 25
18. Price RW. 1998. AIDS Dementia Complex. *HIV InSite Knowledge Base Chapter*
19. Brew BJ, Pemberton L, Cunningham P, and Law PG. 1997. Levels of Human Immunodeficiency Virus Type 1 RNA in Cerebrospinal Fluid Correlate with AIDS Dementia Stage. *J. Infect. Dis.* 175: 963 - 6
20. Ellis RJ, Hsia K, Spector SA, Nelson JA, Heaton RK, Wallace MR, Abramson I, Atkinson JH, Grant I, and McCutchan JA. 1997. Cerebrospinal Fluid Human Immunodeficiency Virus Type 1 RNA Levels are Elevated in Neurocognitively Impaired Individuals with Acquired Immunodeficiency Syndrome. HIV Neurobehavioral Research Center Group. *Ann. Neurol.* 42: 679 - 88
21. Sacktor N, and McArthur J. 1997. Prospects for Therapy of HIV-Associated Neurologic Diseases. *Journal of Neurovirology* 3: 89-101
22. Singh NN, Yahya S, Garewai M, and Thomas FP. 2007. HIV-1 Encephalopathy and AIDS Dementia Complex. *eMedicine*
23. Tyor WR, and Middaugh LD. 1999. Do Alcohol and Cocaine Abuse Alter the Course of HIV-Associated Dementia Complex? *Journal of Leukocyte Biology* 65: 475 - 81

24. Goodwin GM, Pretsell DO, Chiswick A, Egan V, and Brettle RP. 1996. The Edinburgh Cohort of HIV-Positive Injecting Drug Users at 10 Years After Infection: A Case-Control Study of the Evolution of Dementia. *AIDS* 10: 431 - 40

25. Griffin III WC, Middaugh LD and Tyor WR. 2007. Chronic Cocaine Exposure in the SCID Mouse Model of HIV Encephalitis. *Brain Research* 1134: 214 - 9

26. CDC. 2008. HIV/AIDS in the United States: CDC HIV/AIDS Facts.

27. Dougherty RH, Skolasky RL Jr, and McArthur JC. 2002. Progression of HIV-Associated Dementia Treated with HAART. *AIDS Read.* 12: 69 - 74

28. Arango JC, Simmonds P, Brettle RP, and Bell JE. 2004. Does Drug Abuse Influence the Microglial Response in AIDS and HIV Encephalitis? *AIDS* 18: S69 - S74

29. Anthony IC, Ramage SN, Carnie FW, SImmonds P, and Bell JE. 2005. Does Drug Abuse Alter Microglial Phenotype and Cell Turnover in the Context of Advancing HIV Infection? *Neuropathology and Applied Neurobiology* 31: 325 - 38

30. Hauser KF, El-Hage N, Buch S, Nath A, Tyor WR, Bruce-Keller AJ and Knapp PE. 2006. Impact of Opiate-HIV-1 Interactions on Neurotoxic Signaling. *Journal of Neuroimmune Pharmacology* 1: 98 - 105

31. Dore GJ, McDonald A, Li Y, Kaldor JM and Brew BJ. 2003. Marked Improvement in Survival Following AIDS Dementia Complex in the Era of Highly Active Antiretroviral Therapy. *AIDS* 17: 1539-45

32. Sacktor N. 2002. The Epidemiology of Human Immunodeficiency Virus-Associated Neurological Disease in the Era of Highly Active Antiretroviral Therapy *Journal of Neurovirology* 8: 115-21

33. Ferrando S, van Gorp W, McElhiney M, Goggin K, Sewell M, and Rabkin J. 1998. Highly Active Antiretroviral Treatment in HIV Infection: Benefits for Neuropsychological Function. *AIDS* 12: F65 - F70

34. Tyor WR. 2009. Pathogenesis and Treatment of HIV-Associated Dementia: Recent Studies in a SCID Mouse Model. *Handbook of Neurochemistry and Molecular Neurobiology*: 471 - 89

35. Sidtis JJ, Gatsonis C, Price RW, Singer EJ, Collier AC, Richman DD, Hirsch MS, Schaerf FW, Fischl MA, Kieburtz K, et al. 1993. Zidovudine Treatment of the AIDS Dementia Complex: Results of a Placebo-Controlled Trial. AIDS Clinical Trials Group. *Ann. Neurol.* 33: 343 - 9

36. Schmitt FA, Bigley JW, McKinnis R, Logue PE, Evans RW, and Drucker JL. 1988. Neuropsychological Outcome of Zidovudine (AZT) Treatment of Patients with AIDS and AIDS-Related Complex. *New England Journal of Medicine* 319: 1573 - 8

37. Brouwers P, Hendricks M, Lietzau JA, Pluda JM, Mitsuya H, Broder S, and Yarchoan R. 1997. Effect of Combination Therapy with Zidovudince and Didanosine on Neuropsychological Functioning in Patients with Symptomatic HIV Disease: A Comparison of Simultaneous and Alternating Regimens. *AIDS* 11: 59 - 66

38. Yarchoan R, Berg G, Brouwers P, Fischl MA, Spitzer AR, Wichman A, Grafman J, Thomas RV, Safai B, Brunetti A, et al. 1987. Response of Human-Immunodeficiency-Virus-Associated Neurological Disease to 3'-Azido-3'-Deoxythymidine. *Lancet* 1: 132 - 5

39. Chiesi A, Vella S, Dally LG, Pedersen C, Danner S, Johnson AM, Schwander S, Goebel FD, Glauser M, Antunes F, and Lundgren JD. 1996. Epidemiology of AIDS Dementia Complex in Europe. *Journal of Acquired Immune Deficiency Syndromes and Human Retrovirology* 11: 39 - 44

40. Lupia RH, Ferencz N, Lertora JJL, Aggarwal SK, George WJ, and Agrawal KC. 1993. Comparative Pharmacokinetics of Two Prodrugs of Zidovudine in Rabbits: Enhanced Levels of Zidovudine in Brain Tissue. *Antimicrobial Agents and Chemotherapy* 37: 818 - 24

41. Dore GJ, and Correll PK. 1999. Changes to AIDS Dementia Complex in the Era of Highly Active Antiretroviral Therapy. *AIDS* 13: 1249 - 53

42. Nicholas PK, Mauceri L, Slate Ciampa A, Corless IB, Raymond N, Barry DJ and Viamonte Ros A. 2007. Distal sensory polyneuropathy in the Context of HIV/AIDS. *J. Assoc. Nurses AIDS Care.* 18: 32 - 40

43. Wang T, Rumbaugh JA, and Nath A. 2006. Viruses and the Brain from Inflammation to Dementia. *Clin. Sci. (Lond.)* 110: 393 - 407

44. Ghafouri M, Amini S, Khalili K and Sawaya BE. 2006. HIV-1 Associated Dementia: Symptoms and Causes. *Retrovirology* 3: 28-38

45. McGee B, Smith N, and Aweeka F. 2006. HIV Pharmacology: Barriers to the Eradication of HIV from the CNS. *HIV Clinical Trials* 7: 142 - 53

46. Piacenti FJ. 2006. An Update and Review of Antiretroviral Therapy. *Pharmacotherapy* 26: 1111 - 33

47. Groothius DR, and Levy RM. 1997. The Entry of Antiviral and Antiretroviral Drugs into the Central Nervous System. *Journal of Neurovirology* 3: 387-400

48. Gallo JM. 1994. Delivery of Anti-HIV Nucleosides to the Central Nervous System. *Advanced Drug Deliv. Rev.* 14: 299 - 309

49. Wu D, Boado RJ, et al. 1996. Pharmacokinetics and Blood-Brain Barrier Transport of [3H]-Biotinylated Phosphorothioate Oligodeoxynucleotide Conjugated to a Vector Mediated Drug Delivery System. *J. Pharmacol. Exp. Ther.* 276: 206 - 11

50. Simpson DM, and Tagliati M. 1995. Nucleoside Analogue-Associated Peripheral Neuropathy in Human Immunodeficiency Virus Infection. *J. Acquir. Immune Defic. Syndr. Hum. Retrovirol.* 9: 153 - 61

51. Taylor S, and Pereira A. 2000. Penetration of HIV-1 Protease Inhibitors in the CSF and Semen. *HIV Med.* 1: 18 - 22

52. Wynn HE, Brundage RC, and Fletcher CV. 2002. Clinical Implications of CNS Penetration of Antiretroviral Drugs. *CNS Drugs* 16: 595 - 609

53. McNicholl I. 2007. Adverse Effects of Antiretroviral Drugs. *HIV InSite*

54. Nath A, and Sacktor N. 2006. Influence of Highly Active Antiretroviral Therapy on Persistence of HIV in the Central Nervous System. *Curr Opin Neurol* 19: 358-61

55. Enting RH, Hoetelmans RM, Lange JMA, Burger AM, Beijnen JH and Portegies P. 1998. Antivretroviral Drugs and the Central Nervous System. *AIDS* 12: 1941 - 55

56. Crabb C. 2004. Protease Inhibitors and Risk of Developing HIV-Related Sensory Neuropathy. *AIDS* 18: N10

57. Denissen JF, Grabowski BA, et al. 1997. Metabolism and Disposition of the HIV-1 Protease Inhibitor Ritonavir (ABT-538) in Rats, Dogs and Humans. *Drug Metab. Disp.* 25: 489 - 501

58. Cook-Easterwood J, Middaugh LD, Griffin III WC, Khan I and Tyor WR. 2007. Highly Active Antiretroviral Therapy of Cognitive Dysfunction and Neuronal Abnormalities in SCID Mice with HIV Encephalitis. *Exp. Neurol.* 205: 506 - 12

59. Navia BA, Cho E, Petito CK, and Price RW. 1986. The AIDS Dementia Complex. II. Neuropathology. *Ann. Neurol.* 19: 525 - 35

60. Levin HS, Williams DH, Borucki MJ, Hillman GR, Williams JB, Guinto Jr FC, Amparo EG, Crow NW, and Pollard RB. 1990. Magnetic Resonance Imaging and Neuropsychological Findings In Human Immunodeficiency Virus Infection. *J. Acquir. Immune Defic. Syndr.* 3: 757 - 62

61. Rausch DM, Murray EA and Eiden LE. 1999. The SIV-Infected Rhesus Monkey Model for HIV-Associated Dementia and Implication for Neurological Disease. *Journal of Leukocyte Biology* 65: 466-74

62. Sharer LR. 1992. Pathology of HIV-1 Infection of the Central Nervous System. *J. Neuropathol. Exp. Neurol.* 51: 3 - 11

63. Petito CK. 1988. Review of Central Nervous System Pathology in Human Immunodeficiency Virus Infection. *Ann. Neurol.* 23: 54 - 7

64. Sopper S, Koutsilieri E, Scheller C, Czub S, Riederer P and ter Meulen V. 2002. Macaque Animal Model for HIV-Induced Neurological Disease. *Journal of Neural Transmission* 109: 747-66

65. Wiley C, and Achim C. 1994. Human Immunodeficiency Virus Encephalitis is the Pathological Correlate of Dementia in Acquired Immunodeficiency Syndrome. *Ann. Neurol.* 36: 673 - 6

66. Glass J, Wesselingh S, Selnes O, and McArthur J. 1993. Clinical-Neuropathogenic Correlation in HIV-Associated Dementia. *Neurol.* 43: 2230 - 7

67. Glass J, Fedor H, Wesselingh S, and McArthur J. 1995. Immunocytochemical Quantitation of Human Immunodeficiency Virus in the Brain: Correlations with Dementia. *Ann. Neurol.* 38: 755 - 62

68. Brew BJ, Rosenblum M, Cronin K and Price RW. 1995. AIDS Dementia Complex and HIV-1 Brain Infection: Clinical-Virological Correlations. *Annals of Neurology* 38: 563-70

69. Wiley CA, Soontonniyomkij V, Radhakrishnan L, Masliah E, Mellors J, Hermann SA, Dailey P and Achim CL. 1998. Distribution of Brain HIV Load in AIDS. *Brain Pathology* 8: 277-84

70. Lackner AA, Smith MO, Munn RJ, Martfeld DJ, Gardner MB, Marx PA and Dandekar S. 1991. Localization of Simian Immunodeficiency Virus in the Central Nervous System of Rhesus Macaques. *American Journal of Pathology* 139: 609-21

71. Zink MC, Suryanarayana K, Mankowski JL, Shen A, Piatak Jr M, Spelman JP, Carter DL, Adams RJ, Lifson JD, and Clements JE. 1999. High Viral Load in the Cerebrospinal Fluid and Brain Correlates with Severity of Simian Immunodeficiency Virus Encephalitis. *Journal of Virology* 73: 10480 - 8

72. Graybiel AM. 1995. Building Action Repertoires: Memory and Learning Function of the Basal Ganglia. *Curr. Opin. Neurobiol.* 5: 733 - 41

73. Levy R, Friedman HR, Davachi L, and Goldman RPS. 1997. Differential Activation of the Caudate Nucleus in Primates Performing Spatial and Nonspatial Working Memory Tasks. *J. Neurosci.* 17: 3870 - 82

74. Redgrave P, Prescott TJ, and Gurney K. 1999. The Basal Ganglia: A Vertebrate Solution to the Selection Problem? *Neuroscience* 89: 1009 - 23

75. Morris RGM, Garrud P, Rawlins JNP, and O'Keefe J. 1982. Place Navigation Impaired in Rats with Hippocampal Lesions. *Nature* 297: 681 - 3

76. Squire LR. 1992. Memory and the Hippocampus: A Synthesis from Findings with Rats, Monkeys and Humans. *Psych. Rev.* 99: 195 - 231

77. Fine EJ, Ionita CC, and Lohr L. 2002. The History of the Development of the Cerebellar Examination. *Semin. Neurol.* 22: 375 - 84

78. Everall IP, Luthert PJ, and Lantos PL. 1991. Neuronal Loss in the Frontal Cortex in HIV Infection. *The Lancet* 337: 1119 - 21

79. Williams KC, Corey S, Westmoreland SV, Pauley D, Knight H, deBakker C, Alvarez X and Lackner AA. 2001. Perivascular Macrophages are the Primary Cell Type Productively Infected by Simian Immunodeficiency Virus in the Brains of

Macaques: Implications for the Neuropathogenesis of AIDS. *J. Exp. Med.* 193: 905-15

80. Williams KC, and Hickey WF. 2002. Central Nervous System Damage, Monocytes and Macrophages, and Neurological Disorders in AIDS. *Annu. Rev. Neurosci.* 25: 537 - 62

81. Davis LE, Hjelle BL, Miller VE, Palmer DL, Llewellyn AL, Merlin TL, Young SA, Mills RG, Wachsman W and Wiley CA. 1992. Early Viral Brain Invasion in Iatrogenic Human Immunodeficiency Virus Infection. *Neurology* 42: 1736-9

82. Peluso R, Haase A, Stowring L, Edwards M and Ventura P. 1985. A Trojan Horse Mechanism for the Spread of Visna Virus in Monocytes. *Virology* 147

83. Kedzierska K, and Crowe SM. 2002. The Role of Monocytes and Macrophages in the Pathogenesis of HIV-1 Infection. *Current Medicinal Chemistry* 9: 1893 - 903

84. Sonza S, Maerz A, Deacon N, Meanger J, Mills J, and Crowe S. 1996. Human Immunodeficiency Virus Type 1 Replication is Blocked Prior to Reverse Transcription ad Integration in Freshly Isolated Peripheral Blood Monocytes. *Journal of Virology* 70: 3863 - 9

85. Sedgwick JD, Schwedner S, Imrich H, Dorries R, Butcher GW, and ter Meulen V. 1991. Isolation and Direct Characterization of Resident Microglial Cells from the Normal and Inflamed Central Nervous System. *PNAS* 88: 7438- 42

86. Becher B, and Antel JP. 1996. Comparison of Phenotypic and Functional Properties of Immediately Ex Vivo and Cultured Human Adult Microglia. *Glia* 18: 1 - 10

87. Ford AL, Goodsall AL, Hickey WF, and Sedgwick JD. 1995. Normal Adult Ramified Microglia Separated from Other Central Nervous System Macrophages by Flow Cytometric Sorting. Phenotypic Differences Defined and Direct Ex Vivo Antigen Presentation to Myelin Basic Protein-Reactive CD4+ T Cells Compared. *J. Immunol.* 154: 4309 - 21

88. Pulliam L, Gascon R, Stubblebine M, McGuire D, and McGrath MS. 1997. Unique Monocyte Subset in Patients with AIDS Dementia. *Lancet* 349: 692 - 5

89. Hess DC, Abe T, Hill WD, Studdard AM, Carothers J, Masuya M, Fleming PA, Drake CJ, and Ogawa M. 2004. Hematopoietic Origin of Microglial and Perivascular Cells in Brain. *Experimental Neurology* 186: 134 - 44

90. Nottet HSLM. 1999. Interactions Between Macrophages and Brain Microvascular Endothelial Cells: Role in Pathogenesis of HIV-1 Infection and Blood-Brain Barrier Function. *Journal of Neurovirology* 5: 659 - 69

91. Pelchen-Matthews A, Kramer B, and Marsh M. 2003. Infectious HIV-1 Assembles in Late Endosomes in Primary Macrophages. *J. Cell Biol.* 162: 443 - 55

92. Raposo G, Moore M, Innes Do, Leijendekker R, Leigh-Brown A, Benaroch P, and Geuze H. 2002. Human Macrophages Accumulate HIV-1 Particles in MHCII Compartments. *Traffic* 3: 718 - 29

93. Sharova N, Swingler C, Sharkey M and Stevenson M. 2005. Macrophages Archive HIV-1 Virions for Dissemination In Trans. *The EMBO Journal* 24: 2481 - 9

94. Maslin CLV, Kedzierska K, Webster NL, Muller WA and Crowe SM. 2005. Transendothelial Migration of Monocytes: The Underlying Molecular Mechanisms and Consequences of HIV-1 Infection. *Current HIV Research* 3: 303 - 12

95. Sasseville VG, and Lackner AA. 1997. Neuropathogenesis of Simian Immunodeficiency Virus Infection in Macaque Monkeys. *Journal of Neurovirology* 3: 1 - 9

96. Wong D, and Dorovini-Zis K. 1992. Upregulation of Intercellular Adhesion Molecule-1 (ICAM-1) Expression in Primary Cultures of Human Brain Microvessel Endothelial Cells by Cytokines and Lipopolysaccharide. *Journal of Neuroimmunology* 39: 11 - 21

97. Seguin R, Biernacki K, Rotonodo RL, Prat A, and Antel JP. 2003. Regulation and Functional Effects of Monocyte Migration Across Human Brain-Derived Endothelial Cells. *J. Neuropathol. Exp. Neurol.* 62: 412 - 9

98. Hofman FM, Wright AD, Dohadwala MM, Wong-Staal F, and Walker SM. 1993. Exogenous Tat Protein Activates Human Enodthelial Cells. *Blood* 92: 2774 - 80

99. Albini A, Ferrini S, Benelli R, Sforzini S, Giunciuglio D, Aluigi MG, Proudfoot AEI, Alouani S, Wells TNC, Mariani G, Rabin RL, Farber JM and Noonan DM. 1998. HIV-1 Tat Protein Mimicry of Chemokines. *PNAS* 95: 13153 - 8

100. Albini A, Benelli R, Giunciuglio D, Cai T, Mariani G, Ferrini S and Noonan DM. 1998. Identification of a Novel Domain of HIV Tat Involved in Monocyte Chemotaxis. *Journal of Biological Chemistry* 273: 15895 - 900

101. Eugenin EA, Dyer G, Calderon TM, and Berman JW. 2005. HIV-1 Tat Protein Induces A Migratory Phenotype in Human Fetal Microglia By A CCL2 (MCP-1)-Dependent Mechanism: Possible Role in NeuroAIDS. *Glia* 49: 501 - 10

102. Rao VR, Sas AR, Eugenin EA, Siddappa NB, Bimonte-Nelson H, Berman JW, Ranga U, Tyor WR and Prasad VR. 2008. HIV-1 Clade-Specific Differences in the Induction of Neuropathogenesis. *J. Neurosci.* 28: 10010 - 6

103. Dhawan S, Toro LA, Jones E, and Meltzer MS. 1992. Interactions Between HIV-Infected Monocytes and the Extracellular Matrix: HIV-Infected Monocytes Secrete Neutral Metalloproteases that Degrade Basement Membrane Protein Matrices. *J. Leukoc. Biol.* 52: 244 - 8

104. Wiley CA, Schrier RD, Nelson JA, Lampert PW, and Oldstone MBA. 1986. Cellular Localization of Human Immunodeficiency Virus Infection Within the Brains of Acquired Immune Deficiency Syndrome Patients. *PNAS* 83: 7089 - 93

105. Mankowski JL, Spelman JP, Ressetar HG, Strandberg JD, Laterra J, Carter DL, Clements JE and Zink MC. 1994. Neurovirulent Simian Immunodeficiency Virus Replicates Productively in Endothelial Cells of the Central Nervous System In Vivo and In Vitro. *Journal of Virology* 68: 8202 - 8

106. Liu NQ, Lossinsky AS, Popik W, Li X, Gujuluva C, Kriederman B, Roberts J, Pushkarsky T, Bukrinsky M, Witte M, Weinand M, and Fiala M. 2002. Human Immunodeficiency Virus Type 1 Enters Brain Microvascular Endothelia by Macropinocytosis Dependent on Lipid Rafts and the Mitogen-Activated Protein Kinase Signaling Pathway. *Journal of Virology* 76: 6689 - 700

107. Mukhtar M, Harley S, Chen P, BouHamdan M, Patel C, Acheampong E, and Pomerantz RJ. 2002. Primary Isolated Human Brain Microvascular Endothelial Cells Express Diverse HIV/SIV-Associated Chemokine Coreceptors and DC-SIGN and L-SIGN. *Virology* 297: 78 - 88

108. Mendu DR, Katinger H, Sodroski J, and Kim KS. 2007. HIV-1 Envelope Protein gp140 Binding Studies to Human Brain Microvascular Endothelial Cells. *Biochem. Biophys. Res. Commun.* 363: 466 - 71

109. Stins MF, Pearce D, Choi H, Di Cello F, Pado CA, and Kim KS. 2004. CD4 and Chemokine Receptors on Human Brain Microvascular Endothelial Cells, Implications for Human Immunodeficiency Virus Type 1 Pathogenesis. *Endothelium* 11: 275 - 84

110. Argyris EG, Acheampong E, Nunnari G, Mukhtar M, Williams KJ, and Pomerantz RJ. 2003. Human Immunodeficiency Virus Type 1 Enters Primary Human Brain Microvascular Endothelial Cells by a Mechanism Involving Cell Surface Proteoglycans Independent of Lipid Rafts. *Journal of Virology* 77: 12140 - 51

111. Bobardt MD, Salmon P, Wang L, Esko JD, Gabuzda D, Fiala M, Trono D, van der Schueren B, David G, and Gallay PA. 2004. Contribution of Proteoglycans to Human Immunodeficiency Virus Type 1 Brain Invasion. *Journal of Virology* 78: 6567 - 84

112. Banks WA, Robinson SM, Wolf KM, Bess Jr JW, and Arthur LO. 2004. Binding, Internalization and Membrane Incorporation of Human Immunodeficiency Virus-

1 at the Blood-Brain Barrier is Differentially Regulated. *Neuroscience* 128: 143 - 53

113. Kramer-Hammerle S, Rothenaigner I, Wolff H, Bell JE, and Brack-Werner R. 2005. Cells of the Central Nervous System as Targets and Reservoirs of the Human Immunodeficiency Virus. *Virus Research* 111: 194 - 213

114. Mukhtar M, Acheampong E, Parveen Z, and Pomerantz RJ. 2005. T-Cells and Excitotoxicity: HIV-1 and Other Neurodegenerative Disorders. *Neuromolecular Med.* 7: 265 - 73

115. Svenningsson A, Anderson O, Edsbagge M, and Stemme S. 1995. Lymphocyte Phenotype and Subset Distribution in Normal Cerebrospinal Fluid. *J. Neuroimmunol.* 63

116. Stevenson M. 2003. HIV-1 Pathogenesis. *Nature Medicine* 9: 853 - 60

117. Schnittman SM, et al. 1989. The Reservoir for HIV-1 in Human Peripheral Blood in a T Cell that Maintains Expression of CD4. *Science* 245: 305 - 9

118. Ghorpade A, Nukuna A, Che M, Haggerty S, Persidsky Y, Carter E, Carhart L, Shafer L, and Gendelman HE. 1998. Human Immunodeficiency Virus Neurotropism: An Analysis of Viral Replication and Cytopathicity for Divergent Strains in Monocytes and Microglia. *Journal of Virology* 72: 3340 - 50

119. Igarashi T, et al. 2001. Macrophage are the Principal Reservoir and Sustain High Virus Loads in Rhesus Macaques After the Depletion of CD4+ T Cells by a Highly Pathogenic SImian Immunodeficiency Virus/HIV Type 1 Chimera (SHIV): Implications for HIV-1 Infections of Humans. *PNAS* 98: 658 - 63

120. Eckstein DA, et al. 2001. HIV-1 Vpr Enhances Viral Burden by Facilitating Infection of Tissue Macrophages but Not Dividing CD4+ T Cells. *Journal of Experimental Medicine* 194: 1407 - 19

121. Lewin SR, Kirihara J, Sonza S, Irving L, Mills J, and Crowe SM. 1998. HIV-1 DNA and mRNA Concentrations are Similar in Peripheral Blood Monocytes and Alveolar Macrophages in HIV-1 Infected Individuals. *AIDS* 12: 719 - 27

122. Watry D, Lane TE, Streb M and Fox HS. 1995. Transfer of neuropathogenic simian immunodeficiency virus with naturally infected microglia. *Am. J. Pathol.* 146: 914-23

123. Chakrabarti L, Hurtrel M, Maire M, Vazeux R, Dormont D, Montagnier L and Hurtrel B. 1991. Early Viral Replication in the Brain of SIV-Infected Rhesus Monkeys. *American Journal of Pathology* 139: 1273-80

124. Lackner AA, Vogel P, Ramos RA, Kluge JD, and Marthas M. 1994. Early Events in Tissues During Inection with Pathogenic (SIVmac239) and Nonpathogenic (SIVmac1A11) Molecular Clones of Simian Immunodeficiency Virus. *Am. J. Pathol.* 145: 428 - 39

125. Lane JH, Sasseville VG, Smith MO, Vogel P, Pauley DR, Heyes MP, and Lackner AA. 1996. Neuroinvasion by Simian Immunodeficiency Virus Coincides with Increased Numbers of Perivascular Macrophages/Microglia and Intrathecal Immune Activation. *J. Neurovirol.* 2: 423 - 32

126. Gehrmann J, Matosmoto Y, and Kreutzberg GW. 1995. Microglia: Intrinsic Immuneffector Cell of the Brain. *Brain Research Reviews* 20: 269 - 87

127. Hickey WF, Vass K, and Lassman H. 1992. Bone Marrow Derived Elements in the Central Nervous Systems: An Immunohistochemical and Ultrastructural Survey of Rat Chimeras. *J. Neuropathol. Exp. Neurol.* 5

128. Kreutzberg GW. 1996. Microglia: A Sensor for Pathological Events in the CNS. *TINS* 19: 312 - 8

129. Lassmann H, Schmied M, Vass K, and Hickey WF. 1993. Bone Marrrow Derived Elements and Resident Microglia in Brain Inflammation. *Glia* 7: 19 - 24

130. Hickey WF, and Kimura H. 1988. Perivascular Microglial Cells of the CNS are Bone Marrow-Derived and Present Antigen. *Science* 239: 290 - 2

131. Gehrmann J. 1996. Microglia: A Sensor to Threats in the Nervous System. *Research in Virology* 147: 79 - 88

132. Jordan CA, Watkins BA, Kufta C, and Dubois-Dalcq M. 1991. Infection of Brain Microglial Cells by Human Immunodeficiency Virus Type 1 is CD4 Dependent. *Journal of Virology* 65: 736 - 42

133. Lavi E, Strizki JM, Ulrich AM, Zhang W, Fu L, Wang Q, O'Connor M, Hoxie JA, and Gonzalez-Scarano F. 1997. CXCR-4 (Fusin), A Co-Receptor for the Type 1 Human Immunodeficiency Virus (HIV-1), is Expressed in the Human Brain in a Variety of Cell Types, Including Microglia and Neurons. *Am. J. Pathol.* 151: 1035 - 42

134. He J, Chen Y, Farzan M, Choe H, Ohagen A, Gartner S, Busciglio J, Yang X, Hofmann W, Newman W, et al. 1997. CCR3 and CCR5 are Co-Receptors for HIV-1 Infection of Microglia. *Nature* 385: 645 - 9

135. Albright AV, Shieh JT, Itoh T, Lee B, Pleasure D, O'Connor MJ, Doms RW, and Gonzalez-Scarano F. 1999. Microglia Express CCR5, CXCR4 and CCR3, but of These CCR5 is the Principal Coreceptor for Human Immunodeficiency Virus Type 1 Dementia Isolates. *Journal of Virology* 73: 205 - 13

136. Gabuzda D, He J, Ohagen A and Vallat A. 1998. Chemokine Receptors in HIV-1 Infection of the Central Nervous System. *Seminars in Immunology* 10: 203 - 13

137. Martin-Garcia J, Kolson DL, and Gonzalez-Scarano F. 2002. Chemokine Receptors in the Brain: Their Role in HIV Infection and Pathogenesis. *AIDS* 16: 1709 - 30

138. Ioannidis JP, Reichlin S, and Skolnik PR. 1995. Long-Term Productive Human Immunodeficiency Virus-1 Infection in Human Infant Microglia. *Am. J. Pathol.* 147: 1200 - 6

139. Kootstra NA, Zwart BM, and Schuitemaker H. 2000. Diminished Human Immunodeficiency Virus Type 1 Reverse Transcription and Nuclear Transport in Primary Macrophages Arrested in Early G(1) Phase of the Cell Cycle. *Journal of Virology* 7: 1712 - 7

140. O'Brien WA, Namazi M, Kalhor H, Mao SH, Zack JA, and Chen ISY. 1994. Kinetics of Human Immunodeficiency Virus Type 1 Reverse Transcription in Blood Mononuclear Phagocytes are Slowed by Limitations of Nucleotide Precursors. *Journal of Virology* 68: 1258 - 63

141. Weinberg JB, Matthews TJ, Cullen BR, and Mallim MH. 1991. Productive Human Immunodeficiency Virus Type 1 (HIV-1) Infection of Nonproliferating Human Monocytes. *J. Exp. Med.* 174: 1477 - 82

142. Kootstra NA, and Schuitemaker H. 1998. Proliferation-Dependent Replication in Primary Macrophages of Macrophage-Tropic HIV Type 1 Variants. *AIDS Research and Human Retroviruses* 14: 339 - 45

143. Lassmann H, Zimprich F, Vass K, and Hickey WF. 1991. Microglial Cells are a Component of the Perivascular Limitans. *J. Neurosci. Res.* 28

144. Watkins BA, Dorn HH, Kelly WB, Armstrong RC, Potts BJ, Michaels F, Kufta CV, and Dubois-Dalcq M. 1990. Specific Tropism of HIV-1 for Microglial Cells in Primary Human Brain Cultures. *Science* 249: 549-53

145. Strizki JM, Albright AV, Sheng H, O'Connor M, Perrin L and Gonzalez-Scarano F. 1996. Infection of Primary Human Microglia and Monocyte-Derived Macrophages with Human Immunodeficiency Virus Type 1 Isolates: Evidence of Differential Tropism. *Journal of Virology* 70: 7654-62

146. Dickson DW. 1986. Multinucleated Giant Cells in Acquired Immunodeficiency Syndrome Encephalopathy. Origin from Endogenous Microglia? *Arch. Pathol. Lab. Med.* 110: 967 - 8

147. Fischer-Smith T, Croul S, Sverstiuk AE, Capini C, L'Heureux D, et al. 2001. CNS Invasion by CD14/CD16 Positive Peripheral Blood-Derived Monocytes in HIV Dementia: Perivascular Accumulation and Reservoir of HIV Infection. *J. Neuro. Virol.* 7: 528 - 41

148. Morris A, Marsden M, Halcrow K, Hughes ES, Brettle RP, Bell JE, and Simmonds P. 1999. Mosaic Structure of the Human Immunodeficiency Virus Type 1 Genome Infecting Lymphoid Cells and the Brain: Evidence for Frequent

In Vivo Recombination Events in the Evolution of Regional Populations. *Journal of Virology* 73: 8720 - 31

149. Brack-Werner R. 1999. Astrocytes: HIV Cellular Reservoirs and Important Participants in Neuropathogenesis. *AIDS* 13: 1 - 22

150. Gage FH. 2000. Mammalian Neural Stem Cells. *Science* 287: 1433 - 8

151. Barres BA. 1991. New Roles for Glia. *J. Neurosci.* 11: 3685 - 94

152. Raff MC. 1989. Glial Cell Diversification in the Rat Optic Nerve. *Science* 243: 1450 - 5

153. Saito Y, Sharer LR, Epstein LG, Michaels J, Mintz M, Louder M, Golding K, Cvetkovich TA, and Blumberg BM. 1994. Overexpression of Nef as a Marker for Restricted HIV-1 Infection of Astrocytes in Postmortem Pediatric Central Nervous Tissues. *Neurology* 44: 474 - 81

154. Nuovo GJ, Gallery F, MacConnell P, and Braun A. 1994. In Situ Detection of Polymerase Chain Reaction-Amplified HIV-1 Nucleic Acids and Tumor Necrosis Factor-Alpha RNA in the Central Nervous System. *Am. J. Pathol.* 144: 659 - 66

155. Trillo-Pazos G, Diamanturos A, Rislove L, Menza T, Chao W, Belem P, Sadiq S, Morgello S, Sharer L, and Volsky DJ. 2003. Detection of HIV-1 DNA in Microglia/Macrophages, Astrocytes and Neurons Isolated from Brain Tissue with HIV-1 Encephalitis by Laser Capture Microdissection. *Brain Pathol.* 13: 144 - 54

156. Harouse JM, Kunsch C, Hartle HT, Laughlin MA, Hoxie JA, Wigdahl B, and Gonzalez-Scarano F. 1989. CD4-Independent Infection of Human Neural Cells by Human Immunodeficiency Virus Type 1. *Journal of Virology* 63: 2527 - 33

157. Schweighhardt B, Shieh JT, and Atwood WJ. 2001. CD4/CXCR4-Independent Infection of Human Astrocytes by a T-Tropic Strain of HIV-1. *J. Neurovirol.* 7: 155 - 62

158. Gorry PR, Ong C, Thorpe J, Bannwarth S, Thompson KA, Gatignol A, Vesselingh SL, and Purcell DF. 2003. Astrocyte Infection by HIV-1: Mechanisms of Restricted Virus Replication, and Role in the Pathogenesis of HIV-1-Associated Dementia. *Current HIV Research* 1: 463 - 73

159. Sabri F, Tresoldi E, Di Stefano M, Polo S, Monaco MC, Verani A, Fiore JR, Lusso P, Major E, Chiodi F, and Scarlatti G. 1999. Nonproductive Human Immunodeficiency Virus Type 1 Infection of Human Fetal Astrocytes: Independence from CD4 and Major Chemokine Receptors. *Virology* 264: 370 - 84

160. Nath A, Hartloper V, Furer M, and Fowke KR. 1995. Infection of Human Fetal Astrocytes with HIV-1: Viral Tropism and the Role of Cell to Cell Contact in Viral Transmission. *J. Neuropathol. Exp. Neurol.* 54: 320 - 30

161. Gorry PR, Howard JL, Churchill MJ, Anderson JL, Cunningham A, Adrian D, McPhee DA and Purcell DFJ. 1999. Diminished Production of Human Immunodeficiency Virus Type 1 in Astrocytes Results from Inefficient Translation of gag, env and nef mRNAs Despite Efficient Expression of Tat and Rev. *Journal of Virology* 73: 352-61

162. Neumann M, Afonina E, Ceccherini-Silberstein F, Schlicht S, Erfle V, Pavlakis GN, and Brack-Werner R. 2001. Nucleocytoplasmic Transport in Human Astrocytes: Decreased Nuclear Uptake of the HIV Rev Shuttle Protein. *J. Cell. Sci.* 114: 1717 - 29

163. Bagasra O, Lavi E, Bobroski L, Khalili K, Pestaner JP, Tawadros R, and Pomerantz RJ. 1996. Cellular Reservoirs of HIV-1 in the Central Nervous System of Infected Individuals: Identification by the Combination of In Situ Polymerase Chain Reaction and Immunohistochemistry. *AIDS* 10: 573 - 85

164. Takahashi K, Wesselingh SL, Griffin DE, McArthur JC, Johnson RT, and Glass JD. 1996. Localization of HIV-1 in Human Brain Using Polymerase Chain Reaction/In Situ Hybridization and Immunocytochemistry. *Ann. Neurol.* 39: 705 - 11

165. An SF, Groves M, Giometto B, Beckett AA, and Scaravilli F. 1999. Detection and Localization of HIV-1 DNA and RNA in Fixed Adult AIDS Brain by Polymerase Chain Reaction/In Situ Hybridization Technique. *Acta. Neuropathol. Berl.* 98: 481 - 7

166. Wiley CA, Achim CL, Christopherson C, Kidane Y, Kwok S, Masliah E, Mellors J, Radhakrishnan L, Wang G, and Soontornniyomkij V. 1999. HIV Mediates a Productive Infection of the Brain. *AIDS* 13: 2055 - 9

167. Albright AV, Strizki J, Harouse JM, Lavi E, O'Connor M, and Gonzalez-Scarano F. 1996. HIV-1 Infection of Cultured Human Adult Oligodendrocytes. *Virology* 217: 211 - 9

168. Ensoli F, Cafaro A, Fiorelli V, Vannelli B, Ensoli B, and Thiele CJ. 1995. HIV-1 Infection of Primary Human Neuroblasts. *Virology* 210: 221 - 5

169. Obregon E, Punzon C, Fernandez-Cruz E, Fresno M, and Munoz-Fernandez MA. 1999. HIV-1 Infection Induces Differentiation of Immature Neural Cells Through

Autocrine Tumor Necrosis Factor and Nitric Oxide Production. *Virology* 261: 193 - 204

170. Hurtrel B, Chakrabarti L, Hurtrel M, Maire MA, Dormont D, and Montagnier L. 1991. Early SIV Encephalopathy. *Journal of Medical Primatology* 20: 159 - 66

171. Ho DD, Rota TR, Schooley RT, Kaplan JC, Allan JD, Groopman JE, Resnick L, Felsenstein D, Andrews CA and Hirsch MS. 1985. Isolation of HTLV-III from Cerebrospinal Fluid and Neural Tissues of Patients with Neurologic Syndromes Related to the Acquired Immunodeficiency Syndrome. *New England Journal of Medicine* 313: 1493-7

172. Gouldsmit J, deWolf F, Paul DA, Epstein LG, Lange JMA, Krone WJA, Speelman H, Wolters EC, Van der Noordaa J, Oleske JM, Van der Helm HJ and Coutinho RA. 1986. Expression of Human Immunodeficiency Virus Antigen (HIV-Ag) in Serum and Cerebrospinal Fluid During Acute and Chronic Infection. *Lancet* 2: 177-80

173. Smith MS, Niu Y, Buch S, Li Z, Adany I, Pinson DM, Potula R, Novembre FJ and Narayan O. 2005. Active Simian Immunodeficiency Virus (strain smmPGm) Infection in Macaque Central Nervous System Correlates with Neurological Disease. *J. Acquir. Immune Defic. Syndr* 38: 518-30

174. Clements JE, Babas T, Mankowski JL, Suryanarayana K, Piatak Jr. M, Tarwater PM, Lifson JD and Zink MC. 2002. The Central Nervous System as a Reservoir for Simian Immunodeficiency Virus (SIV): Steady State Levels of SIV DNA in Brain from Acute Through Asymptomatic Infection. *Journal of Infectious Diseases* 186: 905-13

175. Mankowski JL, Flaherty MT, Spelman JP, Hauer DA, Didier PJ, Amedee AM, Murphey-Corb M, Kirstein M, Munoz A, Clements JE, and Zink MC. 1997. Pathogenesis of Simian Immunodeficiency Virus Encephalitis: Viral Determinants of Neurovirulence. *Journal of Virology* 71: 6055 - 60

176. Barber SA, Herbst DS, Bullock BT, Gama L, and Clements JE. 2004. Innate Immune Responses and Control of Acute Simian Immunodeficiency Virus Replication in the Central Nervous System. *J. Neurovirol.* 10: 15 - 20

177. Barber SA, Gama L, Dudaronek JM, Voelker T, Tarwater PM, and Clements JE. 2006. Mechanism for the Establishment of Transcriptional HIV Latency in the Brain in a Simian Immunodeficiency Virus-Macaque Model. *Journal of Infectious Diseases* 193: 963 - 70

178. Henderson AJ, Zou X, and Calame KL. 1995. C/EBP Proteins Activate Transcription from the Human Immunodeficiency Virus Type 1 Long Terminal Repeat in Macrophages/Monocytes. *J. Virol.* 69: 5337 - 44

179. Henderson AJ, Connor RI, Calame KL. 1996. C/EBP Activators are Required for HIV-1 Replication and Proviral Induction in Monocytic Cell Lines. *Immunity* 5: 91 - 101

180. Henderson AJ, and Calame KL. 1997. CCAAT/Enhancer Binding Protein (C/EBP) Sites are Required for HIV-1 Replication in Primary Macrophages but not CD4+ T Cells. *PNAS* 94: 8714 - 9

181. Descombers P, and Schibler U. 1991. A Liver-Enriched Transcriptional Activator Protein, LAP, and a Transcriptional Inhibitory Protein, LIP, are Translated from the Same mRNA. *Cell* 67: 569 - 79

182. Weiden M, Tanaka N, Qiao Y, et al. 2000. Differentiation of Monocytes to Macrophages Switches the Mycobacterium tuberculosis Effect on HIV-1 Replication from Stimulation to Inhibition: Modulation of Interferon Response and CCAAT/Enhancer Binding Protein Beta Expression. *J. Immunol.* 165: 2028 - 39

183. Honda Y, Rogers L, Nataka K, et al. 1998. Type I Interferon Induces Inhibitory 16-kD CCAAT/Enhancer Binding Protein (C/EBP) Beta, Repressing the HIV-1 Long Terminal Repeat in Macrophages: Pulmonary Tuberculosis Alters C/EBP Expression, Enhancing HIV-1 Replication. *J. Exp. Med.* 188: 1255 - 65

184. Griffin DE. 2003. Immune Responses to RNA-Virus Infections of the CNS. *Nat. Rev. Immunol.* 3: 493 - 502

185. Hoshino Y, Nakata K, Hoshino S, et al. 2002. Maximal HIV-1 Replication in Alveolar Macrophages During Tuberculosis Requires both Lymphocyte Contact and Cytokines. *J. Exp. Med.* 195: 495 - 505

186. Gessani S, Puddu P, Varano B, Borghi P, Conti L, Fantuzzi L, Gherardi G, and Belardelli F. 1994. Role of Endogenous Interferon-Beta in the Restriction of HIV Replication in Human Monocyte/Macrophages. *J. Leukocyte Biol.* 56: 358 - 61

187. Dudaronek JM, Barber SA, and Clements JE. 2007. CUGBP1 is Required for IFN-Beta-Mediated Induction of Dominant-Negative CEBP-Beta and Suppression of SIV Replication in Macrophages. *Journal of Immunology* 179: 7262 - 9

188. Haase AT. 1986. Pathogenesis of Lentivirus Infections. *Nature* 322: 130 - 6

189. van Marle G, Rourke SB, Zhang K, Silva C, Ethier J, Gill MJ, and Power C. 2002. HIV Dementia Patients Exhibit Reduced Viral Neutralization and Increased Envelope Sequence Diversity in Blood and Brain. *AIDS* 16: 1905 - 14

190. Baskin GB, Murphey-Corb M, Roberts ED, Didier PJ, and Martin LN. 1992. Correlates of SIV Encephalitis in Rhesus Monkeys. *J. Med. Primatol.* 21: 59 - 63

191. Zhang JY, Martin LN, Watson EA, Montelaro RC, West M, Epstein L, and Murphey-Corb M. 1988. Simian Immunodeficiency Virus/Delta-Induced Immunodeficiency Disease in Rhesus Monkeys: Relation of Antibody Resonse and Antigenemia. *J. Infect. Dis.* 158

192. Daniel MD, Letvin NL, Sehgal PK, Hunsmann G, Schmidt DK, King NW, and Desrosiers RC. 1987. Long-Term Persistent Infection of Macaque Monkeys with the Simian Immunodeficiency Virus. *J. Gen. Virol.* 68: 3183 - 9

193. Petito CK, and Cash KS. 1992. Blood-Brain Barrier Abnormalities in the Acquired Immunodeficiency Syndrome: Immunohistochemical Localization of Serum Proteins in Postmortem Brain. *Ann Neurol* 32: 658 - 66

194. Rhodes RH. 1991. Evidence of Serum-Protein Leakage Across the Blood-Brain Barrier in the Acquired Immunodeficiency Syndrome. *J Neuropathol Exp Neurol* 50: 171 - 83

195. Kanmogne GD, Schall K, Leibhart J, Knipe B, Gendelman HE and Persidsky Y. 2007. HIV-1 gp120 Compromises Blood-Brain Barrier Integrity and Enhance Monocyte Migration Across Blood-Brain Barrier: Implication for Viral Neuropathogenesis. *Journal of Cerebral Blood Flow and Metabolism* 27: 123 - 34

196. Richman DD, Wrin T, Little SJ and Petropoulos CJ. 2003. Rapid Evolution of the Neutralizing Antibody Response to HIV Type 1 Infection. *PNAS* 100: 4144 - 9

197. Wei X, Decker JM, Wang S, Hui H, Kappes JC, Wu X, Salazar-Gonzalez JF, Salazar MG, Kilby JM, Saag MS, Komarova NL, Nowak MA, Hahn BH, Kwong PD and Shaw GM. 2003. Antibody Neutralization and Escape by HIV-1. *Nature* 422: 307 - 12

198. McEntee MF, Anderson MG, Daniel MD, Adams R, Farzadegan H, Desrosiers RC and Narayan O. 1992. Differences in Neutralization of Simian Lentivirus (SIVMAC) in lymphocyte and Macrophage Cultures. *AIDS Res Hum Retroviruses* 8: 1193 - 8

199. Petito CK, and Adkins B. 2003. CD4+ and CD8+ Cells Accumulate in the Brains of Acquired Immunodeficiency Syndrome Patients with Human Immunodeficiency Virus Encephalitis. *J. NeuroVirol* 9: 36 - 44

200. Mukhtar M, Mengistu A, Acheampong E, et al. 2003. Statins Block Enhanced Expression of Matrix Metalloproteinases (MMPs) by Virally Infected Monocytes and T-Cells and Thereby Normalize Their Transvascular Migration. A Novel Therapeutic Approach to HIV-1 Neuroinvasion. *Circulation* 108: 487

201. Schmitz JE, Kuroda MJ, Santra S, Sasseville VG, Simon MA, Lifton MA, Racz P, Tenner-Racz K, Dalesandro M, Scallon BJ, Ghrayeb J, Forman MA, Montefiori DC, Rieber EP, Letvin NL, and Reimann KA. 1999. Control of Viremia in Simian Immunodeficiency Virus Infection of CD8+ Lymphocytes. *Science* 283: 857 - 60

202. Williams K, Alvarez X, and Lackner AA. 2001. Central Nervous System Perivascular Cells are Immunoregulatory Cells that Connect the CNS with the Peripheral Immune System. *Glia* 36: 156 - 64

203. Chang HC, Samaniego F, Nair BC, Buonaguro L, and Ensoli B. 1997. HIV-1 Tat Protein Exits From Cells Via A Leaderless Secretory Pathway and Binds to Extracellular Matrix-Associated Heparan Sulfate Proteoglycans Through Its Basic Region. *AIDS* 11: 1421 - 31

204. Li W, Galey D, Mattson MP, and Nath A. 2005. Molecular and Cellular Mechanisms of Neuronal Cell Death in HIV Dementia. *Neurotoxicity Research* 8: 119 - 34

205. Bruce-Keller AJ, Chauhan A, Dimayuga FO, Gee J, Keller JN, and Nath A. 2003. Synpatic Transport of Human Immunodeficiency Virus-Tat Protein Causes Neurotoxicity and Gliosis in Rat Brain. *J. Neurosci.* 23: 8417 - 22

206. Adle-Biassette H, Chretien F, Wingertsmann L, Hery C, Ereau T, Scaravilli F, Tardieu M, and Gray F. 1999. Neuronal Apoptosis Does Not Correlate With Dementia in HIV Infection But Is Related to Microglial Activation and Axonal Damage. *Neuropathol. Appl. Neurobiol.* 25: 123 - 33

207. Benos DJ, Hahn BH, Bubien JK, Ghosh SK, Mashburn NA, Chaikin MA, Shaw GM, and Benveniste EN. 1994. Envelope Glycoprotein gp120 of Human Immunodeficiency Virus Type 1 Alters Ion Transport in Astrocytes: Implications for AIDS Dementia Complex. *PNAS* 91: 494 - 8

208. Catani MV, Corasaniti MT, Navarra M, Nistico G, Finazzi-Agro A, and Melino G. 2000. gp120 Induces Cell Death in Human Neuroblastoma Cells Through the

CXCR4 and CCR5 Chemokine Receptors. *Journal of Neurochemistry* 74: 2373 - 9

209. Holden CP, Haughey NJ, Nath A, and Geiger JD. 1999. Role of Na+/H+ Exchangers, Excitatory Amino Acid Receptors and Voltage-Operated Ca2+ Channels in Human Immunodeficiency Virus Type 1 gp120-Mediated Increases in Intracellular Ca2+ in Human Neurons and Astrocytes. *Neuroscience* 91: 1369 - 78

210. Lipton SA. 1994. Neuronal Injury Associated with HIV-1 and Potential Treatment with Calcium-Channel and NMDA Antagonists. *Dev. Neurosci.* 16: 145 - 51

211. Kruman II, Nath A, and Mattson MP. 1998. HIV-1 Protein Tat Induces Apoptosis of Hippocampal Neurons by a Mechanism Involving Caspase Activation, Calcium Overload and Oxidative Stress. *Exp. Neurol.* 154: 276 - 88

212. Bonavia R, Bajetto A, Barbero S, Albini A, Noonan DM, and Schettini G. 2001. HIV-1 Tat Causes Apoptotic Death and Calcium Homeostasis Alterations in Rat Neurons. *Biochem. Biophys. Res. Commun.* 288: 301 - 8

213. Pattarini R, Pittaluga A, and Raiteri M. 1998. The Human Immunodeficiency Virus-1 Envelope Protein gp120 Binds Through Its V3 Sequence to the Glycine Site of N-Methyl-D-Aspartate Receptors Mediating Noradrenaline Release in the Hippocampus. *Neuroscience* 87: 147 - 57

214. Pittaluga A, Pattarini R, Severi P, and Raiteri M. 1996. Human Brain N-Methyl-D-Aspartate Receptors Regulating Noradrenaline Release Are Positively Modulated by HIV-1 Coat Protein. *AIDS* 10: 463 - 8

215. Kaul M, Zheng J, Okamoto S, Gendeman HE, and Lipton SE. 2005. HIV-1 Infection and AIDS: Consequences for the Central Nervous System. *Cell Death and Differentiation* 12: 878 - 92

216. Swingler S. 1997. Pathogenic Mechanisms of Neuronal Damage in the AIDS Dementia Complex. *J. Clin. Pathol: Mol. Pathol.* 50: 72-6

217. Acquas E, Bachis A, Nosheny RL, Cernak I, and Mocchetti I. 2004. Human Immunodeficiency Virus Type 1 Protein gp120 Causes Neuronal Cell Death in the Rat Brain by Activating Caspases. *Neurotoxicity Res.* 5: 605 - 15

218. Zheng J, Thylin MR, Ghorpade A, Xiong H, Persidsky Y, Cotter R, NiemannD, Che M, Zeng YC, Gelbard HA, Shepard RB, Swartz JM, and Gendelman HE. 1999. Intracellular CXCR4 Signaling, Neuronal Apoptosis and Neuropathogenic Mechanisms of HIV-1-Associated Dementia. *J. Neuroimmunol.* 98: 185 - 200

219. Hesselgesser J, Taub D, Baskar P, Greenberg M, Hoxie J, Kolson DL and Horuk R. 1998. Neuronal Apoptosis Induced By HIV-1 gp120 and the Chemokine SDF-1 Alpha is Mediated by the Chemokine Receptor CXCR4. *Curr. Biol.* 8: 595 - 8

220. Giulian D, Yu J, Li X, Tom D, Li J, Wendt E, Lin S, Schwarcz R, and Noonan C. 1996. Study of Receptor-Mediated Neurotoxins Released by HIV-1-Infected Mononuclear Phagocytes Found in Human Brain. *Journal of Neuroscience* 16: 3139 - 53

221. Genis P, Jett M, Bernton EW, Boyle T, Gelbard HA, Dzenko K, Keane RW, Resnick L, Mizrachi Y, Volsky DJ, Epstein LG, and Gendelman HE. 1992. Cytokines and Arachidonic Metabolites Produced During Human Immunodeficiency Virus (HIV)-Infected Macrophage-Astroglia Interactions:

Implications for the Neuropathogenesis of HIV Disease. *Journal of Experimental Medicine* 176: 1703 - 18

222. Takeda-Hirokawa N, Neoh LP, Akimoto H, Kaneko H, Hishikawa T, Sekigawa I, Hashimoto H, Hirose S, Murakami T, Yamamoto N, Mimura T, and Kaneko Y. 1997. Role of Curdlan Sulfate in the Binding of HIV-1 gp120 to CD4 Molecules and the Production of gp120-Mediated TNF-Alpha. *Microbiol. Immunol.* 41: 741 - 5

223. Giulian D, Wendt E, Vaca K, and Noonan C. 1993. The Envelope Glycoprotein of HIV-1 Stimulates Monocyte Release of Neurotoxins. *PNAS* 90: 2769 - 73

224. Power C, McArthur JC, Nath A, Wehrly K, Mayne M, Nishio J, Langelier T, Johnson RT, and Chesebro B. 1998. Neuronal Death Induced by Brain-Derived Human Immunodeficiency Virus Type 1 Envelope Genes Differs Between Demented and Nondemented AIDS Patients. *Journal of Virology* 72: 9045 - 53

225. Viviani B, Corsini E, Binaglia M, Galli CL, and Marinovich M. 2001. Reactive Oxygen Species Generated by Glia are Responsible for Neuron Death Induced by Human Immunodeficiency Virus-Glycoprotein 120 In Vitro. *Neuroscience* 107: 51 - 8

226. Misse D, Esteve PO, Renneboog B, Vidal M, Cerutti M, St. Pierre Y, Yssel H, Parmentier M, and Veas F. 2001. HIV-1 Glycoprotein 120 Induces the MMP-9 Cytopathogenic Factor Production That is Abolished By Inhibition of the p38 Mitogen-Activated Protein Kinase Signaling Pathway. *Blood* 98: 541 - 7

227. Brenneman DE, McCune SK, Mervis RF, and Hill JM. 1994. gp120 As An Etiologic Agent for NeuroAIDS: Neurotoxicity and Model Systems. *Adv. Neuroimmunol.* 4: 157 - 65

228. Masliah E, Ge N, Achim CL, Hansen LA, and Wiley CA. 1992. Selective Neuronal Vulnerability in HIV Encephalitis. *J. Neuropathol. Exp. Neurol.* 51: 585 - 93

229. Nosheny RL, Bachis A, Acquas E, and Mocchetti I. 2004. Human Immunodeficiency Virus Type 1 Glycoprotein gp120 Reduces the Levels of Brain-Derived Neurotrophic Factor In Vivo: Potential Implication for Neuronal Cell Death. *European Journal of Neuroscience* 20: 2857 - 64

230. Mocchetti I, and Bachis A. 2004. Brain-Derived Neurotrophic Factor Activation of TrkB Protects Neurons from HIV-1/gp120-Induced Cell Death. *Crit. Rev. Neurobiol.* 16: 51 - 8

231. Pulliam L, West D, Haigwood N, and Swanson RA. 1993. HIV-1 Envelope gp120 Alters Astrocytes in Human Brain Cultures. *AIDS Research and Human Retroviruses* 9: 439 - 44

232. Brenneman DE, Westbrook GL, Fitzgerald SP, Ennist DL, Elkins KL, Ruff MR, and Pert CB. 1988. Neuronal Cell Killing by the Envelope Protein of HIV and Its Prevention by Vasoactive Intestinal Peptide. *Nature* 335: 639 - 42

233. Otake K, Fujii Y, Nakaya T, Nishino Y, Zhong Q, Fujinaga K, Kameoka M, Ohki K, and Ikuta K. 1994. The Carboxyl-Terminal Region of HIV-1 Nef Protein is a Cell Surface Domain That Can Interact with CD4+ T Cells. *Journal of Immunology* 153: 5826 - 37

234. Guy B, Riviere Y, Dott K, Regnault A, and Kieny MP. 1990. Mutational Analysis of the HIV Nef Protein. *Virology* 176: 413 - 25

235. Kaminchik J, Bashan N, Pinchasi D, Amit B, Sarver N, Johnston MI, Fischer M, Yavin Z, Gorecki M, and Panet A. 1990. Expression and Biochemical Characterization of Human Immunodeficiency Virus Type 1 Nef Gene Product. *Journal of Virology* 64: 3447 - 54

236. Wesselingh SL, and Thompson KA. 2001. Immunopathogenesis of HIV-Associated Dementia. *Curr. Opin. Neurol.* 14: 375 - 9

237. van Marle G, Henry S, Todoruk T, Sullivan A, Silva C, Rourke SB, Holden J, McArthur JC, Gill MJ and Power C. 2004. Human Immunodeficiency Virus Type 1 Nef Protein Mediates Neural Cell Death: A Neurotoxic Role for IP-10. *Virology* 329: 302-18

238. Sui Y, Stehno-Bittel L, Li S, Loganathan R, Dhillon NK, Pinson D, Nath A, Kolson D, Narayan O, and Buch S. 2006. CXCL10-Induced Cell Death in Neurons: Role of Calcium Dysregulation. *Eur. J. Neurosci.* 23: 957 - 64

239. Lane BR, King SR, Bock PJ, Strieter RM, Coffey MJ, and Markovitz DM. 2003. The C-X-C Chemokine IP-10 Stimulates HIV-1 Replication. *Virology* 307: 122 - 34

240. Tillo-Pazos G, McFarlane-Abdulla E, Campbell IC, Pilkington GJ, and Everall IP. 2000. Recombinant Nef HIV-IIIB Protein is Toxic to Human Neurons in Culture. *Brain Research* 864: 315 - 26

241. Werner T, Ferroni S, Saermark T, Brack-Werner R, Banati RB, Mager R, Steinaa L, Kreutzberg GW, and Erfle V. 1991. HIV-1 Nef Protein Exhibits Structural and

Functional Similarity to Scorpion Peptides Interacting with K+ Channels. *AIDS* 5: 1301- 8

242. Cheng J, Nath A, Knudsen B, Hochman S, Geiger JD, Ma M, and Magnuson DS. 1998. Neuronal Excitatory Properties of Human Immunodeficiency Virus Type 1 Tat Protein. *Neuroscience* 82: 97 - 106

243. Sabatier J, Vives E, Mabrouk K, Benjouad A, Rochat H, Duval A, Hue B and Bahraoui E. 1991. Evidence for Neurotoxic Activity of Tat from Human Immunodeficiency Virus Type 1. *Journal of Virology* 65: 961 - 7

244. Haughey NJ, Holden CP, Nath A, and Geiger JD. 1999. Involvement of Inositol 1,4,5-Trisphosphate-Regulated Stores of Intracellular Calcium in Calcium Dysregulation and Neuron Cell Death Caused by HIV-1 Protein Tat. *J. Neurochem.* 73: 1363 - 74

245. Haughey NJ, Nath A, Mattson MP, Slevin JT, and Geiger JD. 2001. HIV-1 Tat Through Phosphorylation of NMDA Receptors Potentiates Glutamate Excitotoxicity. *J. Neurochem.* 78: 457 - 67

246. Zhou BY, Liu Y, Kim B, Xiao Y, and He JJ. 2004. Astrocyte Activation and Dysfunction and Neuron Death by HIV-1 Tat Expression in Astrocytes. *Mol. Cell. Neurosci.* 27: 296 - 305

247. Magnuson DS, Knudsen BE, Geiger JD, Brownstone RM, and Nath A. 1995. Human Immunodeficiency Virus Type 1 Tat Activates Non-N-Methyl-D-Aspartate Excitatory Amino Acid Receptors and Causes Neurotoxicity. *Ann. Neurol.* 37: 373 - 80

248. New DR, Maggirwar SB, Epstein LG, Dewhurst S and Gelbard HA. 1998. HIV-1 Tat Induces Neuronal Death via Tumor Necrosis Factor Alpha and Activation of Non-N-Methyl-D-Aspartate Receptors by a NFkappaB-Independent Mechanism. *Journal of Biological Chemistry* 273: 17852 - 8

249. Bennasser Y, Badou A, Tkaczuk J, and Bahraoui E. 2002. Signaling Pathways Triggered by HIV-1 Tat in Human Monocytes to Induce TNF-Alpha. *Virology* 303: 174 - 80

250. Khan NA, Di Cello F, Nath A, and Kim KS. 2003. Human Immunodeficiency Virus Type 1 Tat-Mediated Cytotoxicity off Human Brain Microvascular Endothelial Cells. *J. Neurovirol.* 9: 584 - 93

251. Conant K, St. Hillaire C, Anderson C, Galey D, Wang J, and Nath A. 2004. Human Immunodeficiency Virus Type 1 Tat and Methamphetamine Affect the Release and Activation of Matrix-Degrading Proteinases. *J. Neurovirol.* 10: 21 - 8

252. Smith DG, Guillemin GJ, Pemberton L, Kerr S, Nath A, Smythe GA, and Brew BJ. 2001. Quinolinic Acid is Produced by Macrophages Stimulated by Platelet-Activating Factor, Nef and Tat. *J. Neurvirol.* 7: 56 - 60

253. Brew BJ, Corbeil J, Pemberton L, Evans L, Saito K, Penny R, Cooper DA, and Heyes MP. 1995. Quinolinic Acid Production is Related to Macrophage Tropic Isolates of HIV-1. *J. Neurovirol.* 1: 369 - 74

254. Haughey NJ, Cutler RG, Tamara A, McArthur JC, Vargas DL, Pardo CA, Turchan J, Nath A, and Mattson MP. 2004. Perturbation of Sphingolipid Metabolism and Ceramide Production in HIV-Dementia. *Ann. Neurol.* 55: 257 - 67

255. Piller SC, Ewart GD, Jans DA, Gage PW, and Cox GB. 1999. The Amino-Terminal Region of Vpr From Human Immunodeficiency Virus Type 1 Forms Ion Channels and Kills Neurons. *Journal of Virology* 73: 4230 - 8

256. Patel CA, Mukhtar M, and Pomerantz RJ. 2000. Human Immunodeficiency Virus Type 1 Vpr Induces Apoptosis in Human Neuronal Cells. *Journal of Virology* 74: 9717 - 26

257. Nottet HS, and Gendelman HE. 1995. Unraveling the Neuroimmune Mechanisms for the HIV-1-Associated Cognitive/Motor Complex. *Immunol. Today* 16: 441 - 8

258. Matthews S, Barlow P, Boyd J, Barton G, Russell R, Mills H, Cunningham M, Meyers N, Burns N, Clark N, Kingsman S, Kingsman A, and Campbell I. 1994. Structural Similarity Between the p17 Matrix Protein of HIV-1 and Interferon-Gamma. *Nature* 370: 666 - 8

259. Adamson DC, Wildemann B, Sasaki M, Glass JD, McArthur JC, Christov VI, Dawson TM, and Dawson VL. 1996. Immunologic NO Synthase: Elevation in Severe AIDS Dementia and Induction by HIV-1 gp41. *Science* 274: 1917 - 21

260. Hu S, Ali H, Sheng WS, Ehrlich LC, Peterson PK, and Chao CC. 1999. Gp-41-Mediated Astrocyte Inducible Nitric Oxide Synthase mRNA Expression: Involvement of Interleukin-1 Beta Production by Microglia. *J. Neurosci.* 19: 6468 - 74

261. Chong YH, Seoh JY, and Park HK. 1998. Increased Activity of Matrix Metalloproteinase-2 In Human Glial and Neuronal Cell Lines Treated with HIV-1 gp41 Peptides. *J. Mol. Neurosci.* 10: 129 - 41

262. Leveque T, Le Pavec G, Boutet A, Tardieu M, Dormont D, and Gras G. 2004. Differential Regulation of Gelatinase A and B and TIMP-1 and -2 by TNFalpha and HIV Virions in Astrocytes. *Microbes Infect.* 6: 157 - 63

263. Mabrouk K, van Rietschoten J, Vives E, Darbon H, Rochat H, and Sabatier JM. 1991. Lethal Neurotoxicity in Mice of the Basic Domains of Hiv and SIV Rev Proteins. Study of These Regions By Circular Dichroism. *FEBS Letters* 289: 13 - 7

264. Ewart GD, Sutherland T, Gage PW, and Cox GB. 1996. The Vpu Protein of Human Immunodeficiency Virus Type 1 Forms Cation-Selective Channels. *Journal of Virology* 70: 7108 - 15

265. Parmentier HK, van Wichen DF, Meyling FH, Goudsmit J, and Schuurman HJ. 1992. Epitopes of Human Immunodeficiency Virus Regulatory Proteins Tat, Nef and Rev are Expressed in Normal Human Tissue. *Am. J. Pathol.* 141: 1209 - 16

266. Parravicini CL, Klatzmann D, Jaffray P, Costanzi G, and Gluckman JC. 1988. Monoclonal Antibodies to the Human Immunodeficiency Virus p18 Protein Cross-React with Normal Human Tissues. *AIDS* 2: 171 - 7

267. Yamada M, Zurbriggen A, Oldstone MBA, and Fujinami RS. 1991. Common Immunological Determinant Between Human Immunodeficiency Virus Type 1 gp41 and Astrocytes. *Journal of Virology* 65: 1370 - 6

268. Achim CL, Heyes MP, and Wiley CA. 1993. Quantitation of Human Immunodeficiency Virus, Immune Activation Factors and Quinolinic Acid in AIDS Brains. *J. Clin. Invest.* 91: 2769 - 75

269. Wesselingh SL, Power C, Glass JD, Tyor WR, McArthur JC, Farber JM, Griffin JW, Griffin DE. 1993. Intracerebral Cytokine Messenger RNA Expression in Acquired Immunodeficiency Syndrome Dementia. *Ann. Neurol.* 33: 576 - 82

270. Schmidtmayerova H, Nottet HS, Nuovo G, Raabe T, Flanagan CR, Dubrovsky L, Gendelman HE, Cerami A, Bukrinsky M, and Sherry B. 1996. Human Immunodeficiency Virus Type 1 Infection Alters Chemokine Beta Peptide Expression in Human Monocytes: Implications for Recruitment of Leukocytes in Brain and Lymph Nodes. *PNAS* 93: 700 - 4

271. Wilt SG, Milward E, Zhou JM, Nagasato K, Patton H, Rusten R, Griffin DE, O'Connor M, Dubois-Dalcq M. 1995. In Vitro Evidence for a Dual Role of Tumor Necrosis Factor-Alpha in Human Immunodeficiency Virus Type 1 Encephalopathy. *Ann. Neurol.* 37: 381 - 94

272. Talley AK, Dewhurst S, Perry SW, Dollard SC, Gummuluru S, Fine SM, New D, Epstein LG, Gendelman HE, and Gelbard HA. 1995. Tumor Necrosis Factor Alpha-Induced Apoptosis in Human Neuronal Cells: Protection by the Antioxidant N-Acetylcysteine and the Genes Bcl-2 and CrmA. *Mol. Cell. Biol.* 15: 2359 - 66

273. Rath PC, and Aggarwal BB. 1999. TNF-Induced Signaling in Apoptosis. *J. Clin. Immunol.* 19: 350 - 64

274. Sheikh MS, and Huang Y. 2003. Death Receptor Activation Complexes: It Takes Two to Activate TNF Receptor 1. *Cell Cycle* 2: 550 - 2

275. Gelbard HA, Dzenko KA, DiLoreto D, del Cerro C, del Cerro M, and Epstein LG. 1993. Neurotoxic Effects of Tumor Necrosis Factor Alpha in Primary Human

Neuronal Cultures are Mediated by Activation of the Glutamate AMPA Receptor Subtype: Implications for AIDS Neuropathogenesis. *Dev. Neurosci.* 15: 417 - 22

276. Benos DJ, McPherson S, Hahn B, Chaikin MA, and Benveniste EN. 1994. Cytokines and HIV Envelope Glycoprotein gp120 Stimulate Na+/H+ Exchange in Astrocytes. *J. Biol. Chem.* 269: 13811 - 6

277. Fine SM, Angel RA, Perry SW, Epstein LG, Rothstein JD, Dewhurst S, and Gelbard HA. 1996. Tumor Necrosis Factor Alpha Inhibits Glutamate Uptake by Primary Human Astrocytes. Implications for Pathogenesis of HIV-1 Dementia. *J. Biol. Chem.* 271: 15303 - 6

278. Shi B, Raina J, Lorenzo A, Busciglio J, and Gabuzda D. 1998. Neuronal Apoptosis Induced by HIV-1 Tat Protein and TNF-Alpha: Potentiation of Neurotoxicity Mediated by Oxidative Stress and Implications for HIV-1 Dementia. *J. Neurovirol.* 4: 281 - 90

279. Andrieu-Abadie N GV, Salvayre R, and Levade T. 2001. Ceramide in Apoptosis Signaling: Relationship with Oxidative Stress. *Free Radic. Biol. Med.* 31: 717 - 28

280. Sacktor N, Haughey N, Cutler R, Tamara A, Turchan J, Pardo C, Vargas D, and Nath A. 2004. Novel Markers of Oxidative Stress in Actively Progressive HIV Dementia. *Journal of Neuroimmunology* 157: 176 - 84

281. Aloisi F, Care A, Borsellino G, Gallo P, Rosa S, Bassani A, Cabibbo A, Testa U, Levi G, and Peschle C. 1992. Production of Hemolymphopoietic Cytokines (IL-6, IL-8, Colony-Stimulating Factors) by Normal Human Astrocytes in Response to IL-1 Beta and Tumor Necrosis Factor-Alpha. *J. Immunol.* 149: 2358 - 66

282. Guillemin GJ, Croitoru-Lamoury J, Dormont D, Armati PJ, and Brew BJ. 2003. Quinolinic Acid Upregulates Chemokine Production and Chemokine Receptor Expression in Astrocytes. *Glia* 41: 371 - 81

283. Mattson MP, and Camandola S. 2001. NF-Kappa-B in Neuronal Plasticity and Neurodegenerative Disorders. *J. Clin. Invest.* 107: 247 - 54

284. Cheng B, Cristakos S, and Mattson MP. 1994. Tumor Necrosis Factors Protect Neurons Against Metabolic-Excitotoxic Insults and Promote Maintenance of Calcium Homeostasis. *Neuron* 12: 139 - 53

285. Giulian D, and Lachman LB. 1985. Interleukin-1 Stimulation of Astroglial Proliferation After Brain Injury. *Science* 228: 497 - 9

286. Lee SC, Dickson DW, Liu W, and Brosnan CF. 1993. Induction of Nitric Oxide Synthase Activity in Human Astrocytes by Interleukin-1 Beta and Interferon-Gamma. *J. Neuroimmunol.* 46: 19 - 24

287. Liu J, Zhao ML, Brosnan CF, and Lee SC. 1996. Expression of Type II Nitric Oxide Synthase in Primary Human Astrocytes and Microglia: Role of IL-1beta and IL-1 Receptor Antagonist. *J. Immunol.* 157: 3569 - 76

288. daCunha A, Jefferson JJ, Tyor WR, Glass JD, Jannotta FS and Vitkovic L. 1993. Control of Astrocytes by Interleukin-1 and Transforming Growth Factor-beta-1 in Human Brain. *Brain Res.* 631: 39 - 45

289. Lee SC, Liu W, Brosnan CF, and Dickson DW. 1994. GM-CSF Promotes Proliferation of Human Fetal and Adult Microglia in Primary Cultures. *Glia* 12: 309 - 18

290. Si Q, Cosenza M, Zhao ML, Goldstein H, and Lee SC. 2002. GM-CSF and M-CSF Modulate Beta-Chemokine and HIV-1 Expression in Microglia. *Glia* 39: 174 - 83

291. Kandanearatchi A, Zuckerman M, Smith M, Vyakarnam A, and Everall IP. 2002. Granulocyte-Macrophage Colony-Stimulating Factor Enhances Viral Load in Human Brain Tissue: Amelioration with Stavudine. *AIDS* 16: 413 - 20

292. Appay V, Brown A, Cribbes S, Randle E, and Czaplewski LG. 1999. Aggregation of RANTES is Responsible for Its Inflammatory Properties: Characterization of Nonaggregating, Noninflammatory RANTES Mutants. *J. Virol.* 274: 27505 - 12

293. Kitai R, Zhao ML, Zhang N, Hua LL, and Lee SC. 2000. Role of MIP-1beta and RANTES in HIV-1 Infection of Microglia: Inhibition of Infection and Induction by IFNbeta. *J. Neuroimmunol.* 110: 230 - 9

294. Haine V, Fischer-Smith T, and Rappaport J. 2006. Macrophage Colony-Stimulating Factor in the Pathogenesis of HIV Infection: Potential Target for Therapeutic Intervention. *J. Neuroimmune Pharmacol.* 1: 32 - 40

295. Bergamini A, Perno CF, Dini L, Capozzi M, Pesce CD, Ventura L, Cappannoli L, Falasca L, Milanese G, and Calio R. 1994. Macrophage Colony-Stimulating Factor Enhances the Susceptibility of Macrophages to Infection by Human Immunodeficiency Virus and Reduces the Activity of Compounds that Inhibit Virus Binding. *Blood* 84: 3405 - 12

296. Oravecz T, Pall M, Roderiquez G, Gorrell MD, Ditto M, Nguyen NY, Boykins R, Unsworth E, and Norcross MA. 1997. Regulation of the Receptor Specificity and Function of the Chemokine RANTES (Regulated on Activation, Normal T Cell

Expressed and Secreted) by Dipeptidyl Peptidase IV (CD26)-Mediated Cleavage. *J. Exp. Med.* 186: 1865 - 72

297. Komuro I, Yokota Y, Yasuda S, Iwamoto A, Kagawa KS. 2003. CSF-Induced and HIV-1-Mediated Distinct Regulation of Hck and C/EBPbeta Represent A Heterogenous Susceptibility of Monocyte-Derived Macrophages to M-tropic HIV-1 Infection. *J. Exp. Med.* 198: 443 - 53

298. Shapshak P, Duncan R, Minagar A, Rodriguez de la Vega P, Stewart RV, and Goodkin K. 2004. Elevated Expression of IFN-Gamma in the HIV-1 Infected Brain. *Front. Biosci.* 9: 1073 - 81

299. Tyor WR, Glass J, Becker S, Griffin J, Bezman L, McArthur J and Griffin DE. 1992. Cytokine Expression in the Brain During AIDS. *Ann. Neurol.* 31: 349 - 60

300. Heyes MP, Saito K, and Markey SL. 1992. Human Macrophages Convert L-Tryptophan into the Neurotoxin Quinolinic Acid. *J. Biochem.* 83: 633 - 5

301. Merrill JE, Koyanagi Y, and Chen ISY. 1989. Interleukin-1 and Tumor Necrosis Factor-Alpha Can Be Induced from Mononuclear Phagocytes by Human Immunodeficiency Virus Type 1 Binding to CD4 Receptor. *J. Virol.* 63: 4404 - 8

302. Wright SC, Jewett A, Mitsuyasu R, and Bonavida B. 1988. Spontaneous Cytotoxicity and Tumor Necrosis Factor Production by Peripheral Blood Monocytes from AIDS Patients. *J. Immunol.* 141: 99 - 104

303. Xiong H, Boyle J, Winkelbauer M, Gorantia S, Zheng J, Ghorpade A, Persidsky Y, Carlson KA, and Gendelman HE. 2002. Inhibition of Long-Term Potentiation by Interleukin-8: Implications for Human Immunodeficiency Virus-1-Associated Dementia. *Journal of Neuroscience Research* 71: 600 - 7

304. Gerszten RE, Garcia-Zepeda EA, Lim YC, Yoshida M, Ding HA, Gimbrone Jr MA, Luster AD, Luscinskas FW, and Rosenzweig A. 1999. MCP-1 and IL-8 Trigger Firm Adhesion of Monocytes to Vascular Endothelium Under Flow Conditions. *Nature* 398: 718 - 23

305. Gruol DL, and Nelson TE. 1997. Physiological and Pathological Roles of Interleukin-6 in the Central Nervous System. *Molecular Neurobiology* 15: 307 - 39

306. Eugenin EA, Osiecki K, Lopez L, Goldstein H, Calderon TM, and Berman JW. 2006. CCL2/Monocyte Chemoattractant Protein-1 Mediates Enhanced Transmigration of Human Immunodeficiency Virus (HIV)-Infected Leukocytes Across the Blood-Brain Barrier: A Potential Mechanism of HIV-CNS Invasion and NeuroAIDS. *J. Neurosci.* 26: 1098 - 106

307. Eugenin EA, D'Aversa TG, Lopez L, Calderon TM, and Berman JW. 2003. MCP-1 (CCL2) Protects Human Neurons and Astrocytes from NMDA or HIV-Tat-Induced Apoptosis. *J. Neurochem.* 85: 1299 - 311

308. Chao CC, Molitor TW, and Hu S. 1993. Neuroprotective Role of IL-4 Against Activated Microglia. *J. Immunol.* 151: 1473 - 81

309. Brew BJ. 1994. The Clinical Spectrum and Pathogenesis of HIV Encephalopathy, Myelopathy and Peripheral Neuropathy. *Curr. Opin. Neurol.* 7: 209 - 16

310. Kim JP, and Choi DW. 1987. Quinolinate Neurotoxicity in Cortical Cell Culture. *Neuroscience* 23: 423 - 32

311. Stone TW. 1993. Neuropharmacology of Quinolinic and Kynurenic Acids. *Pharmacol. Rev.* 45: 309 - 79

312. Guillemin GJ, Wang L, and Brew BJ. 2005. Quinolinic Acid Selectively Induces Apoptosis of Human Astrocytes: Potential Role in AIDS Dementia Complex. *Journal of Neuroinflammation* 2: 16 - 22

313. Miller B, Sarantis M, Traynelis SF, and Attwell D. 1992. Potentiation of NMDA Receptor Currents by Arachidonic Acid. *Nature* 355: 722 - 5

314. Volterra A, Trotti D, Cassutti P, Tromba C, Salvaggio A, Melcangi RC, and Racagni G. 1992. High Sensitivity of Glutamate Uptake to Extracellular Free Arachidonic Acid Levels in Rat Cortical Synaptosomes and Astrocytes. *J. Neurochem.* 59: 600 - 6

315. Nicotera P, Bonfoco E, and Brune B. 1995. Mechanisms for Nitric Oxide-Induced Cell Death: Involvement of Apoptosis. *Adv. Neuroimmunol.* 5: 411 - 20

316. Rostasy K, Monti L, Yiannoutsos C, Kneissl M, Bell J, Kemper TL, Hedreen JC and Navia BA. 1999. Human Immunodeficiency Virus Infection, Inducible Nitric Oxide Synthase Expression, and Microglial Activation: Pathogenic Relationship to the Acquired Immunodeficiency Syndrome Dementia Complex. *Ann. Neurol.* 46: 207 - 16

317. Bukrinsky MI, Nottet HS, Schmidtmayerova H, Dubrovsky L, Flanagan CR, Mullins ME, Lipton SA, and Gendelman HE. 1995. Regulation of Nitric Oxide Synthase Activity in Human Immunodeficiency Virus Type 1 (HIV-1)-Infected Monocytes: Implications for HIV-Associated Neurological Disease. *J. Exp. Med.* 181: 735 - 45

318. Boven LA, Gomes L, Hery C, Gray F, Verhoef J, Portegies P, Tardieu M, and Nottet HS. 1999. Increased Peroxynitrite Activity in AIDS Dementia Complex:

Implications for the Neuropathogenesis of HIV-1 Infection. *J. Immunol.* 162: 4319 - 27

319. Dawson VL, Dawson TM, Uhl GR, and Snyder SH. 1993. Human Immunodeficiency Virus Type 1 Coat Protein Neurotoxicity Mediated by Nitric Oxide in Primary Cortical Cultures. *PNAS* 90: 3256 - 9

320. Beckman JS, and Koppenol WH. 1996. Nitric Oxide, Superoxide, and Peroxynitrite: The Good, the Bad and Ugly. *Am. J. Physiol.* 271: C1424 - C37

321. Ischiropoulos H, Zhu L, Chen J, Tsai M, Martin JC, Smith CD, and Beckman JS. 1992. Peroxynitrite-Mediated Tyrosine Nitration Catalyzed by Superoxide Dismutase. *Arch. Biochem. Biophys.* 298: 431 - 7

322. Turchan J, Pocernich CB, Gairola C, Chauhan A, Schifitto G, Butterfield DA, Buch S, Narayan O, Sinai A, Geiger J, Berger JR, Elford H, and Nath A. 2003. Oxidative Stress in HIV Demented Patients and Protection Ex Vivo with Novel Antioxidants. *Neurology* 60: 307 - 14

323. Esterbauer H, Schaur RJ, and Zollner H. 1991. Chemistry and Biochemistry of 4-Hydroxynonenal, Malonaldehyde and Related Aldehydes. *Free Radic. Biol. Med.* 11: 81 - 128

324. Gelbard HA, Nottet HSLM, Swindells S, Jett M, Dzenko KA, Genis P, White R, Wang L, Choi Y, Zhang D, Lipton SA, Tourtellotte WW, Epstein LG, and Gendelman HE. 1994. Platelet-Activating Factor: A Candidate Human Immunodeficiency Virus Type 1-Induced Neurotoxin. *Journal of Virology* 68: 4628 - 35

325. Hogan MM, and Vogen SN. 1988. Production of TNF by rIFNgamma-Primed CC3HH/HeJ (LPSd) Macrophages Requires the Presence of Lipid-A-Associated Proteins. *J. Immunol.* 141: 196 - 9

326. Bito H, Nakamura M, Honda Z, Izumi T, Iwatsubo T, Seyama Y, Ogura A, Kudo Y, and Shimizu T. 1992. Platelet-Activating Factor (PAF) Receptor in Rat Brain: PAF Mobilizes Intracellular Ca2+ in Hippocampal Neurons. *Neuron.* 9: 285 - 94

327. Conant K, McArthur JC, Griffin DE, Sjulson L, Wahl LM, and Irani DN. 1999. Cerebrospinal Fluid Levels of MMP-2, 7 and 9 are Elevated in Association with Human Immunodeficiency Virus Dementia. *Ann. Neurol.* 46: 391 - 8

328. Belichenko PV, Miklossy J, and Celio MR. 1997. HIV-1 Induced Destruction of Neocortical Extracellular Matrix Components in AIDS Victims. *Neurobiol. Dis.* 4: 301 - 10

329. Zhang K, McQuibban GA, Silva C, Butler GS, Johnston JB, Holden J, Clark-Lewis I, Overall CM, and Power C. 2003. HIV-Induced Metalloproteinase Processing of the Chemokine Stromal Cell Derived Factor-1 Causes Neurodegeneration. *Nat. Neurosci.* 6: 1064 - 71

330. Freed EO. 2001. HIV-1 Replication. *Somatic Cell and Molecular Genetics* 26: 13 - 33

331. Westervelt P, Trowbridge DB, Epstein LG, Blumberg BM, Li Y, Hahn BH, Shaw GM, Price RW, and Ratner L. 1992. Macrophage Tropism Determinants of Human Immunodeficiency Virus Type 1 In Vivo. *Journal of Virology* 66: 2577 - 82

332. Boyd MT, Simpson GR, Cann AJ, Johnson MA, and Weiss RA. 1993. A Single Amino Acid Substitution in the V1 Loop of Human Immunodeficiency Virus Type 1 gp120 Alters Cellular Tropism. *Journal of Virology* 67: 3649 - 52

333. Shioda T, Levy JA, and Cheng-Meyer C. 1991. Macrophage and T-Cell Line Tropisms of HIV-1 are Determined by Specific Regions of the Envelope gp120 Gene. *Nature* 349: 167 - 9

334. Rossi F, Querido B, Nimmagadda M, Cocklin S, Navas-Martin S, and Martin-Garcia J. 2008. The V1 - V3 Region of a Brain-Derived HIV-1 Envelope Glycoprotein Determines Macrophage Tropism, Low CD4 Dependence, Increased Fusogenicity and Altered Sensitivity to Entry Inhibitors. *Retrovirology* 6: 89

335. Rudensey LM, Kimata JT, Long EM, Chackerian B, and Overbaugh J. 1998. Changes in the Extracellular Envelope Glycoprotein of Variants That Evolve During the Course of Simian Immunodeficiency Virus SIVMne Infection Affect Neutralizing Antibody Recognition, Syncytium Formation and Macrophage Tropism but not Replication, Cytopathicity or CCR5 Coreceptor Recognition. *Journal of Virology* 72: 209 - 17

336. Ogert RA, Lee MK, Ross W, Buckler-White A, Martin MA, and Cho MW. 2001. N-Linked Glycosylation Sites Adjacent to and Within the V1/V2 and V3 loops of Dualtropic Human Immunodeficiency Virus Type 1 Isolae DN12 gp120 Affect Coreceptor Usage and Cellular Tropism. *Journal of Virology* 75: 5998 - 6006

337. Ross TM, and Cullen BR. 1998. The Ability of HIV Type 1 to Use CCR-3 as a Coreceptor is Controlled by Envelope V1/V2 Sequences Acting in Conjunction with a CCR-5 Tropic V3 Loop. *PNAS* 95: 7682 - 6

338. Masciotra S, Owen SM, Rudolph D, Yang C, Wang B, Saksena N, Spira T, Dhawan S, and Lal RB. 2002. Temporal Relationship Between V1V2 Variation, Macrophage Replication and Coreceptor Adaptation During HIV-1 Disease Progression. *AIDS* 16: 1887 - 98

339. Laird ME, Igarashi T, Martin MA, and Desrosiers RC. 2008. Importance of the V1/V2 Loop Region of Simian-Human Immunodeficiency Virus Envelope Glycoprotein gp120 in Determining the Strain Specificity of the Neutralizing Antibody Response. *Journal of Virology* 82: 11054 - 65

340. Rencher SD, and Hurwitz JL. 1997. Effect of Natural HIV-1 Envelope V1-V2 Sequence Diversity on the Binding of V3-Specific and Non-V3-Specific Antibodies. *J. Acquir. Immune Defic. Syndr. Hum. Retrovirol.* 16: 69 - 73

341. McKeating JA, Shotton C, Cordell J, Graham S, Balfe P, Sullivan N, Charles M, Page M, Bolmstedt A, Olofsson S, Kayman SC, Wu Z, Pinter A, Dean C, Sodorski J, and Weiss RA. 1993. Characterization of Neutralizing Monoclonal Antibodies to Linear and Conformation-Dependent Epitopes Within the First and Second Variable Domains of Human Immunodeficiency Virus Type 1 gp 120. *Journal of Virology* 67: 4932 - 44

342. Moore JP, Sattentau Q, Yoshiyama H, Thali M, Charles M, Sullivan N, Poon S, Fung MS, Traincard F, Robinson JE, Ho DD, and Sodroski J. 1993. Probing the Structure of the V2 Domain of the Human Immunodeficiency Virus Type 1

Surface Glycoprotein gp120 with a Panel of Eight Monoclonal Antibodies: The Human Immune Response to the V1 and V2 Domains. *Journal of Virology* 67: 6136 - 51

343. Jurkiewicz E, Hunsmann G, Schaffner J, Nisslein T, Luke W and Petry H. 1997. Identification of the V1 Region as a Linear Neutralizing Epitope of the Simian Immunodeficiency Virus SIVmac Envelope Glycoprotein. *Journal of Virology* 71: 9475-81

344. Burns DPW, and Desrosiers RC. 1991. Selection of Genetic Variants of Simian Immunodeficiency Virus in Persistently Infected Rhesus Monkeys. *Journal of Virology* 65: 1843 - 5

345. Overbaugh J, Rudensky LM, Papenhausen MD, Beneviste RE, and Morton WR. 1991. Variation in Simian Immunodeficiency Virus env is Confined to V1 and V4 During Progression to Simian AIDS. *Journal of Virology* 65: 7025 - 31

346. Almond N, Jenkins A, Heath AB and Kitchin P. 1993. Sequence Variation in the Env Gene of Simian Immunodeficiency Virus Recovered from Immunized Macaques is Predominantly in the V1 Region. *Journal of General Virology* 74: 865 - 71

347. Li M, Salazar-Gonzalez JF, Derdeyn CA, Morris L, Williamson C, Robinson JE, Decker JM, Li Y, Salazar MG, Polonis VR, Mlisana K, Karim SA, Hong K, Greene KM, Bilska M, Zhou J, Allen S, Chomba E, Mulenga J, Vwalika C, Gao F, Zhang M, Korber BTM, Hunter E, Hahn BH, and Montefiori DC. 2006. Genetic and Neutralization Properties of Subtype C Human Immunodeficiency

Virus Type 1 Molecular env Clones from Acute and Early Heterosexually Acquired Infections in Southern Africa. *Journal of Virology* 80: 11776 - 90

348. Chackerian B, Rudensey LM, and Overbaugh J. 1997. Specific N-Linked and O-Linked Glycosylation Modifications in the Envelope V1 Domain of Simian Immunodeficiency Virus Variants That Evolve in the Host Alter Recognition by Neutralizing Antibodies. *Journal of Virology* 71: 7719 - 27

349. Geyer H, Holschbach C, Hunsmann G, and Schneider J. 1988. Carbohydrates of Human Immunodeficiency Virus. Structures of Oligosaccharides Linked to the Envelope Glycoprotein 120. *J. Biol. Chem.* 263: 11760 - 7

350. Leonard CK, Spellman MW, Riddle L, Harris RJ, Thomas JN, and Gregory TJ. 1990. Assignment of Intrachain Disulfide Bonds and Characterization of Potential Glycosylation Sites of the Type 1 Recombinant Human Immunodeficiency Virus Envelope Glycoprotein (gp120) Expressed in Chinese Hamster Ovary Cells. *J. Biol. Chem.* 265: 10373 - 82

351. Auwerx J, Francois KO, Covens K, Van Laethem K, and Balzarini J. 2008. Glycan Deletions in the HIV-1 gp120 V1/V2 Domain Compromise Viral Infectivity, Sensitize the Mutant Virus Strains to Carbohydrate-Binding Agents and Represent a Specific Target for Therapeutic Intervention. *Virology* 382: 10 - 9

352. Karpa KD, Lidow MS, Pickering MT, Levenson R, and Bergson C. 1999. N-Linked Glycosylation is Required for Plasma Membrane Localization of D5, but Not D1, Dopamine Receptors in Transfected Mammalian Cells. *Molecular Pharmacology* 56: 1071 - 8

353. Hansen JE, Lund O, Tolstrup N, Gooley AA, Williams KL, and Brunak S. 1998. NetOglyc: Prediction of Mucin Type O-Glycosylation Sites Based on Sequence Context and Surface Accessibility. *Glycoconjugate Journal* 15: 115 - 30

354. Wang Y, Abernethy JL, Eckhardt AE, and Hill RL. 1992. Purification and Characterization of a UDP-GalNAc:Polypeptide N-Acetylgalactosaminyltransferase Specific for Glycosylation of Threonine Residues. *J. Biol. Chem.* 267: 12709 - 16

355. Overbaugh J, and Rudensey LM. 1992. Alterations in Potential Sites for Glycosylation Predominate During Evolution of the Simian Immunodeficiency Virus Envelope Gene in Macaques. *Journal of Virology* 66: 5937 - 48

356. Management I. 2006. 00.061.1.06.009. Human Immunodeficiency Virus 1. *ICTVdB - The Universal Virus Database* 4

357. Health NIoAaID-NIo. HIV/AIDS - More on How HIV Causes AIDS.

358. Abfalterer W, Athreya G, Fischer W, Funkhouser B, Gaschen B, Hraber P, Lo C, Macke J, Szinger JJ, Thurmond J, Yoon H, Zhang M, Kuiken C (ed), Leitner T (ed), Foley B (ed), Hahn B (ed), Marx P (ed), McCutchan F (ed), Wolinsky S (ed), Korber B (ed), and Bansal G. 2008. Landmarks of the Genome. *HIV Sequence Compendium 2008*: 5 - 6

359. Piguet V, and Trono D. 1999. A Structure-Function Analysis of the Nef Protein of Primate Lentiviruses. *Human Retroviruses and AIDS*: 448-59

360. Niederman TMJ, Hastings WR and Ratner L. 1993. Myristoylation-Enhanced Binding of the HIV-1 Nef Protein to T Cell Skeletal Matrix. *Virology* 197: 420 - 5

361. Das SR, and Jameel S. 2005. Biology of the Nef Protein. *Indian J. Med. Res* 121: 315-32

362. Wei BL, Arora VK, Foster JL, Sodora DL and Garcia JV. 2003. In Vivo Analysis of Nef Function. *Current HIV Research* 1: 41 - 50

363. Geyer M, Fackler OT, and Peterlin BM. 2001. Structure-Function Relationships in HIV-1 Nef. *EMBO Rep.* 2: 580 - 5

364. Kirchhoff F, Schindler M, Bailer N, Renkema GH, Saksela K, Knoop V, Muller-Trutwin MC, Santiago ML, Bibollet-Ruche F, Dittmar MT, Heeney JL, Hahn BH and Munch J. 2004. Nef Proteins from Simian Immunodeficiency Virus-Infected Chimpanzees Interact with p21-Activated Kinase 2 and Modulate Cell Surface Expression of Various Human Receptors. *Journal of Virology* 78: 6864 - 74

365. Kirchhoff F, Munch J, Carl S, Stolte N, Matz-Rensing K, Fuchs D, Haaft PT, Heeney JL, Swigut T, Skowronski J and Stahl-Hennig C. 1999. The Human Immunodeficiency Virus Type 1 nef Gene Can to a Large Extent Replace Simian Immunodeficiency Virus Nef In Vivo. *Journal of Virology* 73: 8371 - 83

366. Schindler M, Munch J, Kutsch O, Li H, Santiago ML, Bibollet-Ruche F, Muller-Trutwin MC, Novembre FJ, Peeters M, Courgnaud V, Bailes E, Roques P, Sodora DL, Silverstri G, Sharp PM, Hahn BH and Kirchhoff F. 2006. Nef-Mediated Suppression of T Cell Activation was Lost in a Lentiviral Lineage that Gave Rise to HIV-1. *Cell* 125: 1055 - 67

367. Schindler M, Wurfl S, Benaroch P, Greenough TC, Daniels R, Easterbrook P, Brenner M, Munch J and Kirchhoff F. 2003. Down-Modulation of Mature Major Histocompatibility Complex Class II and Up-Regulation of Invariant Chain Cell

Surface Expression Are Well-Conserved Functions of Human and Simian Immunodeficiency Virus nef Alleles. *Journal of Virology* 77: 10548 - 56

368. Fackler OT, and Baur AS. 2002. Live and Let Die: Nef Functions Beyond HIV Replication. *Immunity* 16: 493 - 7

369. Greenway AL, Holloway G, McPhee DA, Ellis P, Cornall A and Lidman M. 2003. HIV-1 Nef Control of Cell Signaling Molecules: Multiple Strategies to Promote Virus Replication. *J. Biosci.* 28: 323 - 35

370. Tolstrup M, Ostergaard L, Laursen AL, Pedersen SF and Duch M. 2004. HIV/SIV Escape from Immune Surveillance: Focus on Nef. *Current HIV Research* 2: 141 - 51

371. Ross TM, Oran AE, and Cullen BR. 1999. Inhibition of HIV-1 Progeny Virion Release By Cell-Surface CD4 is Relieved by Expression of the Viral Nef Protein. *Curr. Biol.* 9: 613 - 21

372. Lama J. 2003. The Physiological Relevance of CD4 Receptor Downmodulation During HIV-1 Infection. *Current HIV Research* 1: 167 - 84

373. Michel N, Allespach I, Venzke S, Fackler OT and Keppler OT. 2005. The Nef Protein of Human Immunodeficiency Virus Establishes Superinfection Immunity by a Dual Strategy to Downregulate Cell-Surface CCR5 and CD4. *Current Biology* 15: 714 - 23

374. Lu X, Yu H, Liu SH, Brodsky FM, and Peterlin BM. 1998. Interactions Between HIV-1 Nef and Vacuolar ATPase Facilitate the Internalization of CD4. *Immunity* 8: 647 - 56

375. Janvier K, Kato Y, Boehm M, Rose JR, Martina JA, Kim B, Venkatesan S, and Bonifacino JS. 2003. Recognition of Dileucine-Based Sorting Signals from HIV-1 Nef and LIMP-II by the AP-1 Gamma-Sigma1 and AP-3 Delta-Sigma3 Hemicomplexes. *J. Cell. Biol.* 163: 1281 - 90

376. Craig HM, Reddy TR, Riggs NL, Dao PP, and Guatelli JC. 2000. Interactions of HIV-1 Nef with the Mu Subunits of Adaptor Protein Complexes 1, 2 and 3: Role of the Dileucine-Based Sorting Motif. *Virology* 271: 9 - 17

377. Piguet V, Gu F, Foti M, Demaurex N, Gruenberg J, Carpentier JL, and Trono D. 1999. Nef-Induced CD4 Degradation: A Diacidic-Based Motif in Nef Functions as a Lysosomal Targeting Signal Through the Binding of beta-COP in Endosomes. *Cell* 97: 63 - 73

378. Mandic R, Fackler OT, Geyer M, Linnemann T, Zheng YH, and Peterlin BM. 2001. Negative Factor from SIV Binds to the Catalytic Subunit of the V-ATPase to Internalize CD4 and to Increase Viral Infectivity. *Mol. Biol. Cell.* 12: 463 - 73

379. Crump CM, Xiang Y, Thomas L, Gu F, Austin C, Tooze SA, and Thomas G. 2001. PACS-1 Binding to Adaptors is Required for Acidic Cluster Motif-Mediated Protein Traffic. *EMBO J* 20: 2191 - 201

380. Piguet V, Chen YL, Mangasarian A, Foti M, Carpentier JL, and Trono D. 1998. Mechanism of Nef-Induced CD4 Endocytosis: Nef Connects CD4 with the Mu Chain of Adaptor Complexes. *EMBO J* 17: 2472 - 81

381. Salghetti S, Mariani R, and Skowronski J. 1995. Human Immunodeficiency Virus Type 1 Nef and p56lck Protein-Tyrosine Kinase Interact with a Common Element in CD4 Cytoplasmic Tail. *PNAS* 92: 349 - 53

382. Greenberg ME, Bronson S, Lock M, Neumann M, Pavlakis GN, and Skowronski J. 1997. Co-Localization of HIV-1 Nef with the AP-2 Adaptor Protein Complex Correlates with Nef-Induced CD4 Down-Regulation. *EMBO J* 16: 6964 - 76

383. Mangasarian A, Foti M, Aiken C, Chin D, Carpentier JL, and Trono D. 1997. The HIV-1 Nef Protein Acts as a Connector with Sorting Pathways in the Golgi and at the Plasma Membrane. *Immunity* 6: 67 - 77

384. Aiken C, Konner J, Landau NR, Lenburg ME, and Trono D. 1994. Nef Induces CD4 Endocytosis: Requirement for a Critical Dileucine Motif in the Membrane-Proximal CD4 Cytoplasmic Domain. *Cell* 76: 853 - 64

385. Swigut T, Shohdy N, and Skowronski J. 2001. Mechanism for Downregulation of CD28 by Nef. *EMBO J* 20: 1593 - 604

386. Munch J, Schindler M, Wildum S, Rucker E, Bailer N, Knoop V, Novembre FJ and Kirchhoff F. 2005. Primary Sooty Mangabey Simian Immunodeficiency Virus and Human Immunodeficiency Virus Type 2 Nef Alleles Modulate Cell Surface Expression of Various Human Receptors and Enhance Viral Infectivity and Replication. *Journal of Virology* 79: 10547 - 60

387. Chaudhry A, Das SR, Jameel S, George A, Bal V, Mayor S, and Rath S. 2007. A Two-Pronged Mechanism for HIV-1 Nef-Mediated Endocytosis of Immune Costimulatory Molecules CD80 and CD86. *Cell Host Microbe* 1: 37 - 49

388. Chaudhry A, Das SR, Hussain A, Mayor S, George A, Bal V, Jameel S and Rath S. 2005. The Nef Protein of HIV-1 Induces the Loss of Cell Surface Costimulatory Molecues CD80 and CD86 in APCs. *Journal of Immunology* 175: 4566 - 74

389. Greenberg ME, Iafrate AJ, and Skowronski J. 1998. The SH3 Domain-Binding Surface and An Acidic Motif in HIV-1 Nef Regulate Trafficking of Class I MHC Complexes. *EMBO J* 17: 2777 - 89

390. Cohen GB, Gandhi RT, Davis DM, Mandelboim O, Chen BK, Strominger JL, and Baltimore D. 1999. The Selective Downregulation of Class I Major Histocompatibility Complex Proteins by HIV-1 Protects HIV-Infected Cells from NK Cells. *Immunity* 10: 661 - 71

391. Blagoveshchenskaya AD, Thomas L, Feliciangeli SF, Hung C and Thomas G. 2002. HIV-1 Nef Downregulates MHC-I by a PACS-1- and PI3K-Regulated ARF6 Endocytic Pathway. *Cell* 111: 853 - 66

392. Piguet V, Wan L, Borel C, Mangasarian A, Demaurex N, Thomas G and Trono D. 2000. HIV-1 Nef Protein Binds to the Cellular Protein PACS-1 to Downregulate Class I Major Histocompatibility Complexes. *Nature Cell Biology* 2: 163 - 7

393. Pamer E, and Cresswell P. 1998. Mechanisms of MHC Class I - Restricted Antigen Processing. *Annu. Rev. Immunol.* 16: 323 - 58

394. Stumptner-Cuvelette P, Morchoisne S, Dugast M, Le Gall S, Raposo G, Schwartz O, and Benaroch P. 2001. HIV-1 Nef Impairs MHC Class II Antigen Presentation and Surface Expression. *PNAS* 98: 12144 - 9

395. Hrecka K, Swigut T, Schindler M, Kirchhoff F and Skowronski J. 2005. Nef Proteins from Diverse Groups of Primate Lentiviruses Downmodulate CXCR4 to Inhibit Migration to the Chemokine Stromal Derived Factor 1. *Journal of Virology* 79: 10650 - 9

396. Hanna Z, Priceputu E, Hu C, Vincent P and Jolicoeur P. 2006. HIV-1 Nef Mutations Abrogating Downregulation of CD4 Affect Other Nef Functions and Show Reduced Pathogenicity in Transgenic Mice. *Virology* 346: 40 - 52

397. Michel N, Ganter K, Venzke S, Bitzegeio J, Fackler OT and Keppler OT. 2006. The Nef Protein of Human Immunodeficiency Virus is a Broad-Spectrum Modulator of Chemokine Receptor Cell Surface Levels that Acts Independently of Classical Motifs for Receptor Endocytosis and Galphai Signalling. *Molecular Biology of the Cell* 17: 3578 - 90

398. Baur AS, Sass G, Laffert B, Willbold D, Cheng MC, and Peterlin BM. 1997. The N-Terminus of Nef from HIV-1/SIV Associates with a Protein Complex Containing Lck and a Serine Kinase. *Immunity* 6: 283 - 91

399. Zheng YH, Plementius A, Linnemann T, Fackler OT, and Peterlin BM. 2001. Nef Increases Infectivity of HIV via Lipid Rafts. *Curr. Biol.* 11: 875 - 9

400. Xu XN, Laffert B, Screaton GR, Kraft M, Wolf D, Kolanus W, Mongkolsapay J, McMichael AJ, and Baur AS. 1999. Induction of Fas Ligand Expression by HIV Involves the Interaction of Nef with the T Cell Receptor Zeta Chain. *J. Exp. Med.* 189: 1489 - 96

401. Linnemann T, Zheng YH, Mandic R, and Peterlin BM. 2002. Interaction Between Nef and Phosphatidylinositol-3-Kinase Leads to Activation of p21-Activated Kinase and Increased Production of HIV. *Virology* 294: 246 - 55

402. Fackler OT, Luo W, Geyer M, Alberts AS, and Peterlin BM. 1999. Activation of Vav by Nef Induces Cytoskeletal Rearrangements and Downstream Effector Functions. *Mol. Cell.* 3: 729 - 39

403. Smith BL, Krushelnycky BW, Mochly RD, and Berg P. 1996. The HIV Nef Protein Associates with Protein Kinases C Theta. *J. Biol. Chem.* 271: 16753 - 7

404. Lee CHSK, Mirza UA, Chait BT, and Kuriyan J. 1996. Crystal Structure of the Conserved Core of HIV-1 Nef Complexed with a Src Family SH3 Domain. *Cell* 85: 931 - 42

405. Saksela K, Cheng G, and Baltimore D. 1995. Proline-Rich (PxxP) Motifs in HIV-1 Nef Bind to SH3 Domains of a Subset of Src Kinases and Are Required for the Enhanced Growth of Nef+ Viruses But Not for Down-Regulation of CD4. *EMBO J* 14: 484 - 91

406. Renkema GH, Manninen A, Mann DA, Harris M, and Saksela K. 1999. Identification of the Nef-Associated Kinase as p21-Activated Kinase 2. *Curr Biol* 9: 1407 - 10

407. Sawai ET, Khan IH, Montbriand PM, Peterlin BM, Cheng MC, and Luciw PA. 1996. Activation of PAK by HIV and SIV Nef: Importance for AIDS in Rhesus Macaques. *Curr. Biol.* 6: 1519 - 27

408. Lee CH, Leung B, Lemmon MA, Zheng J, Cowburn D, Kuriyan J, and Saksela K. 1995. A Single Amino Acid in the SH3 Domain of HcK Determines Its High Affinity and Specificity in Binding to HIV-1 Nef Protein. *EMBO J* 14: 5006 - 15

409. Howe AYM, Jung JU and Desrosiers RC. 1998. Zeta Chain of the T-Cell Receptor Interacts with Nef of Simian Immunodeficiency Virus and Human Immunodeficiency Virus Type 2. *Journal of Virology* 72: 9827 - 34

410. Bell I, Ashman C, Maughan J, Hooker E, Cook F and Reinhart TA. 1998. Association of Simian Immunodeficiency Virus Nef with the T-Cell Receptor

(TCR) Zeta Chain Leads to TCR Down-Modulation. *Journal of General Virology* 79: 2717 - 27

411. Kirchhoff F. 2009. Is the High Virulence of HIV-1 an Unfortunate Coincidence of Primate Lentiviral Evolution? *Nature Reviews Microbiology* 7: 467 - 76

412. Hindmarsh P, and Leis J. 1999. Retroviral DNA Integration. *Microbiology and Molecular Biology Reviews* 63: 836 - 43

413. Craigie R. 2001. HIV Integrase: A Brief Overview from Chemistry to Therapeutics. *Journal of Biological Chemistry* 276: 23213 - 6

414. Asante-Appiah E, and Skalka AM. 1997. Molecular Mechanisms in Retrovirus DNA Integration. *Antiviral Research* 36: 139 - 56

415. Chiu TK, and Davies DR. 2004. Structure and Function of HIV-1 Integrase. *Current Topics in Medicinal Chemistry* 4: 965-77

416. Jenkins TM, Esposito D, and Engelman A. 1997. Critical Contacts Between HIV-1 Integrase and Viral DNA Identified By Structure-Based Analysis and Photo-Crosslinking. *EMBO Journal* 16: 6849 - 59

417. Al-Mawsawi LQ, and Neamati N. 2007. Blocking Interactions Between HIV-1 Integrase and Cellular Co-Factors: An Emerging Anti-Retroviral Strategy. *Trends Pharmacol. Sci.* 28: 526 - 35

418. Dyda F, Hickman AB, Jenkins TM, Engelman A, Craigie R, and Davies DR. 1994. Crystal Structure of the Catalytic Domain of HIV-1 Integrase - Similarity to Other Polynucleotidyl Transferases. *Science* 266: 1981 - 6

419. Bujacz G, Jaskoski M, Alexandratos J, Wlodawer A, Merkel G, Katz RA, and Skalka AM. 1995. High-Resolution Structure of the Catalytic Domain of Avian-Sarcoma Virus Integrase. *Journal of Molecular Biology* 253: 333 - 46

420. Chen ZG, Yan YW, Munshi S, Li Y, Zugay-Murphy J, Xu B, Witmer M, Felock P, Wolfe A, Sardana V, Emini EA, Hazuda D, and Kuo LC. 2000. X-Ray Structure of Simian Immunodeficiency Virus Integrase Containing the Core and C-Terminal Domain (Residues 50 - 293) - An Initial Glance of the Viral DNA Binding Platform. *Journal of Molecular Biology* 296: 521 - 33

421. Mumm SR, and Grandgenett DP. 1991. Defining Nucleic Acid-Binding Properties of Avian Retrovirus Integrase by Deletion Analysis. *Journal of Virology* 65: 1160 - 7

422. Shibagaki Y, Holmes ML, Appa RS, and Chow SA. 1997. Characterization of Feline Immunodeficiency Virus Integrase and Analysis of Functional Domains. *Virology* 230: 1 - 10

423. van Gent DC, Oude Groeneger AA, and Plasterk RH. 1993. Identification of Amino Acids in HIV-2 Integrase Involved in Site-Specific Hydrolysis and Alcoholysis of Viral DNA Termini. *Nucleic Acids Research* 21: 3373 - 7

424. Yang ZN, Mueser TC, Bushman FD, and Hyde CC. 2000. Crystal Structure of an Active Two-Domain Derivative of Rous Sarcoma Virus Integrase. *Journal of Molecular Biology* 296: 535 - 48

425. Engelman A, and Craigie R. 1992. Identification of Conserved Amino Acid Residues Critical for Human Immunodeficiency Virus Type 1 Integrase Function In Vitro. *Journal of Virology* 66: 6361 - 9

426. Bushman FD, Engelman A, Palmer I, Wingfield P, and Craigie R. 1993. Domains of the Integrase Protein of Human Immunodeficiency Virus Type 1 Responsible for Polynucleotidyl Transfer and Zinc Binding. *PNAS* 90: 3428 - 32

427. Drelich M, Wilhelm R, and Mous J. 1992. Identification of Amino-Acid Residues Critical for Endonuclease and Integration Activities of HIV-1 Protein In Vitro. *Virology* 188: 459 - 68

428. Ellison V, and Brown PO. 1994. A Stable Complex Between Integrase and Viral-DNA Ends Mediates Human Immunodeficiency Virus Integration In Vitro. *PNAS* 91: 7316 - 20

429. Jenkins TM, Hickman AB, Dyda F, Ghirlando R, Davies DR, and Craigie R. 1995. Catalytic Domain of Human Immunodeficiency Virus Type 1 Integrase: Identification of a Soluble Mutant By Systematic Replacement of Hydrophobic Residues. *PNAS* 92: 6057 - 61

430. Mazumder A, Engelman A, Craigie R, Fesen M, and Pommier Y. 1994. Intermolecular Disintegration and Intramolecular Strand Transfer Activities of Wild-Type and Mutant HIV-1 Integrase. *Nucleic Acids Research* 22: 1037 - 43

431. Zheng RL, Jenkins TM, and Craigie R. 1996. Zinc Folds the N-Terminal Domain of HIV-1 Integrase, Promotes Multimerization and Enhances Catalytic Activity. *PNAS* 93: 13659 - 64

432. Weihe E, Hohr D, Sharer L, Murray E, Rausch P, and Eiden L. 1993. Cortical Astrocytosis in Juvenile Rhesus Monkeys Infected with Simian Immunodeficiency Virus. *Neuroreport* 4: 263 - 6

433. Berman NE, Yong C, Raghavan R, Raymond LA, Joag SV, Narayan O, and Cheney PD. 1998. Neurovirulent Simian Immunodeficiency Virus Induces Calbindin-D-28K in Astrocytes. *Mol. Chem. Neuropathol.* 34: 25 - 38

434. Rausch DM, Heyes MP, Murray EA, Lendvay J, Sharer LR, Ward JM, Rehm S, Nohr D, Weihe E, and Eiden LE. 1994. Cytopathologic and Neurochemical Correlates of Progression to Motor/Cognitive Impairment in SIV-Infected Rhesus Monkeys. *J. Neuropathol. Exp. Neurol.* 53: 165 - 75

435. Sharer LR. 1994. Neuropathology and Pathogenesis of SIV Infection of the Central Nervous System. *Res. Publ. Assoc. Res. Nerv. Ment. Dis.* 72: 133 - 45

436. Greenier JL, Miller CJ, Lu D, Dailey PJ, Lu FX, Kunstman KJ, Wolinsky SM and Marthas ML. 2001. Route of Simian Immunodeficiency Virus Inoculation Determines the Complexity But Not the Identity of Viral Variant Populations That Infect Rhesus Macaques. *Journal of Virology* 75: 3753-65

437. Ringler DJ, Hunt RD, Desrosiers RC, Daniel MD, Chalifoux LV, and King NW. 1988. Simian Immunodeficiency Virus-Induced Meningoencephalitis: Natural History and Retrospective Study. *Ann. Neurol.* 23: S101 - S7

438. Baskerville A, Ramsay A, Cranage MP, Cook N, Cook RW, Dennis MJ, Greenaway PJ, Kitchin PA, and Stott EJ. 1990. Histopathological Changes in Simian Immunodeficiency Virus Infection. *Journal of Pathology* 162: 67 - 75

439. Westmoreland SV, Halpern E, and Lackner AA. 1998. Simian Immunodeficiency Virus Encephalitis in Rhesus Macaques is Associated with Rapid Disease Progression. *Journal of Neurovirology* 4: 260 - 8

440. Sharma DP, Zink MC, Anderson M, Adams R, Clements JE, Joag SV, and Narayan O. 1992. Derivation of Neurotropic Simian Immunodeficiency Virus from Exclusively Lymphocytetropic Parental Virus: Pathogenesis of Infection in Macaques. *Journal of Virology* 66: 3550 - 6

441. Raghavan R, Stephens EB, Joag SV, Adany I, Pinson DM, Li Z, Jia F, Sahni M, Wang C, Leung K, Foresman L and Narayan O. 1997. Neuropathogenesis of Chimeric Simian/Human Immunodeficiency Virus Infection in Pigtailed and Rhesus Macaques. *Brain Pathology* 7: 851 - 61

442. Roberts ES, Zandonatti MA, Watry DA, Madden LJ, Henriksen SJ, Taffe MA, and Fox HS. 2003. Induction of Pathogenic Sets of Genes in Macrophages and Neurons in NeuroAIDS. *American Journal of Pathology* 162: 2041 - 57

443. Zink MC, Amedee AM, Mankowski JL, Craig L, Didier P, Carter DL, Munoz A, Murphey-Corb M and Clements JE. 1997. Pathogenesis of SIV Encephalitis. Selection and Replication of Neurovirulent SIV. *American Journal of Pathology* 151: 793 - 803

444. Novembre FJ, De Rosayro J, O'Neil SP, Anderson DC, Klumpp SA and McClure HM. 1998. Isolation and Characterization of a Neuropathogenic Simian Immunodeficiency Virus Derived from a Sooty Mangabey. *Journal of Virology* 72: 8841-51

445. McClernon DR, Lanier R, Gartner S, Feaser P, Pardo CA, St Clair M, Liao Q and McArthur JC. 2001. HIV in the Brain: RNA Levels and Patterns of Zidovudine Resistance. *Neurology* 57: 1396 - 401

446. Wain-Hobson S. 1992. Human Immunodeficiency Virus Type 1 Quasispecies in vivo and ex vivo. *Curr. Top. Microbiol. Immunol.* 176: 181-93

447. Gerhardt M, Mloka D, Tovanabutra S, Sanders-Buell E, Hoffman O, Maboko L, Mmbando D, Birx DL, McCutchan FE, and Hoelscher M. 2005. In-Depth, Longitudinal Analysis of Viral Quasispecies from an Individual Triply Infected with Late-Stage Human Immunodeficiency Virus Type 1, Using a Multiple PCR Primer Approach. *Journal of Virology* 79: 8249 - 61

448. Jetzt AE, Yu H, Klarmann GJ, Ron Y, Preston BD, and Dougherty JP. 2000. High Rate of Recombination Throughout the Human Immunodeficiency Virus Type 1 Genome. *Journal of Virology* 74: 1234 - 40

449. Bebenek K, Abbotts J, Roberts JD, Wilson SH, and Kunkel TA. 1989. Specificity and Mechanism of Error-Prone Replication by Human Immunodeficiency Virus-1 Reverse Transcriptase. *J. Biol. Chem.* 264: 16948 - 56

450. Babas T, Munoz D, Mankowski JL, Tarwater PM, Clements JE and Zink MC. 2003. Role of Microglial Cells in Selective Replication of Simian Immunodeficiency Virus Genotypes in the Brain. *Journal of Virology* 77: 208-16

451. Goodenow M, Huet T, Saurin W, Kwok S, Sninsky J, and Wain-Hobson S. 1989. HIV-1 Isolates Are Rapidly Evolving Quasispecies: Evidence for Viral Mixtures and Preferred Nucleotide Substitutions. *J. Acquir. Immune Defic. Syndr.* 2: 344 - 52

452. Poss M, Rodrigo AG, Gosink JJ, Learn GH, Panteleeff DDV, Martin Jr. HL, Bwayo J, Kreiss JK and Overbaugh J. 1998. Evolution of Envelope Sequences

from the Genital Tract and Peripheral Blood of Women Infected with Clade A Human Immunodeficiency Virus Type 1. *Journal of Virology* 72: 8240-51

453. Campbell BJ, and Hirsch VM. 1994. Extensive Envelope Heterogeneity of Simian Immunodeficiency Virus in Tissues from Infected Macaques. *Journal of Virology* 68: 3129 - 37

454. Fulcher JA, Hwangbo Y, Zioni R, Nickle D, Lin X, Heath L, Mullins JI, Corey L, and Zhu T. 2004. Compartmentalization of Human Immunodeficiency Virus Type 1 between Blood Monocytes and CD4+ T Cells During Infection. *Journal of Virology* 78: 7883 - 93

455. Wang TH, Donaldson YK, Brettle RP, Bell JE and Simmonds P. 2001. Identification of Shared Populations of Human Immunodeficiency Virus Type 1 Infecting Microglia and Tissue Macrophages Outside the Central Nervous System. *Journal of Virology* 75: 11686 - 99

456. Clarke JR, White NC, and Weber JN. 2000. HIV Compartmentalization: Pathogenesis and Clinical Implications. *AIDS Rev.* 2: 15 - 22

457. Cheng-Mayer C, Weiss C, Seto D, and Levy JA. 1989. Isolates of Human Immunodeficiency Virus Type 1 from the Brain May Constitute a Special Group of the AIDS Virus. *PNAS* 86: 8575 - 9

458. Shapshak P, Segal DM, Crandall KA, Fujimura RK, Zhang B, Xin K, Okuda K, Petito CK, Eisdorfer C and Goodkin K. 1999. Independent Evolution of HIV Type 1 in Different Brain Regions. *AIDS Research and Human Retroviruses* 15: 811-20

459. Korber BTM, Kunstman KJ, Patterson BK, Furtado M, McEvilly MM, Levy R and Wolinsky SM. 1994. Genetic Differences between Blood- and Brain-Derived Viral Sequences from Human Immunodeficiency Virus Type 1-Infected Patients: Evidence of Conserved Elements in the V3 Region of the Envelope Protein of Brain-Derived Sequences. *Journal of Virology* 68: 7467-81

460. Haggerty S, and Stevenson M. 1991. Predominance of Distinct Viral Genotypes in Brain and Lymph Node Compartments of HIV-1-Infected Individuals. *Viral Immunology* 4: 123 - 31

461. Chen MF, Westmoreland S, Ryzhova EV, Martin-Garcia J, Soldan SS, Lackner A and Gonzalez-Scarano F. 2006. Simian Immunodeficiency Virus Envelope Compartmentalizes in Brain Regions Independent of Neuropathology. *Journal of Neurovirology* 12: 73-89

462. Sankale J, de la Tour RS, Marlink RG, Scheib R, Mboup S, Essex ME, and Kanki PJ. 1996. Distinct Quasi-Species in the Blood and the Brain of an HIV-2-Infected Individual. *Virology* 226: 418 - 23

463. Collins KR, Quinones-Mateu ME, Wu M, Luzze H, Johnson JL, Hirsch C, Toossi Z and Arts EJ. 2002. Human Immunodeficiency Virus Type 1 Quasispecies at the Sites of Mycobacterium tuberculosis Infection Contribute to Systemic HIV-1 Heterogeneity. *Journal of Virology* 76: 1697-706

464. Pang S, Vinters HV, Akashi T, O'Brien WA, and Chen ISY. 1991. HIV-1 Env Sequence Variation in Brain Tissue of Patients with AIDS-Related Neurologic Disease. *Journal of Acquired Immune Deficiency Syndromes* 4: 1082 - 92

465. Itescu S, Simonelli PF, Winchester RJ, and Ginsberg HS. 1994. Human Immunodeficiency Virus Type 1 Strains in the Lungs of Infected Individuals Evolve Independently from those in Peripheral Blood and are Highly Conserved in the C-Terminal Region of the Envelope V3 Loop. *PNAS* 91: 11378 - 82

466. Epstein LG, Kuiken C, Blumberg BM, Hartman S, Sharer LR, Clement M, and Goudsmit J. 1991. HIV-1 V3 Domain Variation in Brain and Spleen of Children with AIDS: Tissue-Specific Evolution with Host-Determined Quasispecies. *Virology* 180: 583 - 90

467. Chang J, Jozwiak R, Wang B, Ng T, Ge YC, Bolton W, Dwyer DE, Randle C, Osborn R, Cunningham AL, and Saksena NK. 1998. Unique HIV Type 1 V3 Region Sequences Derived from Six Different Regions of Brain: Region-Specific Evolution within Host-Determined Quasispecies. *AIDS Res. Hum. Retroviruses* 14: 25 - 30

468. Gatanaga H, Oka S, Ida S, Wakabayashi T, Shioda T, and Iwamoto A. 1999. Active HIV-1 Redistribution and Replication in the Brain with HIV Encephalitis. *Arch. Virol.* 144: 29 - 43

469. Kuiken CL, Goudsmit J, Weiller GF, Armstrong JS, Hartman S, Portegies P, Dekker J, and Cornelissen M. 1995. Differences in Human Immunodeficiency Virus Type 1 V3 Sequences from Patients With and Without AIDS Dementia Complex. *Journal of General Virology* 76: 175 - 80

470. Power C, McArthur JC, Johnson RT, Griffin DE, Glass JD, Perryman S, and Chesebro B. 1994. Demented and Nondemented Patients with AIDS Differ in

Brain-Derived Human Immunodeficiency Virus Type 1 Envelope Sequences. *Journal of Virology* 68: 4643 - 9

471. Keys B, Karis J, Fadeel B, Valentin A, Norkrans G, Hagberg L, and Chiodi F. 1993. V3 Sequences of Paired HIV-1 Isolates from Blood and Cerebrospinal Fluid Cluster According to Host and Show Variation Related to the Clinical Stage of Disease. *Virology* 196: 475 - 83

472. Steuler H, Storch-Hagenlocher B, and Wildemann B. 1992. Distinct Populations of Human Immunodeficiency Virus Type 1 in Blood and Cerebrospinal Fluid. *AIDS Research and Human Retroviruses* 8: 53 - 9

473. Ait-Khaled M, McLaughlin JE, Johnson MA, and Emery VC. 1995. Distinct HIV-1 Long Terminal Repeat Quasispecies Present in Nervous Tissues Compared to that in Lung, Blood and Lymphoid Tissues of an AIDS Patient. *AIDS* 9: 675 - 83

474. Corboy JR, and Garl PJ. 1997. HIV-1 LTR DNA Sequence Variation in Brain-Derived Isolates. *Journal of Neurovirology* 3: 331 - 41

475. van Marle G, Gill MJ, Kolodka D, McManus L, Grant T and Church DL. 2007. Compartmentalization of the Gut Viral Reservoir in HIV-1 Infected Patients. *Retrovirology* 4: 87-101

476. Wong JK, Ignacio CC, Torriani F, Havlir D, Fitch NJS and Richman DD. 1997. In Vivo Compartmentalization of Human Immunodeficiency Virus: Evidence from the Examination of pol Sequences from Autopsy Tissues. *Journal of Virology* 71: 2059-71

477. Ritola K, Robertson K, Fiscus SA, Hall C and Swanstrom R. 2005. Increased human immunodeficiency virus type 1 (HIV-1) env compartmentalization in the presence of HIV-1-associated dementia. *Journal of Virology* 79: 10830-4

478. Reinke R, Steffen NR and Robinson WE. 2001. Natural Selection Results in Conservation of HIV-1 Integrase Activity Despite Sequence Variability. *AIDS* 15: 823-30

479. Skinner LM, Lamers SL, Sanders JC, Eyster ME, Goodenow MM and Klatzman M. 1998. Analysis of a Large Collection of Natural HIV-1 Integrase Sequences, Including Those from Long-Term Nonprogressors. *J. Acquir. Immune Defic. Syndr. Hum. Retrovirol* 19: 99-110

480. Acheampong EA, Parveen Z, Muthoga LW, Kalayeh M, Mukhtar M and Pomerantz RJ. 2005. Human Immunodeficiency Virus Type 1 Nef Potently Induces Apoptosis in Primary Human Brain Microvascular Endothelial Cells via the Activation of Caspases. *Journal of Virology* 79: 4257-69

481. Mankowski JL, Flaherty MT, Spelman JP, Hauer DA, Didier PJ, Amedee AM, Murphey-Corb M, Kirstein LM, Munoz A, Clements JE and Zink MC. 1997. Pathogenesis of Simian Immunodeficiency Virus Encephalitis: Viral Determinants of Neurovirulence. *Journal of Virology* 71: 6055-60

482. Overholser ED, Coleman GD, Bennett JL, Casaday RJ, Zink MC, Barber SA and Clements JE. 2003. Expression of Simian Immunodeficiency Virus (SIV) Nef in Astrocytes During Acute and Terminal Infection and Requirement of Nef for Optimal Replication of Neurovirulent SIV In Vitro. *Journal of Virology* 77: 6855-66

483. Kim S, Pang H and Kay MS. 2008. Peptide Mimic of the HIV Envelope gp120-gp41 Interface. *J. Mol. Biol* 376: 786-97

484. Dreyer EB, Kaiser PK, Offermann JT and Lipton SA. 1990. HIV-1 Coat Protein Neurotoxicity Prevented by Calcium Channel Antagonists. *Science* 248: 364-7

485. Starcich BR, Hahn BH, Shaw GM, McNeely PD, Modrow S, Wolf H, Parks ES, Parks WP, Josephs SF, Gallo RC and Wong-Staal F. 1986. Identification and Characterization of Conserved and Variable Regions in the envelope Gene of HTLV-III/LAV, the Retrovirus of AIDS. . *Cell* 45: 637-48

486. Petry H, Pekrun K, Hunsmann G, Jurkiewicz E and Luke W. 2000. Naturally Occurring V1-Env Region Variants Mediate Simian Immunodeficiency Virus SIVmac Escape from a High-Titer Neutralizing Antibodies Induced by a Protective Subunit Vaccine. *Journal of Virology* 74: 11145-52

487. Burkala EJ, He J, West JT, Wood C, Petito CK. 2005. Compartmentalization of HIV-1 in the central nervous system: Role of the choroids plexus. *AIDS* 19: 675-84

488. Zarate S, Pond SLK, Shapshak P and Frost SDW. 2007. Comparative Study of Methods for Detecting Sequence Compartmentalization in Human Immunodeficiency Virus Type 1. *Journal of Virology* 81: 6643-51

489. Renjifo B, Chung M, Gilbert P, Mwakagile D, Msamanga G, Fawzi W and Essex M. 2003. In-Utero Transmission of Quasispecies Among Human Immunodeficiency Type 1 Genotypes. *Virology* 307: 278-82

490. Neildez O, Le Grand R, Caufour P, Vaslin B, Cheret A, Matheux F, Theodoro F, Roques P and Dormont D. 1998. Selective Quasispecies Transmission After

Systemic or Mucousal Exposure of Macaques to Simian Immunodeficiency Virus. *Virology* 243: 12-20

491. Walter BL, Wehrly K, Swanstrom R, Platt E, Kabat D and Chesebro B. 2005. Role of Low CD4 Levels in the Influence of Human Immunodeficiency Virus Type 1 Envelope V1 and V2 Regions on Entry and Spread in Macrophages. *Journal of Virology* 79: 4828 - 37

492. Rybarcyzk B. 2008. Molecular Evolution: The HIV Envelope Protein. *Evo. Edu. Outreach* 1: 179 - 83

493. Kazazi F, Mathijs J, Foley P and Cunningham AL. 1989. Variations in CD4 Expression by Human Monocytes and Macrophages and Their Relationship to Infection with the Human Immunodeficiency Virus. *Journal of General Virology* 70: 2661 - 72

494. Badley AD, Pilon AA, Landay A and Lynch DH. 2000. Mechanisms of HIV-Associated Lymphocyte Apoptosis. *Blood* 96: 2951 - 64

495. Olivetta E, and Federico M. 2006. HIV-1 Nef Protects Human-Monocyte-Derived Macrophages from HIV-1-Induced Apoptosis. *Exp. Cell. Res.* 312: 890 - 900

496. Sharpless N, Gilbert D, Vandercam B, Zhou JM, Verdin E, Ronnett G, Friedman E and Dubois-Dalcq M. 1992. The Restricted Nature of HIV-1 Tropism for Cultured Neural Cells. . *Virology* 191: 813-25

497. Ohagen A, Devitt A, Kunstman KJ, Gorry PR, Rose PP, Korber B, Taylor J, Levy R, Murphy RL, Wolinsky SM and Gabudza D. 2003. Genetic and Functional Analysis of Full-Length Human Immunodeficiency Virus Type 1 env Genes

Derived from Brain and Blood of Patients with AIDS. *Journal of Virology* 77: 12336-45

498. Sharp P. 1997. In Search of Molecular Darwinism. *Nature* 385: 111-2

499. Reeve AB, Patel K, Pearce NC, Augustus KV, Domingues HG, O'Neil SP, Novembre FJ. 2009. Reduced Genetic Diversity in Lymphoid and Central Nervous System Tissues and Selection-Induced Tissue-Specific Compartmentalization of Neuropathogenic SIVsmmFGb During Acute Infection. *AIDS Research and Human Retroviruses* 25: 583 - 601

500. Harrington PR, Connell MJ, Meeker RB, Johnson PR and Swanstrom R. 2007. Dynamics of Simian Immunodeficiency Virus Populations in Blood and Cerebrospinal Fluid Over the Full Course of Infection. *J Infect Dis.* 196: 1058 - 67

501. Gray ES, Moore PL, Choge IA, Decker JM, Bibollet-Ruche F, Li H, Leseka N, Treurnicht F, Mlisana K, Shaw GM, Karim SSA, Williams C, Morris L and the CAPRISA 002 Study Team. 2007. Neutralizing Antibody Responses in Acute Human Immunodeficiency Virus Type 1 Subtype C Infection. *Journal of Virology* 81: 6187 - 96

502. Jones NA, Wei X, Flower DR, Wong ML, Michor F, Saag MS, Hahn BH, Nowak MA, Shaw GM and Borrow P. 2004. Determinants of Human Immunodeficiency Virus Type 1 Escape from the Primary CD8+ Cytotoxic T Lymphocyte Response. *JEM* 200: 1243 - 56

503. Borrow P, Lewicki H, Wei X, Horwitz MS, Peffer N, Meyers H, Nelson JA, Gairin JE, Hahn BH, Oldstone MBA and Shaw GM. 1997. Antiviral Pressure

Exerted by HIV-1-Specific Cytotoxic T Lymphocytes During Primary Infection Demonstrated by Rapid Selection of CTL Escape Virus. *Nature Medicine* 3: 205 - 11

504. Swigut T, Iafrate AJ, Muench J, Kirchhoff F and Skowronski J. 2000. Simian and Human Immunodeficiency Virus Nef Proteins Use Different Surfaces to Downregulate Class I Major Histocompatibility Complex Antigen Expression. *Journal of Virology* 74: 5691 - 701

505. Lemey P, Pond SLK, Drummond AJ, Pybus OG, Shapiro B, Barroso H, Taveira N and Rambaut A. 2007. Synonymous Substitution Rates Predict HIV Disease Progression as a Result of Underlying Replication Dynamics. *PLoS Computational Biology* 3: 282 - 92

506. Gunthard HF, Leigh-Brown AJ, D'Aquila RT, Johnson VA, Kuritzkes DR, Richman DD and Wong JK. 1999. Higher Selection Pressure from Antiretroviral Drugs in Vivo Results in Increased Evolutionary Distance in HIV-1 pol. *Virology* 259: 154 - 65

507. Rodriguez WR, Addo MM, Rathod A, Fitzpatrick CA, Yu XG, Perkins B, Rosenberg ES, Altfeld M and Walker BD. 2004. CD8+ T Lymphocyte Responses Target Functionally Important Regions of Protease and Integrase in HIV-1 Infected Subjects. *Journal of Translational Medicine* 2: 15 - 30

508. Erickson AL, and Walker CM. 1994. An Epitope in the V1 Domain of the Simian Immunodeficiency Virus (SIV) gp120 Protein is Recognized by CD8+ Cytotoxic T Lymphocytes from an SIV-Infected Rhesus Macaque. *Journal of Virology* 68: 2756 - 9

509. Peut V, and Kent SJ. 2007. Utility of Human Immunodeficiency Virus Type 1 Envelope as a T-Cell Immunogen. *Journal of Virology* 81: 13125 - 34

510. Frost SDW, Wrin T, Smith DM, Pond SLK, Liu Y, Paxinos E, Chappey C, Galovich J, Beauchaine J, Petropoulos CJ, Little SJ and Richman DD. 2005. Neutralizing Antibody Responses Drive the Evolution of Human Immunodeficiency Virus Type 1 envelope During Recent HIV Infection. *PNAS* 102: 18514 - 9

511. Wang JY, Ling H, and Yang W. 2001. Structure of a Two-Domain Fragment of HIV-1 Integrase: Implications for Domain Organization in the Intact Protein. *EMBO Journal* 20: 7333 - 43

512. MacArthur MW, and JM Thornton. 1991. Influence of Proline Residues on Protein Conformation. *Journal of Molecular Biology* 218: 397 - 412

513. Bajaj K, MS Madhusudhan, BV Adkar, P Chakrabarti, C Ramakrishnan, A Sali and R Varadarajan. 2007. Stereochemical Criteria for Prediction of the Effects of Proline Mutations on Protein Stability. *PLoS Computational Biology* 3: 2465 - 75

514. Sigma-Aldrich. Amino Acids Reference Chart.

515. Bentham M, S Mazaleyrat and M Harris. 2006. Role of Myristoylation and N-Terminal Basic Residues in Membrane Association of the Human Immunodeficiency Virus Type 1 Nef Protein. *Journal of General Virology* 87: 563 - 71

516. Weiss A, and DR Littman. 1994. Signal Transduction by Lymphocyte Antigen Receptors. *Cell* 76: 263 - 74

517. Kahn JO, and Walker BD. 1998. Acute Human Immunodeficiency Virus Type 1 Infection. *New England Journal of Medicine* 339: 33 - 9

518. Liu LX, Heveker N, Fackler OT, Arold S, Le Gall S, Janvier K, Peterlin BM, Dumas C, Schwartz O, Benichou S, and Benarous R. 2000. Mutation of a Conserved Residue (D123) Required for Oligomerization of Human Immunodeficiency Virus Type 1 Nef Protein Abolishes Interaction with Human Thioesterase and Results in Impairment of Nef Biological Functions. *Journal of Virology* 74: 5310 - 9

519. Liu LX, F Margottin, S Le Gall, O Schwartz, L Selig, R Benarous and S Benichou. 1997. Binding of HIV-1 Nef to a Novel Thioesterase Enzyme Correlates with Nef-Mediated CD Down-Regulation. *Journal of Biological Chemistry* 272: 13779 - 85

520. Kyte J, and Doolittle RF. 1982. A Simple Method for Displaying the Hydropathic Character of a Protein. *Journal of Molecular Biology* 157: 105 - 32

521. Geyer M, Yu H, Mandic R, Linnemann T, Zheng Y, Fackler OT and BM Peterlin. 2002. Subunit H of the V-ATPase Binds to the Medium Chain of Adaptor Protein Complex 2 and Connects Nef to the Endocytic Machinery. *Journal of Biological Chemistry* 277: 28521 - 9